

Interpreting Low-Temperature Thermochronometric Data in Fold-and-Thrust Belts: An  
Example from the Western Foothills, Taiwan

Jane Lock

A dissertation submitted in partial fulfillment of the  
requirements for the degree of

Doctor of Philosophy

University of Washington

2007

Program Authorized to Offer Degree:  
Department of Earth & Space Sciences

University of Washington  
Graduate School

This is to certify that I have examined this copy of a doctoral dissertation by

Jane Lock

and have found that it is complete and satisfactory in all respects,  
and that any and all revisions required by the final  
examining committee have been made.

Chair of the Supervisory Committee:

---

Sean Willett

Reading Committee:

---

Sean Willett

---

Darrel Cowan

---

Gerard Roe

Date: \_\_\_\_\_

In presenting this dissertation in partial fulfillment of the requirements for the doctoral degree at the University of Washington, I agree that the Library shall make its copies freely available for inspection. I further agree that extensive copying of the dissertation is allowable only for scholarly purposes, consistent with "fair use" as prescribed in the U.S. Copyright Law. Requests for copying or reproduction of this dissertation may be referred to ProQuest Information and Learning, 300 North Zeeb Road, Ann Arbor, MI 48106-1346, 1-800-521-0600, to whom the author has granted "the right to reproduce and sell (a) copies of the manuscript in microform and/or (b) printed copies of the manuscript made from microform."

Signature \_\_\_\_\_

Date \_\_\_\_\_

University of Washington

**Abstract**

Interpreting Low-Temperature Thermochronometric Data in Fold-and-Thrust Belts:  
An Example from the Western Foothills, Taiwan

Jane Lock

Chair of the Supervisory Committee:

Professor Sean Willett

Department of Earth and Space Sciences

New apatite fission track and (U-Th)/He data document the cooling history and the structural development of the Taiwan Western Foothills fold-and-thrust belt which lies at the edge of one of the worlds most actively growing orogens. This dissertation develops and uses a 2-dimensional thermo-kinematic model of thrust faulting and folding to understand the cooling history recorded by the new low-temperature thermochronometric data. The results of this dissertation provide the previously lacking long-term record of uplift and erosion in the western foothills fold-and-thrust belt.

In western Taiwan, the apatite fission track and (U-Th)/He cooling ages record thrust exhumation over the last 3.5 Ma. Material is rapidly exhumed above a blind thrust ramp buried beneath the eastern part of the thrust belt or western Hsüeshan Range. After exhumation above the ramp, material is transported horizontally along a décollement in the Miocene strata of the western foothills. The thrust ramp links the main Taiwan décollement in the Oligocene rocks of the Hsüeshan Range to the décollement in the Miocene section and migrates with time.

Slip along the deep buried ramp and the upper décollement is passed to thrust ramps at the deformation front along the western edge of the thrust belt. This

deformation explains the distribution of cooling ages, stratigraphy, and the patterns of geodetic shortening across western Taiwan. There is no evidence for out-of-sequence thrusting in the thrust belt and the evolution recorded by the thermochronometric data is a steady southward and westward propagating sequence of thrusts.

The fault structures in southern Taiwan document the transition from subduction to arc-continent collision. The thermo-kinematic model is used to 'retro-deform' thrust faults and thermochronometric samples. This retro-deformation shows that prior to arc-continent collision, stratigraphy and subduction-related faults were buried in a depositional basin. The onset of arc-continent collision is marked by rapid exhumation above a thrust ramp that forms at the rear of the thrust belt beneath the old subduction-related accretionary-prism faults.

The studies in this dissertation highlight the power of using thermo-kinematic-thermochronologic modeling to understand detailed cooling histories in fold-and-thrust belts.

## TABLE OF CONTENTS

	Page
List of Figures .....	ii
List of Tables .....	iv
Chapter 1: Introduction .....	1
Notes to Chapter 1 .....	17
Chapter 2: Using Low-temperature Thermochronometry to constrain Deformation and Exhumation in Fold-and-Thrust Belts .....	25
Notes to Chapter 2 .....	67
Chapter 3: Low Temperature Thermochronometric data in Western Taiwan.....	76
Notes to Chapter 3 .....	134
Chapter 4: Thermal-kinematic modeling of apatite fission track and apatite (U-Th)/He data in the southern Western Foothills fold-and-thrust belt, Taiwan.....	141
Notes to Chapter 4 .....	171
Chapter 5 Summary and Global Applications .....	175
Notes to Chapter 5 .....	180
List of References.....	182

## LIST OF FIGURES

Figure Number	Page
1.1 Tectonic Setting of Taiwan and the western foothills fold-and thrust belt.....	12
1.2 Photo showing fault-related fold in the western foothills fold-and-thrust belt.....	13
1.3 Schematic fault-bend-fold and common terminology .....	14
1.4 Example fold-and-thrust cross-sections.....	15
1.5 Previous kinematic approximations of thrust faulting.....	16
2.1 Example Fold-and-thrust belt and fault-bend-fold.....	53
2.2 Patterns of Thermochronometric Age produced by Thrust Fault Exhumation.....	54
2.3 Change in depth to the 100°C isotherm in 1d and thrust fault models .....	55
2.4 Predicted thermochronometric ages for fault geometries with different base-flat depths .....	56
2.5 Thermochronometric age sensitivity to fault ramp dip.....	57
2.6 Thermochronometric age sensitivity to slip rate .....	58
2.7 Thermochronometric age patterns generated by blind and emergence thrust ramps .....	59
2.8 Results of multiple fault model with 50 km fault spacing .....	60
2.9 Results of multiple fault model with 20 km fault spacing .....	61
2.10 Temperature-depth histories of selected points in 20 km fault spacing model. .....	62
2.11 Results of multiple fault model with 10 km fault spacing .....	63
2.12 Temperature-depth histories of selected points in 10 km fault spacing model	64
2.13 Comparison of single fault and multiple fault models.....	65
2.14 Schematic illustration of factors controlling different multiple fault thermochronometric age patterns .....	66
3.1 Geologic and Tectonic map and sample locations .....	122
3.2 Stratigraphy of western Taiwan .....	123
3.3 Geologic Map and sample locations in our central sampling region .....	124
3.4 Cross section and thermochronometric ages along the central transect.....	125
3.5 Geologic Map and sample locations in our northern sampling region.....	126
3.6 Cross section and thermochronometric ages along the northern transect.....	127
3.7 Geologic Map and sample locations in our southern sampling region.....	128
3.8 Map of samples and their thermochronometric ages around the Tulungwun fault .....	129
3.9 Cross section and thermochronometric ages along the southern transect .....	130
3.10 Kinematic model of five foreland propagating thrust faults with a flat-ramp-flat-ramp geometry.....	131
3.11 Apatite fission track and (U-Th)/He ages generated by fault kinematics shown in figure 3.10 .....	132
3.12 Temperature time histories for points shown in Figure 3.10 .....	133
4.1 Tectonic Setting and Geologic units of Taiwan. ....	163

4.2 Geologic map, stratigraphy and thermochronometric sample location.....	164
4.3 Example of thermo-kinematic-thermochronometric model.....	165
4.4 Results of preferred thermal-kinematic-thermochronometric model of thrust deformation over the last 1 Ma.....	166
4.5 Kinematic Model of thrusting in southern Taiwan over the last 1 Ma.....	167
4.6 Model generated temperature-depth histories of samples 34_04, 35_04, 26_04 & 41_01.....	168
4.7 Samples and 'undeformed' structure prior to thrust deformation at 1 Ma.....	169
4.8 Backthrust thermo-kinematic-thermochronologic model.....	170



## LIST OF TABLES

Table Number	Page
2.1 Thermal Model Parameters.....	49
2.2 Model geometries and kinematics.....	50
2.3 Depth to 100° isotherm for different fault slip rates after 2 Ma of faulting.....	52
3.1 Apatite fission-track age data collected using the conventional AFT method ...	114
3.2 Summary of the apatite fission-track age data collected using LA-ICPMS .....	115
3.3 Fission track sample age interpretations.....	116
3.4 (U-Th)/He in apatite table A. ....	118
3.5 (U-Th)/He in apatite table B. ....	119
3.6 Comparison of AFT and AHe grain ages. ....	120
4.1 Thermal Model Parameters.....	162

## **ACKNOWLEDGEMENTS**

My thanks goes to the faculty and staff of the department of Earth and Space Sciences for their guidance and support. I would particularly like to thank Sean Willett for his insightful advice and endless knowledge. This research was funded by the National Science Foundation Research Grant EAR-0337782. This dissertation would not have been completed without my friends and without the support of fellow graduate students at the University of Washington, Pennsylvania State University, and Eidgenössische Technische Hochschule Zürich.

## Chapter 1

### Introduction

Fold-and-thrust belts lie at the edge of all major convergent orogens marking the edge of deformation that separates the foreland basin from high mountain topography. Thrust belts play a major role in the mountain building process. They accommodate significant amounts of convergence and much of the material in the orogen has been accreted at the fold-and-thrust belt. Their importance makes understanding how thrust belts develop, how motion is partitioned between structures, and the rates and longevity of individual thrust faults key to understanding orogenic growth.

The Taiwan Western Foothills is a classic fold-and-thrust belt. The Western Foothills lie at the western edge of Taiwan, one of the worlds youngest and most rapidly deforming orogens that forms from the oblique collision of the Luzon arc with the Chinese continental margin (Figure 1.1). More than 50 % of the 80-90 mm/yr total plate convergence between the Luzon volcanic arc and the Eurasian continental margin is accommodated by structures in the Western Foothills fold-thrust belt (Yu et al., 1997). The obliquity of the Luzon arc and continental margin has caused collision to propagate to the south at ~ 55-90 mm/yr (Suppe, 1984; Byrne and Liu, 2002). Thus collision is oldest in the north of Taiwan, and is only just beginning in the south, resulting in a space-time equivalence. The north-south propagating collision and rapid rates of deformation make the Western Foothills fold-and-thrust belt an ideal place to study the development of fold-and-thrust belts in general and investigate the role that thrust fault and fold structures play in the mountain building process.

The Western Foothills fold-and-thrust belt contain a series of parallel NE-SW striking faults that fold Neogene passive margin sediments creating the characteristic thrust-belt ridge-and-valley topography (Figure 1.1 & 1.2). The thrust belt is an example of 'thin-skinned' tectonics; faults sole into décollement layers that separate overlying deformed stratigraphy in the hangingwall from the underlying undeformed stratigraphy in the footwall. The stratigraphy in the hangingwall is advected

horizontally above fault flats and is folded above bends in the thrust faults creating fault-bend-folds (Figure 1.3).

Fold-and-thrust belt structures like those in Taiwan develop by the forward propagation of thrust faults which widens the thrust belt as the deformation front steps into the foreland basin (Figure 1.4). It is the stepping of faults into the foreland basin that incorporates material into the growing orogen. In the conventional view, faults are activated sequentially, and once a new fault is activated, older faults are deactivated (Twiss & Moores, 1995). Faults that are active behind the deformation front are termed 'out-of-sequence' faults.

In the Taiwan thrust belt, the conventional view of a foreland-propagating thrust sequence with no out-of-sequence faults is supported by records of short-term deformation which show rapid deformation around the frontal structures and little elsewhere. Across the frontal structure, geodetic measurements record uplift rates  $> 10$  mm/yr and shortening rates  $> 30$  mm/yr (Yu et al., 1997; Hickman et al., 2002; Yue et al., 2005; Fruneau et al., 2001; Hsu et al., 2003; Yue et al., 2005; Huang et al., 2006) and fluvial terraces indicate incision rates of up to 15 mm/yr (Hsieh and Knuepfer, 2001; 2002; Simoes et al., 2007). There is little short-term evidence for any deformation behind the frontal few structures until reaching the Longitudinal and Coast Range fault on the eastern side of Taiwan that accommodates the remainder of the deformation (Yu et al., 1997; Lee et al., 2001; Hsu et al., 2003).

Although there are many short-term ( $<10$  ka) records of uplift and erosion across the thrust belt, there are no longer-term records ( $>1$  Ma) and it is unclear if the rapid uplift and erosion recorded over the short-term are applicable over geologic time scales. The modern day deformation focused at either edge of Taiwan and little elsewhere, appear at odds with the high mountainous topography and oldest, most deeply exhumed rocks toward the hinterland of the thrust belt and into the Hsüehshan Range. The deeply exhumed rocks record significant uplift and erosion over the long term and perhaps indicate out-of-sequence thrust faults which exhume material in the Hsüehshan Range (Figure 1.1).

Balanced cross sections through the Taiwan thrust-belt place good constraints on many aspects of thrust fault geometry and provide a snapshot of the deformation that has evolved over the life of the thrust belt (Suppe, 1980a,b; 1983, Hickman et al., 2002; Huang et al., 2004). These sections do not, however, constrain thrust timing, exhumation rates or the temporal and spatial evolution of the thrust belt.

A primary aim of this dissertation is to provide the missing record of long-term deformation in the Western Foothills fold-and-thrust belt using apatite fission track and apatite (U-Th)/He data and better understand the role of the thrust belt in the mountain building process. Low closure temperature radiometric dating techniques like apatite fission track and apatite (U-Th)/He can provide the long term rates and reveal patterns of deformation in the Western Foothills fold-and-thrust belt by recording cooling ages that date erosion directly related to active thrust-structures. This record of thrust-related cooling can be used to determine the longevity and slip-rate of individual thrust faults and the spatial and temporal evolution of structures in the fold-and-thrust belt on the million year time scale. This dissertation concentrates on the Taiwan thrust belt, but the results and techniques used here are applicable to thrust belts and convergent orogens world-wide.

*Using low-temperature thermochronology in fold-and-thrust belts.*

Radiometric dating by methods such as apatite (U-Th)/He and apatite fission track data are commonly interpreted assuming 1-dimensional constant exhumation and cooling. In fold-and-thrust belts, however, interpreting radiometric data is complicated by the spatially and temporally varying 2-dimensional kinematics of thrust faulting and folding (Figure 1.3). The varying kinematics generate complex exhumation paths and perturb the temperature field making it difficult to directly convert a cooling age to a cooling rate using traditional techniques.

Previous studies have interpreted thermochronometric data in thrust belts using a variety of techniques. One approach is to assume thermochronometric ages collected from each thrust sheet records timing along each related thrust providing thrust

initiation and thrust fault evolution but not an exhumation amount or a cooling rate (e.g. Blythe et al., 1999; Arne et al., 1997; Theide et al., 2005; Malusa et al., 2005; McQuarrie et al., 2005, Figure 1.5A). Converting a cooling age to an amount of exhumation and a cooling rate requires approximating the temperature field, cooling history and closure temperature depth.

The temperature field and closure temperature depth resulting from thrust faulting has been calculated assuming a 1d linear geotherm and constant cooling (Omar et al., 1994; Spotila et al., 2004; Bullen et al., 2001, 2003; Ducea et al., 2003; Kirby et al., 2002) and by solving the 1d advection-diffusion equation (Zeitler, 1985, Parrish, 1982; 1985, Safran, 2003, Mancktelow and Graseman, 1997, House et al. 2002; Moore & England, 2001, Braun, 2002, Stuwe, 1994). However, 2d thermal models of thrust faulting have shown that assuming a linear geotherm or using a 1d thermal model fails to capture heat advection and/or the two dimensional thrust kinematics that cause lateral temperature gradients (Brewar, 1981; England & Thompson, 1984; Oxburgh and Turcott, 1974; Mailhe et al, 1986; Davy and Gillet, 1986; Brown and Summerfield, 1997; Moore and England, 2001; Molnar and Enlgand, 1990; Karabinos and Ketcham, 1988; Ruppel and Hodges, 1994). These two dimensional thermal-kinematic models range from fairly simple kinematics with material moving parallel to the fault (Molnar and Enlgand, 1990; Karabinos and Ketcham, 1988; Ruppel and Hodges, 1994, Figure 1.5 B) a slightly more complex single flat with a surface breaking ramp (Huntington et al., 2006; 2007 Whipp et al., 2007, figure 1.5 B) to modeling a fault with a flat-ramp-flat geometry which more closely approximates thrust kinematics (Shi and Wang, 1987; ter Voorde, 2004; Bollinger et al., 2004; 2006; Huerta and Rodgers, 2006, Brewer et al., 2007; Figure 1.5 C).

Many workers (e.g. Shi and Wang, 1987; ter Voorde, 2004; Bollinger et al., 2004; 2006; Huerta and Rodgers, 2006; Huntington et al., 2006; 2007, Brewer et al., 2006 & Whipp et al., 2007) use the results of their thermal-kinematic thrust fault models to interpret thermochronometric data in a variety of tectonic settings. However, with the exception of ter Voorde's (2004) models of two faults and associated fault-

bend-folds, these 2-dimensional thrust fault studies have focused on the exhumation history of an individual thrust sheet and do not include the foreland propagation of thrust faults, a fundamental feature of fold-and-thrust belts. Using the existing single-fault model approach in fold-and-thrust belts is overly simplistic. A single fault model fails to capture the salient kinematics of a sequence of thrust faults and folds, and cannot be used to investigate the temporal development of thrust faults or identify features such as 'out-of-sequence' faults.

This dissertation is separated into three main chapters followed by a conclusions chapter. The next chapter of this dissertation, Chapter 2, 'Using Low-Temperature Thermochronometry to constrain Deformation and Exhumation in Fold-and-Thrust Belts', develops a 2-dimensional numerical thermal-kinematic model of thrust-faulting and folding that includes realistic fault geometries and kinematics, and includes multiple thrust faults. I present thermochronometric age patterns generated by a variety of geometries that include individual and multiple thrust faults and fault-bend-folds. This chapter presents the currently lacking systematic study of the patterns of low-temperature thermochronometric ages across a fold-and-thrust belt and investigates how these patterns vary with thrust rate and fault geometry for individual and multiple fault scenarios. The results of this study (Chapter 2) are necessary to use low-temperature thermochronometric data to answer fundamental questions such as the how long thrust faults are active, the amount and rate of exhumation and the role of out-of-sequence faulting in the Taiwan Western Foothills fold-and-thrust belt. Chapter 3 uses the results of this new thermo-kinematic model to interpret thermochronometric data in the Western Foothills fold-and-thrust belt and Chapter 4 extends the thermochronometric model to constrain detailed thrust fault geometries and patterns of burial and exhumation that record the process of incipient collision. Chapter 5 summarizes the key results of this dissertation and discusses the implications of this study to convergent orogens world wide.

*Low-temperature thermochronometry in western Taiwan*

There is a large set of existing thermochronometric data from the center of Taiwan, but there is little thermochronometric data from the Western Foothills fold-and-thrust belt, and what data do exist record ‘partially reset’ ages reflecting the shallow burial depths of material in the thrust belt (Liu et al., 2001; Willett et al., 2003; Fuller et al., 2006). Though partially and unreset ages constrain the amount of exhumation to be less than the closure temperature depth, they do not record the timing of thrust faults, the rate of exhumation or the sequence of thrust development. An important contribution of this dissertation is to obtain cooling ages from the Western Foothills fold-and-thrust belt that were acquired with measuring, sampling and analysis techniques that maximize the chance of recording reset apatite fission track and (U-Th)/He ages and allow the interpretation of a cooling age in material that is partially reset. This new data and the techniques used to obtain cooling ages in Western Taiwan is described in Chapter 3. Also in Chapter 3, I interpret the new apatite fission track and (U-Th)/He cooling age using a combination of the structure and stratigraphy of the Western Foothills, and in light of the results of the thermokinematic modeling described in Chapter 2. The thermochronometric age patterns in the foothills are used to interpret the onset of thrust exhumation, identify active out-of-sequence faults, and constrain the total amount of exhumation in the thrust belt.

The north to south propagating collision is a consequence of the obliquity between the Luzon arc and Chinese continental margin. However, still debated are the time collision began, the rate of collision propagation, and how collision evolves over time (Suppe, 1984; Covey, 1994; Teng, 1990; Wu et al., 1997; Huang et al., 1997; 2000; 2006; Liu et al., 2001; Montheureau et al., 2001; Byrne and Liu, 2002; Willett et al., 2003; Sibuet & Hsu, 2004; Lee et al., 2006; Simoes & Avouac, 2006). The long term cooling and exhumation history in the thrust belt provided by thermochronometric ages presented and interpreted in Chapter 3, are an important missing record in Taiwan’s tectonic history and the history of the thrust belt.



Although the exact timing and nature of collision in Taiwan is debated, it is clear that there is a southward propagating signal. The southern part of the Taiwan fold-and-thrust belt provides an excellent opportunity to investigate incipient collision and the transition from the subduction setting that currently exists to the south of Taiwan, to arc-continent collision. Compared with farther north, the structures in southern Taiwan in the first stage of collision are simpler having experienced less overprinting by multiple thrust faulting and deformation. The well defined geology and density of thermochronometric data collected allow for a detailed investigation of the onset of arc-continent collision and the transition from subduction to collision using the new thermokinematic model. The final chapter of this dissertation, Chapter 4, describes this detailed modeling study.

### *Overview of dissertation*

#### *Chapter 2*

The second chapter presents my new thermo-kinematic-thermochronometric model of thrust faulting and folding. This approach uses a kinematic model that is easily manipulated to include complex fault geometries, multiple faults and different thrust fault histories.

The model links a kinematic model of fault-bend-folding (Figure 1.3) that provides the advection term in a 2 dimensional finite element advection-diffusion thermal model. This linked model tracks the temperature response to thrust faulting and generates material cooling histories. The modeled material cooling histories are used to generate apatite fission track and (U-Th)/He ages to produce the thermochronometric age pattern that results from thrust faulting and folding.

In Chapter 2, I use the model to systematically investigate the different patterns of thermochronometric age produced by a variety of thrust fault geometries and extend the model to include multiple thrust faults. An important prediction of the thermal model is the complex material cooling histories. This is the first study of its kind and raises questions about the applicability of traditional techniques such as age-elevation

transects and 1d steady-state models commonly used to interpret thermochronometric data in regions with thrust faults.

The cooling histories generated by the model show that the age of material exhumed by thrust faulting exhibits a characteristic U-shaped age as a function of distance formed by young cooling ages at its base surrounded by partially reset and unreset ages. The young cooling ages are fairly insensitive to thrust geometry and most sensitive to exhumation rate, but the thermochronometric age distribution is very sensitive to fault geometry. Changing the thrust slip and exhumation rate changes the minimum predicted age, but changing the geometry of the fault ramp does not.

Material exhumed by a sequence of thrust ramps produces thermochronometric age patterns that are not at first intuitive. Depending on the fault spacing and amount of slip along each fault, young cooling ages that record the most recent thrusting event can be preserved in the hinterland *or* in the foreland of a thrust belt. Importantly, there are no sharp age 'breaks' across each thrust fault.

The results of the modeling study are generally applicable to all thrust belts. In Chapter 3, we use the results of the generally applicable thrust fault models presented in Chapter 2 to interpret apatite fission track and (U-Th)/He data in the Western Foothills. Locally, the flexibility of our thermokinematic model with the power to include complex kinematics allows the numerical model to investigate the thermochronometric age pattern generated by thrust structures whose geometry and history is constrained by the actual stratigraphy and structure along a cross-section through the Taiwan thrust-belt.

### *Chapter 3*

Chapter 3, 'Low-Temperature Thermochronometric data in Western Taiwan', presents new apatite fission track and U-Th/He data collected along three transects, a northern, central and southern transect that cross the Western Foothills fold and thrust belt. The new thermochronometric data span the length of Taiwan and greatly extend the spatial coverage and increase the density of existing thermochronometric data.

This chapter describes the sampling, measuring and analysis technique that used to acquire cooling ages from shallowly buried sedimentary rocks of the Western Foothills. I interpret the new thermochronometric data in light of the thermochronometric modeling study described in Chapter 2. The data constrain the timing and significance of thrust structures in western Taiwan and the maximum burial across the thrust belt. For example, the fault(s) separating the western-foothills thrust belt from the metamorphosed rocks of the Hsüehshan Range appears to be a significant geological feature and thermochronometric ages from the Hsüehshan Range indicate recent and rapid exhumation. The results presented in this chapter shows how there is no evidence for 'out-of-sequence' faulting along this or any other of the seemingly major surface breaking thrust structures in Taiwan.

Rather than surface breaking structures, the thermochronometric ages record exhumation over a thrust ramp buried beneath the rear of the thrust belt or beneath the Hsüehshan Range. This ramp is identified along each transect from north and south. The detailed geometry of this ramp in southern Taiwan is investigated as part of the study described in Chapter 4. Motion along this ramp is passed to the active structures that accommodate the majority of convergence at the deformation front. This scenario fits both the long-term distribution of exhumation and the short-term distribution of convergence.

The oldest collision-related thrust-cooling age in the Western Foothills is ~3.5 Ma in northern and central Taiwan and 1 Ma in southern Taiwan reflecting the southward propagating collision. There is no evidence for thrust faulting occurring at the commonly accepted 6-8 Ma time that collision began (Byrne and Liu, 2002). The youngest apatite fission track thrust-cooling age is 1.2 Ma in northern Taiwan and 0.5 Ma in central and southern Taiwan. The distribution of the oldest and youngest cooling ages records the southward progression to collision.

*Chapter 4*

The north to south development of Taiwan presents an excellent opportunity to investigate the onset of collision and the transition from subduction to arc-continent collision that is captured in the youngest part of the thrust belt in southern Taiwan. The southern most data transect presented in Chapter 3 crosses this youngest part of the thrust belt. Chapter 4, ‘Thermal-kinematic modeling of apatite fission track and apatite (U-Th)/He ages in the southern Western-foothills fold-and-thrust belt, Taiwan’ is a detailed thermokinematic modeling study of initial arc-continent collision. In Chapter 4, using the thermokinematic model developed in Chapter 2, I retro-deform a geologically constrained cross-section to predict thermochronometric ages and establish the amount, patterns, and rates of burial and exhumation in the southern Taiwan thrust-belt. The retro-deformed model describes the deformation over the last 1 Ma and the beginning of arc continent collision.

The youth of thrust faults in the south of Taiwan results in simpler structures that have been overprinted by fewer deformational events compared to the thrust-faults in the center and north of Taiwan. The well defined structure and stratigraphy provide tight geological controls which, combined with the high density thermochronometric ages in southern Taiwan, allow detailed thermokinematic modeling to constrain the actual geometry of structures, how faults at the surface continue at depth, and local patterns of burial prior to thrust exhumation.

The geology, thermochronology and thermokinematic modeling show that faults which crop out in southern Taiwan are subduction-related thrust-faults that were active as part of the accretionary prism and are not related to collision. These accretionary prism faults were buried by sediments in a depositional subduction wedge-top basin that has a modern day equivalent in southern and offshore Taiwan.

I argue that with the onset of collision, new thrust faults form beneath the old subduction-related accretionary prism faults. The collision-related thrusts sole and roof into décollement beneath the basal décollement of the accretionary prism faults. Thus collision-related thrusts deform older stratigraphy deeper in the stratigraphic section

compared with the accretionary prism thrusts. Exhumation along the collision-related structures deforms and exhumes the inactive subduction accretionary prism faults from beneath the depositional basin.

The study described in Chapter 4 shows the power of detailed thermo-kinematic modeling to extract detailed cooling histories from thermochronometric data in thrust belts.

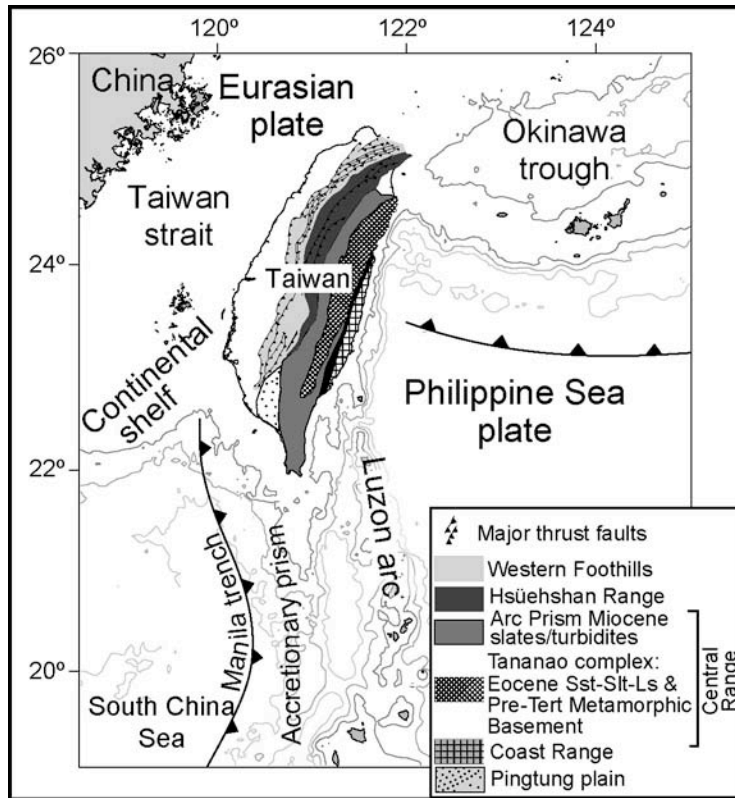


**Figure 1.1** Tectonic Setting of Taiwan and the Western Foothills fold-and-thrust belt. After Ho, 1988; Lundberg et al., 1997; Subuet and Hsu, 1997; Fisher et al., 2002; Lamcombe et al., 2003. Base map from Stolar et al., 2007 showing 1, 2, & 3 km bathymetry.



**Figure 1.2** Photo showing fault-related fold in the Western Foothills fold-and-thrust belt. The Western Foothills fold-and-thrust belt is the site of much of the seminal work on the fault and fold structures in thrust belts by John Suppe in the early 1980's. Beds are folded above changes in the dip of the ramp. This photo shows the back-limb of one of these folds.

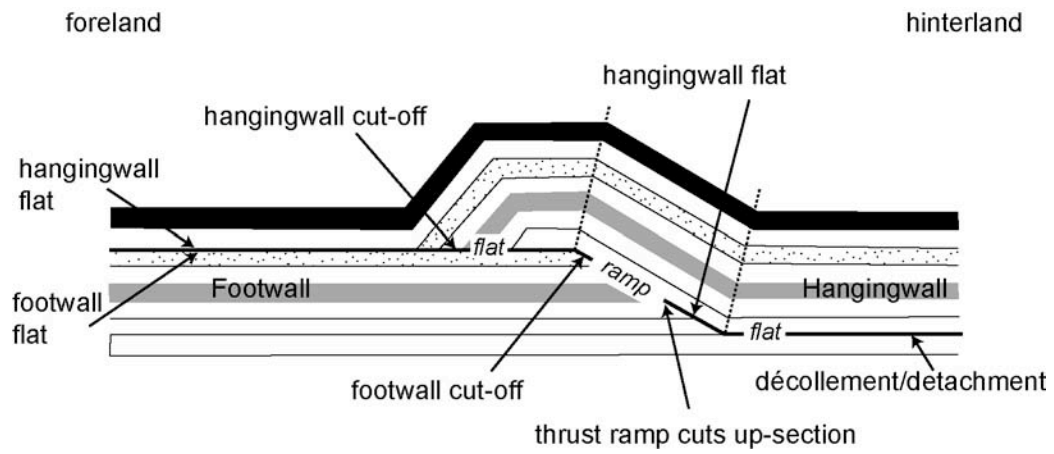


**Figure 1.3** Schematic fault-bend-fold and common terminology. Fault-bend-fold model developed to explain the style of deformation in the Western Foothills fold-and-thrust belt. Faults have a ramp-flat-ramp geometry and sole into a main décollement. The strata fold above changes in the ramp dip.



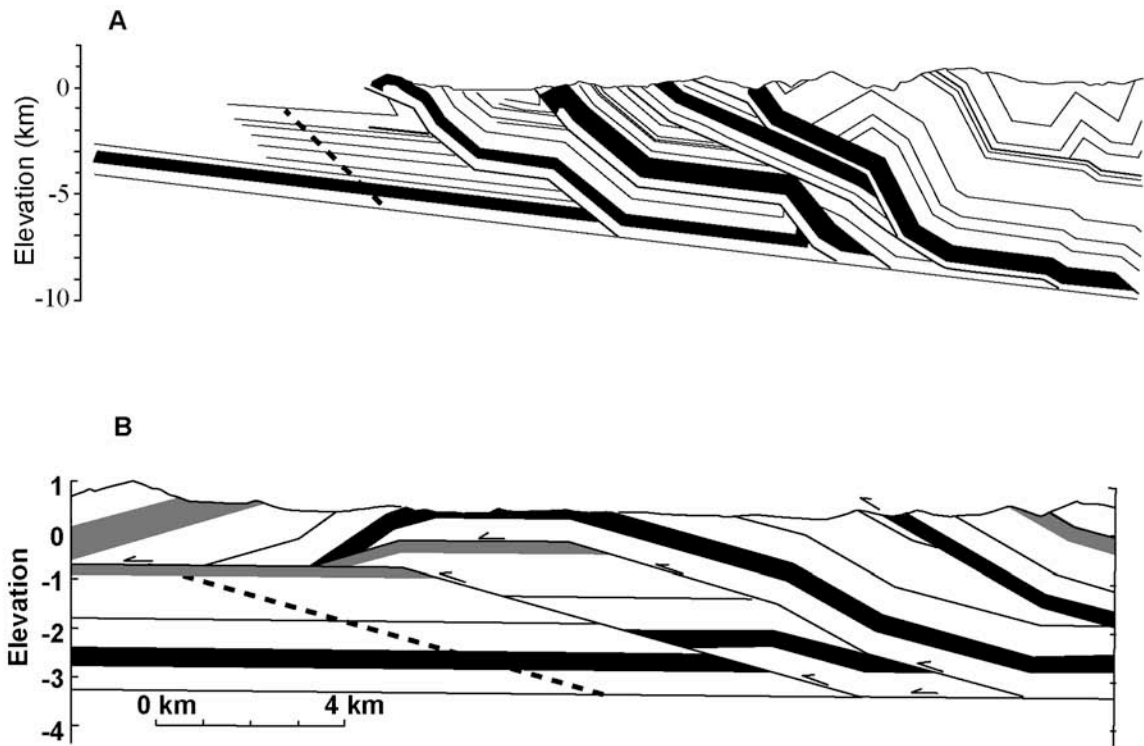


**Figure 1.4** Example fold-and-thrust belt cross-sections

A) Western Foothills Fold and thrust belt after Suppe (1980b). B) Powell anticline from Suppe, 1983. In both sections, dashed line is a schematic representation of a new fault which will activate as convergence continues.

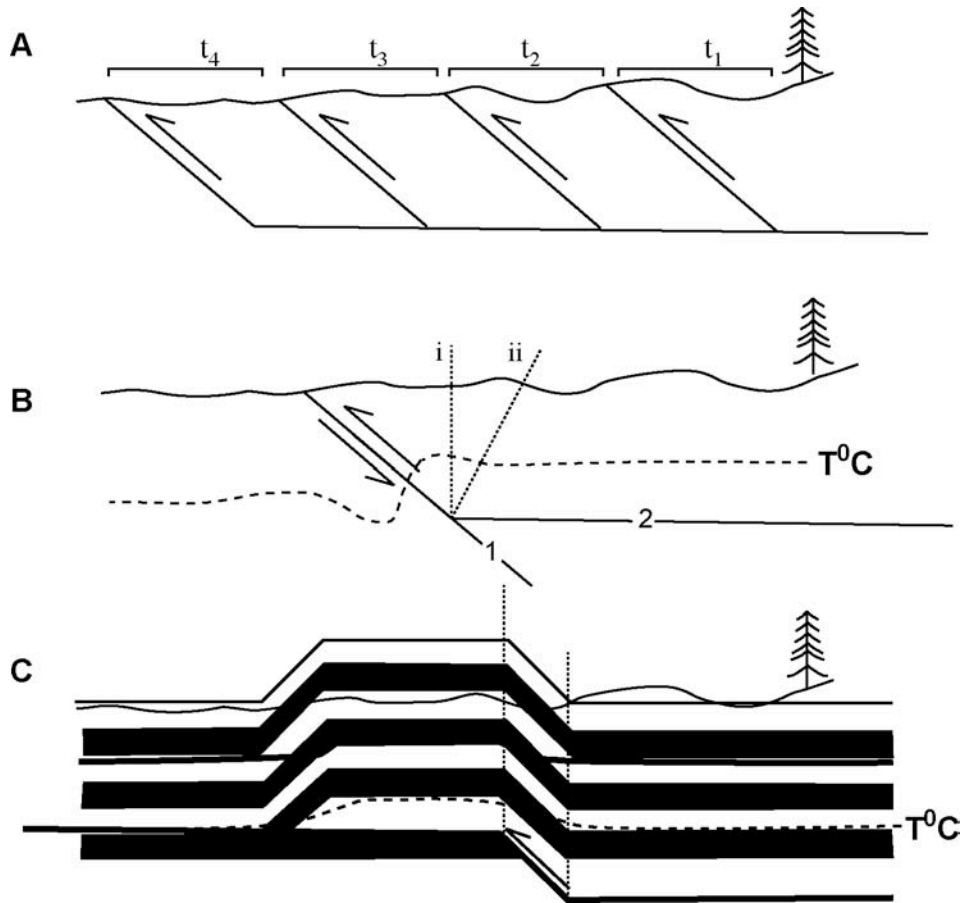


**Figure 1.5** Previous kinematic approximations used to calculate the temperature effects of thrust faulting and/or interpret thermochronometric data.

Previous kinematic approximations used to calculate the temperature effects of thrust faulting and/or interpret thermochronometric data. A) Ages from each thrust sheet records motion on that fault. B) Single fault that reaches surface, material moves parallel to the fault. 1) Fault continues to depth or 2) soles to a décollement level. Dashed line shows a schematic modeled closure temperature. In the single ramp-flat model, material moves horizontally above the bottom flat and is vertically advected above the ramp. Dotted line shows two different fault bisectors. i - material is vertically advected when it is above the fault. ii - material above the fault bisector is vertically advected modified from Huntington et al., 2007. C) Fault bend fold formed above a single thrust fault with a ramp-flat-ramp geometry from Huerta & Rodgers, 2006.

### Notes to Chapter 1

- Arne, D., Worley, B., Wilson, C., Chen, S. F., Foster, D., Luo, Z. L. 1997. Differential exhumation in response to episodic thrusting along the eastern margin of the Tibetan Plateau. *Tectonophysics*, 280(3-4), 239-256.
- Blythe, A. E., Murphy, J., & OSullivan, P. B. 1997. Tertiary cooling and deformation in the south-central Brooks Range: Evidence from zircon and apatite fission-track analyses. *JOURNAL OF GEOLOGY*, 105(5), 583-599.
- Bollinger, L., Avouac, J. P., Beyssac, O., Catlos, E. J., Harrison, T. M., Grove, M. 2004. Thermal structure and exhumation history of the Lesser Himalaya in central Nepal. *Tectonics*, 23.
- Bollinger, L., Henry, P., & Avouac, J. P. 2006. Mountain building in the Nepal Himalaya: Thermal and kinematic model. *Earth and Planetary Science Letters*, 244, 58-71.
- Braun, J. 2002. Quantifying the effect of recent relief changes on age-elevation relationships. *Earth and Planetary Science Letters*, 200(3-4), 331-343.
- Brewer, I. D., & Burbank, D. W. 2006. Thermal and kinematic modeling of bedrock and detrital cooling ages in the central Himalaya. *Journal of Geophysical Research*, 111(B9).
- Brewer, J. 1981). Thermal effects of thrust faulting. *Earth and Planetary Science Letters*, 56, 233-244.
- Brown, R. W., & Summerfield, M. A. 1997). Some uncertainties in the derivation of rates of denudation from thermochronologic data. *Earth Surface Processes and Landforms*, 22(3), 239-248.
- Bullen, M. E., Burbank, D. W., & Garver, J. I. 2003). Building the northern Tien Shan; integrated thermal, structural, and topographic constraints. *Journal of Geology*, 111(2), 149-165.
- Bullen, M. E., Burbank, D. W., Garver, J. I., & Abdrakhmatov, K. Y. 2001). Late Cenozoic tectonic evolution of the northwestern Tien Shan; new age estimates for the initiation of mountain building. *Geological Society of America Bulletin*, 113(12), 1544-1559.

- Byrne, T. B., & Liu, C. (2002). Introduction to the geology and geophysics of Taiwan. *Special Paper - Geological Society of America*, 358, v-viii.
- Carena, S., Suppe, J., & Kao, H. (2002). Active detachment of Taiwan illuminated by small earthquakes and its control of first-order topography. *Geology*, 30(10), 935-938.
- Covey, M. (1984). Lithofacies analysis and basin reconstruction, Plio-Pleistocene western Taiwan foredeep. *Petroleum Geology of Taiwan*, 20, 53-83.
- Davy, P., & Gillet, P. (1986). The stacking of thrust slices in collision zones and its thermal consequences. *Tectonics*, 5(6), 913-929.
- Ducea, M., House, M. A., & Kidder, S. (2003). Late Cenozoic denudation and uplift rates in the Santa Lucia Mountains, California. *Geology (Boulder)*, 31(2), 139-142.
- England, P. C., & Thompson, A. B. (1984). Pressure-temperature-time paths of regional metamorphism; I, Heat transfer during the evolution of regions of thickened continental crust. *Journal of Petrology*, 25(4), 894-928.
- Fisher, D. M., Lu, C., & Chu, H. (2002). Taiwan slate belt; insights into the ductile interior of an arc-continent collision. *Special Paper - Geological Society of America*, 358, 93-106.
- Fruneau, B., Pathier, E., Raymond, D., Deffontaines, B., Lee, C. T., Wang, H. T., et al. (2001). Uplift of Tainan Tableland (SW Taiwan) revealed by SAR interferometry. *Geophysical Research Letters*, 28, 3071-3074.
- Fuller, C., Willett, S., Fisher, D., & Lu, C. (2006). A thermomechanical wedge model of Taiwan constrained by fission-track thermochronometry. *Tectonophysics*, 425(1-4), 1-24.
- Hickman, J. B., Wiltschko, D. V., Hung, J., Fang, P., & Bock, Y. (2002). Structure and evolution of the active fold-and-thrust belt of southwestern Taiwan from Global Positioning System analysis. *Special Paper - Geological Society of America*, 358, 75-92.
- Ho, C. S. (1988). *An Introduction to the Geology of Taiwan:- Explanatory Text of the Geologic Map of Taiwan, 2nd ed.* Taipei, Taiwan: Central Geological Survey.

- House, M. A., Gurnis, M., Kamp, P. J. J., & Sutherland, R. 2002. Uplift in the Fiordland region, New Zealand; implications for incipient subduction. *Science*, 297(5589), 2038-2041.
- Hsieh, M., & Knuepfer, P. L. K. 2002. Synchronicity and morphology of Holocene river terraces in the southern Western Foothills, Taiwan; a guide to interpreting and correlating erosional river terraces across growing anticlines. *Special Paper - Geological Society of America*, 358, 55-74.
- Hsieh, M., & Knuepfer, P. L. K. 2001. Middle-late Holocene river terraces in the Erhjen River Basin, southwestern Taiwan--implications of river response to climate change and active tectonic uplift. *Geomorphology*, 38(3-4), 337-372.
- Hsu, Y., Simons, M., Yu, S., Kuo, L., & Chen, H. 2003. A two-dimensional dislocation model for interseismic deformation of the Taiwan mountain belt. *Earth and Planetary Science Letters*, 211(3-4), 287-294.
- Huang, S-T, Yang, K-M., Hung, J-H., Wu, J-C., Ting, H-H., Mei, W-W., Hsu, S-H., Lee, M. 2004. Deformation Front Development at the Northeast Margin of the Tainan Basin, Tainan-Kaohsiung Area, Taiwan. *Marine Geophysical Researches*, 25(1), 139-156.
- Huang, C., Wu, W., Chang, C., Tsao, S., Yuan, P. B., Lin, C., Xia, K., 1997. Tectonic evolution of accretionary prism in the arc-continent collision terrane of Taiwan. *Tectonophysics*, 281(1-2), 31-51.
- Huang, C., Yuan, P. B., & Tsao, S. 2006. Temporal and spatial records of active arc-continent collision in Taiwan; a synthesis. *Geological Society of America Bulletin*, 118(3-4), 274-288.
- Huang, C., Yuan, P. B., Lin, C., Wang, T. K., & Chang, C. 2000. Geodynamic processes of Taiwan arc-continent collision and comparison with analogs in Timor, Papua New Guinea, Urals and Corsica. *Tectonophysics*, 325(1-2), 1-21. Retrieved October 12, 2007, from <http://www.sciencedirect.com/science/article/B6V72-41JM9C5-2/2/a3240be4772f70971a4ba95ef148422e>
- Huerta, A. D., & Rodgers, D. W. 2006. Constraining rates of thrusting and erosion; insights from kinematic thermal modeling. *Geology (Boulder)*, 34(7), 541-544.
- Huntington, K. W., Ehlers, T. A., Hodges, K. V., & Jr, D. M. W. 2007. Topography, exhumation pathway, age uncertainties, and the interpretation of thermochronometer data. *Tectonics*, 26, TC4012.

- Huntington, K. W., Blythe, A. E., & Hodges, K. V. 2006. Climate change and late Pliocene acceleration of erosion in the Himalaya. *Earth and Planetary Science Letters*, 252(1-2), 107-118.
- Whipp, D. M., Ehlers, T. A., Blythe, A. E., Huntington, K. W., Hodges, K. V., & Burbank, D. W. 2007. Plio-Quaternary exhumation history of the central Nepalese Himalaya: 2. Thermokinematic and thermochronometer age prediction model. *Tectonics*, 26, TC3003.
- Karabinos, P., & Ketchum, R. 1988. Thermal structure of active thrust belts. *Journal of Metamorphic Geology*, 6(5), 559-570.
- Kirby, E., Reiners, P. W., Krol, M. A., Whipple, K. X., Hodges, K. V., Farley, K. A., Tang, W., Chen, Z. 2002. Late Cenozoic evolution of the eastern margin of the Tibetan Plateau; inferences from (super 40) Ar/ (super 39) Ar and (U-Th)/He thermochronology. *Tectonics*, 21(1).
- Lacombe, O., Mouthereau, F., Angelier, J., Chu, H., & Lee, J. 2003. Frontal belt curvature and oblique ramp development at an obliquely collided irregular margin; geometry and kinematics of the NW Taiwan fold-thrust belt. *Tectonics*, 22(3).
- Lee, J., Angelier, J., Chu, H., Hu, J., & Jeng, F. 2001. Continuous monitoring of an active fault in a plate suture zone: a creepmeter study of the Chihshang Fault, eastern Taiwan. *Tectonophysics*, 333(1-2), 219-240.
- Lee, Y., Chen, C., Liu, T., Ho, H., Lu, H., & Lo, W. 2006. Mountain building mechanisms in the Southern Central Range of the Taiwan Orogenic Belt -- From accretionary wedge deformation to arc-continental collision. *Earth and Planetary Science Letters*, 252(3-4), 413-422.
- Liu, T., Hsieh, S., Chen, Y., & Chen, W. 2001. Thermo-kinematic evolution of the Taiwan oblique-collision mountain belt as revealed by zircon fission track dating. *Earth and Planetary Science Letters*, 186(1), 45-56.
- Lundberg, N., Reed, D. L., Liu, C., & Lieske, J. 1997. Forearc-basin closure and arc accretion in the submarine suture zone south of Taiwan. *Tectonophysics*, 274(1-3), 5-23.
- Mailhe, D., Lucazeau, F., & Vasseur, G. 1986. Uplift history of thrust belts; an approach based on fission track data and thermal modelization. *Tectonophysics*, 124(1-2), 177-191.

- Malusa, M. G., Polino, R., Zattin, M., Bigazzi, G., Martin, S., & Piana, F. 2005. Miocene to present differential exhumation in the Western Alps; insights from fission track thermochronology. *Tectonics*, 24(3).
- Mancktelow, N. S., & Grasemann, B. 1997. Time-dependent effects of heat advection and topography on cooling histories during erosion. *Tectonophysics*, 270(3-4), 167-195.
- McQuarrie, N., Horton, B. K., Zandt, G., Beck, S., & DeCelles, P. G. 2005. Lithospheric evolution of the Andean fold-thrust belt, Bolivia, and the origin of the central Andean Plateau. *Tectonophysics*, 399(1-4), 15-37.
- Molnar, P., & England, P. C. 1990. Temperatures, heat flux, and frictional stress near major thrust faults. *Journal of Geophysical Research*, 95(B4), 4833-4856.
- Moore, M. A., & England, P. C. 2001. On the inference of denudation rates from cooling ages of minerals. *Earth and Planetary Science Letters*, 185(3-4), 265-284.
- Mouthereau, F., Lacombe, O., Deffontaines, B., Angelier, J., & Brusset, S. 2001. Deformation history of the southwestern Taiwan foreland thrust belt; insights from tectono-sedimentary analyses and balanced cross-sections. *Tectonophysics*, 333(1-2), 293-322.
- Omar, G. I., Lutz, T. M., & Giegengack, R. 1994. Apatite fission-track evidence for Laramide and post-Laramide uplift and anomalous thermal regime at the Beartooth overthrust, Montana-Wyoming. *Geological Society of America Bulletin*, 106(1), 74-85.
- Oxburgh, E. R., & Turcotte, D. L. 1974. Thermal gradients and regional metamorphism in overthrust terrains with special reference to the Eastern Alps. *Schweizerische Mineralogische und Petrographische Mitteilungen = Bulletin Suisse de Mineralogie et Petrographie*, 54(2-3), 641-662.
- Parrish, R. R. 1983. Cenozoic thermal evolution and tectonics of the Coast Mountains of British Columbia; 1, Fission track dating, apparent uplift rates, and patterns of uplift. *Tectonics*, 2(6), 601-631.
- Ruppel, C., & Hodges, K. V. 1994. Pressure-temperature-time paths from two-dimensional thermal models; prograde, retrograde, and inverted metamorphism. *Tectonics*, 13(1), 17-44.

- Safran, E. B. 2003. Geomorphic interpretation of low-temperature thermochronologic data; insights from two-dimensional thermal modeling. *Journal of Geophysical Research*, 108(B4).
- Shi, Y., & Wang, C. 1987. Two-dimensional modeling of the P-T-t paths of regional metamorphism in simple overthrust terrains. *Geology (Boulder)*, 15(11), 1048-1051.
- Shyu, J. B. H., Sieh, K., Chen, Y., & Chung, L. 2006. Geomorphic analysis of the Central Range Fault, the second major active structure of the Longitudinal Valley suture, eastern Taiwan. *Geological Society of America Bulletin*, 118(11-12), 1447-1462.
- Shyu, J. B. H., Sieh, K., Chen, Y., & Liu, C. 2005. Neotectonic architecture of Taiwan and its implications for future large earthquakes. *Journal of Geophysical Research*, 110, B08402.
- Sibuet, J., & Hsu, S. 1997. Geodynamics of the Taiwan arc-arc collision. *Tectonophysics*, 274(1-3), 221-251.
- Sibuet, J., Hsu, S., & Debayle, E. 2004. Geodynamic context of the Taiwan Orogen. *Geophysical Monograph*, 149, 127-158.
- Simoës, M., & Avouac, J. P. 2006. Investigating the kinematics of mountain building in Taiwan from the spatiotemporal evolution of the foreland basin and western foothills. *Journal of Geophysical Research*, 111, B10401.
- Simoës, M., Avouac, J. P., Chen, Y., Singhvi, A. K., Wang, C., Jaiswal, M., Chan, Y., Bernard, S. 2007. Kinematic analysis of the Pakuashan fault tip fold, west central Taiwan: Shortening rate and age of folding inception. *Journal of Geophysical Research*, 112, B03S14.
- Spotila, J. A., Buscher, J. T., Meigs, A. J., & Reiners, P. W. 2004. Long-term glacial erosion of active mountain belts; example of the Chugach-St. Elias Range, Alaska. *Geology (Boulder)*, 32(6), 501-504.
- Stolar, D. B., Willett, S. D., & Montgomery, D. R. 2007. Characterization of topographic steady state in Taiwan. *Earth and Planetary Science Letters*, 261(3-4), 421-431.
- Stuewe, K., White, L., & Brown, R. 1994. The influence of eroding topography on steady-state isotherms; application to fission track analysis. *Earth and Planetary Science Letters*, 124(1-4), 63-74.



- Suppe, J., & Anonymous. 1981. Mechanics of mountain-building and metamorphism in Taiwan. *Chung Kuo Ti Ch'ih Hsueh Hui Chuan Kan = Memoir of the Geological Society of China*, 4, 67-89.
- Suppe, J. 1980a. Imbricated structure of Western Foothills Belt, southcentral Taiwan. *Petroleum Geology of Taiwan*, (17), 1-16.
- Suppe, J. 1980b. A retrodeformable cross section of northern Taiwan. *Proceedings of the Geological Society of China*, (23), 46-55.
- Suppe, J. 1983. Geometry and kinematics of fault-bend folding. *American Journal of Science*, 283(7), 684-721.
- Suppe, J., Chen, C., Chen, J., Lee, C., & Pan, K. 1984. Kinematics of arc-continent collision, flipping of subduction, and back-arc spreading near Taiwan. *Chung Kuo Ti Ch'ih Hsueh Hui Chuan Kan - Memoir of the Geological Society of China*, 6, 21-33.
- Teng, L. S. 1990. Geotectonic evolution of late Cenozoic arc-continent collision in Taiwan. *Tectonophysics*, 183(1-4), 57-76.
- ter Voorde, M., de Bruijne, C. H., Cloetingh, S. A. P. L., & Andriessen, P. A. M. 2004. Thermal consequences of thrust faulting: simultaneous versus successive fault activation and exhumation. *Earth and Planetary Science Letters*, 223(3-4), 395-413.
- Thiede, R. C., Arrowsmith, J. R., Bookhagen, B., McWilliams, M. O., Sobel, E. R., & Strecker, M. R. 2005. From tectonically to erosionally controlled development of the Himalayan Orogen. *Geology (Boulder)*, 33(8), 689-692.
- Twiss, R. J., & Moores, E. M. 1992. *Structural geology*. New York: W.H. Freeman and Company.
- Willett, S. D., Fisher, D., Fuller, C., Yeh, E., & Lu, C. 2003. Erosion rates and orogenic-wedge kinematics in Taiwan inferred from fission-track thermochronometry. *Geology (Boulder)*, 31(11), 945-948.
- Willett, S. D., Hovius, N., Brandon, M. T., & Fisher, D. M. 2006. Tectonics, climate, and landscape evolution; introduction. *Special Paper - Geological Society of America*, 398, vii-xi.
- Wu, F. T., Rau, R., & Salzberg, D. 1997. Taiwan orogeny: thin-skinned or lithospheric collision? *Tectonophysics*, 274(1-3), 191-220.

- Yu, S., Chen, H., & Kuo, L. 1997. Velocity field of GPS stations in the Taiwan area. *Bulletin of the Institute of Earth Sciences*, 17, 43-44.
- Yue, L., Suppe, J., & Hung, J. 2005. Structural geology of a classic thrust belt earthquake: the 1999 Chi-Chi earthquake Taiwan (Mw=7.6). *Journal of Structural Geology*, 27(11), 2058-2083.
- Zeitler, P. K. 1985. Cooling history of the NW Himalaya, Pakistan. *Tectonics*, 4(1), 127-151.

## Chapter 2

### **Using Low Temperature Thermochronometry to constrain Deformation and Exhumation in Fold-and-Thrust Belts**

Submitted to Tectonophysics, July 2007. Co-author, S. Willett.

#### **2.1 Summary**

We use a new 2-dimensional thermal-kinematic thrust fault model to generate low-temperature thermochronometric age in a fold-and-thrust belt and understand the rates and timing of thrust-deformation recorded by a cooling age. Our model links the kinematic structural model *2DMove* to a finite-element advection-diffusion thermal model to track the cooling history of material exhumed by thrust faulting and fault bend folding. We use this cooling history to model fission track annealing and He retention and predict apatite fission track and U-Th/He in apatite and zircon thermochronometric age.

We show model-generated thermochronometric age patterns in material exhumed by individual and multiple forward-propagating thrust faults and explore the effects of fault slip rate and fault geometry. All our models have a characteristic U-shaped thermochronometric age pattern. This pattern is formed by the distribution of reset, unreset and partially reset thermochronometric ages. Above the thrust ramp, reset material forms a zone of the young thermochronometric ages. Partially reset and unreset material lies either side of this zone of young ages. Although some thermochronometric ages predicted by our fault-bend-fold model are similar to those predicted using a 1-d thermal model, the patterns of ages are markedly different.

The smooth U-shaped pattern exists in both the single thrust fault and multiple thrust-fault models. In the foreland-propagating multiple fault models, there are no distinct changes in age across individual thrust faults and the thermochronometric age pattern changes with thrust-fault spacing. In multiple fault models, depending on the

fault-spacing and amount of slip along each fault, early faulting can be recorded either in the hinterland or foreland of the modeled thrust-belt, a pattern which is non-intuitive.

## 2.2 Introduction

Fold-and-thrust belts are important features of almost all modern convergent orogens, defining the leading edge of deformation, the zone of tectonic accretion of shallow crustal rocks, and the boundary that separates an orogen and its foreland basin. In order to understand the rates and mechanisms of orogenic growth, it is important to determine how deformation is partitioned across a thrust belt, the sequence of structural development, and the rates and longevity of specific structures.

A variety of techniques have been applied to the problem of unraveling the rates and kinematic history of fold and thrust belts. Structural analysis is instrumental in determining the style, relative timing, and sequence of deformation, but does not constrain absolute timing or deformation rates. Short term rates of deformation can be measured using geodetic data such as satellite-based (GPS) and vertical re-leveling (e.g., Hickman et al., 2002; Bürgmann et al., 1994; Banerjee and Bürgmann, 2004) and over a longer timescale (~10 kyr), geomorphic studies using uplifted terraces and dated terrace fill or strath surfaces can provide deformation rates across active structures (e.g., Coward et al. 1999; Jackson et al., 2002, Benedetti, et al., 2000; Wesnousky, et al, 1999). Over longer timescales (>100 kyr), absolute fault timing and even deformation rates can come from syn-orogenic sediments if they are preserved and datable (e.g., Zapata & Allmendinger, 1996; Suppe et al., 1992; Medwedeff, 1989; Ford et al., 1997; Hardy et al., 1996; De Celles et al., 1991; Burbank et al., 1992; 1996). Only this last technique is capable of measuring rates over million-year time scales. Low closure temperature radiometric dating techniques, such as apatite fission track dating and (U-Th)/He dating of apatite, have the potential to resolve thrust fault timing and slip rates averaged over the longer term by providing cooling ages that record erosion directly associated with active structures.

Some studies have used radiometric dating to constrain the absolute timing of thrust faulting. Radiometric dating has been used to constrain the age of initiation of a thrust belt (Blythe et al., 1996) and the timing of individual thrust sheets by identifying ‘steps’ in the cooling age across thrust sheets (Theide et al, 2005; Malusa et al., 2005; Sobel et al, 2006; McQuarrie et al., 2005; Arne et al., 1997). Low closure-temperature thermochronometry can also constrain the amount of exhumation (Lin et al., 1998; Omar et al, 1994) and the style and geometry of thrust fault deformation (O’Sullivan and Wallace, 2002).

If a cooling age can be related to a closure-temperature depth, thermochronometry can potentially measure thrust-related exhumation rates. To convert a cooling age to exhumation or exhumation rate, it is common to assume a linear geotherm and a constant cooling rate (Omar et al., 1994; Spotila et al., 2004; Bullen et al., 2001, 2003; Ducea et al., 2003; Kirby et al., 2002). However, assuming a steady, linear geotherm and constant cooling rate to convert a thermochronometric age to an exhumation rate may not be appropriate in rapidly exhuming thrust belts where exhumation vertically advects heat, perturbing the geotherm (Brown and Summerfield, 1997; Moore and England, 2001).

Thrust faulting perturbs the temperature field by footwall cooling, hanging wall heating, and thrust-driven exhumation that upwardly advects heat and changes the depth to a closure isotherm. Solving the one-dimensional heat advection-diffusion equation either numerically (Zeitler, 1985, Parrish, 1982; 1985, Safran, 2003, Mancktelow and Graseman, 1997, House et al. 2002) or analytically (e.g., Moore & England, 2001, Braun, 2002, Stuwe, 1994), demonstrates the thermal effects of exhumation and has been used to interpret thermochronometric data in many tectonic settings. Initial investigations of the one-dimensional thermal response to thrust faulting typically assumed material in the hanging wall is placed instantaneously over material in the footwall (e.g., Brewar, 1981; England & Thompson, 1984; Oxburgh and Turcott, 1974; Mailhe et al, 1986; Davy and Gillet, 1986) producing a ‘saw-tooth’ or inverted geotherm immediately following thrust faulting. Subsequent diffusion relaxed this inversion, heating the footwall and cooling the

hanging wall of the fault, although the importance of this diffusive process remains debated.

Faulting and fault-related folding are two- or three-dimensional processes which are not captured in one-dimensional models. Two-dimensional temperature effects of thrust faulting have been explored using two-dimensional kinematic patterns ranging from a single dipping fault with material moving parallel to the fault (e.g., Molnar and England, 1990; Karabinos and Ketcham, 1988; Ruppel and Hodges, 1994), to more sophisticated flat-ramp-flat fault geometries (Shi and Wang, 1987; ter Voorde, 2004; Huerta and Rodgers, 2006). Two-dimensional thrust-fault models produce temperature patterns that differ from the predictions of one-dimensional thrust fault thermal models. For example, two-dimensional models do not produce the inverted geotherms seen in one-dimensional models, except under extreme rates of fault slip.

Shi and Wang (1987), Ter Voorde (2004) and Huerta and Rodgers (2006) use results of their 2-dimensional thermal models to interpret thermochronological data in material exhumed by thrust faulting using different erosion models and assuming constant thermochronometer closure temperatures. Shi and Wang (1987) model the temperature in response to an individual thrust fault and fault-bend-fold followed by erosion. Huerta and Rodgers (2006) use a synchronous thrust fault and erosion model to predict apatite fission track cooling age patterns above a thrust fault and fault-bend-fold. Ter Voorde (2004) present a thermal-kinematic model and cooling histories of material in the footwall and hanging wall of a fault with a ramp-flat-ramp geometry and above multiple thrust faults to investigate effects of erosion following or occurring synchronously with faulting.

These thermal studies demonstrate that two-dimensional heat conduction and the two-dimensionality of the rock kinematics during thrust faulting influence cooling histories and thermochronometric ages in fold-and-thrust belts. These studies have focused primarily on the thermal history of a single thrust sheet. Still lacking is a systematic study of the patterns of low-T thermochronometric ages across a fold-and-thrust belt encompassing a complex series of faults, and consideration of how these

patterns change with fault geometry and thrust rate. In this paper, we present a study of the patterns of thermochronometric ages generated by material exhumed by thrust fault and fault-related folds. We use a linked thermal-kinematic-thermochronometric model to generate cooling ages above thrust faults and fault-related-folds and present these modeled thermochronometric age patterns for individual and multiple thrust faults. We include the current thermochronometric models for fission track annealing and He diffusion in apatite to precisely predict low-temperature thermochronometers. Our results can be used to help interpret thermochronometric data in thrust belts and to address fundamental questions such as the length of time each fault is active, the amount and rate of exhumation, and the role of ‘out-of-sequence’ thrusting.

### **2.3 Modeling Approach**

We apply a model that couples 2-dimensional kinematic-structural and 2-dimensional advection-diffusion thermal models, linked to a ‘state-of-the-art’ model of fission track annealing and He retention to predict low-T thermochronometric ages. The kinematic model allows representation of diverse styles of deformation in a fold-and-thrust belt. We use the deformation kinematics to advect heat in a finite-element, advection-diffusion thermal model thus tracking the thermal response to the faulting and fault-related folding to generate cooling histories and predict thermochronometric ages.

#### *2.3.1 Fold-and-Thrust-belts and the Kinematic Model*

Classic examples of fold-and-thrust belts include the North Sevier thrust belt, the Valley and Ridge province of the Appalachians, the Himalayan thrust belt, the Jura Mountains and the Western foothills of Taiwan (Chapple, 1976, Dahlstrom, 1990, Nemcock et al., 2005). Thrust belts are characterized by a sequence of reverse and thrust faults and associated folds overlying a shallow-dipping detachment surface (Fig. 1A). A variety of kinematic models have been proposed to describe deformation in a thrust belt. One kinematic model that is widely applied is Suppe’s fault-bend-fold geometric model

(Suppe and Namson, 1979, Suppe, 1980a, Fig 1). In this model, bedding folds at a kink above a change in the fault dip as faults step up from a basal décollement to a footwall ramp and again to a top flat (Fig. 1B).

To simulate the Suppe fault-bend-fold style of deformation, we use the fault-parallel flow algorithm in the kinematic structural geology software package 2DMove (Midland Valley Ltd). The fault parallel flow algorithm assumes particle flow is parallel to the fault and deformation occurs discretely by flexural slip. All material in the hanging wall of the fault moves parallel to the fault and all material in the footwall remains undeformed. Bed area and length is conserved and beds thin along the forelimb of the anticline. The output from this kinematic model is a grid of material points tracked through the fault-bend-fold deformation. The algorithm produces folds which are geometrically equivalent to Suppe-style fault-bend-folds (Figure 2.1, Suppe, 1983).

The complex rock motion and kinematic paths implicit to these kinematic fault-related fold models imply two-dimensional, time-dependent heat transfer that we approximate with a two-dimensional thermal model.

### 2.3.2 Thermal Model

In a fold-and-thrust belt, the temperature of the crust is controlled by the thermal properties of the crust and the heat flux at the base of the crust, and by heat advection as material in the hanging wall moves over the footwall and nearer the earths surface. These thermal mechanisms are described by the two-dimensional advection diffusion heat flow equation (1) that we use to numerically model the temperature structure of the crust deformed by thrust faulting and fault-bend-folding.

$$\frac{dT}{dt} = \frac{\nabla(k\nabla T)}{\rho c} - v\nabla T + \frac{A}{\rho c} \quad (1)$$

where  $T$  is the temperature,  $v$  is velocity,  $k$  is the thermal conductivity,  $\rho$  the density,  $c$  the specific heat,  $A$  is the heat production and  $t$  is time. Equation 1 is solved for the temperature field over an Eulerian mesh with nodes spaced < 400 m apart using a finite element method based on 3-node triangular elements with linear basis functions and an



fully implicit time stepping scheme. The advection term for each element in the Eulerian thermal mesh is obtained by spatially linking the thermal model and kinematic model. A Lagrangian mesh is constructed over a grid of points that are deformed by thrust faulting and fault-bend-folding using the 2dMove fault parallel flow algorithm described above. At each time step, each node in the Eulerian thermal mesh is assigned a velocity determined from the Lagrangian element in which it is contained. If the Lagrangian element has been folded by thrust deformation, the Eulerian node is assigned the velocity of the closest Lagrangian node. This same interpolation technique is used to derive the temperature for each node in the kinematic Lagrangian mesh.

The thermal model boundary conditions are a constant surface temperature (0 °C), a constant flux at 30 km depth ( $0.05 \text{ W/m}^2$ ) and no-flux boundary conditions at the sides (Table 1). There is no radiogenic heat production in the models presented in this paper. Initial condition is a steady state geotherm for the prescribed boundary conditions with no advection.

At each time step ( $<0.1 \text{ Ma}$ ) the model predicts the temperature of each node in the thermal mesh and the temperature of each node in the Lagrangian mesh. In this way, we obtain the modeled temperature of the crust through time and the temperature history of each point in the deforming Lagrangian mesh which can be used to calculate a thermochronometric age.

### *2.3.3 Thermochronometric Model*

Thermochronometric ages are a function of the path taken by exhumed particles as they pass through the temperature field. Material will not, in general, experience constant exhumation or cooling rates and thus thermochronometric ages are best calculated by integrating the temperature history through a thermochronologic kinetic model of radiogenic daughter product loss. We model the low temperature radiometric systems of interest in this study; zircon fission track, apatite fission track, and (U-Th)/He in apatite. For fission track dating of apatite, the closure temperature is approximately 110-125°C, depending on cooling rate, but the partial annealing zone (PAZ) where tracks

significantly anneal at Ma-timescales is between 60°C and 100°C (Donelick et al., 2005). For zircon fission track dating, the partial annealing zone is between 160 and 350°C at Ma-timescales (Tagami and O'Sullivan, 2005). (U-Th)/He in apatite has a closure temperature of around 70°, although <sup>4</sup>He continues to diffuse from apatite at temperatures as low as ~ 40°C (Farley et al., 1996, 2002; Wolf et al., 1996). These temperature ranges define partial annealing or retention spatial zones separating the regions of total decay product retention and total decay product loss. The exact temperature of these zones are not constant but change with cooling rate and chemical composition of the grain. Given the variable cooling rates and complex cooling histories of material in thrust belts, using a single closure temperature to define an age is simplistic. In a model where we have complete knowledge of the temperature history, it is more appropriate to use a full model of daughter product loss. We predict thermochronometric ages using the temperature histories derived from the linked thermal-kinematic model to calculate apatite (U-Th)/He, apatite fission track, and zircon fission track thermochronometric age (Fuller et al., 2006). To predict thermochronometric age, fission track annealing in apatite is calculated using a modification of the approach of Ketcham et al. (1999) who used the fanning Arrhenius model of Laslett et al. (1987), and the spherical diffusion of Helium in apatite is calculated using the technique of Ehlers et al. (2001; 2003). The algorithms used in the thermochronometric model thus do not explicitly include partial annealing and retention zones, but include a more precise representation of the influence of the cooling rate, and, in fact, the complete temperature history on age.

## 2.4 Modeling Results

We use our linked modeling approach to investigate apatite fission track and apatite (U-Th)/He thermochronometric age patterns in response to a variety of fault geometries and fault slip rates. We explore the different thermochronometric age patterns that result from varying slip rate, depth to décollement, and thrust ramp angle, and contrast our model results to 1d and steady state solutions. We then extend our model to calculate thermochronometric age for material exhumed by multiple thrust faults.

In this study, we assume a completely efficient erosion model such that all topography is removed instantaneously. Once material reaches the model surface, it is removed. Using this approach, no topography is generated. In the other end-member model, there is no erosion so uplift-generated topography exactly mimics the integrated amount of rock uplift. In the no-erosion end-member model exhumation occurs only if erosion is applied following deformation (e.g., Shi and Wang, 1987; ter Voorde et al., 2004). Huerta and Rodgers (2006) assume an erosion model based on surface process laws which occurs synchronously and postdates thrust faulting. We focus here on the first end-member model, where erosion equals rock uplift, thereby concentrating on thrust-driven exhumation. This case is more appropriate for thrust belts in which structural relief is large compared to topography (e.g., Taiwan fold-and-thrust belt).

#### **2.4.1 Thermochronometric Age and Temperature Structure of Fault-Bend-Folding**

##### *i) General Pattern of thermochronometric Age above a Thrust Fault and Fault-bend-fold*

In fault-bend-folding, a column of rock is moved horizontally above the bottom flat before being exhumed above the thrust ramp. The shallow particle paths of thin-skinned deformation limits the amount of material that is exhumed from beneath the closure temperature zone. The limited depth of exhumation means much material exhumed by fault-bend-folding records a thermochronometric age inherited from a previous regime (unreset) or a partially reset age intermediate between an inherited age and a young cooling age. The patterns of the thrust-cooling ages, partially reset ages, and inherited ages form a U-shaped thermochronometric age pattern that is characteristic of all fault-bend-folds modeled in this study (Figure 2.2). An inherited age can not be used to interpret thrust fault exhumation rates, but does constrain exhumation to be less than the depth to the closure temperature zone. Material that is above the closure temperature zone when it resides above the bottom flat retains its inherited age (unreset) and material exhumed from the partial closure zone (partially reset) records an intermediate age (Figure 2.2). As faulting continues, material is continually advected laterally and exhumed from above and within the partial annealing/retention zones. Fully reset

material that records thrust faulting is exhumed from beneath the partial annealing/retention zones by vertical motion that only occurs above the thrust ramp.

The deepest material exhumed is in the hanging wall immediately next to the ramp and has the greatest chance of recording a reset thrust-cooling age rather than an inherited age. There is a zone of consistently young thrust-cooling ages that form the flat base of the ‘U-shaped’ thermochronometric age pattern. We call this zone with the same young cooling ages located above the thrust ramp the ‘ramp-reset zone’. The ramp-reset zone is wider for lower closure-temperature thermochronometers. In model FBF0 (Table 2) the apatite (U-Th)/He ramp-reset zone is 25 km wide compared with the 15 km wide apatite fission track ramp-reset zone (Figure 2.2).

In the *2D Move* fault-parallel-flow model, the region of vertical uplift is defined by the dip bisectors (Figure 2.2D) so material directly above the ramp tip is advected horizontally and not vertically in its most recent history. Therefore, the very youngest ages are not found immediately above the top of the fault ramp but are slightly offset toward the hinterland.

As slip continues, the ramp-reset zone widens toward the foreland as reset material is carried horizontally above the top flat. Thrust initiation is recorded by the material in the foreland furthest from the thrust ramp. At the edge of the ramp reset zone, this oldest fission track cooling age is slightly (0.2 Ma) younger than thrust initiation because material is at first isothermally advected. The oldest (U-Th)/He cooling age almost exactly equals thrust initiation because the lower closure temperatures recorded by (U-Th)/He in apatite respond to exhumation rapidly. For the fault geometries and amount of slip presented, thrust initiation is not recorded behind the top of the ramp (i.e. toward the hinterland).

Huerta & Rodgers (2006) note that, if preserved, the widening of the reset zone above the top flat can be used to calculate horizontal slip rate by dividing the distance from the top of the ramp by the cooling age. Initially, before 2 Ma, the reset zone widens slightly toward the hinterland until material which passed through the critical closure isotherms at their thermal steady state, reaches the surface. This is a type of local or

spatially-limited exhumational steady state (Willett and Brandon, 2002). Once this exhumational steady state is reached (in FBF0 at approximately 3 Ma for apatite fission track and by approximately 1 Ma for (U-Th)/He in apatite) the location of the change from reset to unreset ages in the hinterland remains fixed (Figure 2.2 A-C). Toward the foreland, the transition between reset and unreset ages never reaches a fixed position, so this system never reaches a full exhumational steady-state.

*ii) Temperature Structure of fault bend folding*

Faulting and fault-bend-folding advects the critical closure isotherms upwards above the fault ramp (Figure 2.2E). The maximum perturbation occurs approximately above the center of the thrust ramp and decays in both directions from this maxima. For fault geometry FBF0, the low temperature isotherms are perturbed by thrust-driven advection over a 30 km wide zone.

Material in the footwall immediately adjacent to the fault experiences footwall heating, but this is a small effect limited to a distance of less than 10 km from the fault and becomes almost insignificant more than ~5 km from the fault. Beneath the basal décollement or footwall flat the temperature field is virtually undisturbed by faulting.

The low-temperature isotherms reach a steady position at around 2 Ma and the most rapid shallowing of the isotherms occurs in the first 1 Ma (Figure 3). We use a flux boundary condition at the base of our thermal model, but because advection occurs above the décollement, using a thermal bottom boundary condition produces identical results.

*iii) 1D models vs 2D fault-bend-fold models*

In a 1d advection-diffusion model, advection is assumed to be constant over an infinitely wide region. This 1d advection pattern is in contrast to thrust fault kinematics where uplift and thus heat advection varies vertically and laterally. In the case of fault-bend-folding, vertical uplift is limited to the area above the ramp, and in the case of fault-propagation folding, vertical uplift is limited to the area above a growing fault-tip (Suppe and Meddweff, 1990). The limited vertical and lateral extent of vertical heat advection

in the fault-bend-fold model causes the isotherms to be perturbed over a similarly narrow zone centered above the thrust ramp resulting in lateral temperature gradients and horizontal heat flow. This average depth to a specific isotherm is deeper in the thrust fault model than in the 1d model. Initially, the difference between the depth to the low-temperature isotherms in the 1d and fault-bend-folding model is small, and the difference between the youngest cooling ages between the two models is small. The difference between the depth to the closure isotherms in the 1d and fault-bend-fold models increases with time and with vertical advection rate (table 3, figure 3). For example, after 2 Ma of exhumation at fault-parallel slip rates of 4 mm/yr or less, the depth to the 100° C isotherm in the fault-bend-fold model is closer to the 1d steady state solution with no advection (the initial geotherm) than to the steady state solution with advection. Thus, although ignoring heat advection can lead to an overestimate of the rate and amount of exhumation (Mancktelow and Grassman, 1997, Brown and Summerfield, 1997), assuming a 1d model to interpret the temperature effects of thrusting in a fold-and-thrust belt, may lead instead to an underestimate of the true advection rate.

The different temperature fields in the 1d and 2d models and the 2d kinematics of fault-bend-folding produce different thermochronometric age patterns. For the time and rates shown here, there is little difference between the youngest cooling ages in the ramp-reset zone in the fault-bend-fold and the ages in the 1d model in the first 2 Ma (Figure 2.2A & B). The 1d model approximates the youngest cooling ages above the ramp in the thrust fault model before 2 Ma because material cooled through the closure isotherms at the beginning of the model run when the difference between the 1d and 2d models is small. The cooling age difference between the 1-d and ramp-reset zone in the thrust fault models increases with time because the difference between the depth to the closure isotherm between the models increases with time (Figure 2.2E). The 1-d models do not predict the variable spatial pattern of ages outside of the center of the ramp-reset zone.

The most rapid changes in the temperature field in the fault-bend-fold model occur during the first million years of faulting and most models reach a nearly steady temperature field within 2 Ma. The rapid approach of the shallow isotherms to a thermal

steady state in the fault-bend-fold model (figure 3) is a feature common to the 2d thrust fault and 1d models at the  $> 1$  mm/yr rates typical of fold-and-thrust belts. Exhumational steady state measured by the thermochronometers lags the thermal steady state.

## 2.4.2 Fault-Bend-Folding Parameter Sensitivity

### *i) Sensitivity to basal décollement depth.*

With a deeper décollement, material is exhumed from greater depths and higher temperatures, more material (and heat) is advected, and the closure isotherms are more significantly perturbed. Shallower deformation in fold-and-thrust belts causes less vertical advection and, all else being equal, isotherms remain deeper than for faulting that extends into the deeper crust. In models with a 15 km deep décollement (FBF0, Table 2), after 2 Ma the 100° isotherm is  $> 0.5$  km deeper than an equivalently wide block advecting at the same rate but with no basal flat (model BW17, table 2, Figure 4). With a shallower basal décollement, the closure isotherms deepen. For example, in the model with a 10 km décollement depth (FBF4), the 100° isotherm is  $\sim 0.7$  km shallower than in the model with a 15 km décollement depth (FBF1) (Figure 4).

For the rates and time shown here (2 Ma run time, slip rate 8 mm/yr) the variations in décollement depth and the resultant temperature field cause only slight differences in the youngest cooling age (the youngest cooling age is approximately 1.2 Ma for apatite fission track and 0.7 Ma for (U-Th)/He, figure 4). However, there are large changes in the spatial distribution of ages. For the same ramp dip and upper flat depth, the ramp-reset zone is wider with a deeper décollement, and higher temperature thermochronometers are reset (figure 4). When the décollement depth is specified at 10 km (FBF4) apatite fission track ages are unreset and remain unreset even as faulting continues. With the décollement at 15 km depth, material with reset apatite fission track ages is exhumed after  $\sim 1.25$  Ma.

*ii) Sensitivity to fault dip*

The dip of the thrust ramp affects the distribution and amount of material exhumed and the path material takes to the surface. We investigate the variation in predicted thermochronometric age with thrust ramp dip ranging from a 30° ramp dip (FBF1) to a steeply dipping 60° fault ramp (FBF3)(figure 5). For a constant décollement depth and rate of vertical exhumation, as the dip of the fault ramp decreases, the amount of material exhumed increases and material is exhumed over a wider zone. Thus, less dip to the ramp results in shallower isotherms perturbed over a wider zone.

As the ramp dip decreases, the ramp-reset zone increases in width (Figure 5). This is mostly an artifact of the model, in that we hold the vertical component of velocity constant between models in order to hold the vertical heat advection constant thus the horizontal component of velocity must increase as the fault dip decreases. The greater horizontal advection results in the greater translation of reset ages towards the foreland. The zone of reset ages also widens toward the hinterland as the ramp dip decreases because material is exhumed over a wider zone.

The value of the youngest reset ages predicted in the ramp-reset zone is insensitive to fault dip. The shallower closure isotherms in the 30°-ramp model cause the ages in the ramp-reset zone to be slightly younger than ages recorded by material exhumed above the more steeply dipping faults, but this variation is less than 20%.

*iii) Sensitivity to fault slip rate.*

Fault slip rate dictates the exhumation rate and thus is the most direct control on thermochronometric age. In addition, fault slip rate affects the rate of heat advection, so that age dependence is non-linearly dependent on fault slip rate. With increasing fault slip rate and advection rate, the depth to the closure isotherm decreases (Figure 6). Therefore as the fault slip rate increases, younger modeled ages reflect the decreased depth to the closure temperature and the increased rate of exhumation. Figure 6 shows the pattern of thermochronometric age for faults with slip rates ranging from 2-8 mm/yr and 16 km total slip. For a 30° thrust ramp, this is a 1-4 mm/yr exhumation rate. We hold the total



thrust displacement constant so the total time of modeled fault motion varies from 16-2 Ma.

At exactly half the slip rate, cooling ages are more than twice as old even though material travels to the surface in exactly twice the time, reflecting the non-linear dependence discussed above. The width of the ramp-reset zone is wider with faster advection rates because the increased advection has a larger lateral heating effect.

For all models shown in figure 6 (slip rates of 2 – 8 mm/yr), the minimum depth to the 100° isotherm is more than 1 km deeper in the thrust fault model than the equivalent 1d transient and steady state solutions (Table 3).

#### *iv) Emergent Fault Ramp*

Models shown thus far focus on fault-bend-folds in which the thrust fault never reaches the surface. However, emergent thrust faults where the thrust ramp reaches the surface exist in many fold-and-thrust belts, particularly as ‘out of sequence’ thrusts (thrusts that are active behind the deformation front and crosscut existing structures). If a fault ramp reaches the surface, there is no top flat and thus no horizontal translation above the ramp.

Figure 7 shows model results for two fault configurations that are identical except that the ramp reaches the surface in one model (EFR) and in the other becomes horizontal and remains beneath the surface (FBF0). The thermal response to these two kinematic patterns are almost identical. The only temperature difference is that the coolest (< 75°) isotherms are perturbed over a slightly wider area in the emergent thrust case.

Despite the almost identical temperature response between a flat-ramp-flat thrust (FBF0) and a thrust ramp that reaches the surface (EFR), these two different fault geometries produce distinct differences in the pattern of predicted thermochronometric age. The youngest cooling ages in the ramp-reset zone are the same for both models, reflecting the same exhumation rate and similar temperature fields. The difference in age distribution occurs above the top-flat. When the thrust ramp reaches the surface (Model EFR), predicted age changes abruptly across the fault from a thrust-cooling age to an

inherited age (Figure 7A). The abrupt change in modeled age from unreset to fully reset contrasts with the smooth progression from reset to partially reset to unreset age for a fault-bend-fold. The abrupt age change in the emergent thrust model evolves to a steady pattern. A steady-state age pattern is never reached in the fault-bend-fold model because the zone of reset ages widens indefinitely toward the foreland above the top flat (Figures 8B&C). In the emergent thrust model, material is not preserved above a top flat, thus thermochronometric ages do not record thrust initiation.

In the emergent thrust fault model, the youngest ages in the hanging wall do not occur immediately adjacent to the fault where rocks are exhumed from the greatest depths, but are offset slightly toward the hinterland. This offset occurs because the minimum depth to the closure temperature is not immediately adjacent to the fault, but is offset by cooling of the hanging wall by the footwall.

### **2.4.3 Propagating Thrust Faults**

We have discussed thermochronologic ages in material exhumed by an individual fault, but thrust faults often occur in fold-and-thrust belts made up of multiple thrust faults. Thrust faults in a fold-and-thrust belt generally propagate sequentially toward the foreland as convergence continues and material in the foreland basin is subsumed by the thrust belt. Although the initiation of new faults tends to progress towards the foreland, it is not necessary that more-interior thrusts stop moving as new faults develop. In addition, there are out-of-sequence faults that post-date and cross-cut earlier faults in the thrust-belt interior. Thermochronometric ages have the potential to document the sequence of thrust activation, longevity, and rate, provided the exhumational and thermal history of individual faults can be resolved. In many fold-and-thrust belts, for example, the Western Foothills fold-and-thrust belt in Taiwan (Suppe, 1980a), the Sevier thrust belt (DeCelles and Mitra, 1995), and the Brooks Range of Alaska (O'Sullivan et al., 1995), more-hinterlandward thrusts and material in the hanging wall of more-hinterlandward thrusts are deformed and exhumed by fault activity in the foreland, complicating the relationship between a cooling age, thrust slip rate, and fault propagation. Material in the hanging

wall of one thrust has the potential to record exhumation due to uplift on a ramp associated with another thrust, a process we examine here.

To investigate the thermochronometric age patterns in fold-and-thrust belts, we model a sequence of foreland propagating faults and fault-bend-folds with different fault spacing. In each case, faults dip at  $30^\circ$  and are activated sequentially from the hinterland to the foreland creating a duplex (McClay, 1992). Each fault is active for 1.2 Ma, and slips at 10 mm/yr (corresponding to a vertical rate of 5 mm/yr) producing 12 km of displacement across each fault and a total model time of 4.8 Ma. Once a new fault activates, the old fault is deactivated.

*i) 50 km fault spacing*

When the faults are spaced 50 km apart, each fault is independent of the others and material in the hanging wall of one fault is not deformed by other faults (Figure 8). This geometry is referred to as an independent ramp anticline (Mitra, 1986) and, provided the assumptions made above hold, the analysis of the preceding sections applies. The thermochronometric age pattern within each thrust sheet records slip solely along one thrust and shows the same U-shaped thermochronometric age pattern as in the single fault models (e.g., Fig. 4) repeated above each thrust ramp. The initiation and exhumation rate of each thrust is recorded by thermochronometric cooling ages in its hanging wall, with the foreland progressing sequence of faulting reflected in the progressively younger thermochronometric ages.

*ii) 20 km fault spacing*

For the fault geometry and amount of slip used here, once the fault ramp spacing is less than 50 km, faults can no longer be treated independently of each other. Inactive faults toward the hinterland are deformed and exhumed as they move up the ramp of the other faults towards the foreland. The fault spacing, amount of slip, and fault configuration of model MULTI2 (Figure 9), generates a foreland sloping duplex (Mitra, 1986). With faults spaced at 20 km, despite exhumation along four independently moving faults, the pattern of predicted age is a single U-shape similar to rocks exhumed by an individual thrust (compare Fig. 2 & 9A). However, the explanation of this pattern is

somewhat different. With a single fault, the age gradient is the result of the transition from partially reset to fully reset ages. With closely-spaced, interacting faults, the gradual age decrease from unreset material in the hinterland to the youngest cooling ages reflects partial resetting, but also reflects exhumation associated with slip on the younger faults and motion up each associated ramp. Interestingly and importantly, our models show no distinct change or break in the thermochronometric age moving from the hangingwall to the footwall of a fault even when older thrust ramps are exhumed.

Some material experiences a relatively simple cooling history. Material in the hanging wall of the oldest fault (fault 1, Figure 2.10) records slip along the oldest fault and is not exhumed by slip along younger frontal thrusts (an example of this cooling history is shown by point F, Figure 2.10). Material in the hanging wall of the youngest fault, fault 4, records exhumation only in response to motion on fault 4 (points A & B, Figure 2.10). Thus these more simple example temperature histories record information to resolve motion on just these individual faults and can be interpreted simply (zone marked by black arrow, Figure 2.10A).

Material from the center of this fault series is exhumed by more than one fault and thus has a composite thermal history reflecting the timing of motion on multiple faults (points C, D & E, Figure 2.10, zone marked by grey arrow, Figure 2.10A). There are a variety of different cooling histories. Thermochronometers record cooling along a single fault; for example, fission track and (U-Th)/He ages for material-point E both record cooling by slip along fault 3. However, different thermochronometers can also record cooling along more than one fault; point D has a fission track age set during motion of fault 3 and a (U-Th)/He age set during motion of fault 2.

The sequential development of each thrust in the fold-and-thrust belt is recorded by a progressive age decrease from the oldest ages in the hinterland to the youngest ages in the foreland. The youngest ages (the flat 'base' of the U-shaped pattern) all record slip along the youngest thrust and can be interpreted fairly simply. For this fault geometry and spacing, the youngest ages are ~0.5 Ma for apatite (U-Th)/He and ~0.8 Ma for apatite

fission track and could be used to infer the correct vertical exhumation rate on the youngest fault.

Forelandward of the very youngest ages are a small set of slightly older cooling ages (at ~0 km in Figure 9). These ages are in material that has been horizontally translated above the active fault's top flat in its most recent history. This material records the initiation of the most recent fault. It is the only material that records early faulting that is located forelandward of the active thrust. All other material recording early faulting is located hinterlandward of the active thrust ramp. Thus, for this fault and slip rates, the spatial distribution of cooling histories means the modeled age pattern is still the same U-shape seen in the individual fault-bend-fold model, but 'skewed' toward the foreland.

Material is not exhumed and does not cool significantly during horizontal motion along the bottom flat in the hangingwall of an active thrust, or when it is in the footwall of the active thrust. A small amount of cooling can occur when material is located in the footwall immediately next to an active fault because it is heated by the adjacent hanging wall (e.g., Figure 2.10, Points B & C) or, similarly, if material is in the hanging wall of a thrust and moved horizontally into the region of perturbed isotherms (Figure 2.12, Point D); these both are relatively minor effects. It is not modeled here, but material would cool along the top and bottom décollements if the bottom or top 'flats' dip toward the hinterland.

### *iii) 10 km fault spacing*

When the faults are even more closely spaced, faults in the hinterland are greatly deformed by the younger foreland thrusts producing an antiformal stack (McClay, 1995). A 10-km fault spacing produces a thermochronometric age pattern that differs significantly from the models with a wider fault spacing. With a 10 km fault spacing (Figure 2.11, MULTI3, Table 2), the skewness of the U-shape pattern of thermochronometric ages is reversed compared to models with more widely spaced faults (compare Fig. 9 and Fig. 11). This spatial pattern occurs because material is at first exhumed through the closure temperature above the active fault ramp, then is

horizontally translated above the top flat until it is forelandward of the ramp of the next younger fault. Then, when the new fault is activated, the material that records exhumation by the older fault is not in the zone of exhumation above the new thrust ramp but is horizontally translated above the top flat of the younger fault without being exhumed and removed. Points A & B in Figure 2.12 illustrate this complex cooling history. With these cooling histories, material toward the hinterland records slip along foreland thrusts and material in the foreland records slip along hinterland thrusts.

As in the one-fault models, in the 10 km multiple fault model, the predicted cooling ages increase toward the foreland from the youngest ages at the flat base of the U-shape, to the ages that record the earliest faulting (Figure 2.11A). This age increase toward the foreland has been used by Huerta & Rodgers (2006) in their individual fault model and by Bollinger et al. (2004; 2006) to calculate the horizontal slip rate; the inverse of the age gradient is the horizontal shortening rate. However, in the multiple fault model, unlike the age increase above the top ramp in the individual fault models (e.g., Figure 2.2) the predicted age increase toward the foreland is not linear (Figure 2.13). The age increase records the horizontal fault slip rate, but it also records the rate that faults step into the foreland. The result is a non-linear age gradient that is steeper than the inverse of the shortening rate. Consequently, unless there is only one stationary thrust ramp, the inverse of the age gradient underestimates the rate of fault slip.

The width of the reset zone in the one fault model shown in Figure 2.13 is 30 km wider than the multiple fault model with the same fault-slip rate. 30 km is the total distance that the modeled thrust-ramp has migrated into the footwall since thrust initiation (MULTI3). Thrust initiation is recorded by the oldest cooling age (4.8 Ma in model MULTI3). Thus, if a fault slip rate is known, for example, using geomorphic or geodetic constraints, the rate of fault ramp migration can be determined using the oldest and youngest cooling ages and their spatial separation. In the absence of independent constraints on the fault slip, if the fault ramp geometry is known, identifying the flat base in a thermochronometric age pattern is a way of determining the vertical fault-slip rate (assuming our erosion end member model), and thermochronometric ages alone can

constrain the rate of fault slip and rate of fault ramp migration. For example, using the pattern of thermochronometric ages generated by the model MULTI3 (Figure 2.11), the rate of ramp migration, which is independent of the rate of fault slip, can be calculated as follows:

$$\text{Foreland age gradient} = \frac{\text{Distance between oldest cooling age and youngest cooling age}}{(\text{oldest cooling age} - \text{youngest cooling age})}$$

$$\text{Foreland age gradient} = \frac{10.3 \text{ km}}{(4.8 \text{ Ma} - 0.55 \text{ Ma})} = 2.4 \text{ km/Myr}$$

Rate of ramp migration ( $V_{\text{ramp}}$ ) = Horizontal velocity ( $V_x$ ) – Foreland age gradient

$$V_{\text{ramp}} = 6.25 \text{ Km/Myr, the model imposed ramp migration (30 km in 4.8 Ma)}$$

*iv) Fault Spacing, slip rate, and the patterns of thermochronometric age*

In all models, regardless of fault spacing (10-50 km, Figures 8-12), the oldest cooling age is approximately (within 0.2 Ma) the time the thrust belt became active. This record of fault initiation is in the hinterland of the thrust belt when faults are spaced 20 km and 50 km apart, but in the foreland of the thrust belt when faults are spaced 10 km apart. Therefore, unless exhumation removes all the material that records slip on the oldest fault, the oldest cooling age records the initiation of the thrusts in a fold-and-thrust belt, but the location of this information may be quite different.

The skewness of the U-shaped age patterns generated by the models with differing fault spacing is a function of the initial fault spacing, the final fault spacing, the total slip, the depth to the partial retention zone for the thermochronometric system of interest, the dip of the ramp, and the shape of the anticline described in the models here by the fault bisector.

**PATTERN 1. EARLIEST FAULTING RECORDED IN THE THRUST BELT FORELAND**

A foreland skewed U-shaped pattern of thermochronometric age occurs when the slip on the initial fault is great enough that it reaches the top flat of the younger fault, without being exhumed by slip along this younger thrust. This material must pass out of the zone of vertical exhumation above the ramp of the new thrust before it is removed (Point A, Figure 2.14). Given two faults with identical geometry, the fold kinematics

used in this study, and an idealized single closure temperature depth, for the earliest faulting to be recorded forelandward of a later fault, the minimum slip distance on the initial fault is approximately:

$$Slip_{fault1} \geq a + \left( \frac{D_{Tc} - 2D_{topflat}}{\sin \theta} \right) \quad \text{for } D_{topflat} < D_{Tc}$$

$$Slip_{fault1} \geq a + \left( \frac{D_{Tc}}{\sin \theta} \right) \quad \text{for } D_{topflat} > D_{Tc}$$

where  $a$  is fault spacing,  $D_{topflat}$  is the depth to the top flat,  $D_{Tc}$  is the depth to the closure temperature,  $\theta$  is the dip of the fault ramp, and  $Slip_{fault1}$  is the slip along the initial fault (Figure 2.14).

Holding all other parameters constant, if slip on the older fault is not enough to satisfy the above inequality, material is exhumed above the ramp of the younger fault before it reaches the top flat of the younger fault and older faults are not recorded in the foreland.

PATTERN 2. EARLIEST FAULTING RECORDED IN THE HANGINGWALL OF A YOUNGER FAULT (E.G., MODELS WITH A 20 & 50 KM FAULT SPACING, FIGS. 8, 9)

To preserve material that records earlier faulting in the hangingwall of a younger fault, if the two faults have the same geometry, the slip on the younger fault must respect the condition that:

$$Slip_{fault2} < a + \frac{D_{Tc}}{\sin \theta}$$

Where  $Slip_{fault2}$  is the amount of slip along the younger fault. If this condition is not met, the most hinterlandward material that records older fault slip is not preserved. The most hinterland material that records slip on the older fault is the intersection between the bottom bisector and the depth to the closure temperature at the end of slip along the older fault (Point B, Figure 2.13).

v) *Higher Temperature Thermochronometers.*

Antiformal stacks like the structure produced in the 10-km fault-spacing model, can exhume material from greater depths than can be achieved by single or widely spaced thrust faults. Thus, unlike the models with a wider fault-spacing, the 10-km fault-spaced



model exhumes material from the depth to the bottom flat to expose reset zircon fission track ages. Slip across any individual fault with the parameters of this study is not great enough to exhume material with reset zircon fission track ages, but the combined slip along multiple faults exhumes material with reset zircon fission track ages (e.g., points E, Figure 2.12). In this 10 km fault-spacing model, Point E (Figure 2.12) has cooled almost constantly above the ramp of each fault. Thus, the zircon fission track age of this material, which is located behind the active frontal thrust, has been exhumed and cooled at the slip rate of the active frontal thrust and the cooling rate determined from these zircon thermochronometric age can be compared to short-term rates (e.g., river terraces) measured at the frontal thrust.

*vi) Age-Elevation Relationships in fold-and-thrust belts.*

Age-elevation relationships are commonly used to interpret exhumation rates by assuming that material at high elevations passed through the closure isotherms before material at low elevations and that all material passes vertically through the closure temperature at the same rate. Although theoretically, samples for age-elevation transects are thought of as being collected along a vertical transect this is impossible and in reality these transects are horizontally distributed. Therefore, in a fold-and-thrust belt, an age elevation transect might record the sequential activation of thrusts in addition to any change in elevation. For example, the thermochronometric ages generated in the model with a 20 km fault-spacing (MULTI2), show an age increase from the foreland to the hinterland of approximately 1.8 Ma over only 10 km. Such an age increase from the foreland to the hinterland records the sequential fault activation and would complicate the interpretation of an age-elevation relationship.

## **2.5 Conclusions**

The distribution of the predicted low-T thermochronometric ages is a ‘U-shaped’ pattern with reset ages in the center, surrounded by partially-reset, and unreset ages. This

pattern is characteristic of the individual fault-bend folds, and the multiple fault duplexes and antiformal stacks that we investigated in this study.

Material with the youngest reset cooling ages is located above the thrust ramp as part of the ‘ramp-reset-zone’ to form the flat base of the U-shaped pattern of predicted age. With a constant rate of fault slip, the material with the youngest ages is cooled at a near-constant rate after passing through the closure temperature. This steady cooling rate permits almost direct correspondence between age and the vertical exhumation rate along an individual fault. Thus, identifying the youngest ages comprising the flat ‘base’ of the cooling age pattern permits direct comparison between thermochronometric ages and modern geomorphic and geodetic estimates of deformation and exhumation.

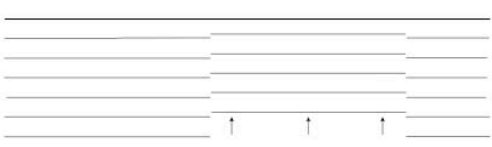
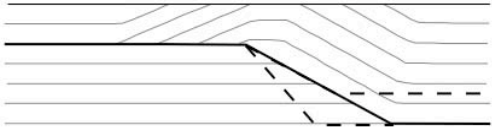
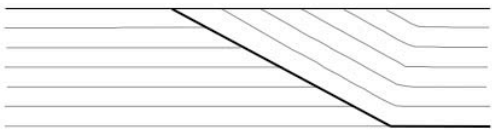
The youngest cooling ages are most sensitive to fault slip rate and fairly insensitive to individual fault geometry. However, when there are multiple thrust faults, the geometry and the amount of slip along each fault has a large impact on the predicted thermochronometric age pattern. The simple interpretation that material in the hanging wall of a fault records slip along that same fault is not generally valid. Typically, faults are closely spaced so that material exhumed in the hangingwall of a fault in the hinterland is also deformed and exhumed by faults in the foreland. Because material is exhumed by multiple faults, predicted cooling ages do not show a step change across each fault and material in the hanging wall of one fault may record slip along a younger fault. Thus, it may be incorrect to use thermochronometric ages in the hanging wall of any individual fault to infer motion along that fault.

In single fault models, material in the ramp-reset zone is horizontally transported without additional exhumation along a top flat, thus preserving the age of thrust initiation. In our multiple fault models, the age of thrust belt initiation is preserved, but, depending on the fault spacing, slip rate, and thermochronometric system, this can be recorded in either the front or the rear of the thrust belt.

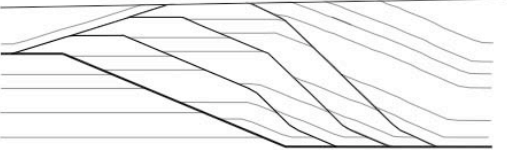
**Table 2.1** Thermal Model Parameters.

<b>Model Parameter</b>	<b>Value</b>
Specific heat	1000 J kg <sup>-1</sup> K <sup>-1</sup>
Thermal conductivity	2.5 Wm <sup>-1</sup> K <sup>-1</sup>
Radioactive Heat Production	0 W/m <sup>2</sup>
Upper Boundary Condition	0 °C
Rock density	2500 (kg/m <sup>3</sup> )
Lower Boundary Condition	0.05 W/m <sup>2</sup>
Model Depth	30 km
Model Width	100 km

**Table 2.2** Model geometries and kinematics

<b>Kinematic Model</b>		<b>Run Time</b>	<b>Parameters Investigated</b>	<b>Model Parameter</b>				<b>Model Name</b>				
		2 Ma	Block Width	17.5				BW17.5				
		2 Ma		20				BW20				
		2 Ma						1D				
<b>Fault-bend Fold FBF</b> 		2 Ma	Fault Ramp Dip Figure 6	Ramp Dip	Depth to Base Flat	Slip rate mm/yr	Vertical Slip rate					
								30°	15	8	4	FBF 0
								30°	15	11.3	5.66	FBF 1
								45°	15	8	5.66	FBF 2
		2 Ma	2 Ma	Depth to base flat Figure 7	30°	15	8	4				
		2 Ma	2 Ma						60°	15	6.5	5.66
		2 Ma	16 Ma	Fault parallel slip rate Figure 8	30°	15	10	8	4			
		16 Ma	8 Ma						1	0.5	FBF 5	
		8 Ma	4 Ma						2	1	FBF 6	
		4 Ma	4 Ma						4	2	FBF 7	
	4.8	4.8		30	15	10	5	5	FBF 8			
<b>Emergent Fault Ramp EFR</b> 		2 Ma	Emergent ramp	30°	15	8	4	EFR				

**Table 2.2** Continued

Multiple faults & fault-bend-folds MULTI		4.8 Ma		Ramp Dip	Depth to base Flat	Slip rate (mm/yr)	Fault Spacing	
		4.8	Multiple faults	30	15	10	50	MULTI 1
		4.8		30	15	10	20	MULTI 2
		4.8		30	15	10	10	MULTI 3

**Table 2.3** Depth to the 100° isotherm for different fault slip rates after 2 Ma of faulting. Analytic solution is the 1d solution to the advection diffusion equation for the vertical advection rate, a surface temperature and flux bottom boundary conditions. The steady state solution is the 1d solution for surface and bottom temperature boundary conditions.

Rate (Fault parallel)	Vertical Rate	Depth to 100° isotherm		
		FBF Model	1d solution	Steady State
8 mm/yr	4 mm/yr	3.1 km	2 km	1.4 km
4 mm/yr	2 mm/yr	3.8 km	2.6 km	2.4 km
2 mm/yr	1 mm/yr	4.3 km	3.1 km	3.4 km
1 mm/yr	0.5 mm/yr	4.6 km	3.5 km	4.1 km

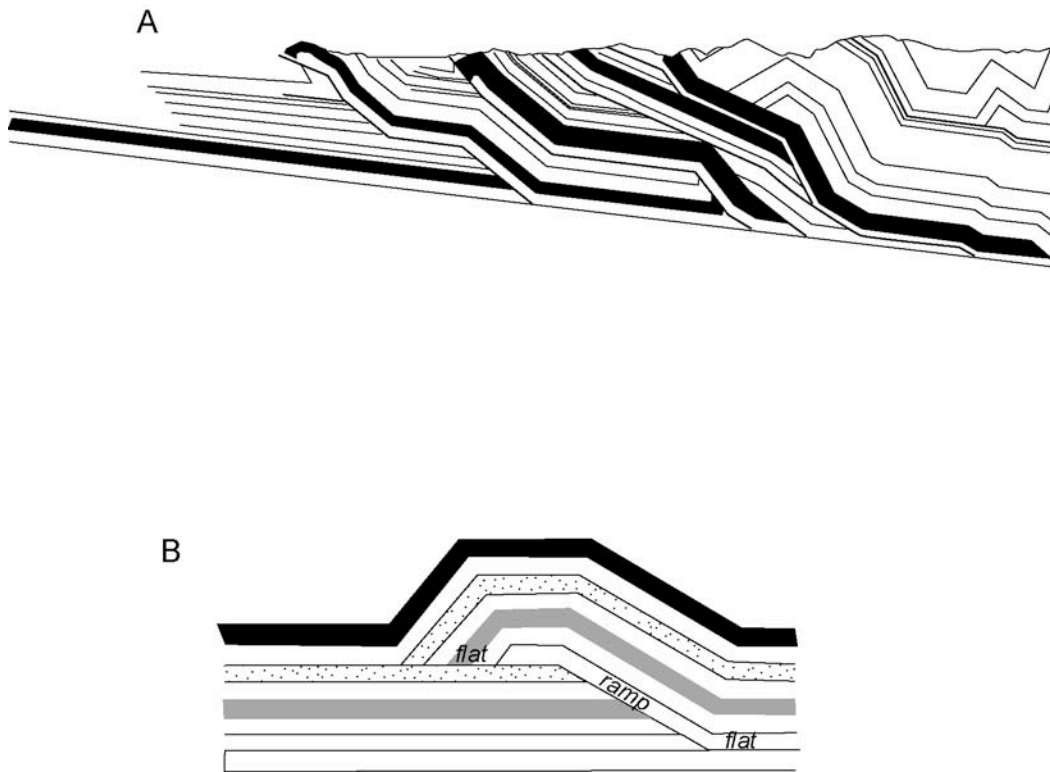


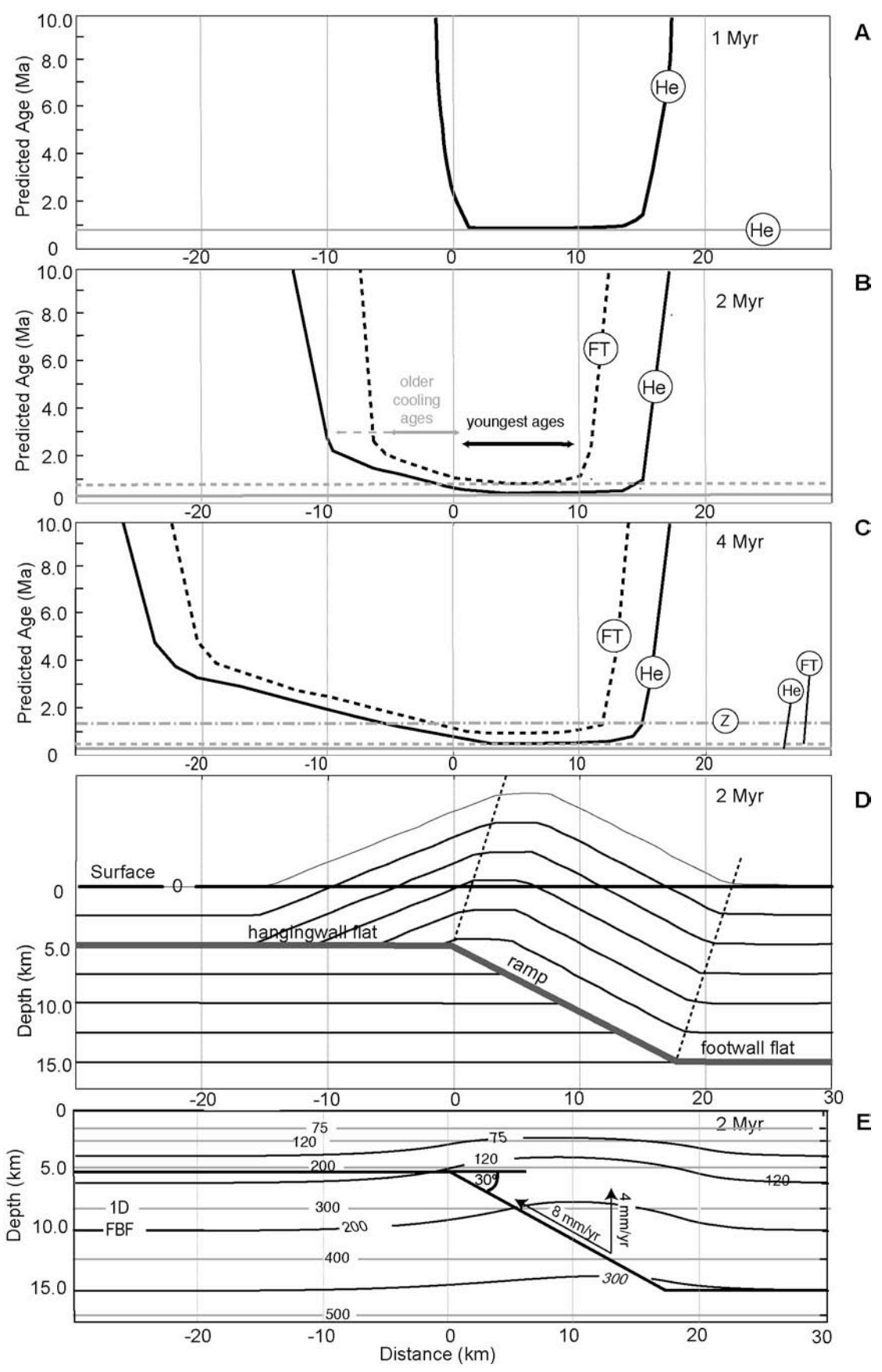
**Figure 2.1** Example Fold-and-thrust belt and fault-bend-fold.

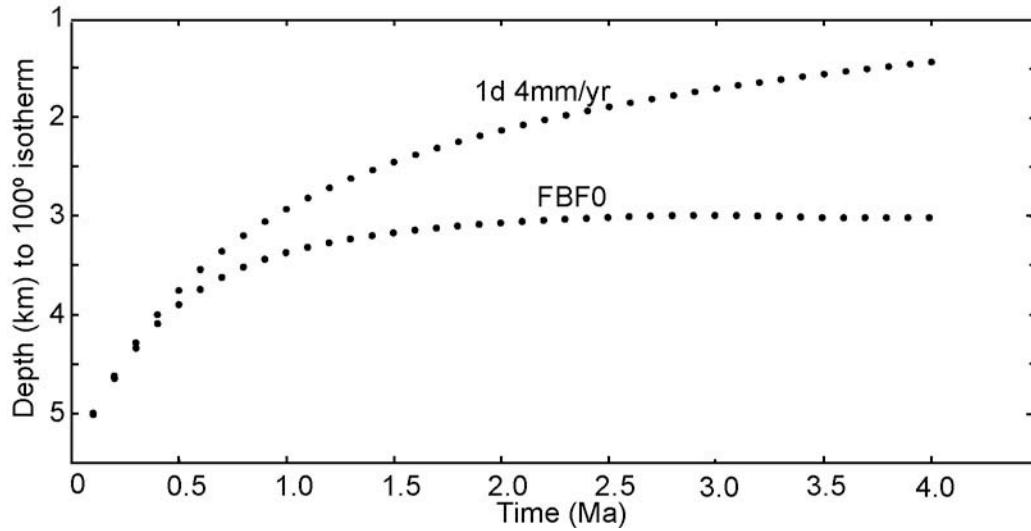
A) Cross section from the Taiwan Western Foothills fold-and-thrust belt showing thrust faults and fault-related fault-bend-folding typical of a fold-and-thrust belt (modified from Suppe 1980a). B) A schematic fault-bend-fold model (Suppe 1980a). In the fault-bend-fold model, beds fold above changes in the fault dip. All material in the hanging wall of the fault moves parallel to the fault and all material in the footwall remains undeformed. Bed area and length is conserved and beds thin along the forelimb of the anticline.

**Figure 2.2** Patterns of Thermochronometric Age produced by Thrust Fault Exhumation

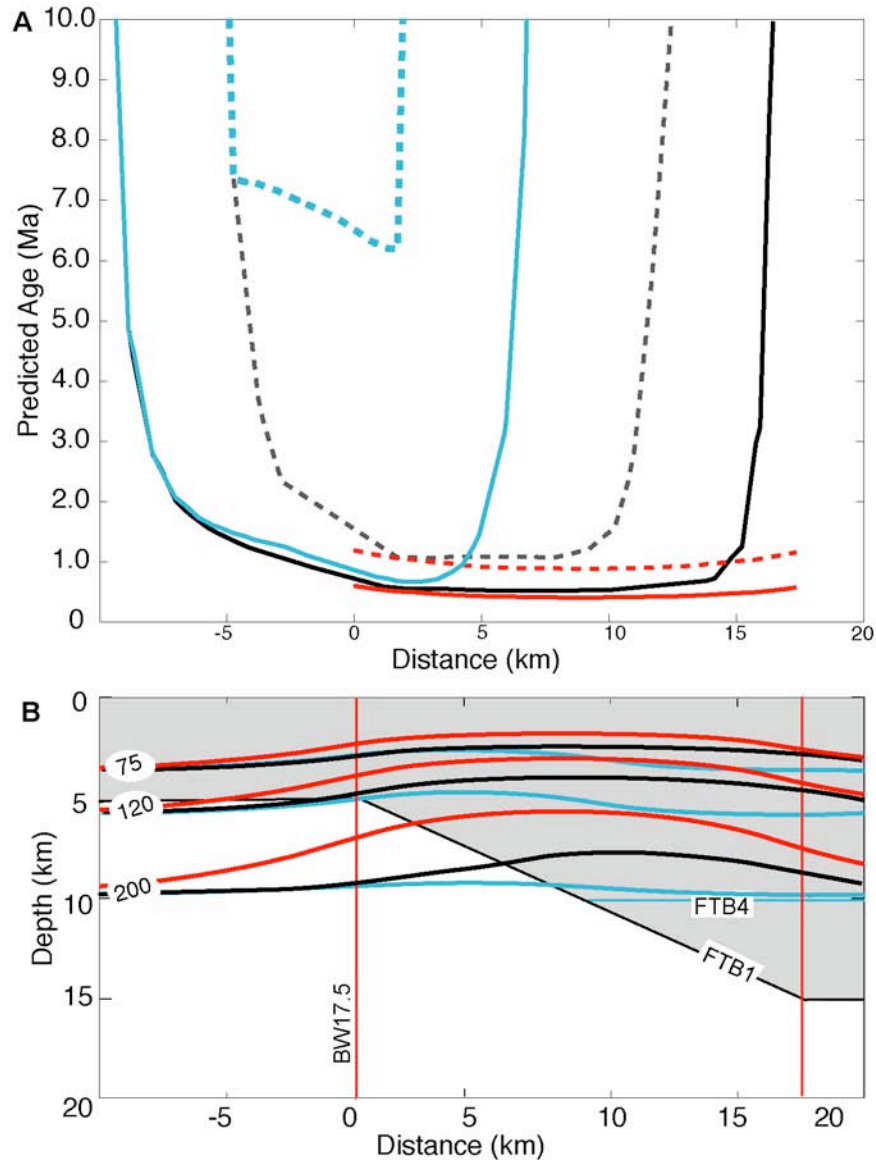
Results of thermal-kinematic fault-bend-fold model FBF0 (black lines, FBF0, Table 2) and comparison to a 1d model (grey lines, 1D, Table 2). In model FBF0, the fault ramp dips at 30°, the basal flat is at 15 km, the top flat is at 5 km, and fault parallel slip is 8 mm/yr. The 1d transient model uses a vertical advection rate of 4 mm/yr and a constant flux bottom boundary condition. Modeled ages given in top 3 panels (A-C) are (U-Th)/He age in apatite (He, dashed lines), apatite fission track (FT, solid lines), zircon fission track (Z, dashed lines). Modeled ages: A) After 1 Ma of faulting. B) After 2 Ma of faulting. C) After 4 Ma of faulting. D) Fault-bend-fold formed using the fault-parallel flow algorithm in 2DMove. E) Select low temperature isotherms after 2 Ma for the 1d model (grey lines) and the fault bend fold model (black lines). Grey and black arrows in B mark zones of reset ages that experience constant and non-constant cooling after passing through the closure temperatures. The zone width varies with different thermochronometers.



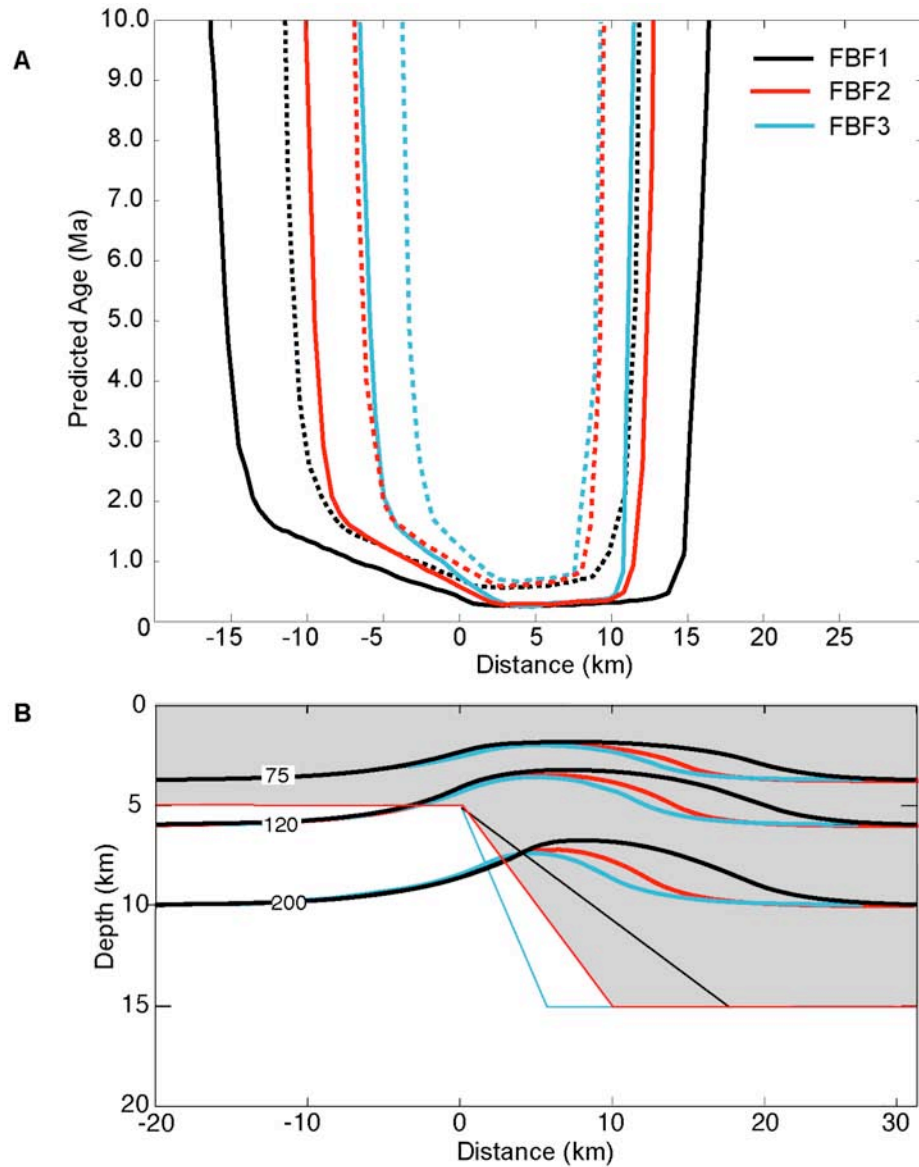




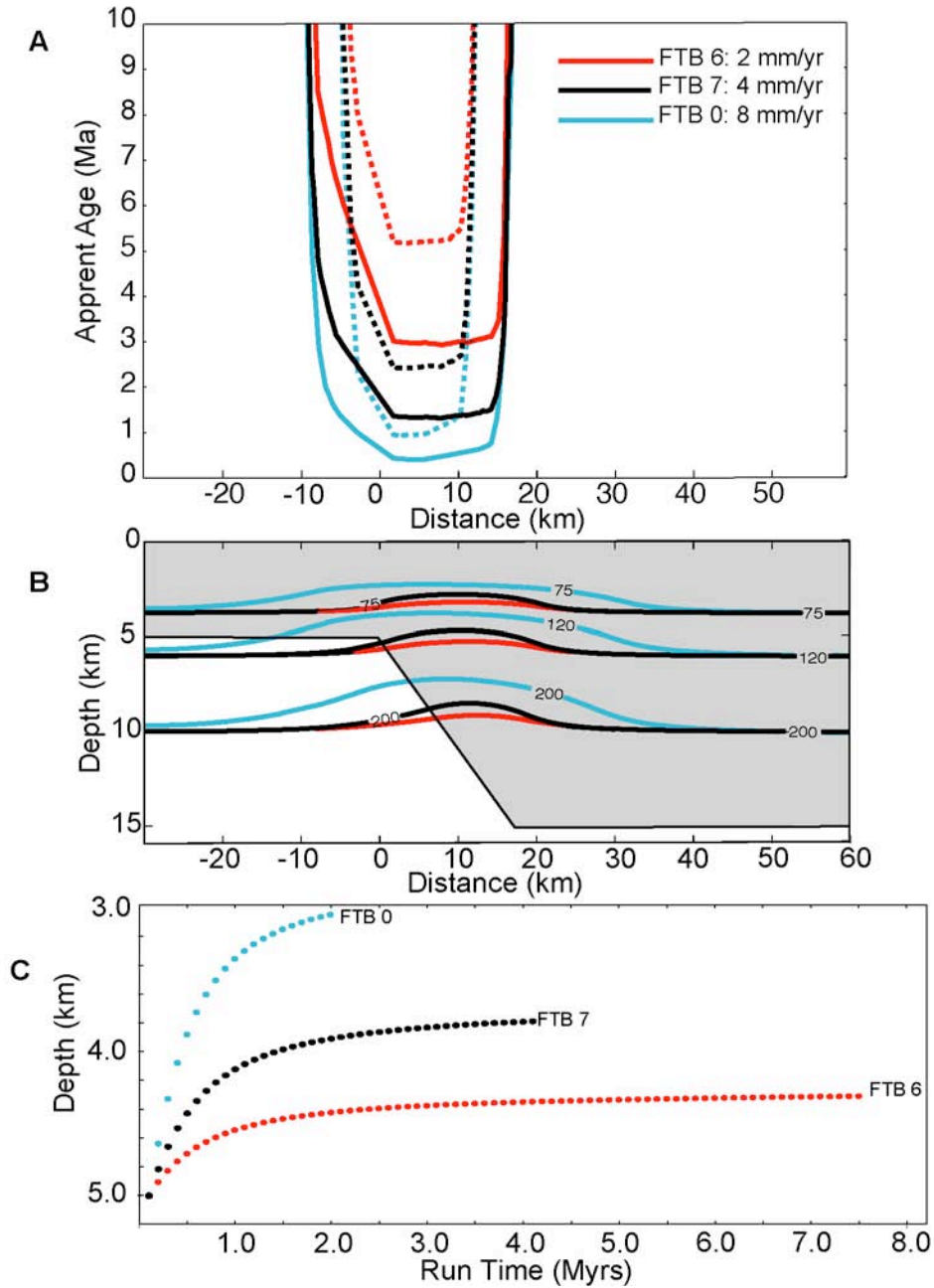
**Figure 2.3** Change in depth to the 100°C isotherm in 1d and thrust fault models  
The depth to the 100° isotherm through time in the 1d transient model (1D) and the minimum depth to the 100°C isotherm (in the thrust fault model, this is the depth of the isotherm above the center of the thrust ramp) in the fault-bend-bold model FBF0 shown in Figure 2.2.



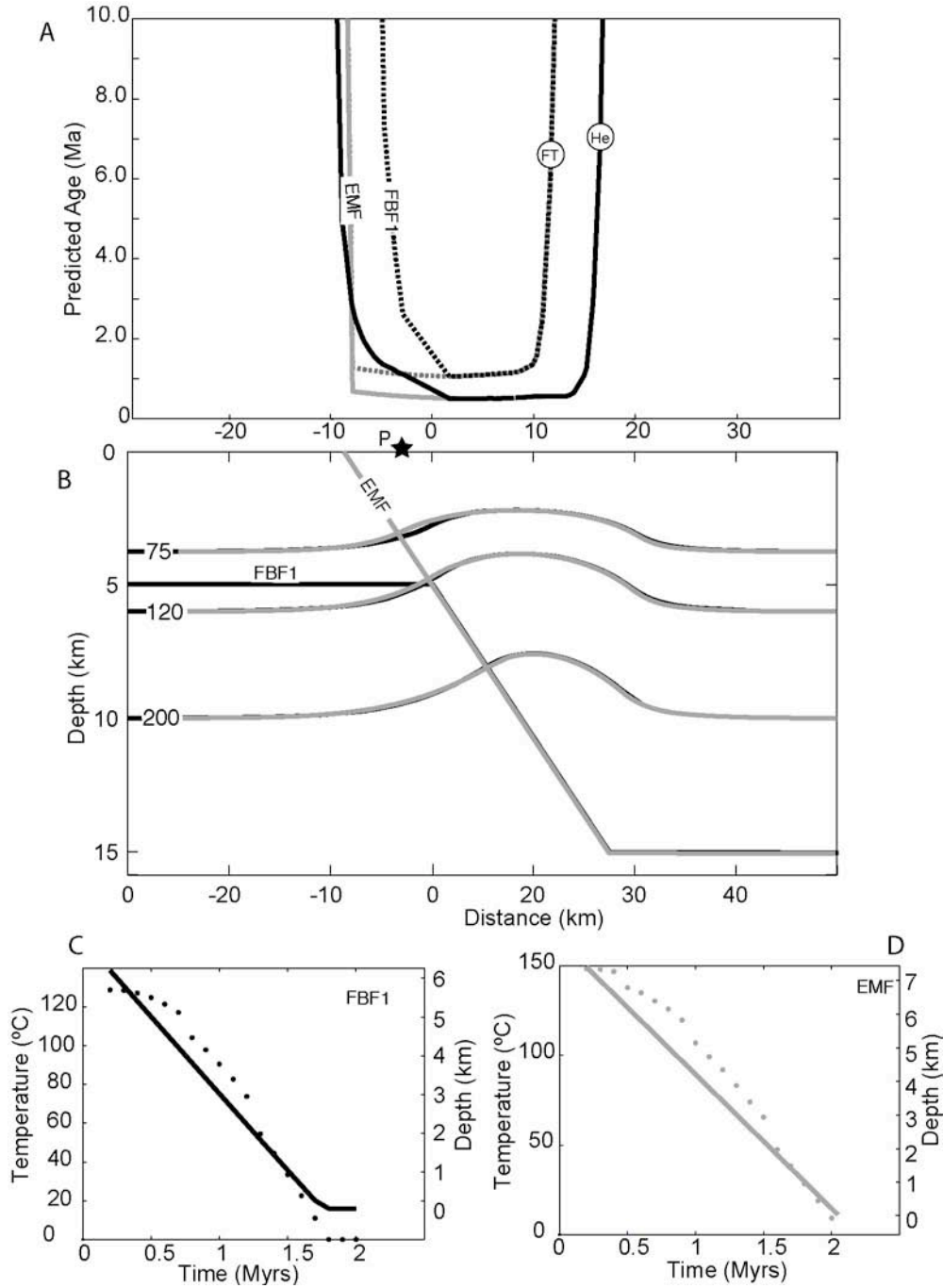
**Figure 2.4** Predicted thermochronometric ages for fault geometries with different base-flat depths (A) Apatite fission track predicted ages (dashed lines) and (U-Th)/He ages (solid lines) for fault geometries shown in B. FBF0: black lines, BW17, red lines, FBF4, blue lines. (B) Fault geometries (thin lines) and select isotherms (thick lines). Models are a fault-bend-fold structure with a basal flat at 15 km (FBF0, black lines), a block uplift with the width of the ramp (BW17, red lines) and a fault-bend-fold model with a basal flat at 10 km (FBF4, blue lines). Models are all run for 2 Ma with a vertical slip rate 4 mm/yr and a fault parallel slip rate of 8 mm/yr. Shaded region marks the hanging wall in model FBF0.



**Figure 2.5** Thermochronometric age sensitivity to fault ramp dip. Fault ramp dips are  $30^\circ$  (FBF1, black lines),  $45^\circ$  (FBF2, red lines) and  $60^\circ$  (FBF3, blue lines). Vertical exhumation rate above the ramp is 5.66 mm/yr, horizontal slip varies (Table 2). Model run time is 2 Ma. A) Predicted apatite fission track (dashed lines) and (U-Th)/He in apatite (solid lines) thermochronometric age B) Select temperature contours (thick lines) for each fault configuration at the end of faulting. Shaded region marks the hanging wall in model FBF1.

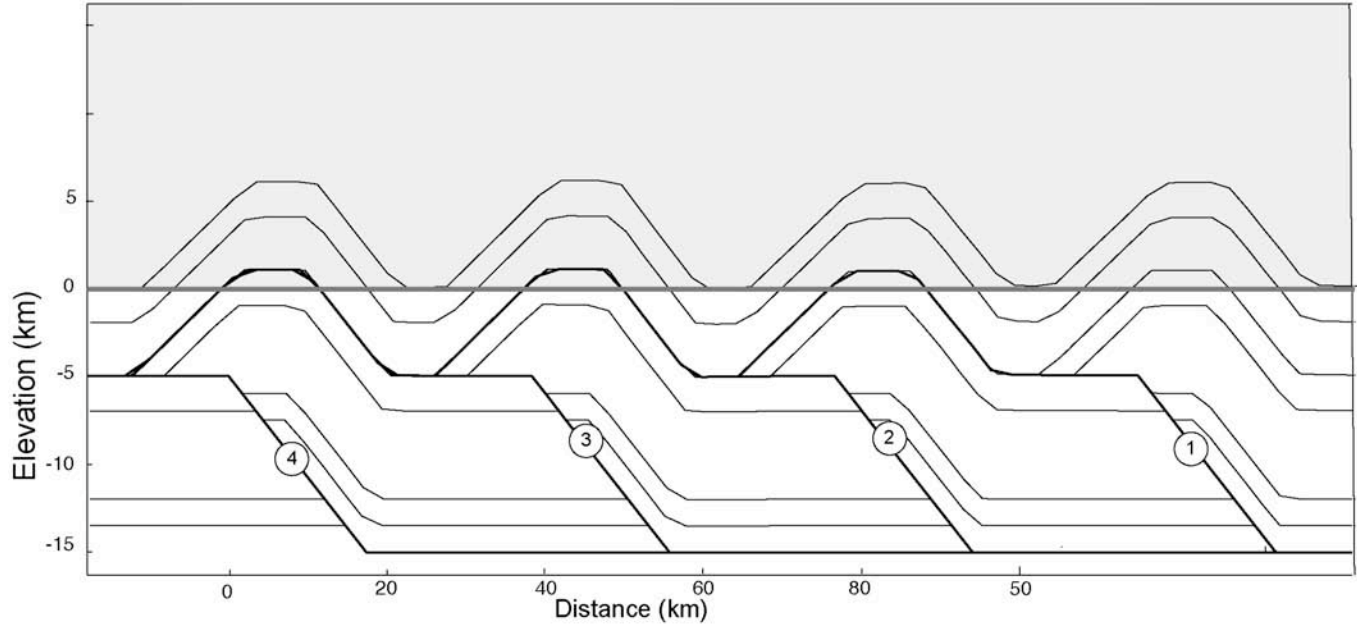
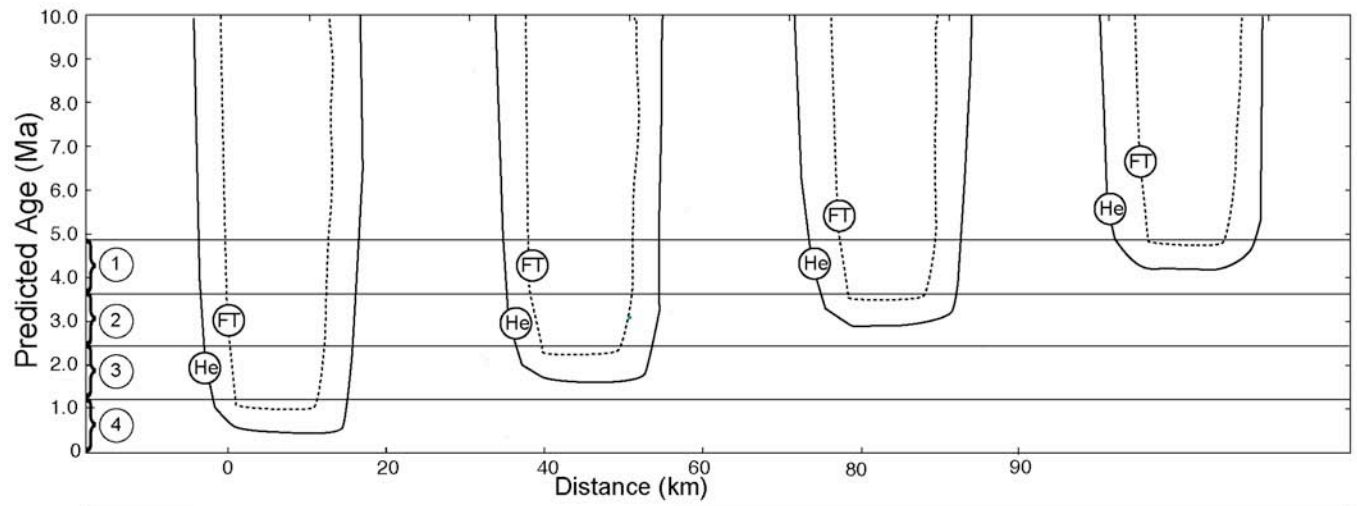


**Figure 2.6** Thermochronometric age sensitivity to slip rate. Vertical slip rate varies from 1 mm/yr - 4 mm/yr (Table 2). The fault dips at  $30^\circ$  and the depth to the base-flat is 15 km. The hanging wall is shown as shaded region in B. Fault parallel slip varies from 8 mm/yr run for 2 Ma (FTB0, blue lines), 2 mm/yr run for 8 Ma (FTB6, red lines) and 4 mm/yr (FTB 7, blue lines) run for 4 Ma. A) Predicted thermochronometric age. Apatite fission track are solid lines and (U-Th)/He are dashed lines B) Temperature structure (thick lines) and fault geometry (thin lines) C) Minimum depth to  $100^\circ$  isotherm for each model.

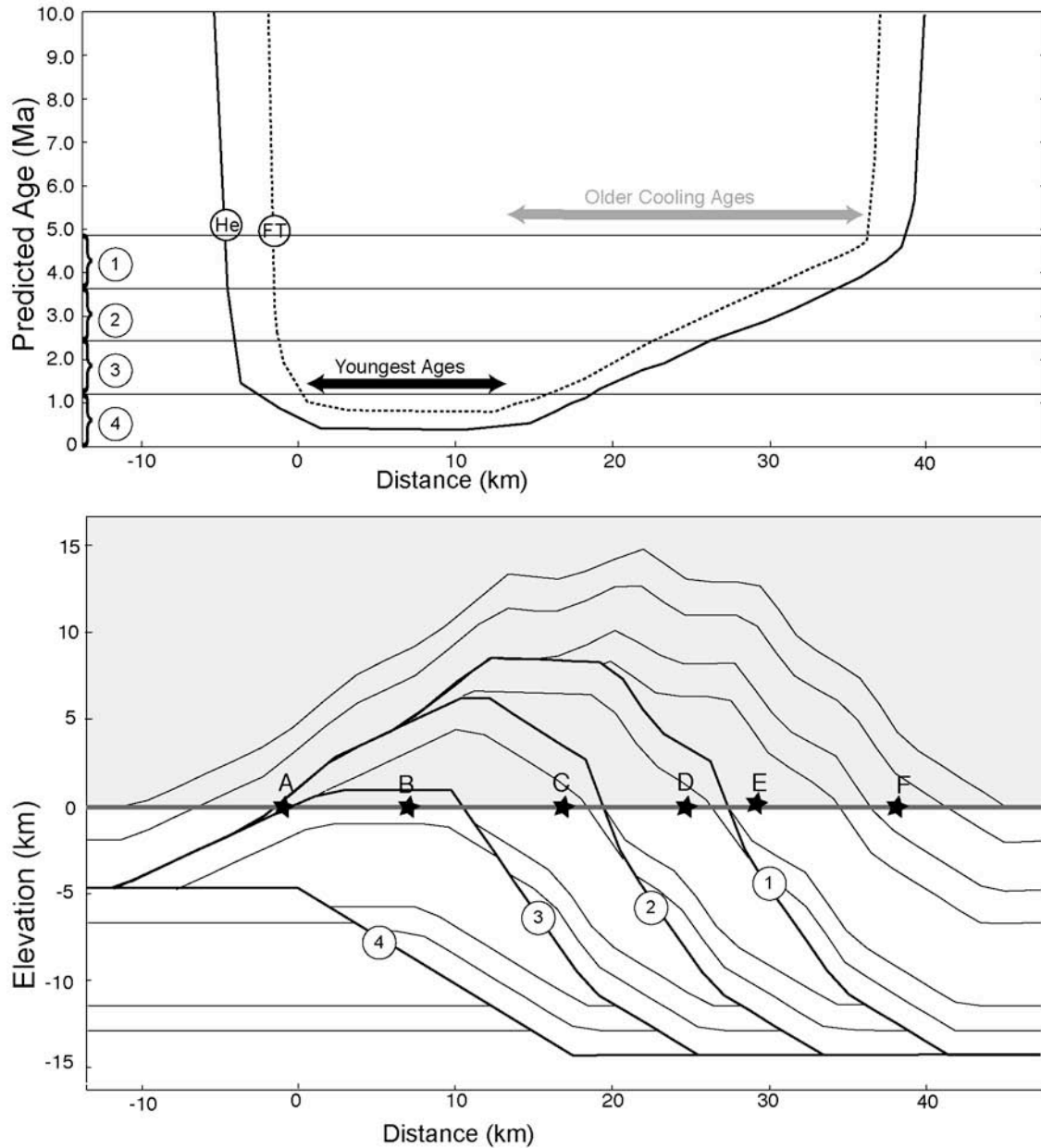


**Figure 2.7** Thermochronometric age patterns generated by blind and emergence thrust ramps. Comparison between a fault-bend-fold (FBF1, black lines) and an emergent thrust (EMF, grey lines) A) Predicted age (apatite fission track: dashed lines, (U-Th)/He in apatite: solid lines). B) Temperature structure. C) Temperature time path for particle in fault-bend-fold model at point P. Line shows depth through time, points show temperature D) Temperature time path for particle in emergent thrust ramp model at point P.

**Figure 2.8** Results of multiple fault model with 50 km fault spacing. Model with multiple faults with a 50 km spacing (MULT1). B) Final structure and A) resulting thermochronometric ages. Each fault slips 10 mm/yr for 1.2 Ma. Fault 1 is active from 4.8-3.6 Ma, fault 2 is active from 3.6-2.4 Ma, fault 3 is active from 2.4-1.2 Ma, and fault 4 is active from 1.2-0 Ma. Shaded box in lower panel is area removed by erosion.



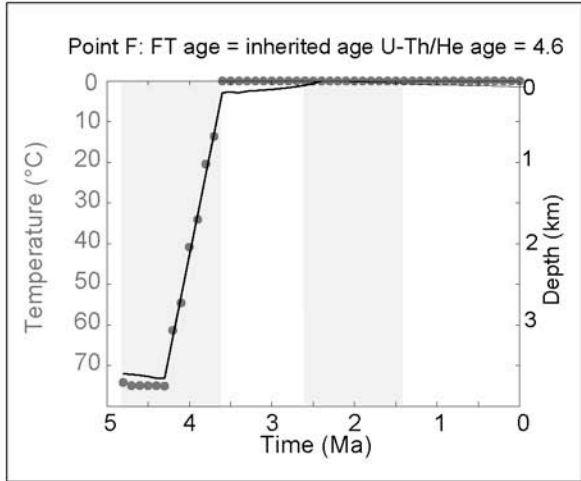
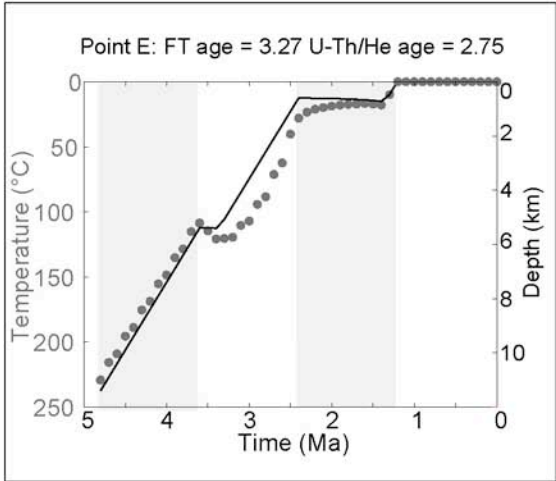
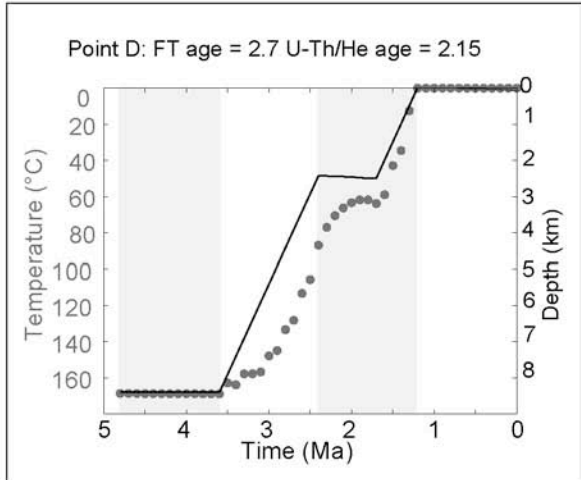
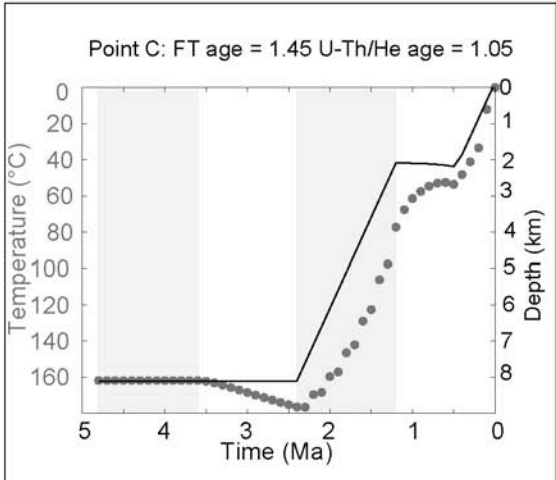
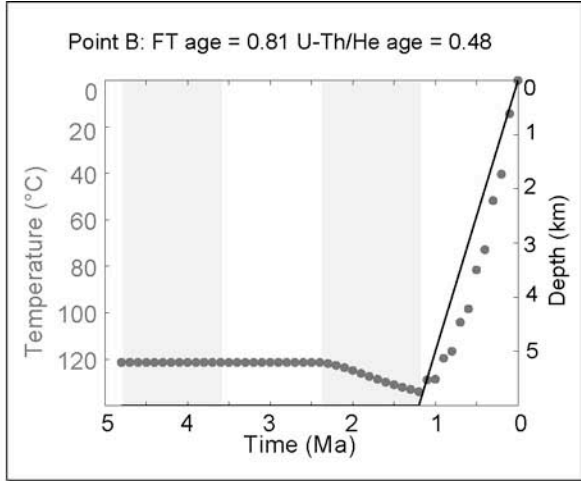
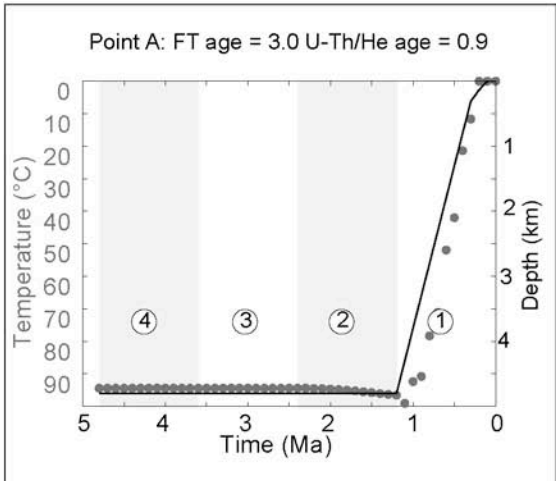




**Figure 2.9** Results of multiple fault model with 20 km fault spacing.

Model with multiple faults and a 20 km spacing (MULTI2). A) Predicted Thermochronometric age for model MULTI2 (Table 2). Black line marks zone of youngest cooling ages that record slip along the active frontal thrust. Grey line marks older cooling ages that are cooled through the closure temperature by older thrusts. B) Final structure at 4.8 Ma. Thick lines are faults and thin lines represent bedding. Faults are labeled 1-4. Fault 1 is active from 4.8-3.6 Ma, fault 2 is active from 3.6-2.4 Ma, 3 is active from 2.4-1.2 Ma, and fault 4 is active from 1.2-0 Ma. Shaded box in B shows area removed by erosion.

**Figure 2.10** Temperature-depth histories of selected points in 20 km fault spacing model. Temperature and depth as a function of model time for selected particles in model shown in Figure 9. Final position of particles A-F shown in Figure 9b. Solid line indicates depth history of particle; grey dots indicate temperature. Shaded regions show the time each fault is active, faults 1-4 (figure 9). Predicted (U-Th)/He and fission track ages for the cooling histories are in give Ma.



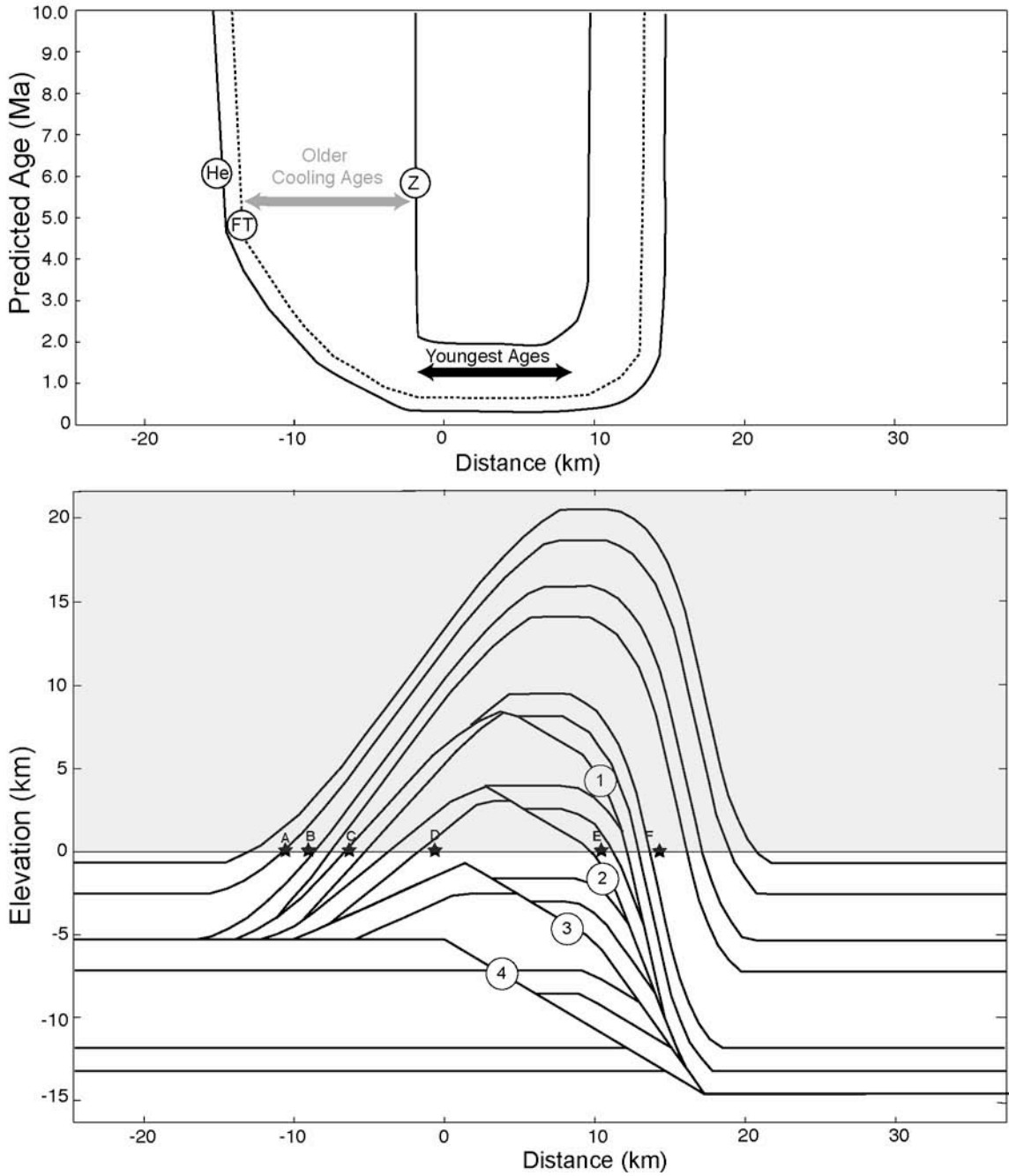


**Figure 2.11** Results of multiple fault model with 10 km fault spacing. Model with multiple faults with a 10 km spacing (MULTI3). A) Predicted Thermochronometric Age for model MULTI3 (Table 2). Grey line marks older cooling ages that are cooled through the closure temperature by older thrusts. B) Structure and pattern of thermochronometric age for fault model MULTI3. Thick lines are faults and thin lines represent bedding. Fault 1 is active from 4.8-3.6 Ma, fault 2 is active from 3.6-2.4 Ma, 3 is active from 2.4-1.2 Ma, and fault 4 is active from 1.2-0 Ma. Shaded box in B shows area removed by erosion.

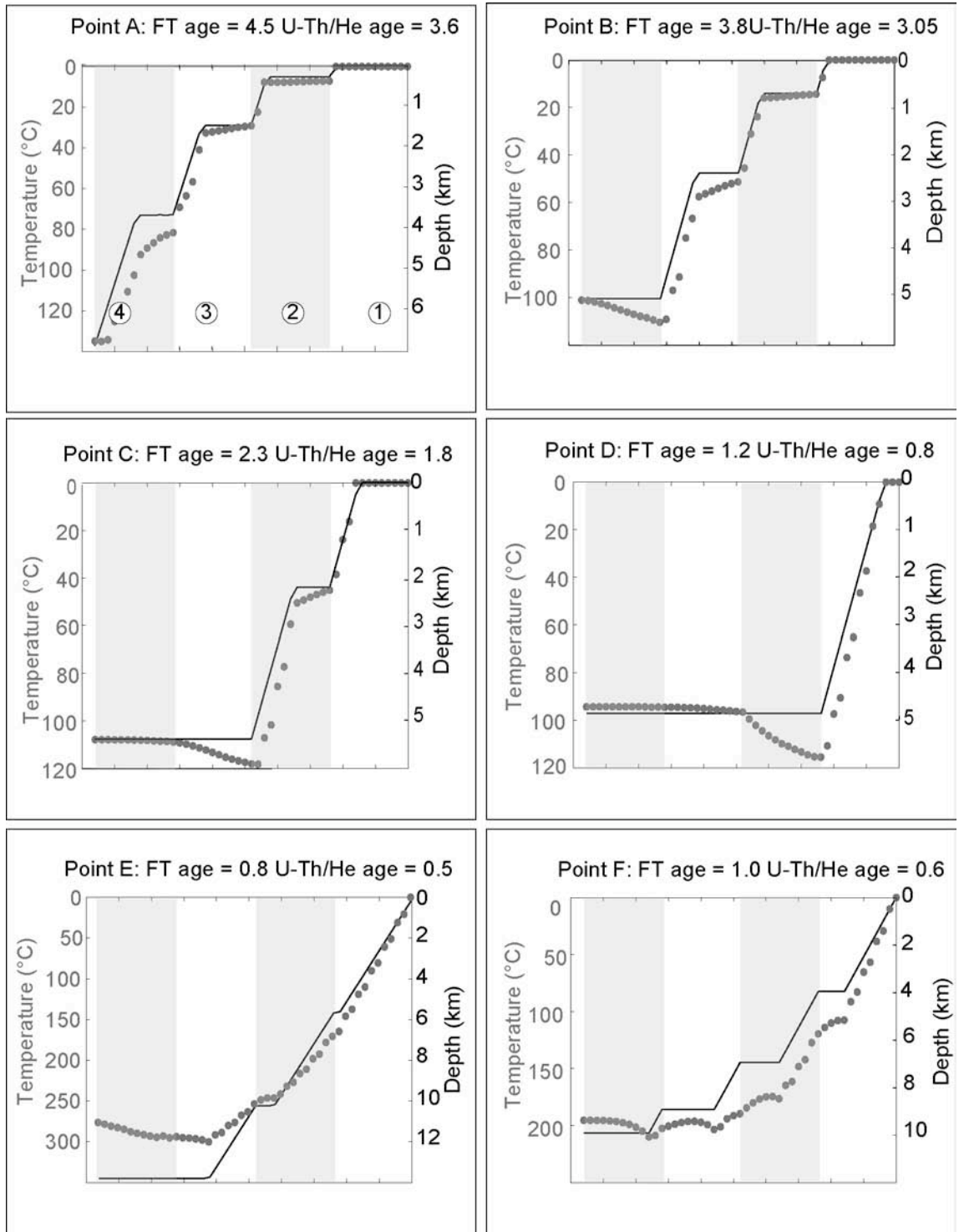


**Figure 2.12** Temperature-depth histories of selected points in 10 km fault spacing model. Temperature and depth as a function of model time for selected particles shown in Figure 11. Final position of particles A-F shown in Figure 11. Solid line indicates depth history of particle; Grey dots indicate temperature; Shaded regions show the time each fault is active, faults 1-4 (figure 11). Predicted (U-Th)/He and fission track ages for the cooling histories are in give Ma.

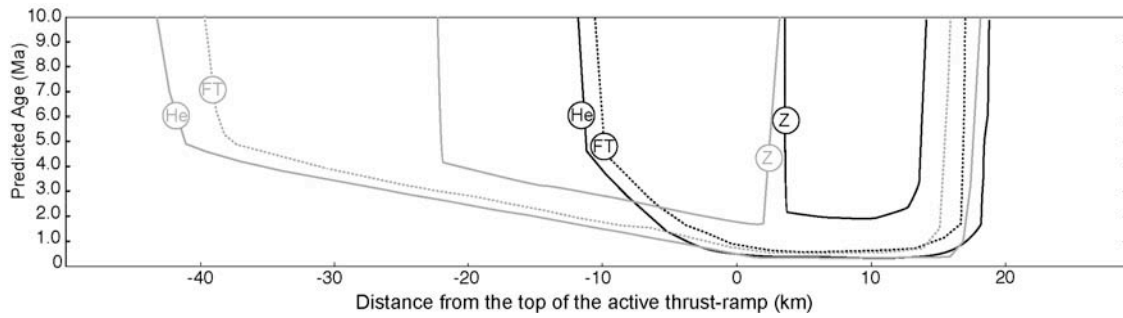


**Figure 2.13** Comparison of single fault and multiple fault models.

Predicted thermochronometric age in material exhumed by an individual fault (grey lines) and multiple faults (black lines). In both models fault dip is  $30^\circ$  and fault slip rate is 10 mm/yr for 4.8 Ma (total slip is 48 km). In the individual fault model, slip is accommodated along one fault (FBF8). In the multiple fault model (MULTI 3, figure 11), slip is accommodated by 4 sequentially activated faults spaced 10 km apart, each fault is active for 1.2 Ma and activated in sequence. Thermochronometric ages are approximately equal above the active fault ramp. In the one-fault model, age increases linearly at a rate equal to the inverse of the horizontal slip rate. In the multiple fault model, the increasing age gradient is steeper and not linear.

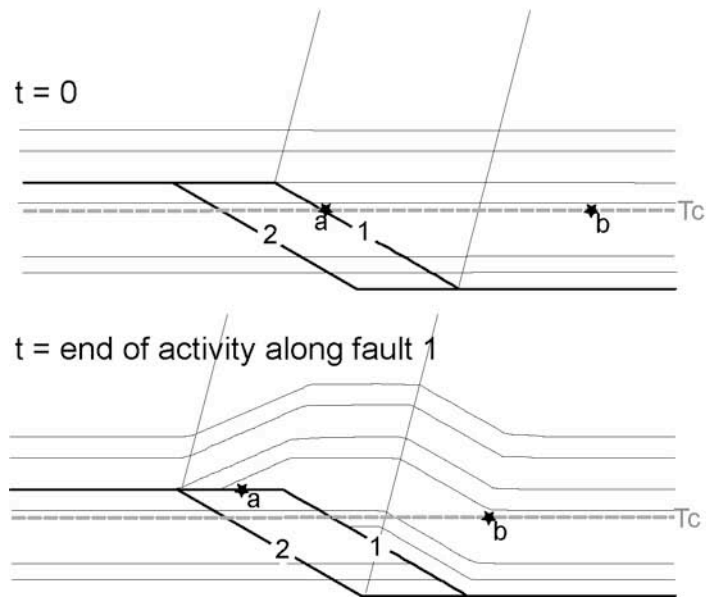


**Figure 2.14** Schematic illustration of factors controlling different multiple fault thermochronometric age patterns.

Schematic illustration showing the factors that determine the different location of material that records slip on an older fault. Fault 1 is older and fault 2 is a younger thrust.  $T_c$  is a schematic representation of the closure temperature. A) At time  $t = 0$ , no thrust deformation. B) At the end of slip along fault 1. Point a is the point closest to the foreland that records activity of fault 1, point b is the most hinterlandward that records activity of fault 1. If slip along fault 2 exhumes point a, the activity of fault 1 will not be preserved in the foreland. If fault 2 exhumes point b, the activity of fault 1 is not preserved in the hinterland.

## Notes to Chapter 2

- Arne, D., B. Worley, C. Wilson, S. Chen, D. Foster, Z. Luo, S. Liu, and P. Dirks, 1997, Differential exhumation in response to episodic thrusting along the eastern margin of the Tibetan Plateau, *Tectonophysics*, 280, 239–256.
- Banerjee, P., and R. Bürgmann, 2002, Convergence across the northwest Himalaya from GPS measurements, *Geophysical Research Letters*, 29(13),30
- Benedetti, L., Tapponnier, P., King, G.C.P., Meyer, B. & Manighetti, I., 2000, Growth folding and active thrusting in the Montello region, Veneto, northern Italy. *J. Geophys. Res.*, 105, 739– 766.
- Blythe, A.E., Bird, J.M., and Omar, G.I., 1998, Constraints on the cooling history of the central Brooks Range, Alaska, from fission-track and  $^{40}\text{Ar}/^{39}\text{Ar}$  analyses, in Oldow, J.S., and Av Lallemand, H. G., eds., *Architecture of the Central Brooks Range Fold and Thrust Belt, Arctic Alaska: Boulder, Colorado, Geological Society of America Special Paper 324*, 163-177.
- Bollinger, L., Avouac, J.P., Beyssac, O., Catlos, E.J., Harrison, T.M., Grove, M., Goffe, B., Sapkota, S., 2004, Thermal structure and exhumation history of the Lesser Himalaya in central Nepal, *Tectonics* 23(5), TC501519.
- Bollinger, L., P. Henry and J.P. Avouac, 2006, Mountain building in the Nepal Himalaya: Thermal and kinematic model, *Earth Planet. Sc. Lett.*, 244, 58-71.
- Brandon, M.T., 1992. Decomposition of fission track age distributions. *Am. J. Sci.*, 292, 535-564.
- J. Braun, 2002, Quantifying the effect of recent relief changes on age – elevation relationships, *Earth and Planetary Science Letters*, 200, 331–343.
- Brown, R.W. and Summerfield, M.A., 1997, Some Uncertainties in the Derivation of Rates of Denudation from Thermochronologic Data, *Earth Surface Processes and Landforms* 22(3),.239-248
- Brewer, J., 1981, Thermal effects of thrust faulting: *Earth and Planetary Science Letters* 56, 233–244.
- Bullen, M.E., Burbank, D.W.; Garver, J.I., 2003, Building the northern Tien Shan; integrated thermal, structural, and topographic constraints. *Journal of Geology* 111(2),149-165.



- Bullen, M E; Burbank, D W; Garver, J I; Abdrakhmatov, K Ye., 2001. Late Cenozoic tectonic evolution of the northwestern Tien Shan; new age estimates for the initiation of mountain building. *Geological Society of America Bulletin*, vol.113, no.12, pp.1544-1559.
- Burbank, D.W., Meigs, A., and Brozovic, N., 1996, Interactions of growing folds and coeval depositional systems: *Basin Research*, v. 8, p. 199-223.
- Burbank, D.W., Vergés, J., MUÑOZ, J.A., and Betham, P., 1992, Coeval hindward- and forward-imbricating thrusting in the south-central Pyrenees, Spain: Timing and rates of shortening and deposition *Geological Society of America Bulletin*, 3–17.
- Burbank, D.W., Blythe, A.E., Putkonen, J., Pratt-Sitaula, B., Gabet, E., Oskin, M., Barros, A., and Ojha, T.P., 2003, Decoupling of erosion and precipitation in the Himalayas, *Nature* 426, 652-655.
- Bürgmann, R., Arrowsmith, R., Dumitru, T., and McLaughlin, R., 1994, Rise and fall of the southern Santa Cruz Mountains, California, from fission tracks, geomorphology, and geodesy, *Journal of Geophysical Research*, 99, 20181-20, 202.
- Byrne, T.B. and Liu, C.S., 2002, Preface: Introduction to the geology and geophysics of Taiwan. In: T.B. Byrne and C.S. Liu, Editors, *Geology and Geophysics of an Arc-Continent Collision, Taiwan*, pp. v-viii.
- Carena, S., Suppe, J., Kao, H., 2002, Active detachment of Taiwan illuminated by small earthquakes and its control of first-order topography. *Geology* 30, 10, 935-938.
- Chapple, W.M., 1978, Mechanics of thin-skinned fold-and-thrust belts. *Geological Society of America Bulletin*, 89 (8), 1189-1198
- Coward, M. P., M. De Donatis, S. Mazzoli, W. Paltrinieri, and F. Wezel, 1999, Frontal part of the northern 85222 fold and thrust belt in the Romagna-Marche area (Italy): Shallow and deep structural styles. *Tectonics* 18(3), 559–574
- Dadson, S. J., Hovius, N., Chen, H., Dade, W.B., Lin, J. C., Hsu, M.-L., Lin, C.-W., Horng, M.-J., Chen, T.-C., Milliman, J., Stark, C. P., 2004, Earthquake-triggered increase in sediment delivery from an active mountain belt. *Geology* 32, 733-736.
- Dahlstrom, C. D. A., 1970, Structural geology in the eastern margin of the Canadian Rocky Mountains. *Bull. Can. Petrol. Geol.* 18, 332-406

- Dahlstrom, C.D.A., 1969, Balanced cross sections. *Canadian Journal of Earth Sciences*, vol.6, no.4, Part 1, 743-757.
- Davis, D., Suppe, J., Dahlen, F. A., 1983, Mechanics of fold-and-thrust belts and accretionary wedges. *Journal of Geophysical Research* 88, 1153-1172.
- Davy, P., and Gillet, P., 1986, The stacking of thrust slices in collision zones and its thermal consequences. *Tectonics* 5, 913–929.
- DeCelles, P. G., Gray, M. B., Ridway, K. D., Cole, R. B. Srivastava, , P., Pequera, N., Pivnik, D. A., 1991, Kinematic history of a foreland uplift from Paleocene synorogenic conglomerate, Beartooth Range, Wyoming and Montana, *Geological Society of America Bulletin* 103(11) 1458–1475.
- DeCelles, P.G., Gautam, M.,1995, History of the Sevier orogenic wedge in terms of critical taper models, Northeast Utah and Southwest Wyoming. *Geological Society of America Bulletin* 107(4), 454-462.
- Donelick, R.A., O’Sullivan, P.B., Ketcham, R.A., 2005, Apatite Fission-Track Analysis. *Reviews in Mineralogy and Geochemistry*. 58(1), 49-94.
- Ducea, M. N., House, M. A., Kidder, S., 2003, Late Cenozoic denudation, bedrock and surface uplift rates in the Santa Lucia Mountains, California. *Geology*, 31, 139-142.
- Ehlers, T.A., Willett, S.D., Armstrong, P.A., Chapman, D.S., 2003, Exhumation of the central Wasatch Mountains, Utah; 2, Thermokinematic model of exhumation, erosion, and thermochronometer interpretation, *Journal of Geophysical Research* 108(B3), 2173.
- Ehlers, T.A., Farley, K.A., 2003, Apatite (U–Th)/He thermochronometry: methods and applications to problems in tectonic and surface processes. *Earth and Planetary Science Letters* 206(1-2), 1-14.
- England, P., Thompson, A., 1984, Pressure-temperature-time-paths of regional metamorphism I. Heat transfer during the evolution of regions of thickened crust, *J. Petrol.* 25, 894-928.
- Farley, K.A., Wolf, R.A., Silver, L.T., 1996, The effects of long alpha-stopping distances on (U-Th)/He dates, *Geochim. et Cosmochim. Acta*, 60, 4223-4229.
- Farley, K.A., 2002, (U-Th)/He dating: Techniques, calibrations, and applications, in: *Noble Gases in Geochemistry and Cosmochemistry*. *Reviews in Mineralogy and Geochemistry*, 47, 819-844.

- Ford, M., Williams, E.A., Artoni, A., Verges, J., Hardy, S., 1997, Progressive evolution of a fault-related fold pair from growth strata geometries, Sant Llorenç de Morunys. SE Pyrenees. *Journal of Structural Geology*, 19, 413-441.
- Fuller, C.W., Willett, S.D., Fisher, D., Lu, C-Y., 2006, A thermomechanical wedge model of Taiwan constrained by fission-track thermochronometry. *Tectonophysics*, Volume 425(1-4), 1-24.
- Hardy, S., Poblet, J., McClay, K., and Waltman, D., 1996, Mathematical modelling of growth strata associated with fault-related fold structures, in Buchanan, P.G., and Nieuwland, D.A., Editors, *Modern developments in structural interpretation, validation and modelling: Geological Society [London] Special Publication 99*, 265–282.
- Hickman, J. B., Wiltschko, D. V., Hung, J.-H., Fang, P., Bock, Y., 2002, Structure and evolution of the active fold-and-thrust belt of Southwestern Taiwan from Global Positioning System analysis. *Geological Society of America Special Paper 358*, 75-92.
- House, M.A., Gurnis, M., Kamp, P.J.J., Sutherland, R., 2002, Uplift in the Fiordland region, New Zealand; implications for incipient subduction, *Science*, v. 297, 2038-2041.
- Hsieh, M.-L., Knuepfer, P. L. K., 2001, Middle-late Holocene river terraces in the Ehrjen River Basin, southwestern Taiwan - implications of river response to climate change and active tectonic uplift., *Geomorphology* 38, 337-372.
- Hsieh, M.-L., Knuepfer, P. L. K., 2002, Synchronicity and morphology of Holocene river terraces in the southern Western Foothills, Taiwan: a guide to interpreting and correlating erosional river terraces across growing anticlines. In *Geology and geophysics of an arc-continent collision, Taiwan.*, Byrne T. B., Liu, C. S., Editors, 55-74.
- Huerta, A.D., Rodgers, D.W., 2006, Constraining rates of thrusting and erosion: Insights from kinematic thermal modeling *Geology*, 34(7), 541–544.
- Jackson, J., Ritz, J.F., Siame, L., Raisbeck, G., Yiou, F., Norris, R., Youngson, J. & Bennett, E., 2002, Fault growth and landscape development rates in Otago, New Zealand, using in situ cosmogenic <sup>10</sup>Be. *Earth Planet. Sci. Lett.*, 195, 185– 193.
- Karabinos, P. and Ketcham, R., 1988, Thermal structure of active thrust belts. *Journal of Metamorphic Geology*, 6, 559-570.

- Ketcham, R.A., Donelick, R.A. and Carlson, W.D., 1999, Variability of apatite fission-track annealing kinetics: III. Extrapolation to geological timescales. *American Mineralogist*, 84, 1235-1255.
- Kirby, E. Reiners, P.W. M.A. Krol, K.X. Whipple, K.V. Hodges, K.A. Farley, W. Tang and Z. Chen, 2002, Late Cenozoic evolution of eastern margin of the Tibetan Plateau: inferences from  $^{40}\text{Ar}/^{39}\text{Ar}$  and (U/Th)/He thermochronology, *Tectonics*, 21(1), 1001, doi:10.1029/2000TC001246, 2002.
- Lacombe, O., F. Mouthereau, F., B. Deffontaines, B., and Angelier, J., 1999, Geometry and Quaternary kinematics of fold and-thrust units of southwestern Taiwan., *Tectonics*, 18, 1198-1223.
- Lacombe, O., Mouthereau, F., 2002, Basement-involved shortening and deep detachment tectonics in forelands of orogens: Insights from recent collision belts (Taiwan, western Alps, Pyrenees). *Tectonics*, 21(4).
- Lacombe, O., Mouthereau, F., Angelier, J., Chu, H.-T., Lee, J.-C., 2003, Frontal belt curvature and oblique ramp development at an obliquely collided irregular margin: Geometry and kinematics of the NW Taiwan fold-thrust belt. *Tectonics* 22(3) 1025, doi:10.1029/2002TC001436, 2003.
- Laslett, G.M., Green, P.F., Duddy, I.R., Gleadow, A.J.W., 1987, Thermal annealing of fission tracks in apatite. *Chemical Geology Isotope Geoscience Section* 65(1), 1-13.
- Mailhe, D., Lucazeau, F., and Vasseur, G., 1986, Uplift history of thrust belts; an approach based on fission track data and thermal modelization., *Tectonophysics* 124, 177–191.
- Malusa, M. G., Polino, R., Zattin, M., Bigazzi, G., Martin, S., Piana, F., 2005, Miocene to Present differential exhumation in the Western Alps: Insights from fission track thermochronology. *Tectonics* 24, TC3004, doi:10.1029/2004TC001782
- Mancktelow, N.S., Grasemann, B., 1997, Time dependent effects of heat advection and topography on cooling histories during erosion., *Tectonophysics* 270, 167–195.
- McClay, K. R., 1992, Glossary of thrust tectonics terms, in McClay, K. R., ed., *Thrust tectonics*: London, Chapman & Hall, 419-433.
- McQuarrie, N., Horton, B.K., Zandt, G., Beck, S., DeCelles, P.G., , 2005, Lithospheric evolution of the Andean fold–thrust belt, Bolivia, and the origin of the central Andean plateau. *Tectonophysics*, 399(1-4), 15-37.

- Medwedeff, D.A., 1989, Growth fault-bend folding at southeast Lost Hills, San Joaquin Valley, California: *American Association of Petroleum Geologists Bulletin*, 73, 54–67.
- Mitra, S. (1986) Duplex structures and imbricate thrust systems: Geometry, structural position and hydrocarbon potential. *Bulletin of the American Association of Petroleum Geologists* 70, 1087-1112. *Memoir*. 171,489-514.
- Molnar, P. and England, P., 1990, Temperatures, heat flux, and frictional stress near major thrust faults. *Journal of Geophysical Research*, 95(B4), 4833-4856.
- Moore, M.A., England, P.C., 2001, On the inference of denudation rates from cooling ages of minerals., *Earth Planet. Sci. Lett.* 185, 265–284.
- Naeser, C. W., Faul, H., 1969, Fission track annealing in apatite and sphene., *Journal of Geophysical Research* 74, 705-710.
- Omar, G.I., Lutz, T.M., Giegengack, R., 1994, Apatite fission-track evidence for Laramide and post-Laramide uplift and anomalous thermal regime at the Beartooth overthrust, Montana-Wyoming, *Geological Society of America Bulletin*, 106, 74-85.
- O'Sullivan, P.B., Hanks, C.L., Wallace, W.K., Green, P.F., 1995, Multiple episodes of Cenozoic denudation in the northeastern Brooks Range; fission-track data from the Okpilak Batholith, Alaska. *Canadian Journal of Earth Sciences Journal Canadien des Sciences de la Terre* 32(8), 1106-1118.
- O'Sullivan, P.B., Wallace, W.K., 2002, Out-of-sequence, basement-involved structures in the Sadlerochit. Mountains region of the Arctic National Wildlife Refuge, Alaska: Evidence and implications from fission-track thermochronology. *GSA Bulletin*, 114 (11), 1356–1378.
- Oxburgh, E.R., Turcotte, D.L., 1974, Thermal gradients and regional metamorphism in overthrust terrains with special reference to the eastern Alps., *Schweizerische Mineralogische und Petrographische Mitteilungen* 54, 641–662.
- Parrish, R. R. 1983. 'Cenozoic thermal evolution and tectonics of the coast mountains of British Columbia 1. Fission track dating, apparent uplift rates, and patterns of uplift', *Tectonics*, 2, 601–631.
- Parrish, R. R. 1985. 'Some cautions which should be exercised when interpreting fission track and other data with regard to uplift rate calculations' (abstract), *Nuclear Tracks and Radiation Measurements* 10, 425.

- Ruppel, C.; Hodges, K. V., 1994, Pressure-temperature-time paths from two-dimensional thermal models: Prograde, retrograde, and inverted metamorphism., *Tectonics*, 13(1) 17-44.
- Safran, E.B., 2003, Geomorphic interpretation of low-temperature thermochronologic data: Insights from two-dimensional thermal modeling. *Journal of Geophysical Research*, 108(B4), 2189.
- Shaw, J.H., Suppe, J., 1994, Active faulting and growth folding in the eastern Santa Barbara Channel. *California GSA Bulletin* 106(5) 607-626.
- Shi, Y., and Wang, C.Y., 1987, Two-dimensional modeling of the P-T-t paths of regional metamorphism in simple overthrust terrains., *Geology* 15, 1048–1051.
- Spotila, J.A., Jamie T. Buscher, J.T., Meigs, A.J., Reiners, P.W., 2004, Long-term glacial erosion of active mountain belts., Example of the Chugach–St. Elias Range, Alaska. *Geology*, 32(6), 501–504.
- Stewart, R.J., Brandon, M.T., 2004, Detrital zircon fission-track ages for the "Hoh Formation": Implications for late Cenozoic evolution of the Cascadia subduction wedge., *Geological Society of America Bulletin* 116, 60-75.
- Stuwe, K., White, L. and Brown, R. 1994. 'The influence of eroding topography on steady-state isotherms. Application to fission track analysis', *Earth and Planetary Science Letters*, 124, 63–174.
- Sibuet, J., Hsu, S., 1997, Geodynamics of the Taiwan arc-arc collision., *Tectonophysics*, vol.274, p.221-251.
- Sobel E. R., Oskin, M., Burbank, D., Mikolaichuk A., 2006, Exhumation of basement-cored uplifts: Example of the Kyrgyz Range quantified with apatite fission track thermochronology, *Tectonics* 25, TC2008, doi:10.1029/2005TC001809.
- Suppe, J., 1980a, Imbricated Structure of Western Foothills Belt, South Central Taiwan., *Petroleum Geology of Taiwan*, 17, 1-16.
- Suppe, J., 1980b, A retrodeformable cross section of northern Taiwan., *Geological Society of China Proceedings*, 23, 46–55.
- Suppe, J., 1981, Mechanics of mountain building and metamorphism in Taiwan., *Memoir of the Geological Society of China.*, 4, 67-89.
- Suppe, J., 1983, Geometry and kinematics of fault-bend folding, *American Journal of Science* 283(7), 684-721.

- Suppe, J., 1984, Kinematics of arc-continent collision, flipping of subduction, and back-arc spreading near Taiwan., Geological Society of China Memoir 6, 21–33.
- Suppe, J., Medwedeff, D.A., Geometry and kinematics of fault-propagation folding, *Eclogae Geologicae Helvetiae*, 1990, 83(3), 409-454.
- Suppe, J., Chou, G.T., and Hook, S.C., 1992, Rates of folding and faulting determined from growth strata, in McClay, K.R., ed., Thrust tectonics: London, Chapman & Hall, 105-121.
- Suppe, J., Namson, J., 1979, Fault-bend origin of frontal folds of the western Taiwan fold-and-thrust belt., *Petroleum Geology of Taiwan*, 16, 1–18.
- Tagami, T., O'Sullivan, P.B., 2005, Fundamentals of fission-track thermochronology, in Low-temperature thermochronology; techniques, interpretations, and applications, *Reviews in Mineralogy and Geochemistry*, 58(1), 19-47, Reiners, P.W., Ehlers, T.A., Editors.
- Thompson, S.C., Weldon, R.J., Rubin, C.M., Abdrakhmatov, K., Molnar, R. & Berger, G.W., 2002, Late Quaternary slip rates across the central Tien Shan, Kyrgyzstan, central Asia. *J. Geophys. Res.*, 107(B9), 2203.
- Thiede, R.C., Arrowsmith, J.R., Bookhagen, B., McWilliams, M.O., Sobel, E.R., Strecker, M.R., 2005, From tectonically to erosionally controlled development of the Himalayan orogen, *Geology* 33(8), 689–692.
- Willett, S., Fisher, D., Fuller, C., Yeh, E.-C., and Lu, C.-Y., 2003, Erosion rates and orogenic-wedge kinematics in Taiwan inferred from fission-track thermochronometry., *Geology* 31, 945–948.
- Willett, S.D., Brandon, M.T., 2002. On steady states in mountain belts, *Geology* 30(2), 175–178.
- Wesnousky, S.G., Kumar, S., Mohindra, R., Thakur, V.C., 1999, Uplift and convergence along the Himalayan Frontal Thrust of India. *Tectonics* 18, 967–976.
- Wolf, R.A., Farley, K.A., Silver, L.T., 1996, Helium diffusion and low temperature thermochronometry of apatite. *Geochim. et Cosmochim. Acta*, 60, 4231-4240.
- Yu, S.-B., Chen, H.-Y., Kuo, L.-C., 1997, Velocity field of GPS stations in the Taiwan area. *Tectonophysics*, 274, 41-59.

- Yu, S.-B., Kuo, L.-C., Hsu, Y.-J., Su, H.-H., Liu, C.C., Hou, C.-S., Lee, J.-F., Lai, T.-C., C.C. Liu, Liu, C.-L., Tseng, T.-F., Tsai, C.-S., Shin, T.-C., 2001, Preseismic deformation and coseismic displacements associated with the 1999 Chi-Chi, Taiwan, earthquake., *Bulletin of the Seismological Society of America.*, 91 (5), 995-1012.
- Yue L.F., Suppe, J., and Hung, J.H., 2005, Structural geology of a classic thrust belt earthquake: the 1999 Chi-Chi earthquake Taiwan (MW=7.6)., *Journal of Structural Geology* 27, 2058–2083.
- ter Voorde, M., de Bruijne, C.H., Cloetingh, S.A.P.L., Andriessen, P.A.M., 2004, Thermal consequences of thrust faulting: simultaneous versus successive fault activation and exhumation. *Earth and Planetary Science Letters* 223, 395– 413.
- Wesnousky, S.G., Kumar, S., Mohindra, R. & Thakur, V.C., 1999, Uplift and convergence along the Himalayan Frontal Thrust of India. *Tectonics*, 18, 967–976.
- Zapata, T., Allmendinger, R.W., 1996, Growth stratal records of instantaneous and progressive limb rotation in the Precordillera thrust belt and Bermejo basin, Argentina, *Tectonics* 15, 1065–1083.
- Zeitler, P.K., 1985, Cooling history of the NW Himalaya, Pakistan. *Tectonics*, 4(1), 127-151.



## Chapter 3

### Low-Temperature Thermochronometric data in Western Taiwan

#### 3.1 Summary

New apatite fission track and apatite (U-Th)/He data document the cooling history and constrain the timing and significance of fault structures in western Taiwan. We present 43 apatite fission track (AFT) ages and 62 apatite (U-Th)/He (AHe) grain ages collected along three transects that cross the Taiwan Western Foothills fold-and-thrust belt and the eastern Hsüehshan Range. AFT ages range from  $> 60$  Ma to 0.5 Ma and AHe ages range from 7 to 0.34 Ma. The data presented here greatly expand the northern and western spatial extent of thermochronometric ages in Taiwan and are the first thermochronometric cooling ages from the Taiwan thrust belt.

The thermochronometric ages record deeper and more recent exhumation in the rear of the thrust belt and in the Hsüehshan Range and older shallower exhumation toward the front of the thrust belt. We interpret this age distribution records exhumation above a thrust ramp that is now located beneath the Hsüehshan Range. The ramp links two décollements, the main Taiwan décollement in Eocene-Oligocene formations which crop out in the Hsüehshan Range, to a décollement that is at or above the AFT and AHe closure temperatures in the upper Miocene - Pliocene strata of the Western foothills. Motion along this ramp rapidly exhumes material in the hangingwall through the AFT and AHe closure temperatures. Material is then transported along the décollement in upper Miocene-Pliocene stratigraphic units that links to the thrust faults at the deformation front.

The earliest thermochronometric record of thrust-motion is recorded in the western foothills at 3.5 Ma in northern and central Taiwan, and at 1 Ma in southern Taiwan. The youngest cooling age related to thrust faulting is 0.5 Ma in central and southern Taiwan and 1.2 Ma in northern Taiwan. This spatial distribution of the youngest and oldest cooling ages records arc-continent collision that is younger in the south and now inactive in the north of Taiwan. The ages in western Taiwan document a

steady southward and westward propagating deformation with no evidence of ‘out-of-sequence’ faulting.

### 3.2 Introduction

The Taiwan orogen is formed by the collision of the Luzon Arc with the Chinese continental margin (Figure 3.1). The western Foothills fold-and-thrust belt lies at the western periphery of Taiwan. The thrust-belt accommodates more than 50% of the ~80-90 mm/yr total current plate convergence between the Philippine Sea and Eurasian plates (Yu et al., 1997; Sella et al., 2002) and plays an important role in arc-continent collision. Despite its importance in the Taiwan mountain building process, how convergence is partitioned across the thrust belt, and the significance of individual thrust faults remain as fundamental questions.

As is characteristic of all thrust belts, the majority of convergence in western Taiwan is accommodated by the frontal structures at the deformation front along the very western edge of the thrust belt. Across the frontal structure, geodetic measurements record uplift rates  $> 10$  mm/yr and shortening rates  $> 30$  mm/yr (Yu et al., 1997; Hickman et al., 2002; Fruneau et al., 2001; Hsu et al., 2003; Yue et al., 2005; Huang et al., 2006) and fluvial terraces indicate incision rates of up to 15 mm/yr (Hsieh and Knuepfer, 2001; 2002; Simoes et al., 2007). In 1999, the devastating Chi Chi earthquake ruptured the Chelungpu fault which, while not the western-most structure, is part of frontal thrust system at the western edge of the thrust belt (Shin and Teng, 2001; Yue et al., 2005).

The distribution of short term deformation focused around the frontal structures in the Taiwan thrust belts is consistent with a general westward sequential development of thrust faults in the western foothills. The general view is that once a new fault is initiated, older faults toward the hinterland of the thrust belt cease to be active. Faults active behind the deformation front are termed ‘out-of-sequence’ thrusts. There is evidence for out-of-sequence thrusting in Taiwan (Tillman & Byrne, 1996; Mouthereau et al., 2001; Ching et al., 2007) and out-of-sequence thrust are suggested as important

features of other convergent thrust fault settings (Marques and Cobbold, 2002; Hoth et al., 2003; Wobus et al., 2003; Hodges et al., 2004; Kimura et al., 2007).

Despite the rapid shortening, uplift and erosion, the fold-and-thrust belt contains mostly Plio-Pleistocene unmetamorphosed sediments indicating small amounts of total exhumation. In contrast, the hinterland of the western-foothills, the Hsüehshan and Backbone range toward the center of the Taiwan show little record of active deformation or shortening but rapid and deep exhumation over the longer term (Dadson et al., 2003). AFT and zircon fission track thermochronometric ages from the Hsüehshan and Backbone range record recent, rapid exhumation (Liu et al., 2001; Willett et al. 2003; Fuller et al. 2006) and the oldest most deeply exhumed and highest grade stratigraphy is exposed in the high topography of the Hsüehshan and Backbone Range (Ho, 1988; Figure 3.1). In the western foothills fold-and-thrust belt, apart from the pattern of older and younger stratigraphic units, there are no measures of erosion, uplift and exhumation that average over million year times scales. Thus, whether shorter term rapid deformation focused along thrust faults at the front of the western foothills reflect the longer term spatial distribution of deformation, and whether 'out-of-sequence' faults are an important feature in the development of the thrust belt is unclear.

Low closure temperature radiometric dating techniques like apatite fission track (AFT) and apatite (U-Th)/He (AHe) dating can resolve exhumation rates and amounts on the  $10^6$  year time scale and by inference, the deformation and erosion history of material in western Taiwan. However, the shallow material paths in the thin-skinned thrust belt makes it difficult to obtain cooling rather than detrital ages. The few AFT thermochronometric ages that exist in the thrust belt have been exhumed from above the AFT closure temperature and all zircon fission track ages are detrital not cooling ages (Fuller et al., 2006).

To acquire the data presented in this paper, we use sampling and analysis techniques that minimize the traditional obstacles to using radiometric dating in thrust belts. Using these techniques, we are able to obtain AFT and AHe thermochronometric cooling ages along three transects in northern, central and southern Taiwan that cross

the western foothills fold-and-thrust belt. Our sampling technique maximizes the potential of acquiring reset AFT and AHe ages, and our analysis technique enables us to identify AFT cooling ages in partially reset samples.

Interpreting these new AFT and AHe ages and converting the cooling ages to cooling histories is complicated by the 2 dimensionality to thrust faulting which drives spatially and temporally varying cooling histories and temperature perturbations (Chapter 2). Chapter 2 describes a 2-dimensional thermal-kinematic numerical model to investigate the complex cooling histories and the temperature response to the 2-dimensional sequential thrust-fault activation to predict patterns of thermochronometric ages in fold-and-thrust belts. This study described in Chapter 2 shows the different thermochronometric age patterns generated by a foreward propagating thrust system with different fault geometries. In this study, the results of that analysis are used to interpret the new AFT and AHe ages in the western Taiwan fold-and-thrust belt along each of the 3 sampling transects.

We first introduce the stratigraphy and structure in western Taiwan, then describe the sampling, measuring and analysis techniques we use to acquire AFT and AHe data and cooling ages in the western Taiwan. Following, we discuss the AHe and AFT ages and the interpretation of these ages along each of the three sampling transects, north, central and south. The thermochronometric data are used to document the amount, patterns, and rates of exhumation in the western foothills over the long term. The ages constrain the geometry, timing, and significance of the different thrust fault structures in western Taiwan and are used to understand the role of the thrust belt in the mountain building process.

### **3.3 Taiwan Tectonic Setting**

Taiwan is at the convergent boundary between the Eurasian plate and Philippine Sea Plates. North and south of Taiwan, subduction zones accommodate the ~80-90 mm/yr of NW directed convergence (Yu et al, 1997; Sella et al., 2002, Figure 3.1). To the south, the oceanic Eurasian plate subducts beneath the Eurasian plate along the

Manila trench. To the north, the Philippine Sea plate subducts northward beneath the Eurasian plate along the Ryuku trench. Between these two reverse polarity subduction zones, Taiwan forms from the collision of the Luzon arc with the edge of the Chinese continental margin.

The Luzon arc is oblique to the continental shelf causing collision to propagate from north to south with time (Suppe, 1984; Teng, 1992; Mouthereau et al., 2001; Liu et al., 2001; Byrne and Liu, 2002; Lin et al., 2003; Sibuet and Hsu, 2004; Malavieille et al., 2002). In the north, collision began sometime between ~4-6.5 Ma but is no longer active, where as in southern Taiwan, collision is just beginning (Suppe 1984; Covey, 1984; Sibuet & Hsu, 2004, Huang et al., 2006). The propagating collision causes the southward growth of Taiwan. With ongoing collision, Eurasian plate sediments are accreted to the growing orogen and the region offshore southern Taiwan emerges.

### *3.3.1 Taiwan stratigraphy*

Taiwan's geology is divided into six regions from west to east: the Coastal plain, the western foothills fold-and-thrust belt, the Hsüehshan Range, the Central Range, the Longitudinal valley and the Coast Range (Figure 3.1, Huang et al., 2006). These geological units extend from northern to southern Taiwan and their pre-collision submarine equivalents can be traced offshore to the south. The Coast Range is the northern continuation of the Luzon volcanic arc. The Central Range consists of Miocene, and perhaps earlier, slates and phyllites, and the metamorphic basement (Ernst & Jahn, 1987; Ho, 1988). Rocks of the Central Range extend to the Hengchung Peninsula which can be traced offshore as the bathymetrically high Hengchun ridge (Huang et al., 2006).

In southern Taiwan, the Central range abuts the hinterland of the western-foothills fold-and-thrust belt (Figure 3.1). The western foothills fold-and-thrust belt borders the entire western edge of the high topography of Taiwan and forms as a growing belt of thrust faults and fault-related-folds that deform Oligocene to Miocene syn-rift, passive margin and synorogenic sediments.

Offshore southern Taiwan, the western foothills fold-and-thrust belt can be traced to the submarine accretionary prism which is formed by the east-directed subduction of the Eurasian plate, and the western foothills arcuate deformation front can be traced southward to the Manila trench.

In northern and central Taiwan, the Hsüehshan Range separates the Western foothills and the Central Range, but the Hsüehshan Range ‘pinches out’ to the south (Figure 3.1). The Hsüehshan Range, contains Eocene-Oligocene and perhaps earliest Miocene syn-rift and passive-margin weakly-metamorphosed slates and carbonaceous sandstones (Ernst & Jahn, 1987; Ho, 1988). The lithology of rocks in the Hsüehshan Range are similar to the passive margin sediments of the western foothills, but are distinguished from the western foothills by the appearance of slaty cleavage. The western foothills and the Hsüehshan Range are separated by the Chuichui fault (also known locally as the Shuichangliu, Shulikeng and ChaoChao faults)(Ho,1988). The Hsüehshan Range is separated from the Central Range based on lithology; the Hsüehshan Range contains thick sandstone units and almost no limestone, whereas the Backbone Range contains limestone and only thin sandy units. The absence of Hsüehshan Range rocks in southern Taiwan indicates that either this strata never existed in the south because, for example, of basement topography, or indicates that the nascent collision in the south has not yet exposed rocks of the Hsüehshan Range.

With the exception of the Coast Range, the rocks of Taiwan are derived from sediments which were deposited on the Chinese passive margin and subsequently accreted. A significant proportion of the stratigraphy is incorporated into Taiwan by the westward propagation of thrust faults in the fold-and-thrust belt that step into the undeformed passive margin and synorogenic Pliocene to recent sediments of the Coastal plain.

### *3.3.2 Western Taiwan structure*

In western Taiwan, the dominant mechanism of accretion and deformation is brittle faulting. Although there are numerous tight folds and near-vertical beds, the

gross structure is one of fault-bend folding where faults run along different décollement layers linked by ramps (Suppe, 1983). Anticlines and synclines form above changes in dip of the faults. In western Taiwan, the stratigraphy of the western foothills, Hsüehshan Range and Central Range is deformed by a series of west verging thrust faults that presumably sole to the main seismically illuminated Taiwan décollement located within the Eocene - early Miocene section (Suppe, 1980a;b;1981; Tillman & Byrne, 1996; Hickman et al. 2002; Carena and Suppe, 1999). The thrust faulting results in a series of repeated sections.

The thrust faults hinterland-ward of the active faults at the deformation front, the faults in the Hsüehshan Range, and the faults that separate the different geologic regions, despite appearing to be major tectonic features appear to be inactive (Shyu et al., 2005; 2006). Here we document the geometry and evolution of these thrusts and fault-bend-fold structures in the western part of Taiwan using AFT and AHe ages collected along three transects which span the island (Figure 3.1).

### **3.4 Methods**

#### *3.4.1 Sampling Strategy*

Previously measured apatite fission track ages in the western foothills are partially-reset or unreset (Liu et al., 2001; Willett et al. 2003; Fuller et al. 2006) as is typical in fold-and-thrust belts. To maximize the potential of collecting material that yielded reset fission track ages, we tried to sample the more deeply exhumed Miocene stratigraphic units which are exposed in the core of anticlines and in the hangingwall immediately behind a thrust fault. To identify sampling targets, structures and stratigraphic units, we used a combination of field geology, published geology (1:100000 Chinese Petroleum Maps, Tainan (1989) and Taichung (1982) sheets, and MOEA 1:50000 geologic maps, Chasien sheet (2000), Kuoshing sheet (1999), Hsintien (2000) & Taoyuan sheets (1996)). Unfortunately, thrust faults and stratigraphic boundaries are often difficult to detect in the field. Faults juxtapose similar lithologies, and the lithology of each stratigraphic unit varies both laterally and vertically as a result

of accretionary prism processes, inherited syn-rift basement topography, and eustatic sea level change (Ho et al., 1988).

Stratigraphic units deposited in the deeper parts of the depositional Miocene basin are more likely to have been buried to temperatures high enough for fission tracks to anneal and samples to yield reset fission track ages. However, the finer grained rocks deposited in the deeper water are problematic for AFT and AHe dating that need the large apatites found in coarser grained material to obtain meaningful results. Our ultimate samples were thus a compromise between a desire for coarser lithology and the most deeply buried units.

Our three sampling transect locations (Figure 3.1) were chosen to achieve north to south spatial coverage while crossing regions of the thrust belt with good exposure of the deeper Miocene units. The spatial distribution of the transects - northern, central and southern - cross the western Taiwan at 3 different stages of collision. Collision is thought to have begun earliest in the north, and propagated south so the 3 transects provide snapshots of the thrust belt at different stages of arc continent collision (Suppe, 1984). Collision is oldest in the north, developed and ongoing in central Taiwan, and youngest in the south.

Initially we collected samples across fault structures in an attempt to date thrust motion by identifying changes in the cooling age across the fault. However, numerical model results demonstrate that sharp breaks in cooling age do not exist in fold-and-thrust belts with foreland propagating structures without out-of-sequence thrusting (Chapter 2).

The only sharp thermochronometric age difference that might exist in a foreland propagating thrust sequence is the change from reset ages in the hanging wall to unreset thermochronometric ages in the footwall. If there is a thermochronometric age change from reset material in the hanging wall to unreset material in the footwall, then the fault was active at the time recorded by the reset cooling age. In the absence of a mapped fault, the change from unreset to reset age over a short distance (as short as ~1 km) is not necessarily evidence of an unidentified surface breaking thrust but is consistent with



material being exhumed by a ramp located at depth. A change in thermochronometric cooling ages on either side of a thrust fault does indicate ‘out-of-sequence’ fault motion, that is thrust structures that are active behind the deformation front.

There are no vertical relief profiles in our study. Age-elevations transects are problematic in thrust belts because the kinematics of multiple thrust-fault deformation causes rapid age variations over short horizontal distances requiring sample locations to be near vertical to give meaningful results (Chapter 2). If transects are not vertical, a change in age with elevation will in part record the non-constant cooling histories generated by a forward propagation thrust fault sequence.

#### *3.4.2 AFT and AHe Methods and Data*

Samples were dated by the apatite fission track method and by (U-Th)/He in apatite. The apatite fission track method makes use of damage tracks in the apatite crystal lattice left by the spontaneous decay of  $^{238}\text{U}$ . Above  $\sim 120^\circ\text{C}$  tracks anneal and below  $\sim 60^\circ\text{C}$  tracks are retained on Ma timescales (Ketcham et al., 1999). (U-Th)/He in apatite uses the decay of uranium and thorium to helium. Above  $\sim 70^\circ\text{C}$ , helium is lost from the apatite grain and below  $\sim 40^\circ\text{C}$  helium is retained on Ma timescales. These temperature ranges define partial annealing or partial retention zones separating regions of total decay product retention and total decay product loss. The exact temperature of these zones changes with cooling rate and chemical composition of the grain. The low-temperature sensitivity of these two systems makes them a valuable tool for investigating the upper crustal patterns of exhumation and low-temperature material cooling histories that exist in western Taiwan.

AFT analyses were completed by Apatite to Zircon Inc, and (U-Th)/He were completed by Apatite to Zircon Inc, P. Reiners at Yale University, and D. Stockli at the University of Kansas.

##### *Apatite fission track method*

20 fission track samples were analyzed using the conventional external detector method (EDM, Tagami and O’Sullivan, 2005, Table 1) and 23 samples were analyzed

using Laser Ablation-Inductively Coupled Plasma-Mass Spectrometry (LA-ICPMS, Hasebe et al., 2004, Table 2). In the conventional EDM fission track analysis, an external detector records the number of  $^{235}\text{U}$  atom fissions induced when a sample is irradiated with low-energy thermal neutrons. Knowing the thermal neutron flux, the  $^{235}\text{U}$  concentration is calculated from the number of induced tracks, and the abundance of  $^{238}\text{U}$  is estimated using the natural constant ratio  $^{235}\text{U}/^{238}\text{U}$ .

The LA-ICPMS method measures the ratio of  $^{238}\text{U}$  to the isotope  $^{43}\text{Ca}$ .  $^{43}\text{Ca}$  indicates the amount of apatite ablated, and  $^{238}\text{U}/^{43}\text{Ca}$  is used to calculate the  $^{238}\text{U}$  concentration. LA-ICPMS AFT analysis is receiving increased attention because unlike the traditional EDM, it does not require a nuclear reactor and it provides a direct measure of  $^{238}\text{U}$  rather than inferring the concentration of  $^{238}\text{U}$  from the number of induced tracks.

Each of these AFT measurement methods produce an AFT age that is interpreted to be reset, partially-reset, or unreset. Partially-reset and unreset AFT ages are abundant in regions like western Taiwan reflecting the shallow burial and small amounts of exhumation across the thrust belt. Partially-reset and unreset AFT pooled ages place limits on the amount of exhumation but do not constrain the exhumation time or rate. Partially-reset ages result from different fission track annealing temperatures caused by the different chemical and physical properties of each apatite grain (typically > 30 grains in one sample) (Donelick et al., 2005, Carlson et al., 1999).  $D_{\text{par}}$  is used as a proxy for the chemistry controlling the annealing temperature with higher values of  $D_{\text{par}}$  reflecting higher closure temperatures (Ketchum et al., 1999;2000, Donelick et al., 2005). When material is buried to the fission track partial annealing zone, grains with a higher annealing temperature (higher  $D_{\text{par}}$ ) retain fossil tracks while tracks in grains with lower annealing temperatures (lower  $D_{\text{par}}$ ) fully heal. When material is exhumed, only the material with lower closure temperature will record the most recent exhumation, the apatite grains with higher closure temperatures retain an older pre-depositional age. The youngest exhumation event can be determined by identifying the population of reset grains that have a slightly lower closure temperature.

BINOMFIT (Brandon et al. 1992; Brandon, 2002) is a program that uses binomial peak fitting (Galbraith and Green 1990, Galbreith and Laslett, 1993) to separate mixed fission track sample ages into different age populations. This program is widely used in detrital thermochronometry to separate grains with different provenance (e.g., Stewart and Brandon, 2004; Barnes et al., 2006) and is also useful in partially-reset mixed age samples to identify the youngest age population that records the most recent cooling event (Brandon et al., 1998). The peak of the grains with reset ages is referred to as a young peak age (YPA). The ability to extract cooling ages from partially-reset samples makes BINOMFIT an important tool to analyze samples collected from the fold-and-thrust belt which have been exhumed from low temperatures ( $< \sim 140$  °C) and as a result, are often partially-reset. Also, BINOMFIT appropriately analyzes samples with grains that contain a large number of grains that have few to zero spontaneous fission tracks. In western Taiwan, grains with few to no spontaneous tracks are abundant, reflecting the very rapid rates of exhumation. These zero track grains are important and can be used to place an upper limit on the amount of time that material has passed through the closure temperature using appropriate analysis (Sneyd, 1984; Brandon et al., 1998).

The binomial peak fitting method relies on the poissonian nature of nuclear fission counting statistics (Brandon, 1992). Two poissonian processes, in this case the number of spontaneous tracks and the number of induced tracks measured using the conventional fission track method EDM, can be approximated by a single binomial distribution (Galbraith and Green, 1990). In the LA-ICPMS method, the number of spontaneous tracks is poissonian, but measuring the  $^{238}\text{U}/^{43}\text{Ca}$  ratio (Pi) is not. This means the ratio  $N_s/P_i$  can not be approximated by a binomial distribution and it is inappropriate to use BINOMFIT to analyze samples measured with LA-ICPMS.

To analyze our data using the binomial peak fitting method and BINOMFIT, we use  $^{238}\text{U}/^{43}\text{Ca}$  measured with ICPMS as a proxy for the number of induced fission tracks in the conventional EDM (Appendix 1). We then analyze the samples in the conventional way with BINOMFIT. This is not an ideal analysis method, but samples

from similar locations analyzed with the two different methods (ICP-MS and EDM) yield the same approximate age giving confidence in our proxy method (e.g., samples 24\_01 & 41\_05 YPA = 2.0 Ma; samples 06\_04 & 07\_04 YPA = 3.5 Ma, tables 1 & 2).

#### *Apatite (U-Th)/He Method*

(U-Th)/He in apatite dating is an increasingly important low-T thermochronometric method. (U-Th)/He in apatite has a closure temperature of around 70°C making this system particularly attractive in the western foothills fold-and-thrust belt where the slightly higher closure temperature (~110°C) system AFT often results in unreset AFT ages.

Despite the relevance of AHe dating to the fold-thrust belt, it is difficult to obtain good results in detrital sediments like those in the western Foothills. Identifying the inclusion free-grains required for (U-Th)/He dating is complicated by grain frosting, which is a particular problem in detrital sediments, and detrital (U-Th)/He in apatite analyses are hampered by apatite grains with low uranium. Our AFT and AHe dating was completed by Apatite to Zircon Inc who have developed a method of obtaining AFT and AHe ages from the same apatite grain in an attempt to minimize these traditional problems. The apatite grains are first dated using the fission track method making it possible to identify grains with high uranium content. Polishing the grain for fission track dating removes any frosted surfaces that conceal the grain interior. The grain interior can then be viewed at high resolution (1562.5x at Apatite to Zircon Inc) so that inclusion free grains can be picked for (U-Th)/He analysis.

### **3.5 Thermochronometric Data**

#### *3.5.1 Apatite Fission Track Data*

We interpret each AFT age as reset, partially-reset, or unreset (Brandon et al., 1998, Table 3.3). ‘Unreset’ material is exhumed from above the closure temperature and retains a detrital age. These ages do not document cooling, but they do place an upper limit on the total amount of exhumation. ‘Reset’ AFT samples have been buried

to temperatures sufficient to for fission tracks in apatite to fully anneal before being exhumed with the onset of collision. ‘Partially-reset’ AFT samples record that material has not been buried to temperatures sufficient for all apatite grains in the sample to record reset AFT ages, but age population analysis provides the age peak of the population of grains with a slightly lower closure temperature that are reset and do record collision-related cooling (the young peak age, YPA).

Table 3.3 shows the classification of reset, partially-reset, or unreset interpreted for each AFT sample. To classify each sample we consider the depositional age of the sample, the  $\chi^2$  statistic for the sample grain ages, and the annealing properties of the individual grains. The  $\chi^2$  test classifies a grain-age distribution as either concordant ( $P(\chi^2) > 5\%$ ) and passing the  $\chi^2$  test, or discordant ( $P(\chi^2) < 5\%$ ) and failing the  $\chi^2$  test (Galbreith, 1981; Green, 1981). In general, material is interpreted to be fully reset if the sample passes the  $\chi^2$  test and is significantly younger than the depositional age. In a few cases, although a sample fails the  $\chi^2$  test, we classify it as reset because BINOMFIT analysis finds a youngest age population that is approximately equal to the pooled age, and the samples contain only a small number of grains that retain a detrital age. Material is interpreted as partially-reset, if a sample contains grain ages both younger and older than deposition and analysis using BINOMFIT identifies a young peak age which is younger than the depositional age. Material is interpreted as unreset if the pooled age is older than or approximately equal to the depositional age or the YPA is significantly older than the beginning of arc-continent collision. The large number of unreset and partially-reset fission track samples (Table 3.3, Figures 3.2, 3.3, 3.5) and the existence of old grains even in samples that we classify as reset, indicate shallow exhumation across the whole thrust belt and a short time ( $< 10$  Ma) between deposition, burial, and exhumation.

Our samples show a general relationship between  $d_{par}$  and AFT grain age. In reset or partially-reset material, grains that retain an inherited age have  $d_{par} > 2.0$  and grains that are reset have  $d_{par} < 1.6$ .

### 3.5.2 AHe data

We obtained a total of 62 ages from 18 different samples in the central and southern transects (Table 3.4, 3.5). The data shows considerable scatter. We attempted to obtain three consistent repeat AHe ages for each sample dated, but this was achieved only for one sample (sample 08\_04, table 3.5). Two repeat grain ages with overlapping errors were observed in 12 samples, and AHe ages from the remaining 6 samples show no consistent pattern. We interpret the scatter to be in part a signal of partial resetting of the (U-Th)/He system, but scatter is observed even in material with a reset AFT age indicating heating above the AHe closure temperature.

Inconsistent AHe sample ages might arise from 1) variations in the chemical composition of the apatite grain, 2) variations in grain size, or 3) radiation damage. These first two explanations for the scatter do not apply. Unlike AFT, the AHe closure temperature is not thought to be affected by chemical composition and our AHe age variations do not correlate to  $d_{par}$  which is a proxy for chemical composition, and our data shows no relationship between age and grain size measured by the FT correction factor (Table 3.4, 3.5). Farley (2000), Green et al. (2006), Schuster et al. (2006), and Flowers et al. (2007), argue that increased radiation damage can increase the AHe age because He gets ‘trapped’ in a damaged crystal lattice retarding diffusion. The suggestion is that greater radiation damage increases the AHe effective closure temperature resulting in different AHe age for grains with the same cooling history. Material in the fold-thrust belt has been exhumed from temperatures beneath the closure temperature for radiation damage ( $T_{rda} \sim 150^{\circ}\text{C}$ , Schuster et al., 2006) making radiation damage an attractive explanation for the data scatter. However, our AHe ages show no correlation to Uranium or Helium concentration, or to spontaneous fission track density, a form of radiation damage (Table 3.5).

There is some encouraging consistency to the AHe data in that for all grains except two, the fission track grain age is older than the He age for the same grain. In general, AHe sample grain ages show more consistency in material that has a reset AFT

age recording burial to near or above to the radiation damage closure temperature. We favor the explanation that the scatter in the grain ages is a combination of shallow and short burial that results in partially reset AHe ages, and changes in the He diffusion from radiation damage.

### **3.6 Discussion**

Below we discuss our interpretation of the AFT and AHe data along each of the 3 sampling transects (central, northern and southern). Along each transect, the locations of AFT and AHe reset and unreset ages constrain the distribution, amount, and time of exhumation across western Taiwan. The distribution of reset, partially-reset, and unreset AFT and AHe ages also constrains the temperature, and by inference, the maximum burial depth of different stratigraphic units. If there are no lateral variations in the stratigraphic thickness or the geothermal gradient, the AFT and AHe ‘closure temperature’ zone will be contained in one stratigraphic horizon along the length of the transect and the closure temperature zone can be used as a proxy for the formation burial depth.

Constraining the temperature and depth of different stratigraphic units also constrains the geometry of thrust faults along each transect. In the following discussion, previously published geological cross-sections and the observed surface structure is used to identify the stratigraphic unit(s) that contain the décollement(s) into which the surface thrust faults sole. Recognizing the stratigraphic layer that contains the décollement, and having identified the depth of the stratigraphic layer using reset and unreset samples places limits on depth to décollement(s) along each sampling transect. Knowing the depth of the décollement relative to the closure temperature is crucial to recognize the geometry and depth of thrust ramps that are responsible for the exhumation recorded by the AFT and AHe cooling age. Thrust ramps above a décollement that is shallower than the closure temperature zones can not exhume material with reset ages.

### 3.6.1 Central Data Transect

The central transect passes southeast of the 1999 Chi Chi earthquake epicenter rupture, and just to the north of the Puli basin (Figure 3.1). At this latitude, collision is well established and ongoing (Shyu et al., 2005, Yue et al., 2005).

The transect passes through Pleistocene, Pliocene, Miocene, and Oligocene (perhaps Eocene) passive margin and synorogenic rocks of the western Foothills and the eastern Hsüehshan Range (Figure 3.2, Figure 3.3). In central Taiwan, the structure of the active Changhua and Chelungpu thrusts at the very western edge of the foothills has been well constrained by detailed seismic, geomorphic and geological data (e.g., Yue et al, 2005; Simoes et al., 2007). Geodetically and geomorphically measured rates of horizontal shortening are ~25-40 mm/yr and are concentrated across the frontal few thrusts that define the deformation front (Simoes et al., 2006; Yu et al., 2001; Yue et al, 2005).

This transect crosses 5 major faults: the Shuantung fault, the Kueipu fault, the Kuoshing fault, the Shulikeng fault and Meiyun fault. The Shuantung fault is immediately behind the active Chelungpu fault. The youngest Pliocene and Pleistocene stratigraphic units are uplifted and exposed at the west end of the transect in the frontal thrust sheets of the western foothills, and the oldest Oligocene rocks of the Hsüehshan Range are exposed to the east (Figure 3.3, 3.4).

There is structural evidence for at least two different décollement layers in the western foothills. An upper décollement at ~ 3-5 km is in the Pliocene Chinshui shale which is exhumed in the hangingwall of the Chelungpu thrust. Structural constraints in the Chelungpu thrust sheet dictate that this décollement must have extended horizontally beneath the entire thrust belt and almost all of the Hsüehshan Range at the time the Chelungpu thrust was activated (Yue et al., 2005).

A second décollement must exist beneath the Chinshui décollement because Miocene and Oligocene units crop out in the rear of the western foothills and Hsüehshan Range. There are no obvious beds that parallel faults in the Miocene units of the Shuantung thrust sheet to identify the stratigraphic layer that contains décollement.



Yue et al., (2005) use the thickness of the section in the Shuantung thrust to constrain the deep décollement at 10 km in the Tachien sandstone, coincident with the depth of the seismically imaged main décollement (Carena et al., 2002).

#### *Central Transect Thermochronometry*

We collected 14 AFT and 14 AHe ages along the central transect. AFT ages from the western foothills samples are partially-reset and AFT ages from the Hsüehshan Range samples are reset.

The distribution of reset and unreset AFT ages within the stratigraphic column defines the fission track closure temperature to be located at least as deep as the bottom of the Pailiao formation along the central transect (Figure 3.2). Samples in the Peiliao, Talu, and Kuanyinshan formations are partially-reset and exhumed from the AFT partial retention zone (PRZ). To the north the AFT PRZ steps down section to near the base of the Miocene stratigraphy consistent with a northward thinning stratigraphic section (Yue et al., 2005). Samples 1\_04 and 2\_04 are located slightly north of the transect line and record less exhumation than samples in the stratigraphic units to the south (Figure 3.2).

It is surprising that the entire Miocene section has ages that are partially-reset or unreset because along our transect the depth to the overlying Pliocene Chinshui shale is well constrained to be at ~5 km (Yue et al., 2005). Therefore AFT closure temperature depth is > 6 km which implies a low geothermal gradient (< 20°C/km). A low geothermal gradient in the thrust belt is not unreasonable even with the very high exhumation rates. Rapid deposition of thick synorogenic sediments combined with hanging wall cooling by the subducting Chinese basement could depress the geotherm. A second possible explanation is that the Miocene sediments were exhumed before the development of a foreland basin and thus were not buried by a thick package of synorogenic Pliocene sediments like those that overlie the Miocene units today. However, there is sedimentological evidence for a foreland basin at the time of cooling recorded by the oldest AFT ages of 3.5 Ma (Covey, 1984; Simoes and Avouac, 2006).

Either of these two explanations for the AFT closure temperature in the middle to lower Miocene stratigraphy is favored by the short time between burial and exhumation (< 10 Ma) and fast exhumation rates which increase the effective closure temperature and depth (Ketcham et al., 1999).

Eight AFT cooling ages exist along this central transect, 6 are reset and 2 YPA interpreted from samples that are partially-reset. The YPA of partially-reset AFT samples in the Shuantung thrust sheet (including the small Kueipu and Kuoshing thrusts) range from 10.8 Ma to 3.5 Ma. Two samples give consistent YPAs of 10.7 and 10.8 Ma (samples 3\_04 and 4\_04, table 3.2). However, these are interpreted as unrelated to collision as they significantly pre-date the time of the onset of collision based on plate reconstructions (Sibuet et al., 2002). This is also the case for sample 5\_04 (YPA: 8.6 Ma). It is possible that the YPA of 6.9 Ma records the onset of collision related thrusting but because the other AFT YPA and AHe ages in this thrust sheet are significantly younger (~3.5 Ma) we interpret this age as partially-reset and not recording thrust-exhumation.

At the latitude of the central transect, the first record of thrust exhumation is at 3.5 Ma along the Shuantung fault. This places a lower limit on the time of activity of the Shuantung thrust because there is a change from reset to unreset material across the Shuantung thrust (there are no samples in the footwall, but the footwall contains shallowly buried Pleistocene units).

The approximately equal ~3-3.5 Ma AFT and AHe ages in material in the Shuantung thrust sheet indicate this material cooled rapidly through the AFT and AHe closure temperatures at this time (Figure 3.3). The rapid cooling did not occur above the ramp rising from the upper décollement in the Pliocene Chinshui shale because the décollement is above the AFT and AHe closure temperature zone. The rapid cooling indicated by the similar AFT and AHe ages instead records exhumation above the thrust ramp between the upper décollement in the Pliocene stratigraphy and the main Taiwan detachment in the Eocene/Oligocene units (Yue et al., 2005).

The surface exposure of the Shuantung thrust juxtaposes Miocene and the Pleistocene Toukushan formations, therefore this section of the fault must have been active in the Pleistocene during the deposition of the Toukushan formation in the Shuantung thrust at  $< 1.1$  Ma (Simoès and Avouac, 2006).

In the Shuantung thrust sheet, between the time of exhumation above the lower ramp at 3.5 Ma, and exhumation above the ramp that cuts the Toukoushan formation at  $< 1.1$  Ma, material is carried along the upper décollement above the AFT and AHe closure temperature. This scenario is consistent with the regional structural interpretations of Yue et al. (2005) and the above mentioned structural constraint that the décollement in the Chinshui shale extended horizontally beneath the foothills and into the Hsüeshan Range at the onset of activity along the Chelungpu fault at  $< 1$  Ma.

The length of the décollement that separates the surface breaking Shuantung thrust above the upper décollement from the lower ramp linking the upper and lower décollements can be estimated by assuming a slip rate that remains constant through time. We argue that a constant slip rate is a good assumption in western Taiwan. The almost identical AFT and AHe ages indicate fast exhumation at the onset of thrusting at 3.5 Ma and fast rates of shortening and uplift are recorded geomorphically and geodectically today. There is no obvious reason for shortening to slow between the earliest recorded cooling at 3.5 Ma and present. Assuming slip occurred at 15 mm/yr, which is the estimated slip rate across the Chelungpu thrust (Simoès and Avouac, 2006), for 3.5 Ma constrains the length of the ramp to be  $\sim 53$  km. Assuming a higher slip rate 40 mm/yr suggested for the main décollement (Simoès and Avouac, 2006) gives a length of the upper décollement of  $\sim 140$  km.

The age of initiation of the Shuantung thrust of 3.5 Ma is significantly older than the 1.1 Ma of Simoès and Avouac (2006). However, the thermochronometric data does not record the age of initiation of the surface exposure of the Shuantung thrust that is above the AFT and AHe closure temperatures. Instead the 3-3.5 Ma ages record exhumation above a ramp *beneath* the décollement into which the surface trace of the

Shuantung thrust soles. Thus the AFT and AHe data are consistent with a younger age of initiation for the current surface trace of the Shuantung thrust.

In the Shulikeng and Meiyuan thrust sheets (Figure 3.4) AFT cooling ages are reset and, for the most part, younger than the cooling ages in the Shuantung thrust. The youngest age is located significantly north of the transect in the core of the Tachien anticline which can be traced southward to east of our transect (23\_04, 0.7 Ma). The youngest cooling ages located along our central transect are samples 18\_04 (2.3 Ma) and 14\_04 (1.4 Ma) in the Meiyuan thrust sheet. This pattern of the youngest cooling ages in the hinterland and older cooling ages in the foreland of the thrust belt is indicative of material exhumed above a ramp and carried horizontally along an upper flat (Bollinger et al., 2004; 2006; Huerta & Rodgers 2006; Chapter 2). Material becomes progressively younger toward the ramp because it has spent less time above the upper flat since exhumation above the ramp. This interpretation is very different than the interpretation of ages in each thrust sheet as recording slip along each independent thrust fault.

The Shulikeng fault separates the western foothills and the Hsüehshan Range (Figures 3.3, 3.4). This fault is generally accepted as a west-verging thrust although it has also been interpreted as a west dipping normal fault (Yue et al., 2005). Along our transect, the Shulikeng fault juxtaposes the upper Oligocene Shuichangliu formation against the middle Miocene Nankang formation (Figure 3.2, Figure 3.4). Vitrinite reflectance records a thermal offset across this structure ( $< 84^\circ$ , Sakaguchi et al., 2007). AFT are reset on the east side of the Shulikeng fault, and partially-reset on the west side of the fault consistent with higher temperatures to the east recorded by vitrinite reflectance. However, the existence of partially-reset samples in the Shuantung thrust sheet records a maximum temperature that is less than the  $200^\circ\text{C}$  recorded by vitrinite reflectance (Sakaguchi et al., 2007).

The cooling ages on either side of the Shulikeng fault are approximately equal. On the east side, sample 9\_04 has a pooled age of 2.8 Ma and the AHe Ages are 2.6, 2.5 and 3.4 Ma, sample 11\_04 has a pooled age of 2.4 Ma. The similar AHe and AFT ages

indicate rapid cooling though the closure temperature at around 2.6 Ma. In the footwall, AFT young peak age are 3.5 Ma (7\_04) and 3.5 Ma (6\_04). AHe ages are 2.1, 2.6 & 4.4 Ma (3\_04); 3.7, 3.5 & 3.1 (8\_04); & 3.6, 3.5, 4.3 Ma (7\_04). These ages on the west side of the fault indicate rapid cooling from the partial annealing zone at ~3-3.5 Ma, which is identical to the east side within error. There might be a step in cooling age across of the fault of 0.5-1 Ma indicating out-of-sequence thrust motion along the Shulikeng thrust and motion along the thrust above the AFT and AHe closure temperatures, but this is of small magnitude. Our preferred interpretation is that this section of the Shulikeng thrust was active beneath the AFT and AHe closure temperatures and is an exhumed section of the ramp between the lower Pliocene and Oligocene/Miocene décollements. Material in both the hangingwall and footwall of the Shulikeng fault was exhumed though the closure temperature together at around 3 Ma by a younger ramp that formed toward the foreland. This interpretation means the thermochronometric ages do not record the time of activity of the Shulikeng fault though if there is a real change of 0.5-1 Ma between the ages in the hangingwall and footwall, the fault was active at ~ 2.5 Ma.

The youngest age in the core of the Tachien anticline records the most recent exhumation and constrains the present location of the buried thrust ramp that soles into the main Taiwan décollement to be east of our transect beneath the central Hsüehshan Range. Based on balanced cross sections, a ramp at this location was suggested by Yue et al. (2005).

### *3.6.2 Northern Transect*

The northern sampling transect passes through the northern end of Taiwan just south of Taipei (Figure 3.1). At this latitude, because of the southward propagating collision, structures are probably not accommodating collision and the orogen is no longer active (Sibuet and Hsu, 2004). The onshore continuation of the Okinawa trough back-arc basin, the Ilan plane, is located southeast of the transect (Figure 3.1). The Ilan plane is extending as part of the back-arc system of the northward directed Ryuku

subduction zone. It is possible that structures along our northern transect are reactivated as normal faults that accommodate extension as part of the back-arc system (Teng, 1996; Hu et al., 2002; Sibuet and Hsu, 2004; Shyu et al., 2005). However, the characteristics of the structures and stratigraphy along the northern transect are the same as those along central and southern Taiwan; eastward dipping, westward verging thrust faults which deform Pliocene, Miocene, and Oligocene passive margin and synorogenic sediments into a series of fault-bend-folds. Therefore, although these structures might no longer accommodate active convergence, the thrust faults and folds and patterns of long term exhumation have not been significantly overprinted by Quaternary extension.

#### *Northern Transect Stratigraphy and Structure*

The transect crosses Pliocene, Miocene, Oligocene and perhaps Eocene rocks of the Western foothills fold-and-thrust belt and the Hsüehshan Range. This material is deformed by eight major thrust faults; the Hsinchuang fault, Taipei fault, Chengfu fault, Hsientien Fault, Lumintan fault, Chuchih fault, the Fushan fault, and the Chinkualiao fault (Figure 3.1, 3.5). The youngest unit exposed is the Kuichelin formation in the Hsinchang thrust sheet. The oldest and deepest stratigraphic units are exposed in the Hsüehshan Range in the hangingwall of the Chuchi and Chinkualiao faults (Figure 3.6).

The stratigraphic units exposed in each thrust sheet shows the thrust faults along the northern transect sole into at least three décollement layers (Suppe, 1980b). One décollement is in the lower Miocene/upper Oligocene Tatungshan (or Wushihshan) formation (Figure 3.2). The Tatungshan formation crops out in the hangingwall of the Hsintien thrust and the stratigraphy dips parallel to the Hsintien thrust fault indicating that the Tatungshan formation contains a décollement layer (Figure 3.6). West of the Hsintien thrust, the Tatungshan formation is not exposed but it is likely that this stratigraphic unit is also the décollement layer in the Hsinchuang, Taipei and Chengfu faults (Suppe, 1980b, Figure 3.6). There is no evidence that deeper stratigraphic units are involved in the thrust sheets in the western foothills. Suppe (1980b) interprets a second décollement above the décollement in the Tatungshan formation.

The older Oligocene rocks contained in thrust sheet in the Hsüehshan Range are evidence that the décollement steps down the section into a unit stratigraphically beneath the Tatungshan formation. The undifferentiated argillaceous rocks in the Hsüehshan Range make it very difficult to identify any exhumed footwall or hangingwall flats. The deepest stratigraphy exposed in the Hsüehshan Range is the Hsintin formation in the core of anticlines to the east of our transect so a third major décollement must exist in this lower Oligocene unit.

The ramp that links the décollements in the Tatungshan and the Hsintin formations is a major feature on the order of 4 km high (Suppe, 1980b). The largest structure along the northern transect, the Chatienshan anticline, likely forms as an anticline above this major ramp.

#### *Northern Transect Thermochronometry*

Ten apatite fission track ages were obtained along the northern transect (Figure 3.5). Along this transect, AFT ages in the western foothills are partially-reset or unreset, and ages in the Hsüehshan range are reset (Figure 3.5). The two samples collected in the hangingwall of the frontal thrust, the Hsinchuang fault, are unreset (2\_05, 3\_05) and AFT ages in the Hsintien and Lumuntan thrust sheets are partially-reset (samples 4\_05, 8\_05, 10\_05, Figures 3.5, 3.6, table 3.3). In the Taipei thrust sheet between these unreset and partially-reset samples, sample 7\_05 is fully reset even though it is collected from a stratigraphic unit that is above than units containing samples with partially-reset samples. This anomalous record of deeper exhumation of younger stratigraphy must reflect localized burial in the northern part of the sampling region (Figure 3.5). All AFT samples in the Hsüehshan Range Oligocene rocks located behind the Chuchih fault are fully reset (samples 11\_05, 12\_05, 13\_05, 14\_05, Figures 3.5 3.6, table 3.3).

This pattern of reset material in the Hsüehshan Range and unreset AFT ages in the western foothills constrains the depth of the Tatungshan formation, which is a décollement layer, to be approximately equal to the depth of the fission track closure temperature. Local variations in the stratigraphic thickness recorded by the anomalously

reset sample 7\_05 appears to be great enough to place the Tatungshan formation either entirely above or entirely below the AFT closure temperature.

The décollement that exists in the lower Oligocene rocks of the Hsüehshan Range is beneath the AFT closure temperature. If the décollement layer in the Western foothills is around 5 km (the approximate depth to the AFT closure temperature for normal crustal heat flows) and the ramp linking the upper décollement in the Tatungshan formation and the lower décollement in the lower Oligocene strata is on the order of 4 km (Suppe, 1980b), the depth of the lower décollement is ~9 km. This depth is around the depth of the main Taiwan décollement seismically illuminated at ~10 km further south (Carena et al., 2002).

We obtain 7 AFT cooling ages along the northern transect, 5 as reset pooled ages, and 2 as YPA from partially-reset samples. The cooling age pattern shows a general trend of younger cooling ages in the east and older cooling ages in the west (Figure 3.5 & 3.6). The youngest cooling age occurs on the eastern flank of the Chatienshan anticline in the hangingwall of the Chuchih fault (14\_05, 1.2 Ma, Figure 3.6). The oldest cooling ages are around 3 Ma in the Lumintan and Hsintien thrust sheets toward the front of the thrust belt.

This thermochronometric cooling-age pattern of older cooling ages toward the front of the thrust belt and younger cooling ages to the rear, is consistent with material being exhumed over the décollement ramp between the Tatungshan formation and the Hsitsun formation and then carried horizontally along the upper décollement (Bollinger et al., 2004; 2006; Huerta and Rodgers, 2006; Chapter 2). The greater amounts of exhumation in the Hsüehshan Range and the younger ages in the Hsüehshan Range is interpreted to result from the migration of the ramp that links the two identified décollement layers.

### *3.6.3 Southern Transect*

The southern sampling transect is east of Tainan and north of the Pintung basin crossing the youngest part of the western foothills fold-and-thrust belt (Figures 3.1, 3.7).



The southern fold-thrust-belt is a zone of active collision with rapid rates of short-term uplift and shortening recorded across the westernmost structures of the western foothills and at the deformation front (Yu et al., 1997; Fruneau et al., 2002; Shyu et al., 2005).

Samples along the southern transect are collected from Miocene rocks of the western foothills fold-and-thrust belt and Miocene rocks of the eastern Central Range (Figure 3.1). This transect does not cross the Hsüehshan Range that ‘pinches out’ to the north of the transect so that the western foothills directly juxtapose the Central range (Figure 3.1). The sampling transect crosses 5 major faults; the Lunhou, Chutouchi, Pingshi, Chishan and Tulugwun faults (Figures 3.7, 3.8 & 3.9). These faults, and currently active blind thrusts have deformed the Miocene and Pliocene stratigraphy into a sequence of folded repeating sections (Suppe, 1980a; Hickman et al., 2002; Huang et al., 2004; Fruneau et al., 2002).

There is stratigraphic evidence for a décollement at the base of the middle-upper Miocene Changshikeng formation (Nanchuang formation, Figure 3.2). The Changshikeng formation is exposed in the hangingwall of the Lunhou, Chutouchi and Pingshi thrust sheets and run parallel to the faults as is characteristic of a décollement layer (Figures 3.7 & 3.9, MOEA 1:25000 Geologic map, Chasien sheet, 2000). There is evidence for a second deeper décollement. The upper Miocene Changshikeng formation crops out in the Chishan thrust sheet, but as a hangingwall cut-off formed as the thrust steps down section, and the lower Miocene Mushan formation is contained in imbricate thrust sheets beneath the Chaiyi hills (Suppe, 1980a). There is no obvious décollement layer in the Chishan or Tulungwun thrust sheets. Suppe (1980a) places a lower décollement in the lower Miocene Mushan formation at ~6-8 km, and Hung & Wiltschko, 1993, Hung et al., 2000, and Hickman et al., 2002, place this décollement at 9-13 km in the lower Miocene or upper Oligocene stratigraphy. The depth of the deeper décollement is at approximately the depth of the main Taiwan décollement at 10-12 km (Carena et al., 2002).

*Southern transect thermochronometry*

We obtained 19 AFT and 39 AHe ages along the southern transect (Figure 3.7). All AFT ages in the Lunhou and Chutouchi thrust sheets are unreset and AFT ages in the Chishan and Tulungwun faults are partially or fully reset (Figure 3.9). Different stratigraphic depths can not explain this distribution of reset and unreset AFT ages. In the Pingshi thrust, material in the front of the thrust sheet in the Miocene Tatungshan formation is unreset (36\_04), where material from the Aliaochio formation at the rear of the thrust sheet is partially-reset (33\_04). This counterintuitive pattern indicates local burial or burial in the eastward deepening foreland basin.

The majority of AHe ages presented in this paper were collected along the southern transect. The AHe ages show considerable scatter but are generally more consistent to the east. Our interpretation is that the scatter in the western AHe ages are partially or un-reset AHe ages, where as AHe ages in the eastern part of the study area have experienced greater burial and are reset with more consistent AHe sample ages. The relative burial depths recorded by reset and unreset AFT samples are consistent with this interpretation.

In the northern and central transects the AFT cooling ages become older toward the foreland. The opposite cooling age trend is seen along the transect in the south. The youngest AFT age is located in the center of the Chishan thrust sheet (35\_04, 0.6 Ma, Figure 3.7) and the oldest AFT cooling ages are located at the rear of the Chishan thrust sheet and in the Tulungwun thrust sheet (26\_04; 4.1 Ma, 28\_04; 3.2 Ma, 23\_01; 3.4 Ma, Figure 3.7 & 3.8).

The AFT ages are particularly complex around the Tulugnwun fault (Figure 3.8). The Tulugwun fault (also known as the Laonung fault) separates material in the western foothills from material in the Central range (Figure 3.1). This fault appears to be a major tectonic feature but the nature and significance of this structure is unknown. The Tulungwun fault marks a striking topographic boundary between the Pingtung Valley and the Hengchun Peninsula highlands but there is no geomorphic or geodetic evidence of active faulting (Shyu et al., 2005; Ching et al., 2007). This near vertical

fault is assumed to be a inactive thrust fault which may now have a component of strike-slip (Hickman et al., 2002; Lacombe et al., 2003)) and may link to the active strike-slip faults to the south (Shyu et al., 2005). Along our transect, the Tulungwun fault is difficult to identify in the field. At the latitude of the southern transect, the mapped trace of the Tulugwun fault coincides with an crop out of highly weathered conglomerates (Chinese Petroleum Corporation geological map, Tainan Sheet; 1999 & MOEA Geological Survey geological map; Chasien Sheet, 2000).

We collected a dense suite of AFT ages from either side of the mapped traced of the Tulungwun fault (Figure 3.8). The density of data around the Tulungwun fault allows for a detailed analysis of the stratigraphic and structural relationships that exist. The AFT data shows two distinct groups of ages. The first group of ages are fully reset with pooled ages around  $\sim 3.5$  Ma (23\_01, 26\_04, & 28\_04). The second group of ages are partially-reset with a YPA  $\sim 2$  Ma (24\_01, 24\_04, & 41\_05). These two groups are separated by  $< 500$  m (Figure 3.8). The partially-reset samples in group 2 are located in the hangingwall of the Tulungwun fault, in the lower unit of the Changshan formation. The reset samples in group 1 are in the hangingwall *and* footwall of the Tulungwun fault in the upper unit of the Changshan formation and the Changshikeng formation (Figure 4.2).

The amount of burial implied by the distribution of reset and unreset ages is not consistent with the stratigraphic relationships of the Changshan and Changshikeng formations. Samples in the lower Changshan formation are partially-reset but this unit is stratigraphically beneath the upper Changshan and Changshikeng formations that contains reset ages (Figure 3.2). This apparent anomaly can not be explained by burial in an eastward deepening foreland basin because material to the east material is unreset. Nor can local burial explain the pattern because the samples are located closely spaced to one another. The pattern of reset and unreset samples around the Tulungwun fault can not be explained by different chemical properties that change the temperature annealing because the measured  $d_{par}$  is almost identical in all samples ( $\sim 1.7$ , Tables 1 & 2). Thus, in its most recent history, material in the mapped lower member of the

Changshan formation appears to have been exhumed from above the upper member of the Changshan and the Changshikeng formations and the stratigraphic relationships need to be evaluated.

Despite the sharp change from reset to partially-reset AFT ages over  $< 500\text{m}$ , our preferred explanation of the Tulungwun fault reset and partially-reset AFT ages is that they mark the transition from reset to unrest ages expected above a thrust fault and fault-bend-fold (Chapter 2); AFT ages record exhumation at  $\sim 3.5\text{ Ma}$  and partially-reset samples in group 2 are exhumed from above the AFT closure temperature. The  $\sim 3.5\text{ Ma}$  ages cross the trace of the Tulungwun fault, therefore either the Tulungwun fault is mislocated and is west of the mapped trace, or the AFT ages do not record motion along this thrust structure. Regardless of the interpretation, our low-temperature thermochronometric data, record no recent activity across the Tulungwun fault and the nature and significance of this important structure remain an outstanding problem.

The 3-3.5 Ma cooling ages are a robust signal evident more than 50 km along strike to the south (Fuller et al., 2007). These cooling ages significantly pre-date the onset of arc-continent collision in southern Taiwan making it unlikely the ages record collision of the Luzon arc with the Chinese continental margin. Instead we agree with the interpretation of Huang et al. (2000; 2006) and Lee et al. (2006); the  $\sim 3.5\text{ Ma}$  signal in southern Taiwan and the Hengchun Peninsula record erosion in a subaerial part of the accretionary prism formed by subduction at the Manila trench. Sub-aerial exposure of the subduction accretionary prism is suggested to be the first stage of the southward propagating arc-continent collision (Huang et al., 2000; 2006; Lee et al. 2006), but this is incompatible with the southern extent of AFT reset ages. In a southward propagating system, AFT ages would be progressively older to the south, and material at the southern tip of Taiwan would exhibit partially or unreset ages. Instead reset AFT ages extend almost to the southern tip of the Hengchen Peninsula (Figure 3.1).

The 3-3.5 Ma AFT ages in southern Taiwan are coincident with the 3.5 Ma AFT and AHe ages sampled along the central transect which record the first thrust faulting in central Taiwan. The coincident ages provide a possible explanation for the anomalously

old ages in the south. The onset of thrusting may have led to rapid erosion of the passive margin stratigraphy in central Taiwan that was added to the southward deepening Pliocene basin by longitudinal rivers. This sediment influx may have increased the amount of material accreted to the submarine accretionary prism causing growth and sub-aerial exposure of the prism. This same process is not occurring today, and the accretionary prism southward of the Hengchen Peninsula is not sub-aerial because the basin deepens even further to the south creating a greater accommodation space.

The youngest AFT cooling ages are in the center of the Chishan thrust sheet (35\_04, 0.6 Ma; 33\_01; 0.54 Ma) and slightly cooling older ages of 1 Ma are in the western Chishan thrust sheet and eastern Pingshi thrust sheet (21\_01; YPA=1.3 Ma, 33\_04; YPA=1.2 Ma, 34\_04; 1.0 Ma, Figure 3.7). The age trend for this group of samples is that cooling ages become slightly older toward the west. An increase in the age toward the west is the same pattern seen in the northern and central transects, but the increasing cooling age trend along the southern transect spans < 5 km. Like in the north, we interpret that the westward increasing cooling ages indicates exhumation above a buried ramp and subsequent horizontal transport above a décollement at the top of the ramp. The ramp likely links the décollement in the lower Miocene Mushan formation to a décollement in the Oligocene strata. The narrower width of the age increase compared to the northern transects reflects the incipient nature of collision in the south.

#### *3.6.4 Summary of exhumation in western Taiwan*

Along all three transects, ages in the Eocene-lower Miocene rocks in the Hsüehshan Range and eastern part of the thrust-belt are partially-reset and fully-reset, and ages in the middle Miocene and Pliocene rocks in the center and western thrust belt are unreset. In central and northern Taiwan, almost all the Miocene passive margin stratigraphic section has been exhumed from depths above the AFT closure temperature. In southern Taiwan, the AFT closure temperature is near the top of the Miocene section and Miocene units have been exhumed from depths below the AFT closure temperature. The higher stratigraphic position of the AFT closure temperature in

southern Taiwan is consistent with the southward deepening Miocene-Pliocene basin and southward thickening of the sedimentary units (Covey, 1984). In a few cases, a deeper relative burial depth recorded by the thermochronometric data can not be attributed solely to older stratigraphic units indicating differential burial. These thermochronometric records of differential burial are almost all spatially limited and thus do not appear to record burial in a large eastward deepening foreland basin.

In northern and central Taiwan, the youngest AFT cooling ages are recorded in the eastern part of the Hsüehshan Range. In southern Taiwan, the youngest cooling ages are recorded in the eastern part of the thrust belt. Along all three transects, the general trend is that collision-related cooling ages become progressively older to the west. We believe this trend records thrust motion above a ramp that soles into the main Taiwan décollement (Carena et al., 2002). Motion along the thrust ramp exhumes material in the hangingwall through the AFT and AHe closure temperatures. The ramp links the décollement in the Oligocene/Eocene rocks at ~10 km to a décollement in the Miocene section that is around the depth to the AFT effective closure temperature at ~5 km.

Slip along the thrust ramp is transferred to the décollement in the upper Miocene and lower Pliocene units and then to structures around the deformation front that accommodate rapid shortening by imbricate thrusting, fault propagation folding and surface-breaking thrusts such as the Chelungpu fault (Suppe, 1980a; Hung, 1999; Hickman et al., 2002; Huang et al., 2004; Simoes et al., 2007). This described deformation pattern is consistent with the geodetically measured velocities that show little shortening across the eastern Hsüehshan range and western thrust belt and rapid shortening at the deformation front (Yu et al., 2001; Hsu et al., 2003).

Along all three sections the youngest cooling ages occur in or near the core of major anticlines as characteristic fault-bend-fold anticline formed above the thrust ramp. In the northern section the youngest ages are located in the Chatienshan anticline; in the central transect, youngest AFT age is in the core of the Tachien anticline; in the southern section, the youngest age is in the core of the anticline in the Chishan thrust sheet identified by Hickman et al. (2002). These anticline structures that coincide with

the youngest ages expose the oldest strata in western Taiwan supported the deformation history we depict.

Rather than a single ramp that is stationary with respect to the undefining foreland, the thrust ramp we record with the AHe and AFT ages must migrate to the west with time. In both the single and multiple ramp duplex fault geometries, thermochronometric ages would become younger to the west. In the single fault scenario, the inverse of the rate that the ages change with distance is the velocity of material in the hanging wall (Bollinger et al., 2004; 2006; Huerta and Rodgers, 2006). The velocity calculated using the observed age gradient is ~12 mm/yr in the central and southern transects which is more than half the geodetically and geomorphically recorded rates of shortening (>30 mm/yr, Yu et al. 1997; Simoes and Avouac, 2006). A much slower rate of shortening is inconsistent with the fast exhumation rates recorded by the young AFT ages in the Hsüehshan Range and the hinterland of the western foothills (~0.5 Ma), and the older, but approximately equal, AFT and AHe ages along the central transect. Additionally, the west-verging thrust faults exhumed in the hanging wall of faults, for example, the Kueipu and Kuoshing faults in the Shuantung thrust sheet, document the existence of older thrust faults that are active at depth and exhumed by the Shuantung thrust. Also, a single ramp with the geometry outlined above does not exhume material from depths great enough to expose ZFT ages at odds with the reset ZFT ages in the Hsüehshan Range (Liu et al., 2001; Willett et al. 2003; Fuller et al. 2006).

The implication is that as the thrust ramp migrates, slivers of the Eocene-Miocene passive margin stratigraphy are accreted from the footwall into the hangingwall and the old thrust ramp is exhumed with the newly accreted material. Thus, the east-dipping west-verging thrust fault structures in the Hsüehshan Range are exhumed sections of the décollement ramp.

### 3.6.5 Kinematic-thermal Model of western Taiwan.

Thermal-kinematic thrust fault modeling greatly improves our understanding of the fault kinematics which generate the cooling histories recorded by the thermochronometric age and the significance of the thrust structures in western Taiwan. Using the model described in Chapter 2, we use a thermal-kinematic numerical model to generate a thermochronometric age pattern produced by a migrating thrust ramp with the geometry and evolution described (Figure 3.10 & 3.11). The numerical model couples a 2-dimensional kinematic-structural to a 2-dimensional advection-diffusion thermal model, and models fission track annealing and He retention, to predict low-T thermochronometric ages. The kinematic model allows representation of diverse styles of deformation in a fold-and-thrust belt. We use the deformation kinematic model *2DMove* to generate the deformation field of Suppe-style fault-bend-folding (Suppe, 1983, Figure 3.10). The advection term field is fed into a finite-element, advection-diffusion thermal model thus tracking the thermal response to the faulting and fault-related folding and producing material cooling histories that we use to calculate thermochronometric age (Figure 3.11).

The numerical model shown in Figures 3.10 & 3.11 is based on the thrust geometry and thermochronometric ages along the central transect. The basal décollement is at 10 km and the upper décollement is at 5 km (Figure 3.10). The thrust ramp between these décollements dips at 20° to approximately fit the youngest cooling ages recorded in the Hsüehshan Range for the 30 mm/yr fault slip rate used here (0.5-0.7 Ma, Figure 4.3). Each fault is activated sequentially from the hinterland to the foreland. We have chosen fault spacing to be 20 km. The total slip along each fault is shown in Figure 3.10B. The structure, stratigraphy and fault geometry of the frontal thrusts is taken from the balanced cross-sections of Yue et al., 2005, which are located around our central sampling transect (Figure 3.11A). The thermochronometric pattern generated by this numerical model is similar to the pattern of ages observed along the central transect (Figure 3.11B). Example cooling histories that produced the age pattern are shown in Figure 3.12. Material at the front of the thrust belt (Figure 3.12 A) records



initial thrust motion above the thrust ramp. Material recording the most recent exhumation above the thrust ramp is located at the rear of the thrust belt (Figure 3.12 D).

In addition to the good agreement between the modeled AFT and AHe ages and those observed along the central transect, the gross structure generated by the sequential activation of thrust faults matches the gross structure in the western Taiwan (Figure 3.11A & C). There are, however, inconsistencies. A major inconsistency is that there is no roof thrust identified in the Hsüehshan Range or the Western foothills. There are large syncline structures to the west of the anticlines compatible with our model, but there is no roof thrust or east verging thrust between the anticline and syncline separating the Oligocene and Miocene stratigraphy. However, the undifferentiated Miocene and Oligocene argillites, slates and siltstones of the Hsüehshan Range and western foothills make the exact structure of these rocks difficult to distinguish and it is possible that an unidentified roof thrust does indeed exist.

Another inconsistency is that in the numerical model, shallowly buried rocks crop out in the same thrust sheet as the most deeply exhumed material which is not observed along the central transect. However, the age and stratigraphic relationships of material in the Hsüehshan Range are not clear. The Tachien sandstone may be stratigraphically equivalent to the Paileng formation rather than beneath it (Ho, 1988; Yue et al., 2005). If the Tachien sandstone is stratigraphically equivalent to the Paileng formation, the stratigraphy that crops out in the western foothills and eastern Hsüehshan Range closely matches the stratigraphy generated in the numerical model (Figure 3.11C).

### *3.6.6 Onset of collision-related erosion in the Western Foothills.*

The proposed time for the onset of arc-continent collision ranges from as old as 12 Ma to as recently as 2 Ma, though the generally accepted age of onset is ~6-8 Ma (Byrne and Liu, 2002; Huang et al., 2006). There are 7 AFT YPA ages ~ 10-12 Ma. Given their prevalence it is unlikely that all the 10-12 Ma YPA in material with

different stratigraphic ages and cooling histories are partially-reset ages intermediate between the depositional age and the cooling ages. The ~10 Ma ages in the southern section are detrital ages that pre-date the depositional age of the sediments, thus they do not record thrust exhumation (Samples 29\_04 & 36\_04, Table 3.3). In the northern and central sections, the YPA post-date the depositional age (Table 3.3) and are consistent with the earliest time suggested for collision. However, subduction of the Eurasian plate beneath the Luzon arc to form the Manila trench began at ~ 15 Ma (Sibuet et al., 2002), and there is evidence that subduction continued, even in northern Taiwan, until at least 8.5 Ma (Sibuet et al., 2002; Sibuet & Hsu, 2004; Huang et al., 2006). Therefore, the 10-12 Ma YPA may record a minor exhumational event and there is evidence for erosion at this time (Monthereau et al., 2001; Tensai et al., 2006), we do not believe they record the onset of arc-continent collision.

The oldest AFT age that we interpret as recording collision-related thrust faulting is ~3.5 Ma along the northern and central transects, and ~ 1 Ma in southern Taiwan. This age records vertical advection above a thrust ramp that exhumes material through the AFT closure temperatures. AFT and zircon fission track collected from the Central Range show approximately the same 3.5 Ma maximum cooling age (Liu et al., 2001; Willett et al. 2003; Fuller et al. 2006; Lee et al., 2006). These studies do report a few ages older than 3.5 Ma but these are all at the edge of regions of reset ages and are likely partially reset (Fuller et al., 2006). Therefore low-T thermochronometric ages in Taiwan show no record of the generally accepted ~6-8 Ma for the onset of collision. Material recording earlier thrusting could, however, have been removed by erosion and if older thrust-related cooling AFT and AHe ages exist, they will be evident in the detrital record. The first record of thrust motion at 3.5 Ma coincides with an increase sedimentation rate and change in the lithology in the Pliocene depositional basin at around 3-3.5 Ma suggesting this time marks the onset of a major exhumational event (Chang & Chi, 1983; Teng, 1990).

The southward propagating collision is reflected by the younger, 1 Ma, record of thrust faulting in the south compared to the 3.5 Ma in the north. As collision continues

in the south, ongoing exhumation above a migrating thrust ramp will widen the zone of reset AFT ages to the west and expose deeper material above the migrating thrust ramp. Thus with continued collision, the prediction is for rocks of the Hsüehshan Range to be exposed in the south.

The southward propagating collision is also recorded by the youngest age along each of the three transects. Along the central and southern transects, the youngest cooling age is 0.5 Ma recording rapid active exhumation. The youngest cooling age in the northern transect is 1.2 Ma recording that collision is now inactive at this latitude.

### **3.7 Conclusions**

The prevalence of reset and partially-reset AFT and AHe ages in western Taiwan record shallow burial and exhumation. In northern and central Taiwan, the AFT closure temperature is in the lower Miocene stratigraphic units and in southern Taiwan, the AFT closure temperature is in the middle Miocene stratigraphic units.

Along the length of western Taiwan, the thermochronometric thrust-related cooling ages are older in the west and younger toward the east. The gross structure and the thermochronometric cooling age pattern along all 3 transects is consistent with the migration of a buried thrust ramp that is today located beneath the western foothills hinterland/eastern Hsüehshan Range. The cooling ages record vertical exhumation through the AFT and AHe closure temperatures above the thrust ramp, and horizontal transport above an upper décollement in the Miocene or lower Pliocene. Rather than recording a slower exhumation rate, the older ages in the west of the foothills thrust belt record earlier cooling above the thrust ramp, but at the same rapid rate as the youngest sample ages from central Taiwan.

The thermochronometric ages show no evidence for any significant amounts of out-of-sequence faulting along any of the structures. The pattern of young ages toward the rear of the thrust belt and older ages toward the foreland is the result of a sequence of foreland propagating faults that does not require-out-of-sequence thrust motion to exhume material in the hinterland with the youngest ages. The thrust structures that crop

out along each of our transects are exhumed through the closure temperature to the surface by the motion along the main Taiwan décollement.

The southward propagation is reflected in the distribution of oldest and youngest thrust cooling ages. The oldest thermochronometric record of thrust faulting is 3.5 Ma along the northern and central transects, and 1 Ma in the south showing the progressively younger onset of collision in the south. The youngest cooling age is 0.5 Ma in central and southern Taiwan and 1.2 Ma in northern Taiwan recording that thrust faults in northern Taiwan are no longer accommodating collision. Thus the overall deformation history documented by thermochronometric ages in western Taiwan is a steady southward progressing collision that is accommodated by westward propagating thrust faults and fault-related folding of sediments of the Asian passive margin.

### 3.8 Appendix 1: Simulating induced tracks using ICPMS data

We simulate the number of induced tracks using the ICPMS measure of Uranium as follows:

Calculated the amount of Uranium in ppm using the ICPMS measured value  $P_i$  (table 2):

$$P_i = \frac{\text{Number of } ^{238}\text{U atoms}}{\text{Number of } ^{43}\text{Ca atoms}}$$

$$^{238}\text{U}(g) = \frac{P_i \cdot M_{238}}{N_A} \quad (1)$$

*Amount of apatite (g):*

1 atom of  $^{43}\text{Ca}$  = 1/0.135% Ca atoms.

$^{43}\text{Ca}$  is 0.135 weight % Ca

$\therefore$  1 atom of  $^{43}\text{Ca}$  = 740.74 Calcium atoms

$$\therefore 1 \text{ } ^{43}\text{Ca atom} = \frac{1}{0.135\%} = 740.74 \text{ Ca atoms}$$

$$740.74 \text{ Ca atoms} = \frac{740.74 \cdot M_{Ca}}{N_A} = 4.9297e - 20g$$

$$M_{Ca} = 40.78 \text{ g/mol}$$

Calcium is 39.36% weight of apatite

$$\therefore 1 \text{ atom } ^{43}\text{Ca} = 1.25E-19 \text{ g of apatite (2)}$$

$$^{238}\text{U}(\mu\text{g/g}) = \frac{^{238}\text{U}(g) (1)}{\text{apatite}(g) (2)} \cdot 1e6 \cdot \text{fractionation factor}$$

$$\text{U(ppm)} = ^{238}\text{U (ppm)} / A_{238}$$

Where  $A_{238}$  = abundance of  $^{238}\text{U}$  in weight %

The simulated induced track density is calculated by rearranging equation (1) of Hasebe et al., 2004,

$$\rho_i = U \cdot A_{235} \cdot 0.5 \cdot R_{ED} \left[ \frac{\rho_d}{U_{dos} \cdot A_{235dos} \cdot g \cdot R_{EDdos}} \right]$$

where  $\rho_i$  = induced track density ( $\text{cm}^{-2}$ ),  $U$  = total uranium content of apatite ( $\mu\text{g/g}$ ),  $A_{235}$  = Abundance of  $^{235}\text{U}$  in weight for the apatite ( $\text{g/g}$ ), 0.5 is geometry factor because tracks recorded in the external detector originate from only one side of the observed surface, whilst tracks in apatite come from both sides,  $R_{ED}$  = a registration efficiency factor for  $^{235}\text{U}$  induced tracks in the apatite (cm),  $R_{EDdos}$  = a registration efficiency factor for the dosimeter,  $\rho_d$  = induced track density for the dosimeter glass measured in an external detector ( $\text{cm}^2$ ),  $U_{dos}$  = the uranium content of the dosimeter glass ( $\text{Ag/g}$ ),  $A_{235dos}$  =  $^{235}\text{U}$  abundance in weight for the dosimeter glass ( $\text{g/g}$ ) for  $^{235}\text{U}$  induced tracks in the dosimeter glass (cm). The term in parentheses are dosimeter constants which are assumed. This approach uses the derivation of the fission track age equation in the EDM which is explained by Hasebe et al., 2004 and is found in Tagami and O'Sullivan, (2005).

The number of induced tracks is then:

$$N_i = \rho_i \cdot Area$$

Where Area is the area analyzed for the spontaneous tracks (cm<sup>2</sup>).

The  $\zeta$  factor is then calculated by ICPMS measured pooled age = simulated pooled age. This data can now be used as input into BinomFit.

**Table 3.1** Apatite fission-track age data collected using the conventional AFT method.

$\rho_s$  - spontaneous track density;  $N_s$  - total number of spontaneous tracks;  $\rho_i$  - induced track density ;  $\rho_d$  - dosimeter track density; Grains - total number of dated grains; Q is chi squared probability;  $N_d$ —total number of tracks; YPA – Young peak age from BinomFit; % percent of total number of dated grains in the youngest peak. All ages are  $\pm 2\sigma$ .

1. Forced three peaks. BinomFit picks two peaks with YPA = 3.6(-0.8,1.1); 89.8%.

2. Remove 1 young grain with zero tracks to fit YPA. With all grains YPA:1.8(-1.6,12.3); 14%. This is inconsistent with U-Th/He ages. *\*Data in italics are fission track date reported by Fuller et al., 2007, used in this discussion.*

Sample	Latitude	Longitude	Elevation (m)	$\rho_s$ (10 <sup>6</sup> tracks cm <sup>-2</sup> )	$N_s$ (tracks)	$\rho_i$ (10 <sup>6</sup> tracks cm <sup>-2</sup> )	$N_i$ (tracks)	$\rho_d$ (10 <sup>6</sup> tracks cm <sup>-2</sup> )	$N_d$ (tracks)	Grains	Q	Dpar ( $\mu\text{m}$ )	Dper ( $\mu\text{m}$ )	Pooled Fission-Track Age (Ma)	Mean Fission-Track Age (Ma)	YPA (95% confidence interval)	% grains in YPA population
7_04	120.861	24.079	331.763	0.605	397	1.387	911	2.471	4113	37	0	1.96	0.46	61.0 $\pm$ 4.1	69.5 $\pm$ 10.5	3.5(-2.8,13.5) <sup>2</sup>	14
8_04	120.858	24.08	337.971	0.77	205	2.873	765	2.487	4113	37	0	1.88	0.41	37.8 $\pm$ 3.2	62.4 $\pm$ 9.7	18.4(-4.3,5.6)	57.6
9_04	120.87	24.077	313.199	0.026	10	1.287	504	2.502	4113	38	0.16	1.74	0.44	2.82 $\pm$ 0.91	2.98 $\pm$ 1.46	2.1(-1.3,3.5)	92.9
14_04	120.946	24.067	412	0.016	6	1.716	627	2.518	4113	23	0	1.58	0.46	1.37 $\pm$ 0.56	2.70 $\pm$ 1.86	0.9(-0.6,1.7)	94.9
18_04	120.988	24.076	491.856	0.045	31	2.839	1962	2.564	4113	38	0.102	1.64	0.46	2.30 $\pm$ 0.42	2.87 $\pm$ 0.99	2.2(-0.9,1.5)	94.9
23_04	121.123	24.254	1285.68	0.009	6	1.919	1254	2.58	4113	40	0	1.6	0.39	0.702 $\pm$ 0.28	1.52 $\pm$ 1.49	0.5(-0.3,0.8)	97.2
24_04	120.655	23.022	279.43	0.245	119	1.567	760	2.595	4113	36	0	1.77	0.44	23.1 $\pm$ 2.4	15.4 $\pm$ 6.6	1.1(0.7,1.9)	81.2
25_04	120.647	23.03	308.457	0.206	118	2.219	1274	2.611	4113	39	0	1.72	0.4	13.7 $\pm$ 1.4	5.14 $\pm$ 2.46	2.3(-0.9,1.5)	95.8
26_04	120.645	23.031	313.34	0.035	17	1.29	620	2.626	4113	36	0.728	1.73	0.4	4.10 $\pm$ 1.01	5.18 $\pm$ 1.56	4.1(-1.6,2.6)	100
27_04	120.647	23.03	308.457	0.049	1	2.051	42	2.642	4113	1	n.a.	1.53	0.42	3.58 $\pm$ 3.62	n.a	n.a	n.a
28_04	120.648	23.031	297.475	0.07	42	3.341	1993	2.657	4113	38	0.471	1.79	0.42	3.19 $\pm$ 0.51	3.33 $\pm$ 1.00	3.2(-0.9,1.2)	100
29_04	120.51	23.092	175.081	0.74	407	3.478	1912	2.673	4113	38	0	2.03	0.43	32.3 $\pm$ 2.0	43.0 $\pm$ 6.5	10.9(-2.6,3.3)	37.6
30_04	120.513	23.115	360.975	0.516	296	2.851	1635	2.688	4113	37	0	2.06	0.4	27.6 $\pm$ 1.9	48.7 $\pm$ 9.2	15.3(-3.3,4.2)	59.1
31_04	120.503	23.115	153.594	0.918	619	4.186	2824	2.704	4113	40	0	2.03	0.42	33. $\pm$ 8	52.4 $\pm$ 8.3	13.2(-2.3,2.7)	47.4
32_04	120.528	23.097	157.39	0.66	446	3.445	2328	2.719	4113	39	0	2.21	0.42	29.6 $\pm$ 1.8	42.9 $\pm$ 6.8	16.7(-2.5,3.0)	68.5
33_04	120.604	23.086	314.085	0.235	127	4.349	2349	2.735	4113	37	0	2.1	0.47	8.41 $\pm$ 0.81	11.1 $\pm$ 4.1	1.2(-0.7,1.5)	48.8
34_04	120.611	23.083	355.506	0.019	23	2.9	3510	2.75	4113	37	0	1.93	0.46	1.03 $\pm$ 0.22	2.87 $\pm$ 1.53	0.9(-0.3,0.6)	94
35_04	120.642	23.073	459.081	0.012	9	3.382	2567	2.766	4113	35	0	1.87	0.43	0.55 $\pm$ 0.185	1.37 $\pm$ 1.14	0.6(-0.3,0.5)	100
36_04	120.553	23.085	432.394	0.985	554	3.569	2008	2.781	4113	34	0	2.01	0.41	43.5 $\pm$ 2.5	64.7 $\pm$ 8.9	10.9(-2.5,3.3)	23.1
39_04	120.47	23.238	316.828	1.133	729	4.294	2762	2.797	4113	40	0	2.09	0.42	41.9 $\pm$ 2.1	66.7 $\pm$ 10.7	20.5(-4.1,5.1)	38.8
20_01	120.544	23.071	304.01	<i>0.638</i>	<i>471</i>	<i>6.533</i>	<i>4825</i>	<i>4.112</i>	<i>4132</i>	<i>39</i>	<i>0</i>	<i>1.95</i>	<i>n.a</i>	<i>22.8<math>\pm</math>1.3</i>	<i>39.6<math>\pm</math>7.1</i>	<i>n.a</i>	<i>n.a</i>
21-01*	<i>120.621</i>	<i>23.073</i>	<i>570.28</i>	<i>0.119</i>	<i>93</i>	<i>4.972</i>	<i>3885</i>	<i>4.102</i>	<i>4132</i>	<i>37</i>	<i>0</i>	<i>1.96</i>	<i>0.58</i>	<i>5.59<math>\pm</math>0.61</i>	<i>30.1<math>\pm</math>13.7</i>	<i>1.3 (-0.6,1.1)<sup>l</sup></i>	<i>63.7</i>
23-01*	<i>120.65</i>	<i>23.034</i>	<i>330.38</i>	<i>0.069</i>	<i>29</i>	<i>4.79</i>	<i>2005</i>	<i>4.093</i>	<i>4132</i>	<i>37</i>	<i>0.695</i>	<i>1.79</i>	<i>0.53</i>	<i>3.37<math>\pm</math>0.64</i>	<i>4.5<math>\pm</math>1.45</i>	<i>3.4(-1.0,1.5)</i>	<i>100</i>
24-01*	<i>120.662</i>	<i>23.048</i>	<i>276</i>	<i>0.026</i>	<i>6</i>	<i>2.277</i>	<i>532</i>	<i>4.083</i>	<i>4132</i>	<i>28</i>	<i>0.047</i>	<i>1.65</i>	<i>0.49</i>	<i>2.6<math>\pm</math>1.1</i>	<i>2.81<math>\pm</math>2.13</i>	<i>2.0(-1.3,3.6)</i>	<i>96.6</i>

**Table 3.2** Summary of the apatite fission-track age data collected using LA-ICPMS.

Grains - total number of dated grains; N<sub>s</sub> - total number of spontaneous tracks; Area Analyzed- total area analyzed for spontaneous tracks;  $\Sigma(P\Omega)$  = Sum of Pi for each sample,  $P = (^{238}\text{U}/^{43}\text{Ca})$  for each apatite grains;  $\xi_{\text{MS}}$  = ICPMS Zeta factor each sample;  $^{238}\text{U}$  = background-corrected  $^{238}\text{U}$  in cps measured with LA-ICPMS;  $^{43}\text{Ca}$  = background-corrected  $^{43}\text{Ca}$  in cps measured with LA-ICPMS; Q - chi squared probability; Dpar= is the mean maximum diameter of fission-track etch figures parallel to the c-axis; Dper= is the mean maximum diameter of fission-track etch figures perpendicular to the c-axis; YPA - Young peak age from BinomFit; % grains in young peak = percent of total number of dated grains in the youngest peak. All ages are  $\pm 2\sigma$ . 1. forced to fit 3 peaks. BinomFit auto fit is to fit 2 peaks.

Sample	Latitude	Longitude	Elevation (m)	Grains	N <sub>s</sub> (tracks)	Area Analyzed (cm <sup>2</sup> )	$\Sigma(P\Omega)$ (cm <sup>2</sup> )	$1\sigma \Sigma(P\Omega)$ (cm <sup>2</sup> )	$\xi_{\text{MS}}$	$1\sigma \xi_{\text{MS}}$	<sup>43</sup> Ca bkg:sig (dmnls)	<sup>238</sup> U bkg:sig (dmnl)	Q (dmnl s)	Dpar (μm)	Dper (μm)	Pooled Fission-Track Age (Ma)	YPA (95 % confidence interval)	% grains in Young Peak
33-01	120.427	22.839	2049.15	40	6	9.95E-04	9.39E-05	4.08E-06	16.7623	0.3445	3.65E-02	1.67E-01	1	1.61	0.51	0.535+/- 0.220	0.5(-0.3,0.6)	100
1_04	120.849	24.112	915.859	29	176	2.99E-04	2.34E-05	9.78E-07	16.2842	0.3347	6.88E-02	2.59E-01	0	2.04	0.59	61.1+/- 5.4	19.5(-5.0,6.7)	27.4
2_04	120.857	24.11	730.6	37	315	7.56E-04	6.04E-05	2.82E-06	15.8121	0.3251	5.20E-02	9.38E-01	0	1.97	0.67	41.1+/- 3.1	6.9(-2.0,2.7)	6.6
3_04	120.803	24.037	294.3	37	680	7.43E-04	8.51E-05	1.21E-06	11.6053	0.3108	3.10E-02	1.20E-02	0	1.88	0.42	46.2+/- 2.3	10.8(-1.8,2.2)	14.6
4_04	120.832	24.035	371	40	479	7.37E-04	8.95E-05	3.23E-06	15.34	0.3154	6.43E-02	2.40E-01	0	2.05	0.63	40.9+/- 2.5	10.7(-2.3,2.9)	15.4
5_04	120.822	24.033	326.556	39	560	7.96E-04	8.65E-05	2.74E-06	14.8619	0.3056	3.67E-02	7.01E-02	0	2.03	0.58	47.9+/- 2.7	8.6(-2.5,3.4)	14.7
6_04	120.84	24.029	244.12	38	474	6.73E-04	5.77E-05	1.99E-06	14.3838	0.2958	5.95E-02	1.32E-01	0	2.09	0.7	58.8+/- 3.6	16.2(-3.1,3.8)	26
11_04	120.869	24.046	290	39	20	6.68E-04	5.71E-05	4.98E-06	13.9057	0.286	7.31E-02	2.50E-01	0.9709	1.99	0.59	2.43+/- 0.59	2.4(0.9,1.3)	100
13-04	120.897	24.06	329.25	36	14	2.71E-04	2.44E-05	4.68E-07	11.2774	0.2924	3.17E-02	5.58E-02	0.3259	1.64	0.4	3.23+/- 0.87	1.4(0.8,2.0)	43.7
																3.2(1.3,2.2)	100	
1_05	121.371	24.991	188.66	7	88	4.35E-05	4.18E-06	1.04E-07	15.0106	0.5021	1.77E-02	1.29E-03	0	1.64	0.39	156+/-18	n/a	n/a
2_05	121.361	24.997	176.18	40	149	9.16E-04	5.37E-05	7.77E-07	14.818	0.4913	1.66E-02	2.31E-03	0	2.14	0.62	20.5+/-1.8	11.3(-2.6,3.3)	39.6
3_05	121.359	25	201.41	40	524	7.42E-04	7.29E-05	1.08E-06	14.4902	0.4728	2.40E-02	1.78E-02	0	1.87	0.45	51.8+/-2.9	12.5(-3.5,4.8)	34.3
4_05	121.47	24.928	315.39	8	9	6.40E-05	6.51E-06	2.13E-07	14.2894	0.4616	1.81E-02	4.63E-03	0	1.59	0.44	9.86+/- 3.32	n/a	n/a
5_05	121.47	24.925	75.1	1	1	2.56E-06	4.96E-07	3.65E-08	14.2484	0.4593	1.60E-02	9.15E-05	n.a.	1.44	0.51	14.3+/- 14.4	n/a	n/a
7_05	121.474	24.988	16.78	39	27	6.91E-04	7.63E-05	1.26E-06	14.0804	0.4498	2.07E-02	8.46E-03	0.9974	1.65	0.41	2.49+/- 0.49	1.7(-0.8,1.4)	64
8_05	121.499	24.92	257.22	39	53	6.31E-04	5.81E-05	9.40E-07	13.7526	0.4314	2.67E-02	2.44E+00	0	1.63	0.43	6.27+/- 0.89	3.2(-1.0,1.5)	88.9
																1.8(-1.0,2.1) <sup>1</sup>	32.3	
9_05	121.505	24.911	447.16	4	1	2.75E-05	1.76E-06	6.53E-08	13.56	0.4206	3.78E-02	3.53E-01	0.8095	1.59	0.34	3.85+/- 3.85	n/a	n/a
10_05	121.51	24.906	507.2	39	14	5.22E-04	2.57E-05	4.12E-07	13.3674	0.4098	2.65E-02	9.38E-02	0.0029	1.61	0.4	3.65+/- 0.98	0.9(-0.6,1.9)	62
11_05	121.527	24.914	49.16	12	1	7.30E-05	3.51E-06	9.60E-08	13.142	0.3971	4.66E-02	5.87E-01	1	1.54	0.35	1.87+/- 1.88	n/a	n/a
12_05	121.539	24.894	72.63	40	11	5.49E-04	3.11E-05	4.01E-07	12.9166	0.3845	2.84E-02	3.36E-02	0.9999	1.66	0.44	2.28+/- 0.69	2.3(-1.0,1.9)	100
13-05	121.58	24.848	263.53	38	9	5.05E-04	3.45E-05	7.37E-07	12.5888	0.366	3.36E-02	6.61E-02	0.2133	1.63	0.43	1.64+/- 0.55	0.6(-0.4,1.2)	68
14-05	121.549	24.862	164.39	38	5	4.26E-04	2.62E-05	3.37E-07	12.2609	0.3476	2.91E-02	5.37E-02	0.2736	1.66	0.4	1.17+/- 0.52	n/a	n/a
41-05	120.667	23.019	421.44	39	20	7.70E-04	2.20E-05	3.93E-07	11.9331	0.3292	4.15E-02	7.86E-02	0.9201	1.69	0.42	5.41+/- 1.22	2.0(-1.2,3.0)	41



**Table 3.3** Fission track sample age interpretations.

Formation name and age after Tensi et al., 2006. Fission track sample in interpreted as reset, partially reset, or unreset based on the Chi-squared statistic (Q), the difference between the depositional age and the pooled age, and the annealing properties of individual grains in each sample.

Sample	Formation Name	Formation Age (After Tensi et al., 2006)	Pooled Age	Q	YPA	Interpretation	Comments
21_01	Changshikeng	Miocene	9 Ma	5.59±0.61	0	1.32(-0.6,1.1)	Partially reset Three old grains with dpar > 2.98 raises the PA
23_01	Kuanyinshan	Miocene	14.6 Ma	3.37±0.64	0.695	3.4(-1.0,1.5))	Reset Pooled age = YPA
24_01	Kuanyinshan	Miocene	14.6 Ma	2.6±1.1	0.047	2.0(-1.3,3.6)	Partially Reset or reset Almost reset. One old grain with a dpar of 2.13 (higher than average dpar of 1.6). Removing this old grain, binomfit picks one peak with YPA = 1.8(-1.1,3.0)
33_01	Changshikeng	Miocene	9 Ma	0.535±/ -0.220	1	0.5(-0.3,0.6)	Reset Pass Chi squared and YPA = PA
1_04	Peiliao	Miocene	20 Ma	61.1±/ -5.4	0	n.a.	Unreset Only 7 grains
2_04	Mushan	Miocene	24 Ma	41.1±/ -3.1	0	11.3(-2.6,3.3)	Unreset Although the YPA is younger than the depositional age, the YPA is interpreted to represent a partially reset age and is not related to collision
3_04	Kuanyinshan	Miocene	14.6 Ma	46.2±/ -2.3	0	10.8(-1.8,2.2)	Unreset
4_04	Talu	Miocene	17 Ma	46.2±/ -2.3	0	12.5(-3.5,4.8)	Unreset
5_04	Talu	Miocene	17 Ma	40.9±/ -2.5	0	n.a.	Unreset
6_04	Peiliao	Miocene	20 Ma	47.9±/ -2.7	n.a.	n.a.	Unreset
7_04	Peiliao	Miocene	20 Ma	61.0±4.1	0	3.5(-2.8,13.5); 1.8(-1.6,2.3)	Partially Reset Automatic YPA = 1.8, but this is younger than the AHe grains. Removing one young with dpar = 1.7 results in YPA = 3.5
8_04	Kuanyinshan	Miocene	14.6 Ma	37.8±3.2	0.00	18.4(-4.3,5.6)	Unreset No Young grains and YPA is approximately the formation age.
9_04	Shuichangliu	Miocene/Oligocene	32 Ma	2.82±0.91	0.16	2.1(-1.3,3.5)	Reset YPA = Pooled age and passes the Chi <sup>2</sup> distribution
11_04	Paileing Fm	Oligocene	35 Ma <	2.43±/ -0.59	0.970 9	2.4(0.9,1.3)	Reset Passes the Chi <sup>2</sup> distribution and YPA = Pooled age.
13_04	Shuichangliu	Miocene/Oligocene	32 Ma	3.23±/ -0.87	0.325 9	1.4(0.8,2.0); 3.2(1.3,2.2)	Reset Automatic YPA is 1.4 Ma. However, the sample passes the Chi <sup>2</sup> test, therefore this sample is interpreted to be reset.
14_04	Paileing Fm	Oligocene	35 Ma <	1.37±0.56	0	3.21(2.4,10.3) 0.9(-0.6,1.7)	Reset YPA is without one older grain with age of 43.5. Including all grains, BinomFit picks two peaks, one peak 0.9(-0.6,1.7), other peak at 30.9(25,243). This older peak is more consistent with sample (U-Th)/He ages, but younger than the pooled age. All ages younger than collision, and this sample in interpreted as reset.
18_04	Paileing Fm	Oligocene	35 Ma <	2.30±0.42	0.10	2.2(-0.9,1.5)	Reset Pass Chi squared and YPA = PA.
23_04	Paileing Fm	Oligocene	35 Ma <	0.702±0.28	0.00	0.53(-0.3,0.8)	Reset Fails Chi squared but YPA approximately equal to Pooled age.
24_04	Kuanyinshan Fm	Miocene	14.6 Ma	23.1±2.4	0.00	1.1(0.7,1.9)	Partially reset Fails Chi squared and many older grains
25_04	Kuanyinshan Fm	Miocene	14.6 Ma	13.7±1.4	0.00	2.3(-0.9,1.5)	Partially reset Fails Chi squared and many older grains

**Table 3.3** Continued

26_04	Changshikeng	Miocene	9 Ma	4.10±1.01	0.73	4.1(-1.6,2.6)	Reset	Passes the Chi <sup>2</sup> distribution and BiniomFit picks one peak and YPA = Pooled age.
27_04	Kuanyinshan Fm	Miocene	14.6 Ma	3.58±3.62	n.a.	n.a.	n.a.	
28_04	Kuanyinshan Fm	Miocene	14.6 Ma	3.19±0.51	0.47	3.2(-0.9,1.2)	Reset	Pass Chi squared and YPA = PA.
29_04	Yenshuikeng	Pliocene	5.3 Ma	32.3±2.0	0.00	10.9(-2.6,3.3)	Unreset	YPA is older than depositional age.
30_04	Tangenshan	Miocene	7 Ma	27.6±1.9	0.00	15.3(-3.3,4.2)	Unreset	YPA is older than depositional age.
31_04	Chutouchin Fm	Pliocene	3 Ma	33. ±.8	0.00	13.2(-2.3,2.7)	Unreset	YPA is older than depositional age.
32_04	Chutouchin Fm	Pliocene	3 Ma	29.6±1.8	0.00	16.7(-2.5,3.0)	Unreset	YPA is older than depositional age.
33_04	Ailiaochiao	Pliocene	3.7-5.33	8.41± 0.81	0.00	1.2(-0.7,1.5)	Partially reset	Pooled age is older than depositional age. YPA is younger than depositional age
34_04	Tangenshan	Miocene	5.5-8.6 Ma	1.03±0.22	0.00	0.9(-0.3,0.6)	Reset	Fails Chi squared but YPA approximately equal to Pooled age.
35_04	Changshikeng	Miocene	9 Ma	0.55±0.185	0.00	0.6(-0.3,0.5)	Reset	Fails Chi squared but YPA approximately equal to Pooled age and BinomFit picks one peak.
36_04	Changshikeng	Miocene	9 Ma	43.5±2.5	0.00	10.9(-2.5,3.3)	Unreset	Fails Chi squared, no young grains and YPA is approximately equal depositional age.
39_04	Tangenshan	Miocene	5.5-8.6 Ma	41.9±2.1	0.00	20.5(-4.1,5.1)	Unreset	YPA is older than depositional age.
1_05	Peiliao	Miocene	20 Ma	156+/-18	0	n.a.	n.a.	
2_05	Taliao	Miocene	23.8 Ma	20.5+/-1.8	0	11.3(-2.6,3.3)	Unreset	
3_05	Shitii	Miocene	23 Ma	51.8+/-2.9	0	12.5(-3.5,4.8)	Unreset	Although the YPA is younger than the depositional age, the YPA is interpreted to represent a partially reset age and is not related to collision.
4_05	Tatungshan Fm	Oligocene	32 Ma	9.86+/- 3.32	0	n.a.	n.a.	
5_05	Mushan	Miocene	23.8 Ma	14.3+/- 14.4	n.a.	n.a.	n.a.	
7_05	Shihti	Miocene	23 Ma	2.49+/- 0.49	0.9974	1.7(-0.8,1.4)	Reset	Reset. Passes the Chi squared test.
8_05	Kuanyinshan	Miocene	14.6 Ma	6.27+/- 0.89	0	3.2(-1.0,1.5)	Partially reset	Binom fit default YPA is 3.2 Ma. Forcing 3 peaks give a YPA of 1.8. 3.2 Ma is consistent with sample 10_05, but 1.8 is consistent with 07_05 (but this sample is reset)
9_05	Mushan	Miocene	23.8 Ma	3.85+/- 3.85	0.8095	n.a.	n.a.	There are only 4 apatite grains
10_05	Taliao	Miocene	23.8 Ma	3.65+/- 0.98	0.0029	0.9(-0.6,1.9)	Partially Reset	Fails Chi squared and many grains older than Pooled age.
11_05	Tsuku	Oligocene	32 Ma	1.87+/- 1.88	1	n.a.	n.a.	There are only 12 grains
12_05	Tsuku	Oligocene	32 Ma	2.28+/- 0.69	0.9999	2.3(-1.0,1.9)	Reset	Binom fit picks one peak and YPA=PA
13_05	Kankou Fm	Oligocene	33.78 Ma	1.64+/- 0.55	0.2133	0.6(-0.4,1.2)	Reset	Pass Chi squared and YPA = PA.
14_05	Tsuku	Oligocene	32 Ma	1.17+/- 0.52	0.2736	n.a.	Reset	Binom fit won't fit a peak so this is the Normal fit YPA
41_05	Kuanyinshan	Miocene	14.6 Ma	5.41+/- 1.22	0.9201	2.0(-1.2,3.0)	Partially reset	Pass Chi squared, but YPA is similar to ages in samples 24_01 and 24_04, so interpreted as partially reset.

**Table 3.4** (U-Th)/He in apatite table A

(U-Th)/He in Apatite data measured at Yale University. Columns are: Sample - sample number; Age - Corrected age in millions of years;  $\pm$  [Ma] -  $2\sigma$  on age; Th [ng] - Thorium in nanograms; Sm[ng] - Samarium; Th/U - Thorium/Uranium ratio; He[ncc]: measured  $^4\text{Helium}$ ; Ft - fraction of alphas retained; U[ng] - measured Uranium. For sample location, see tables 3.1 and 3.2

Sample	Age [Ma]	$\pm$ [Ma]	Th [ng]	Sm [ng]	Th/U	He [ncc]	Ft	U ng
17_01	0.799	0.100	0.076	0.086	3.247	0.002	0.488	0.024
	14.706	1.077	0.003	0.039	0.694	0.005	0.557	0.005
	1.830	0.293						
20-01	0.416	0.044	0.026	0.131	0.395	0.003	0.685	0.067
	0.273	0.029	0.075	0.271	1.285	0.002	0.730	0.060
	0.027	0.050					0.680	
	1.405	0.084					0.630	
23-01	0.705	0.937	0.009	0.028	6.541	0.000	0.474	0.001
	1.552	0.274					0.607	
	0.968	0.457					0.533	
28_04	2.876	0.398	0.090	0.106	10.491	0.006	0.580	0.009
	1.228	0.475	0.023	0.064	5.444	0.001	0.612	0.004
	0.969	0.385	0.024	0.159	2.927	0.001	0.596	0.008
04-29	1.042	0.354	0.014	0.096	1.307	0.001	0.609	0.011
	4.903	0.518	0.024	0.038	5.550	0.004	0.593	0.004
	25.662	0.944	0.023	0.019	3.722	0.022	0.600	0.006
30_04	154.236	6.999	0.020	0.021	6.487	0.090	0.593	0.003
	0.507	0.039	0.095	0.059	1.370	0.003	0.608	0.071
31_04	0.573	0.074	0.047	0.113	2.006	0.002	0.664	0.024
	2.285	0.070	0.060	0.111	2.127	0.008	0.676	0.029
04-32	0.399	0.029	0.082	0.052	1.532	0.002	0.671	0.055
	0.529	0.106	0.029	0.037	0.959	0.001	0.559	0.031
	1.161	0.042	0.055	0.100	0.937	0.007	0.657	0.061
04-33	0.873	0.193	0.014	0.029	1.165	0.001	0.575	0.013
	0.338	0.104	0.062	0.114	4.305	0.001	0.606	0.015
	0.346	0.057	0.116	0.081	3.412	0.001	0.549	0.035
04-34	2.230	0.288	0.016	0.048	1.693	0.002	0.592	0.010
	0.366	0.058	0.041	0.055	0.960	0.001	0.629	0.044
	0.414	0.048	0.034	0.254	0.493	0.003	0.641	0.071
04-35	0.867	0.118	0.041	0.070	2.468	0.002	0.542	0.017
	0.395	0.021	0.142	0.107	1.137	0.005	0.692	0.128
	0.423	0.018	0.346	0.780	3.432	0.006	0.641	0.103
04-36	1.475	0.376	0.041	0.048	52.059	0.001	0.608	0.001
	12.065	0.291	0.016	0.127	0.441	0.038	0.619	0.038
	2.547	0.087	0.040	0.080	1.014	0.010	0.633	0.041

**Table 3.5** (U-Th)/He in apatite table B

(U-Th)/He in Apatite data measured at University of Kansas. (U-Th)/He in Apatite data measured at Yale University. Columns are: Sample - sample number; Age - corrected age in millions of years;  $\pm$  [Ma] - 2 s on age; U[ppm] - Uranium concentration; Th [ppm] - Thorium concentration; Sm [ppm] - Samarium concentration; Th/U - Thorium/Uranium ratio; He[ncc/mg]: Helium concentration; mass [mg] - mass of grain ablated; Ft - fraction of alphas retained. For sample location, see tables 3.1 and 3.2.

Sample	Age [Ma]	$\pm$ [Ma]	U [ppm]	Th [ppm]	Sm [ppm]	Th/U	He [ncc/mg]	mass [mg]	Ft
03_04	2.1	0.125	51.1	82.7	82.4	1.62	13.1	1.58	0.73
	2.6	0.159	74.9	106.8	78.6	1.43	23.5	1.33	0.72
	4.4	0.262	9.9	8.8	41.5	0.89	4.5	1.06	0.69
07_04	4.3	0.256	9.1	41.6	231.0	4.56	7.1	0.79	0.66
	3.5	0.211	26.0	52.6	114.4	2.02	10.8	0.59	0.64
	3.6	0.216	0.8	7.4	8.3	9.04	0.0	0.55	0.63
08_04	3.7	0.220	15.8	43.0	32.4	2.72	6.9	0.42	0.59
	3.5	0.207	15.6	327.4	246.1	21.04	20.2	0.23	0.51
	3.1	0.184	42.9	46.2	276.6	1.08	12.3	0.35	0.56
09_04	2.6	0.153	5.3	36.8	15.2	6.89	2.3	0.30	0.53
	2.5	0.148	9.9	54.0	89.3	5.43	4.1	0.39	0.59
14_04	52.5	3.148	0.0	5.1	0.0	n.a.	0.1	0.70	0.65
	2.6	0.155	20.9	117.3	184.5	5.60	9.5	0.46	0.61
	4.1	0.248	7.1	21.1	121.7	2.99	4.0	0.46	0.61
	3.4	0.205	0.5	47.4	45.7	88.05	2.9	0.35	0.57
24_04	0.0	0.000	0.0	2.2	0.0	n.a.	0.0	0.99	0.67
	2.7	0.164	13.3	65.3	53.3	4.90	6.0	0.60	0.62
	4.2	0.251	7.5	62.7	60.7	8.36	7.8	1.00	0.67
29_04	1.6	0.098	17.6	34.9	22.1	1.99	3.2	0.62	0.63
	1.5	0.090	167.4	163.4	153.2	0.98	23.9	0.60	0.63
	0.8	0.049	111.7	102.2	362.5	0.92	8.6	0.64	0.62
30_04	2.7	0.163	55.3	92.2	189.1	1.67	13.3	0.27	0.51
	2.0	0.119	0.5	25.3	49.2	48.71	1.0	0.42	0.58
31_04	7.1	0.425	30.9	58.8	245.4	1.90	22.1	0.37	0.55
32_04	1.3	0.079	75.4	199.1	210.8	2.64	11.3	0.40	0.57
33_04	1.1	0.068	72.9	199.4	158.1	2.74	9.9	0.38	0.59
36_04	6.0	0.358	53.6	339.4	271.2	6.33	51.1	0.68	0.64
	6.6	0.398	26.5	56.7	122.2	2.14	21.7	0.80	0.66

**Table 3.6** Comparison of AFT and AHe grain ages.

Columns are: Sample - sample number; Number - grain number; He corr age (Ma) - AHe corrected age in million years; FT Age (Ma) - AFT grain age;  $\rho_s$  - grain spontaneous fission track density; U(ppm) - measured Uranium content; AFT Interp - apatite fission track sample interpretation, see table 3.3 and text for details. Comments - relationship between age,  $\rho_s$  and AHe age.

Sample	Grain Number	He corr age (Ma)	FT Age (Ma)	RhoNs	U (ppm)	AFT Interp	Comments	
17_01	29	0.80	105	1.88E+06	47	Unreset	$\rho_s$ correlates with He age, but U content is consistent.	
	32	14.71	148	2.40E+06	42			
20_01	43	0.42	n.a.	n.a.	n.a.	Unreset	Age increases with decreasing U.	
	46	0.27	n.a.	n.a.	n.a.			
	3	0.027	27.5	3.19E+06	304			
	16	1.40527	65.1	5.08E+06	204			
23_01	27	0.71	16.6	2.19E+06	25	Reset	n.a..	
03_04	6	2.1	n.a.	n.a.	n.a.	Unreset	n.a..	
	3	2.6	n.a.	n.a.	n.a.			
	1	4.4	44.5	9.11E+05	38.52			
07_04	6	4.3	77.9	5.21E+05	15	Partially Reset	Similar Age, U content, and $\rho_s$	
	5	3.5	240.1	1.82E+06	17			
08_04	4	3.7	65.1	6.51E+05	23	Unreset	Consistent age, different U and $\rho_s$	
	2	3.5	28.8	1.37E+06	110			
	1	3.1	24.6	4.69E+05	45			
09_04	5	2.6	36.9	0.00E+00	6	Reset	Age correlates positively to U content.	
	2	2.5	49.6	2.60E+05	12			
	1	3.4	5.9	0.00E+00	53			
14_04	5	2.6	17.5	0.00E+00	9	Reset	Different ages, similar U and $\rho_s$	
	4	4.1	7.3	0.00E+00	11			
24_04	3	2.7	11.8	0.00E+00	11	Partially Reset	Different ages, similar U and $\rho_s$	
	2	4.2	11.8	0.00E+00	14			
28_04	3	2.88	4.16	1.17E+05	74	Reset	Age increases with $\rho_s$ & U constant	
	4	1.23	1.61	4.34E+04	71			
	18	0.97	0	0.00E+00	10			Lower U grain , younger age
29_04	3	1.04	51.45	1.17E+06	51	Unreset	Age increases with decreasing $\rho_s$	
	8	4.90	46.86	4.34E+04	61			
	22	25.66	72.81	0.00E+00	9			Age increases with lower U, lower $\rho_s$
	44	1.6	n.a.	n.a.	17.6			Age does not correlate with U
42	1.5	n.a.	n.a.	167.4				
45	0.8	n.a.	n.a.	111.7				
30_04	14	154.24	16.2	3.91E+05	56	Unreset	AHe grain older than AFT. Contaminant?	
	24	0.51	22.8	1.56E+05	16			
	3	2.7	7.2	0.00E+00	12			Age increases with increasing U
	29	2.0	80.9	3.91E+04	1			

Table 3.6 Continued

<b>31_04</b>	18	0.57	14	1.17E+05	20	Unreset	Different ages. No difference in U content
	29	2.29	29	4.77E+05	32		
	15	7.1	162	1.56E+06	22		Age increases with increasing $\rho_s$ , but U constant
<b>32_04</b>	3	0.40	2.76	1.30E+05	108	Unreset	AHe age varies, but not consistently with in U content or $\rho_s$
	19	0.53	89.4	4.17E+06	106		
	30	1.16	17	2.39E+05	144		
	7	1.3	4.9	4.88E+04	96		
<b>33_04</b>	6	0.87	5.2	5.04E+04	31	Partially Reset	Higher U, lower $\rho_s$ , lower age Higher Age. Lower U content, Higher $\rho_s$
	18	0.34	0.8	0.00E+00	121		
	19	0.35	142.7	5.07E+05	117		
	10	1.1	6.9	1.42E+06	11		
<b>34_04</b>	4	2.23	0.8	0.00E+00	82	Reset	He age is older than fission track age. Contaminant? Same U content, different ages.
	25	0.37	1	0.00E+00	27		
	35	0.41	3.2	4.78E+04	98		
<b>35_04</b>	16	0.87	2	0.00E+00	35	Reset	Same U content, different ages.
	20	0.39	3.7	5.21E+04	30		
	30	0.42	1.5	0.00E+00	52		
<b>36_04</b>	6	1.48	61	3.19E+05	49	Unreset	Weak relationship: He age increases with $\rho_s$ ; AHe age decreases with increasing Uranium.
	8	12.06	56	6.19E+05	53		
	10	2.55	56	1.66E+05	56.6		
	23	6.0	42.2	7.52E+05	27		
	12	6.6	127.6	8.13E+05	14		

**Figure 3.1** Geologic and Tectonic Map and sample locations. Tectonic and Geologic Map of Taiwan (from Ho, 1988, Sibuet and Hsu, 1997 and Lamcombe et al. 2003) showing five major tectonostratigraphic units, associated bounding faults (modified from Fisher et al. (2002) and sample transects. Deformation front from Lamcombe et al. (2003). Inset shows regional tectonic setting from Stolar et al., 2007.

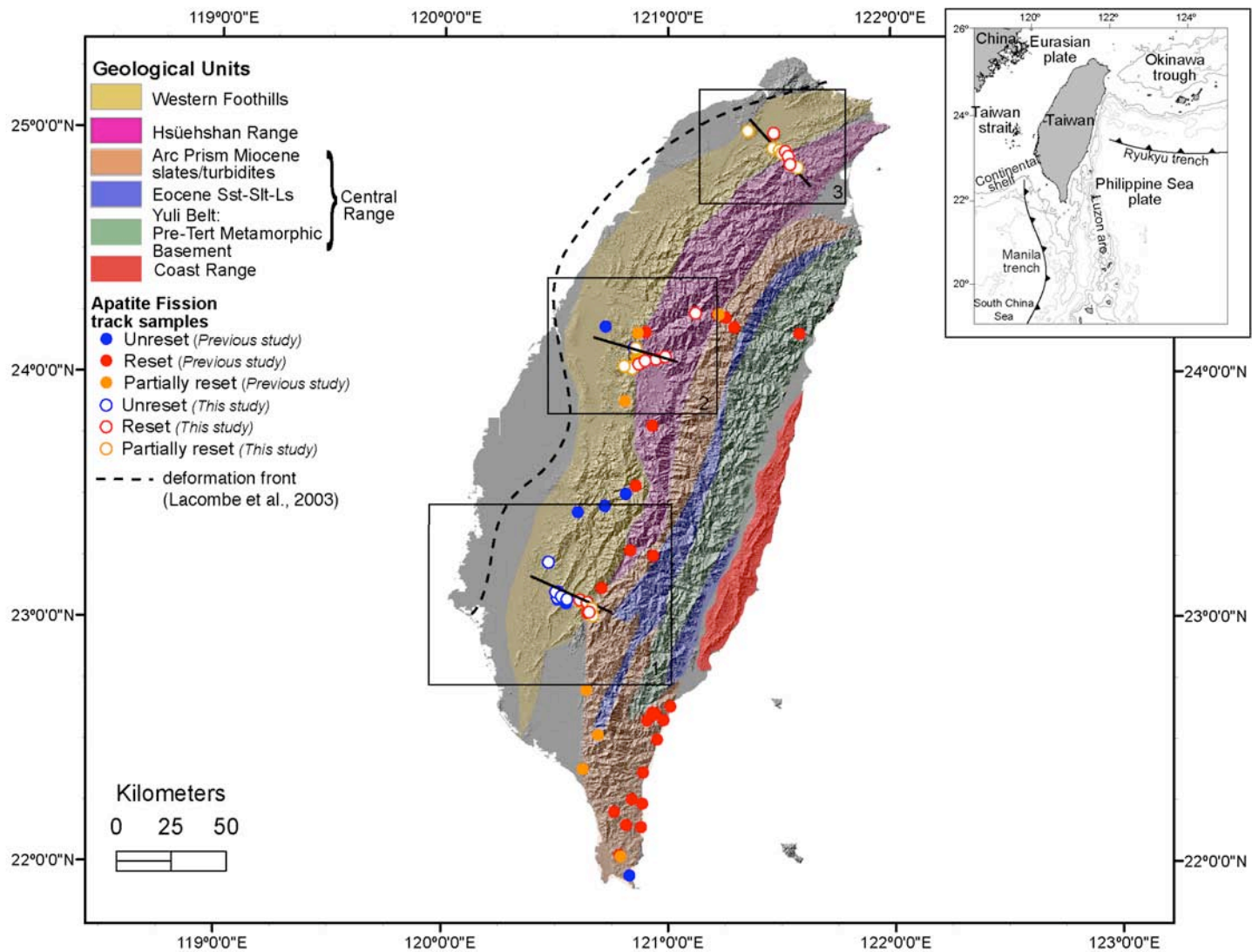




**Figure 3.2** Stratigraphy of Western Taiwan  
Generalized stratigraphy for each of our sample transects in Western foothills and Hsueshan Range. Compiled from Tensi et al., 2006, Ho, 1988, and MOEA Central Geologic Survey Maps, 1999 ; Lee et al., 2002; Huang et al., 2004).

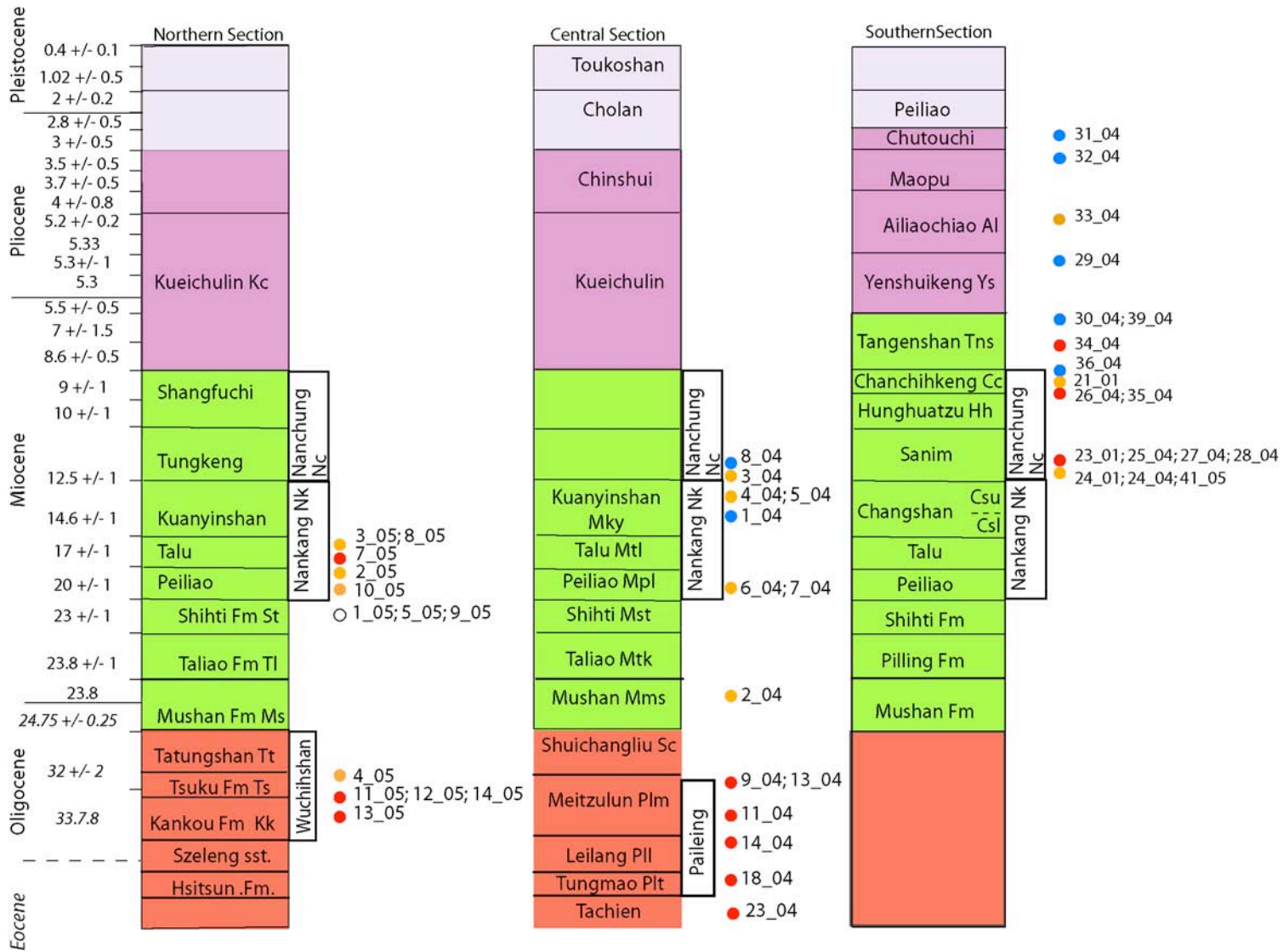


**Figure 3.3** Geologic map and sample locations in our central sampling region  
Location of map shown on figure 1. Structure and stratigraphy from Chinese Petroleum corporation 1:100000 Taichung sheet, 1989.  
Sample locations and thermochronometric age. Fission track ages: given as Pooled ages (PA)  $\pm$  2 s and young peak age (YPA) with asymmetric 95% confidence intervals. (U-Th)/He in apatite grain ages He ages:  $\pm$  95% confidence intervals. Labels are fault names from Chinese Petroleum corporation map. Chi Chi rupture, approximate location of surface rupture of 1999 Chi Chi earthquake after Yue et al., 2005.

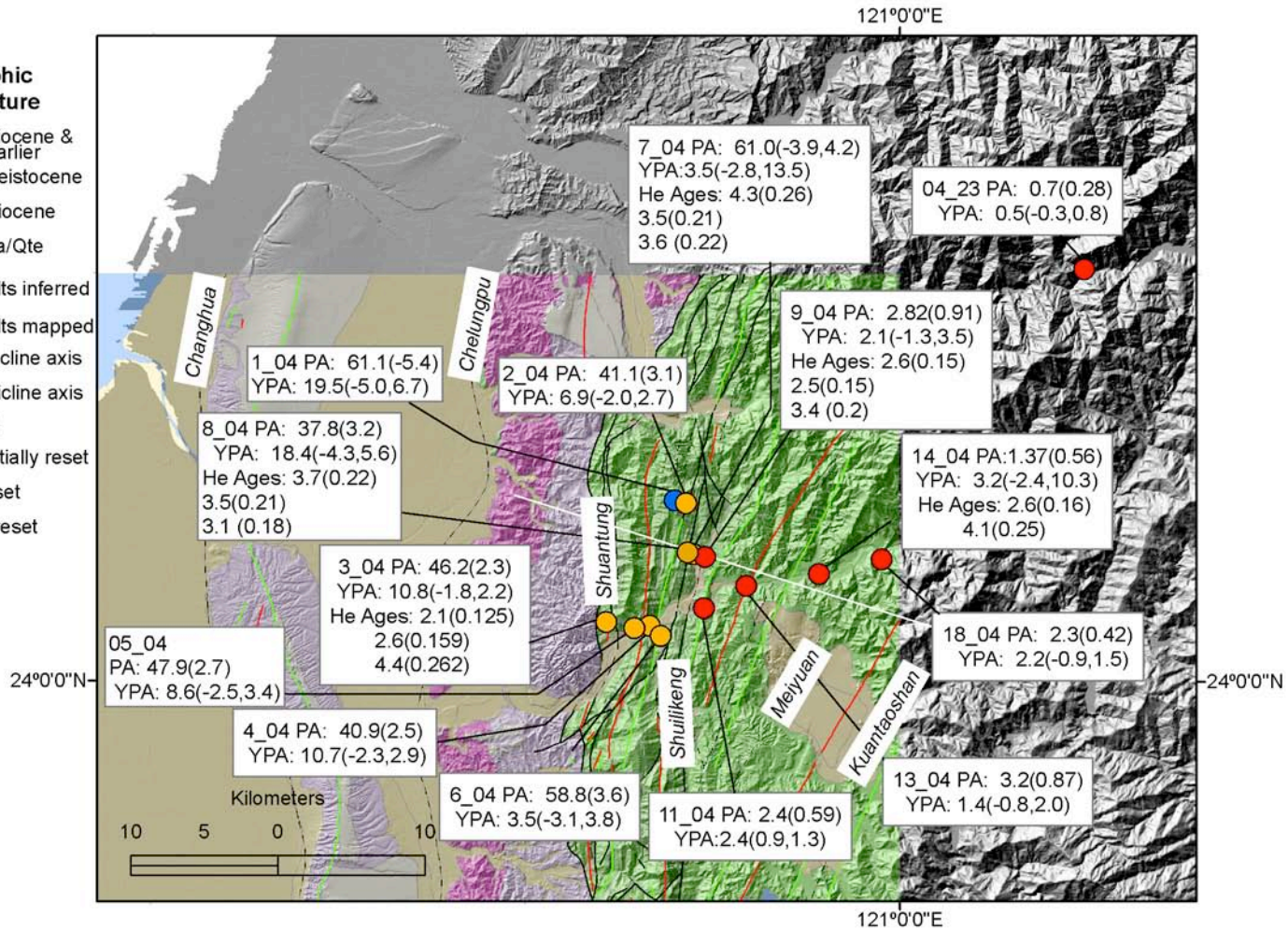
**Stratigraphic and Structure**

- Miocene & earlier
- Pleistocene
- Pliocene
- Qa/Qte

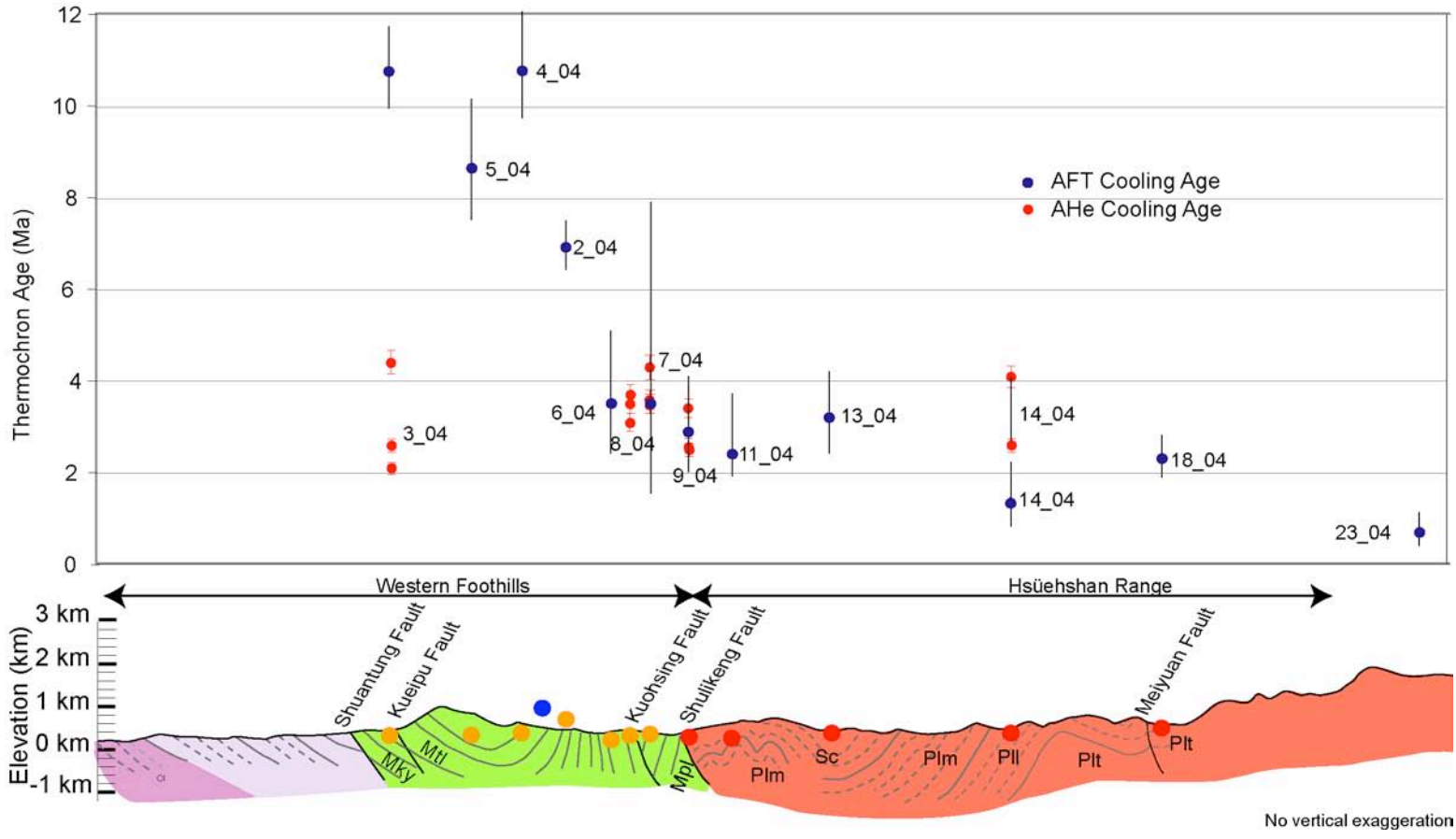
- faults inferred
- faults mapped
- syncline axis
- anticline axis

**Samples**

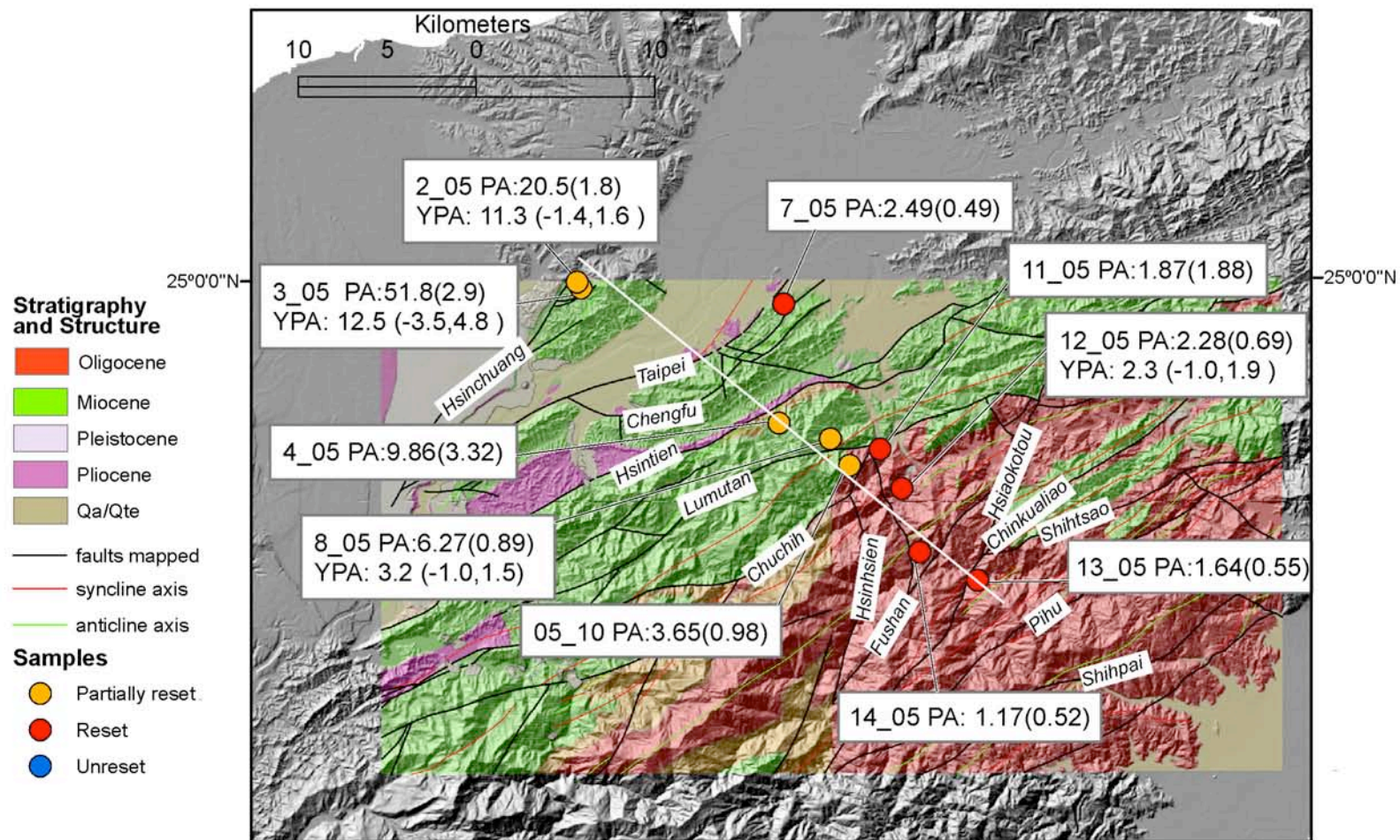
- Partially reset
- Reset
- Unreset



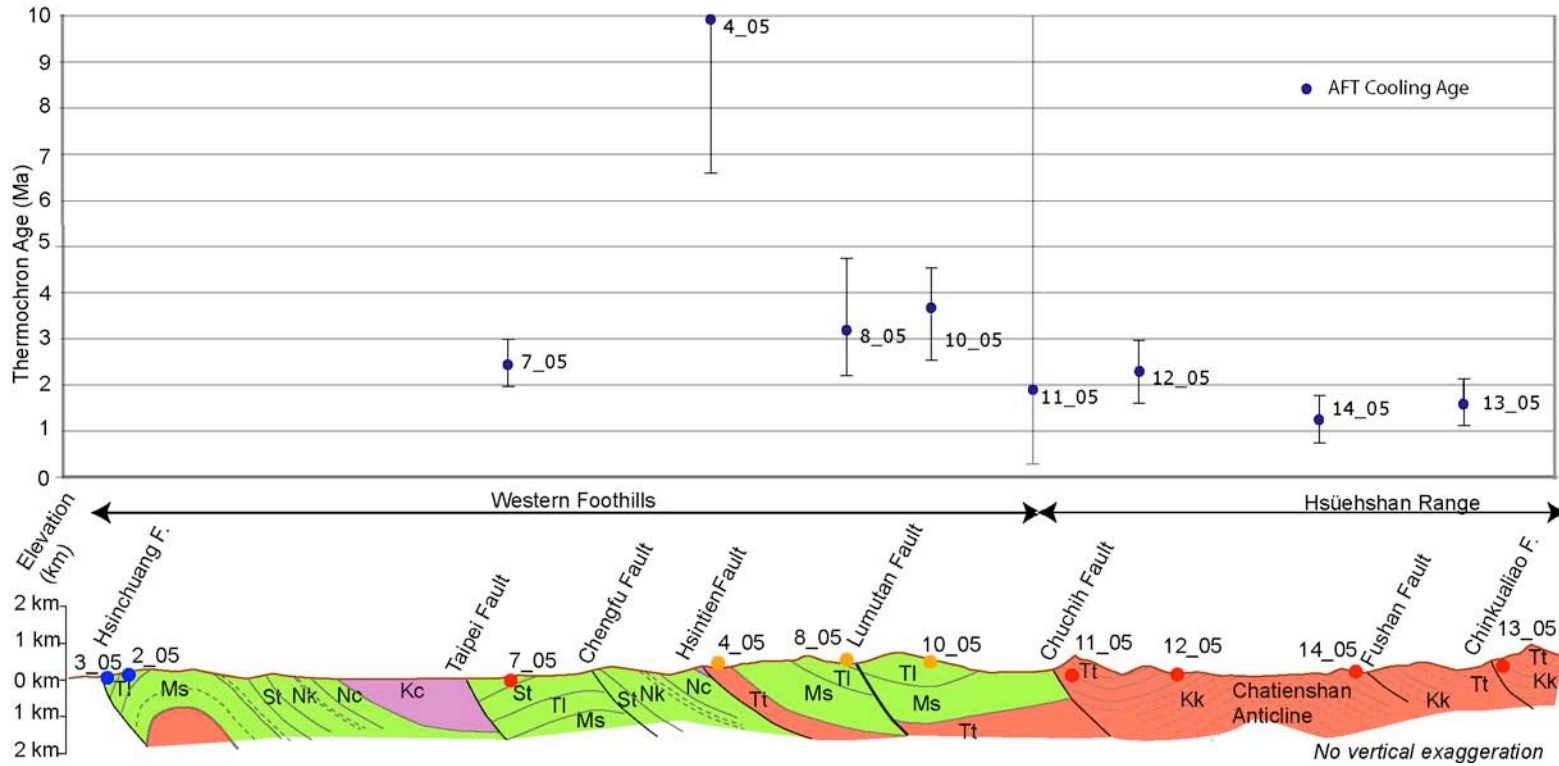
**Figure 3.4** Cross section and thermochronometric ages along the central transect. Structure and stratigraphy modified from Kuohsing geologic maps (and sample (U-Th/He in apatite grain age and apatite fission track interpreted cooling age (table 3). Oligocene units shown in red, Miocene in green. For stratigraphic names and abbreviations, see figure 2., Central Geologic Survey, MOEA, 1999) and sample (U-Th/He in apatite grain age and apatite fission track interpreted cooling age (table 3). Oligocene units shown in red, Miocene in green. For stratigraphic names and abbreviations, see figure 2. For transect location, see figure 1 and 3. Samples shown in red indicate reset, yellow indicates partially reset, blue is unreset. Error on thermochronometric age is 2 s for pooled age and 95% asymmetric confidence intervals for YPA (table 1, 2).



**Figure 3.5** Geologic map and sample locations in our northern sampling region. Location of map shown on figure 1. Structure and stratigraphy modified from Taoyun and Hsintien geologic maps (1:50000, Central Geologic Survey, MOEA, 1996; 2000). Sample locations shown with apatite fission track and (U-Th)/He. Fission track ages: given as Pooled ages (PA)  $\pm$  2 s and young peak age (YPA) with asymmetric 95% confidence intervals. (U-Th)/He in apatite grain ages (He ages) with 95% confidence intervals.



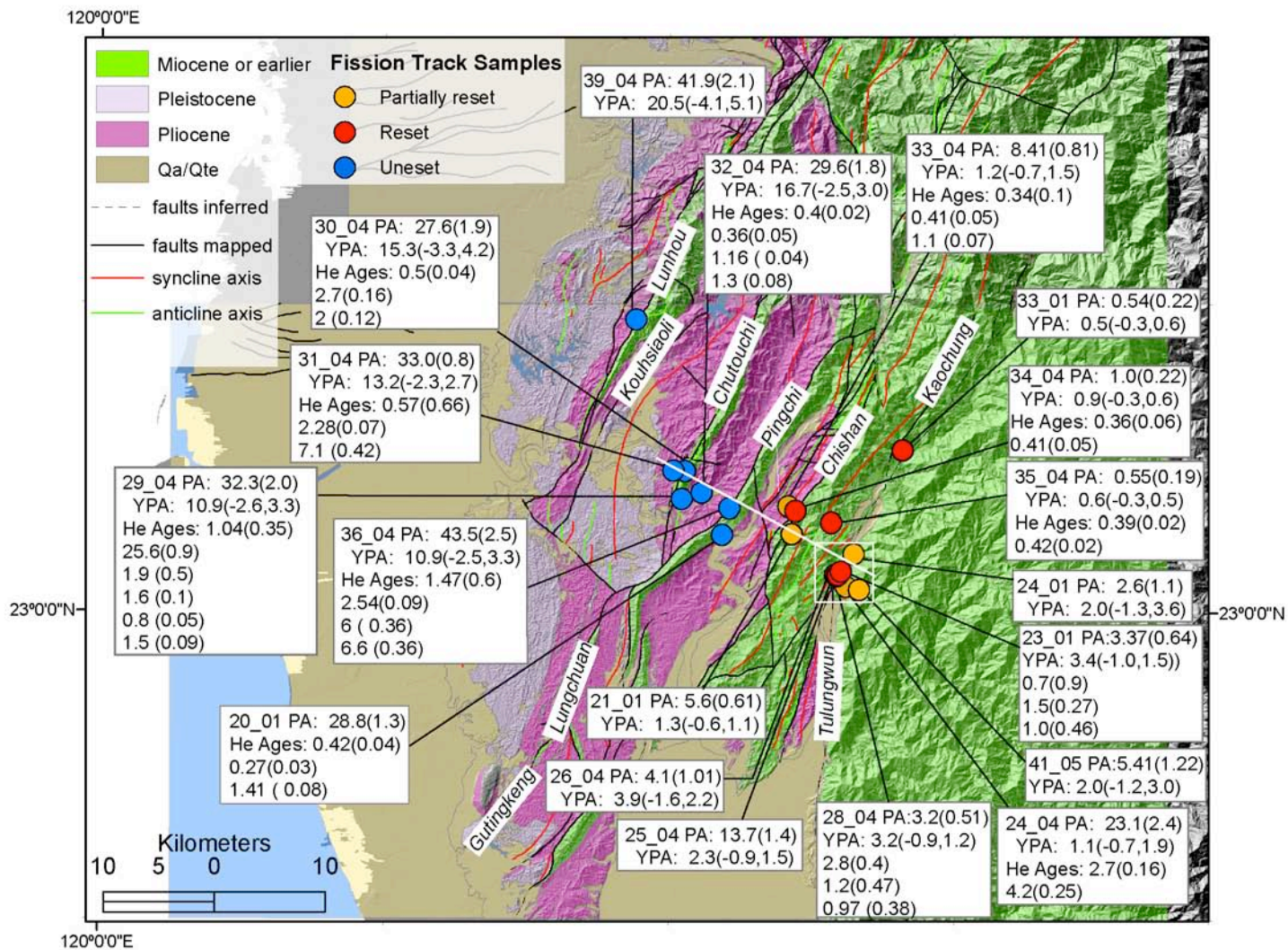


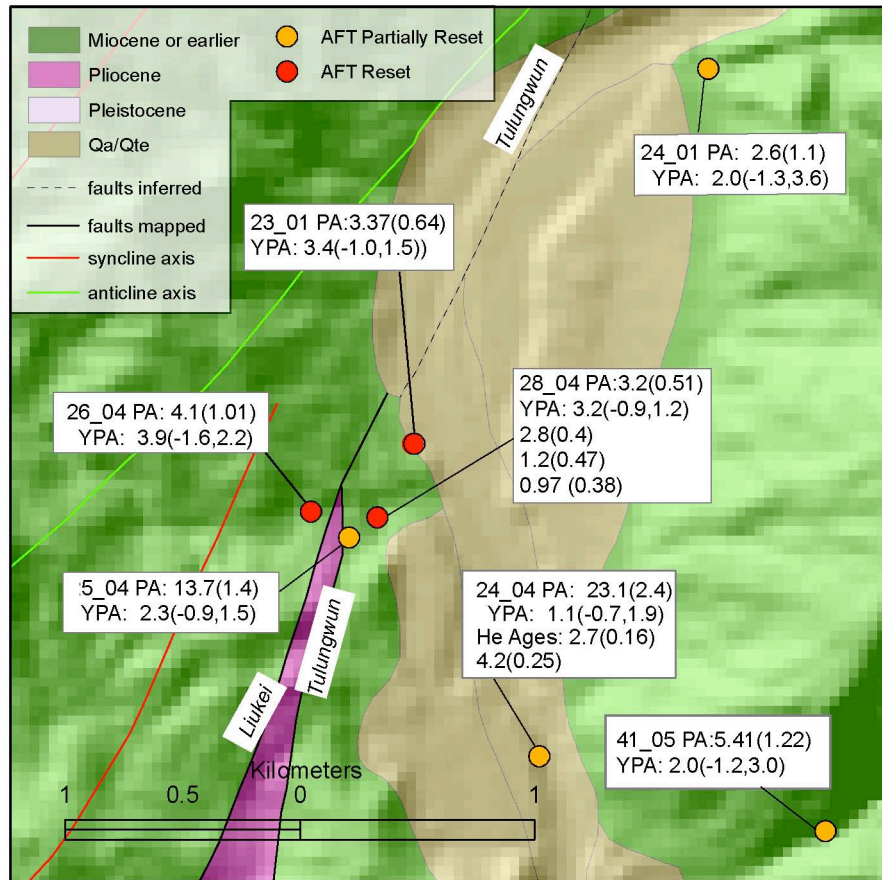


**Figure 3.6** Cross section and thermochronometric ages along the northern transect.

Structure and stratigraphy modified from Taoyun and Hsintien geologic maps (1:50000, Central Geologic Survey, MOEA, 1996; 2000) and sample (U-Th/He in apatite grain age and apatite fission track interpreted cooling age (table 3). For stratigraphic names and abbreviations, see figure 2. For transect location, see figures 1 and 5. Samples shown in red indicate reset, yellow indicates partially reset, blue is unreset. Error on thermochronometric age is  $2\sigma$  for pooled age and 95% asymmetric confidence intervals for YPA (tables 1, 2).

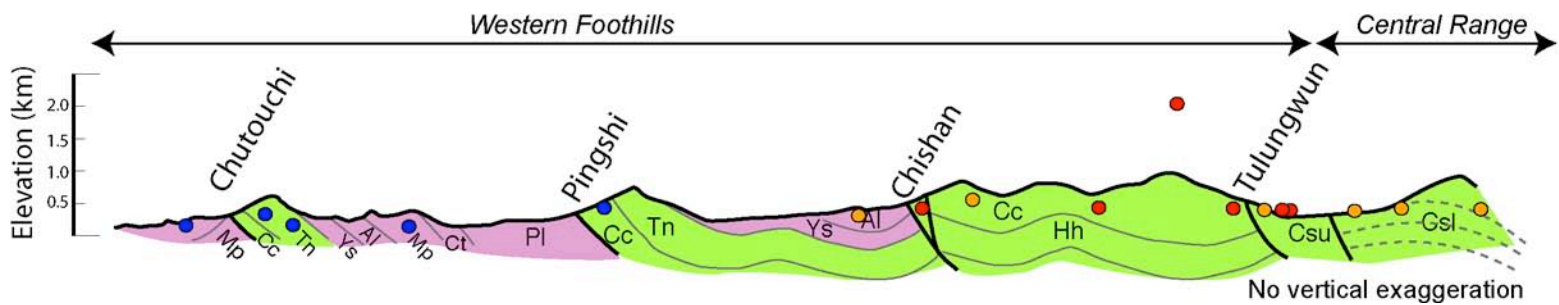
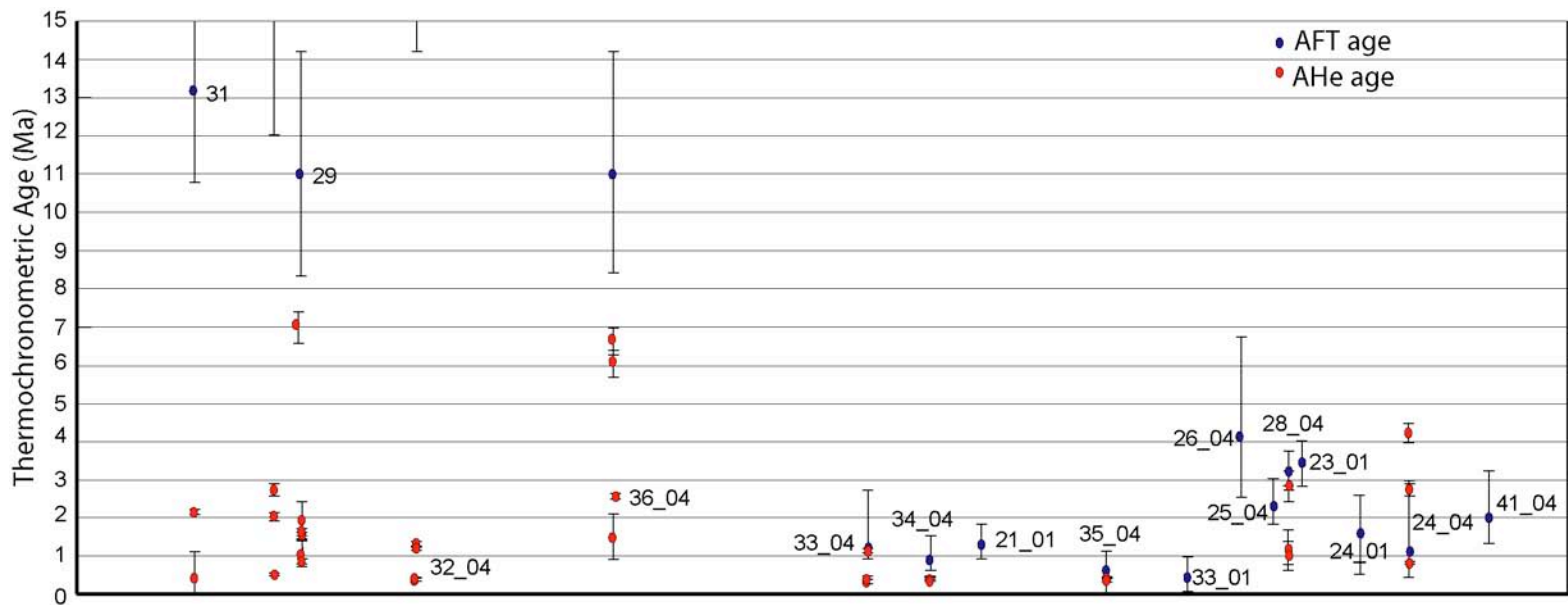
**Figure 3.7** Geologic map and sample locations in our southern sampling section. Location of map shown on figure 3.1. Structure and stratigraphy from Chinese Petroleum corporation 1:100000 Chai-i sheet, 1986. Sample locations and thermochronometric age. Fission track ages: given as Pooled ages (PA)  $\pm 2\sigma$  and young peak age (YPA) with asymmetric 95% confidence intervals. (U-Th)/He in apatite grain ages He ages:  $\pm 95\%$  confidence intervals. White line shows the location of the cross section in figure 3.9.





**Figure 3.8** Map of samples and their thermochronometric ages around the Tulungwun fault. For map location, see figure 7. PA - pooled age. YPA- young peak age. Ages in Ma PA  $\pm 2\sigma$ , YPA  $\pm$  asymmetric 95% confidence intervals.

**Figure 3.9** Cross section and thermochronometric ages the along the southern transect. Structure and stratigraphy modified from Chishan geologic map (1:50000, Central Geologic Survey, MOEA, 1999) and sample (U-Th/He in apatite grain age and apatite fission track interpreted cooling age (table 3). For stratigraphic names and abbreviations, see figure 2. For transect location, see figures 1 and 6. Samples shown in red indicate reset, yellow indicates partially reset, blue is unreset. Error on thermochronometric age is  $2\sigma$  for pooled age and 95% asymmetric confidence intervals for YPA (tables 1, 2).



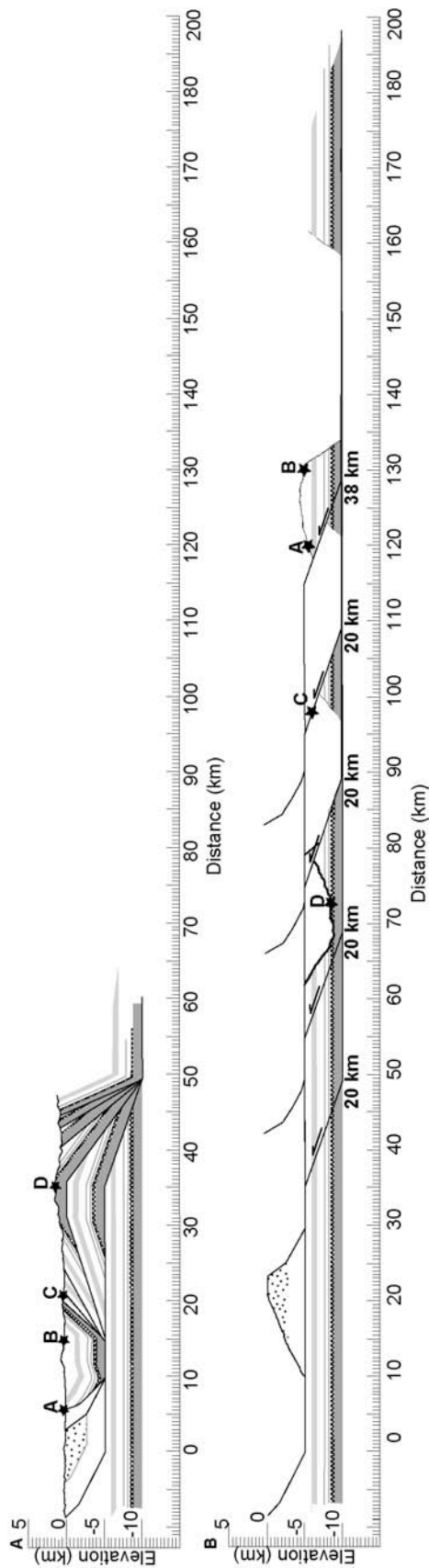


**Figure 3.10** Kinematic model of five foreland propagating thrust faults with a flat-ramp-flat-ramp geometry. A) Kinematic model deformed from undeformed state using the fault-parallel flow algorithm in the kinematic software package 2DMove. B) Initial undeformed state. Topography shown is the observed topography along the central transect. Temperature-time history for each point A-D are shown in figure 3.12. Each fault is activated sequentially and slips at 30 mm/yr for the distance shown on each fault. Each fault's lower ramp dips at 20°. As described in the text, this kinematic model is linked to thermal and thermochronometric models. Thermochronometric age pattern generated by this sequence of deformation is shown in figure 3.11. The kinematic model describes the style of deformation we argue exists in western Taiwan.

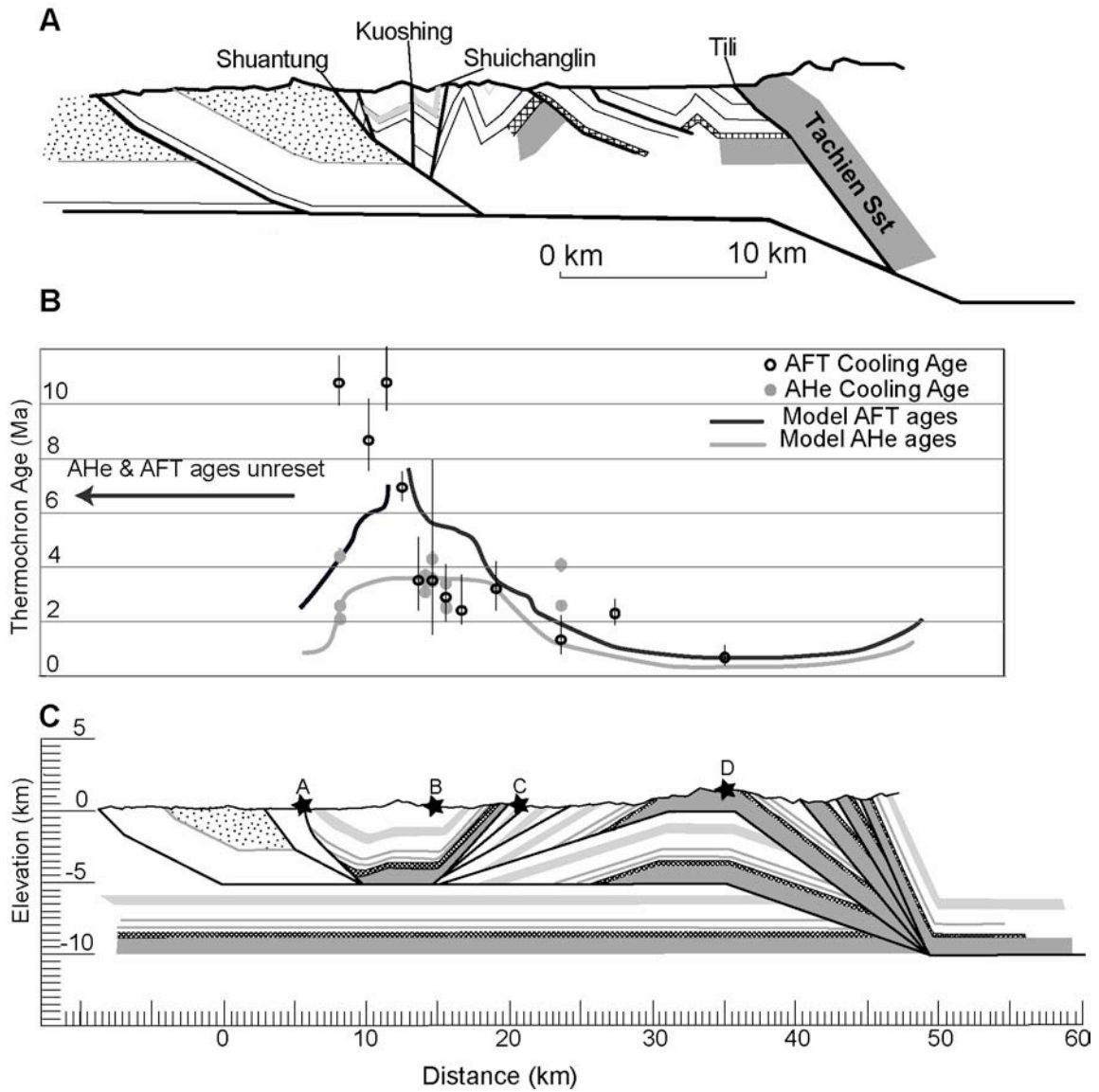


**Figure 3.11** Apatite fission track and (U-Th)/He ages generated by fault kinematics shown in figure 3.10. A) Balanced cross-section through the western foothills fold-thrust belt and eastern Hsuehshan Range in the vicinity of our Central transect from Yue et al., 2005. B) Thermochronometric AFT and AHe thermochronometric age generated from the kinematic model shown in 3.10 and observed thermochronometric age data along the central transect. C) Deformed cross-section. The topography is the actual topography along the central transect. Temperature-time history for points A-D in figure C are shown in figure 3.12.



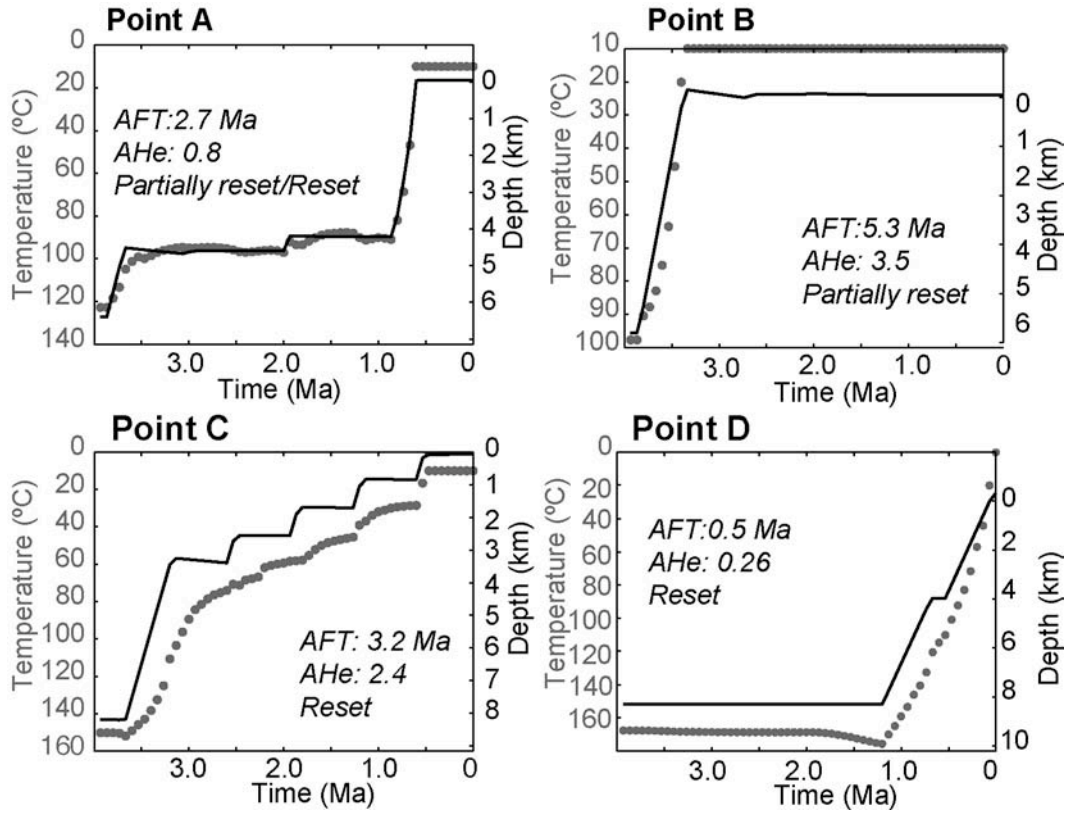


**Figure 3.12** Temperature-time histories for points shown in figure 3.10.

Point A records initial thrust motion. Material is exhumed through the AFT and AHe closure temperature above the thrust ramp and carried along the horizontal décollement at 5 km. In its most recent history, material point A is exhumed above the ramp of the frontal thrust. Point B also records initial thrusting, but is exhumed from the AFT closure temperature zone and AFT is partially-reset. Point C is exhumed by each thrust fault. Point D is exhumed from the greatest depths and records the youngest cooling ages.

**Notes to Chapter 3**

- Barnes, J. B., Ehlers, T. A., McQuarrie, N., O'Sullivan, P. B., & Pelletier, J. D. (2006). Eocene to recent variations in erosion across the central Andean fold-thrust belt, northern Bolivia: Implications for plateau evolution. *Earth and Planetary Science Letters*, 248, 118-133.
- Bollinger, L., Avouac, J. P., Beyssac, O., Catlos, E. J., Harrison, T. M., Grove, M., et al. (2004). Thermal structure and exhumation history of the Lesser Himalaya in central Nepal. *Tectonics*, 23, TC5015.
- Bollinger, L., Henry, P., & Avouac, J. P. (2006). Mountain building in the Nepal Himalaya: Thermal and kinematic model. *Earth and Planetary Science Letters*, 244, 58-71.
- Brandon, M. T. (1992). Decomposition of fission-track grain-age distributions. *American Journal of Science*, 292(8), 535-564.
- Brandon, M. T., Roden-Tice, M. K., & Garver, J. I. (1998). Late Cenozoic exhumation of the Cascadia accretionary wedge in the Olympic Mountains, Northwest Washington State. *Geological Society of America Bulletin*, 110(8), 985-1009.
- Brandon, M.T. (2002) Decomposition of mixed grain-age distributions using BINOMFIT. On Track, v. 24, p. 13-18 (informal report in newsletter)
- Byrne, T. B., & Liu, C. (2002). Introduction to the geology and geophysics of Taiwan. In: *Geology and Geophysics of an Arc-Continent Collision, Taiwan, Republic of China* (Ed. by T.B. Byrne & C.-S. Liu). *Special Paper - Geological Society of America*, 358, v-viii.
- Carena, S., Suppe, J., & Kao, H. (2002). Active detachment of Taiwan illuminated by small earthquakes and its control of first-order topography. *Geology*, 30(10), 935-938 .
- Carlson, W. D., Donelick, R. A., & Ketcham, R. A. (1999). Variability of apatite fission-track annealing kinetics; I, Experimental results. *American Mineralogist*, 84(9), 1213-1223.
- Ching, K., Rau, R., Lee, J., & Hu, J. (2007). Contemporary deformation of tectonic escape in SW Taiwan from GPS observations, 1995-2005. *Earth and Planetary Science Letters*, 262(3-4), 601-619.

- Covey, M. (1984). Lithofacies analysis and basin reconstruction, Plio-Pleistocene western Taiwan foredeep. *Petroleum Geology of Taiwan*, 20, 53-83.
- Dadson, S. J., Hovius, N., Chen, H., Dade, W. B., Hsieh, M., Willett, S. D., et al. (2003). Links between erosion, runoff variability and seismicity in the Taiwan orogen. *Nature*, 426(6967), 648-651.
- Donelick, R. A., O'Sullivan, P. B., & Ketcham, R. A. (2005). Apatite fission-track analysis. *Reviews in Mineralogy and Geochemistry*, 58(1), 49-94.
- Ernst, W. G., & Jahn, B. M. (1987). Crustal Accretion and Metamorphism in Taiwan, a Post-Palaeozoic Mobile Belt. *Philosophical Transactions of the Royal Society of London. Series A, Mathematical and Physical Sciences*, 321(1557), 129-161.
- Farley, K. A. Helium diffusion from apatite: General behavior as illustrated by Durango fluorapatite. *Journal of Geophysical Research*, 105(B2), PAGES 2903-2914.
- Flowers, R. M., Shuster, D. L., Wernicke, B. P., & Farley, K. A. (2007). Radiation damage control on apatite (U-Th)/He dates from the Grand Canyon region, Colorado Plateau. *Geology*, 35(5), 447-450.
- Fruneau, B., Pathier, E., Raymond, D., Deffontaines, B., Lee, C. T., Wang, H. T., et al. (2001). Uplift of Tainan Tableland (SW Taiwan) revealed by SAR interferometry. *Geophysical Research Letters*, 28, 3071-3074.
- Fuller, C., Willett, S., Fisher, D., & Lu, C. (2006). A thermomechanical wedge model of Taiwan constrained by fission-track thermochronometry. *Tectonophysics*, 425(1-4), 1-24.
- Galbraith, R.F., & Green, P.F. (1990) Estimating the component ages in a finite mixture. *Nucl. Tracks Radiat. Meas.*, 17, p196-206.
- Galbraith, R. F., & Laslett, G. M. (1993). Statistical models for mixed fission track ages. *International Journal of Radiation Applications and Instrumentation. Part D. Nuclear Tracks and Radiation Measurements*, 21(4), 459-470.
- Green, P. F., Crowhurst, P. V., Duddy, I. R., Japsen, P., & Holford, S. P. (2006). Conflicting (U Th)/He and fission track ages in apatite: Enhanced He retention, not anomalous annealing behaviour. *Earth and Planetary Science Letters*, 250, 407-427.
- Hasebe, N., Barbarand, J., Jarvis, K., Carter, A., & Hurford, A. J. (2004). Apatite

- fission-track chronometry using laser ablation ICP-MS. *Chemical Geology*, 207(3-4), 135-145.
- Hickman, J. B., Wiltschko, D. V., Hung, J., Fang, P., & Bock, Y. (2002). Structure and evolution of the active fold-and-thrust belt of southwestern Taiwan from Global Positioning System analysis. In: *Geology and Geophysics of an Arc-Continent Collision, Taiwan, Republic of China* (Ed. by T.B. Byrne & C.-S. Liu). *Special Paper - Geological Society of America*, 358, 75-92.
- Ho, C. S. (1988). *An Introduction to the Geology of Taiwan:- Explanatory Text of the Geologic Map of Taiwan, 2nd ed.*. Taipei, Taiwan: Central Geological Survey.
- Hodges, K. V., Wobus, C., Ruhl, K., Schildgen, T., & Whipple, K. (2004). Quaternary deformation, river steepening, and heavy precipitation at the front of the Higher Himalayan ranges. *Earth and Planetary Science Letters*, 220(3-4), 379-389.
- Hoth, S., Adam, J., Kukowski, N., & Oncken, O. (2006). Influence of erosion on the kinematics of bivergent orogens; results from scaled sandbox simulations. *Special Paper - Geological Society of America*, 398, 201-225.
- Hsieh, M., & Knuepfer, P. L. K. (2002). Synchronicity and morphology of Holocene river terraces in the southern Western Foothills, Taiwan; a guide to interpreting and correlating erosional river terraces across growing anticlines. In: *Geology and Geophysics of an Arc-Continent Collision, Taiwan, Republic of China* (Ed. by T.B. Byrne & C.-S. Liu). *Special Paper - Geological Society of America*, 358, 55-74.
- Hsieh, M., & Knuepfer, P. L. K. (2001). Middle-late Holocene river terraces in the Erhjen River Basin, southwestern Taiwan--implications of river response to climate change and active tectonic uplift. *Geomorphology*, 38(3-4), 337-372.
- Hsu, Y., Simons, M., Yu, S., Kuo, L., & Chen, H. (2003). A two-dimensional dislocation model for interseismic deformation of the Taiwan mountain belt. *Earth and Planetary Science Letters*, 211(3-4), 287-294.
- Hu JC, Yu SB, Chu HT, Angelier J (2002) Transition tectonics of northern Taiwan induced by convergence and trench retreat. In: *Geology and Geophysics of an Arc-Continent Collision, Taiwan, Republic of China* (Ed. by T.B. Byrne & C.-S. Liu). *Special Paper - Geological Society of America*, 358, pp. 147-160
- Huang, C., Yuan, P. B., & Tsao, S. (2006). Temporal and spatial records of active arc-continent collision in Taiwan; a synthesis. *Geological Society of America*

*Bulletin*, 118(3-4), 274-288.

- Huang, C., Yuan, P. B., Lin, C., Wang, T. K., & Chang, C. (2000). Geodynamic processes of Taiwan arc-continent collision and comparison with analogs in Timor, Papua New Guinea, Urals and Corsica. *Tectonophysics*, 325(1-2), 1-21.
- Huang, C., Yuan, P. B., & Tsao, S. (2006). Temporal and spatial records of active arc-continent collision in Taiwan: A synthesis. *Geological Society of America Bulletin*, 118(3-4), 274-288.
- Huang, S., Yang, K., Hung, J., Wu, J., Ting, H., Mei, W., et al. (2004). Deformation Front Development at the Northeast Margin of the Tainan Basin, Tainan–Kaohsiung Area, Taiwan. *Marine Geophysical Researches*, 25(1), 139-156.
- Huerta, A. D., & Rodgers, D. W. (2006). Constraining rates of thrusting and erosion; insights from kinematic thermal modeling. *Geology*, 34(7), 541-544.
- Hung, J., & Wiltschko, D. V. (1993). Structure and kinematics of arcuate thrust faults in the Miaoli-Cholan area of western Taiwan. *Petroleum Geology of Taiwan*, 28, 59-96.
- Ketcham, R. A., Donelick, R. A., & Carlson, W. D. (1999). Variability of apatite fission-track annealing kinetics; III, Extrapolation to geological time scales. *American Mineralogist*, 84(9), 1235-1255.
- Ketcham, R.A., Donelick, R.A., and Donelick, M.B., (2000) AFTSolve: A program for multi-kinetic modeling of apatite fission-track data. Geological Materials Research, v2n1.
- Kimura, G., Kitamura, Y., Hashimoto, Y., Yamaguchi, A., Shibata, T., Ujiie, K., et al. (2007). Transition of accretionary wedge structures around the up-dip limit of the seismogenic subduction zone. *Earth and Planetary Science Letters*, 255(3-4), 471-484.
- Lacombe, O., Mouthereau, F., Angelier, J., Chu, H., & Lee, J. (2003). Frontal belt curvature and oblique ramp development at an obliquely collided irregular margin; geometry and kinematics of the NW Taiwan fold-thrust belt. *Tectonics*, 22(3).
- Lee, Y., Chen, C., Liu, T., Ho, H., Lu, H., & Lo, W. (2006). Mountain building mechanisms in the Southern Central Range of the Taiwan Orogenic Belt -- From accretionary wedge deformation to arc-continental collision. *Earth and Planetary Science Letters*, 252(3-4), 413-422.

- Lin, A. T., Watts, A. B., & Hesselbo, S. P. (2003). Cenozoic stratigraphy and subsidence history of the South China Sea margin in the Taiwan region. *Basin Research*, 15(4), 453-478.
- Liu, T., Hsieh, S., Chen, Y., & Chen, W. (2001). Thermo-kinematic evolution of the Taiwan oblique-collision mountain belt as revealed by zircon fission track dating. *Earth and Planetary Science Letters*, 186(1), 45-56.
- Malavieille J, Lallemand SE, Dominguez S, Deschamps A, Lu CY, et al. (2002) Arc-continent collision in Taiwan: New marine observations and tectonic evolution. n: *Geology and Geophysics of an Arc-Continent Collision, Taiwan, Republic of China* (Ed. by T.B. Byrne & C.-S. Liu). *Special Paper - Geological Society of America*. 187-211
- Marques F. O., & Cobbold P. R. (2002) Topography as a major factor in the development of arcuate thrust belts: insights from sandbox experiments. *Tectonophysics*, 348(4), 29, pp. 247-268.
- Mouthereau, F., Lacombe, O., Deffontaines, B., Angelier, J., & Brusset, S. (2001). Deformation history of the southwestern Taiwan foreland thrust belt; insights from tectono-sedimentary analyses and balanced cross-sections. *Tectonophysics*, 333(1-2), 293-322.
- Sakaguchi, A., Yanagihara, A., Ujiie, K., Tanaka, H., & Kameyama, M. (2007). Thermal maturity of a fold-thrust belt based on vitrinite reflectance analysis in the Western Foothills complex, western Taiwan. *Tectonophysics*, 443(3-4), 220-232.
- Sella, G. F., Dixon, T. H., & Mao, A. (2002). REVEL: A model for Recent plate velocities from space geodesy. *Journal of Geophysical Research*, 107(B4), 2081.
- Shin, T., & Teng, T. (2001). An Overview of the 1999 Chi-Chi, Taiwan, Earthquake. *Bulletin of the Seismological Society of America*, 91(5), 895-913.
- Shuster, D. L., Flowers, R. M., & Farley, K. A. (2006). The influence of natural radiation damage on helium diffusion kinetics in apatite. *Earth and Planetary Science Letters*, 249(3-4), 148-161.
- Shyu, J. B. H., Sieh, K., Chen, Y., & Chung, L. (2006). Geomorphic analysis of the Central Range Fault, the second major active structure of the Longitudinal Valley suture, eastern Taiwan. *Geological Society of America Bulletin*, 118(11-12), 1447-1462.

- Shyu, J. B. H., Sieh, K., Chen, Y., & Liu, C. (2005). Neotectonic architecture of Taiwan and its implications for future large earthquakes. *Journal of Geophysical Research*, *110*, B08402.
- Sibuet, J., & Hsu, S. (2004). How was Taiwan created? *Tectonophysics*, *379*(1-4), 159-181.
- Sibuet, J., Hsu, S., Le Pichon, X., Le Formal, J., Reed, D., Moore, G., Liu, C. (2002). East Asia plate tectonics since 15 Ma: constraints from the Taiwan region. *Tectonophysics*, *344*(1-2), 103-134.
- Simoes, M., & Avouac, J. P. (2006). Investigating the kinematics of mountain building in Taiwan from the spatiotemporal evolution of the foreland basin and western foothills. *Journal of Geophysical Research*, *111*, B10401.
- Simoes, M., Avouac, J. P., Chen, Y., Singhvi, A. K., Wang, C., Jaiswal, M., Chan, Y., Bernard, S. (2007). Kinematic analysis of the Pakuashan fault tip fold, west central Taiwan: Shortening rate and age of folding inception. *Journal of Geophysical Research*, *112*, B03S14.
- Sneyd, A. D. (1984). A computer program for calculating exact confidence intervals for age in fission-track dating. *Computers & Geosciences*, *10*(2-3), 339-345.
- Stewart, R. J., & Brandon, M. T. (2004). Detrital-zircon fission-track ages for the "Hoh Formation"; implications for late Cenozoic evolution of the Cascadia subduction wedge. *Geological Society of America Bulletin*, *116*(1-2), 60-75.
- Suppe, J., & Anonymous. (1981). Mechanics of mountain-building and metamorphism in Taiwan. *Chung Kuo Ti Ch'ih Hsueh Hui Chuan Kan, Memoir of the Geological Society of China*, *4*, 67-89.
- Suppe, J. (1980a). A retrodeformable cross section of northern Taiwan. *Proceedings of the Geological Society of China*, *23*, 46-55.
- Suppe, J. (1980b). Imbricated structure of Western Foothills Belt, southcentral Taiwan. *Petroleum Geology of Taiwan*, *17*, 1-16.
- Suppe, J. (1983). Geometry and kinematics of fault-bend folding. *American Journal of Science*, *283*(7), 684-721.
- Suppe, J., Chen, C., Chen, J., Lee, C., & Pan, K. (1984). Kinematics of arc-continent collision, flipping of subduction, and back-arc spreading near Taiwan. *Chung Kuo Ti Ch'ih Hsueh Hui Chuan Kan, Memoir of the Geological Society of China*, *6*, 21-33.

- Tagami, T., & O'Sullivan, P. B. (2005). Fundamentals of fission-track thermochronology. *Reviews in Mineralogy and Geochemistry*, 58(1), 19-47.
- Teng, L. S. (1992) Geotectonic evolution of Tertiary continental margin basins of Taiwan. *Petroleum Geology of Taiwan*, 27, 1-19.
- Teng, L. S. (1996). Extensional collapse of the northern Taiwan mountain belt. *Geology*, 24(10), 949-952.
- Tensi, J., Mouthereau, F., & Lacombe, O. (2006). Lithospheric bulge in the West Taiwan Basin. *Basin Research* 18 (3), 277-299.
- Tillman, K. S., Byrne, T. B., Teng, L. S., & Huang, C. (1996). Out-of-sequence thrusting in the Taiwan slate belt. *Journal of the Geological Society of China*, 39(2), 189-208.
- Willett, S. D., Fisher, D., Fuller, C., Yeh, E., & Lu, C. (2003). Erosion rates and orogenic-wedge kinematics in Taiwan inferred from fission-track thermochronometry. *Geology*, 31(11), 945-948.
- Wobus, C. W., Hodges, K. V., & Whipple, K. X. (2003). Has focused denudation sustained active thrusting at the Himalayan topographic front? *Geology*, 31(10), 861-864.
- Yu, S., Chen, H., & Kuo, L. (1997). Velocity field of GPS stations in the Taiwan area. *Bulletin of the Institute of Earth Sciences*, 17, 43-44.
- Yu, S., Kuo, L., Hsu, Y., Su, H., Liu, C., Hou, C., Lee, C., Lai, T., Liu, C., Liu, C., Tseng, T Tsai, C. Shin T. (2001). Preseismic Deformation and Coseismic Displacements Associated with the 1999 Chi-Chi, Taiwan, Earthquake. *Bulletin of the Seismological society of America*, 91(5), 995-1012.



## Chapter 4

### **Thermal-kinematic modeling of apatite fission track and apatite (U-Th)/He ages in the southern Western Foothills fold-and-thrust belt, Taiwan.**

#### **4.1 Summary**

We use a geologically constrained thermo-kinematic thrust-fault model to track temperature-depth paths to understand the timing and geometry of burial and exhumation along a transect in the southern western-foothills fold-and-thrust belt, Taiwan. A dense suite of new apatite fission track and (U-Th)/He data, combined with surface structure and stratigraphy, allows a detailed analysis of the timing and kinematics of thrust faulting and folding. We retro-deform a geologically constrained cross-section to predict thermochronometric ages and establish the amount, patterns, and rates of burial and exhumation in the southern Taiwan thrust-belt.

Apatite fission track data (AFT) record rapid burial in a depositional basin on the subduction accretionary prism prior to thrust exhumation. The depositional basin is interpreted as wedge-top depozone whose geometry is similar to the modern-day Pingtung Basin. The Chishan, Pingshi and Chutouchi faults at the rear of the thrust belt are inactive sub-marine accretionary prism faults that pre-date burial in the wedge top depositional basin and are not related to arc-continent collision. Arc-continent collision is marked at 1 Ma by the onset of rapid exhumation that cools material through the apatite fission-track and (U-Th)/He closure temperatures. Exhumation occurs at  $\sim 8.5$  mm/yr above a sequence of shallowly dipping ( $\sim 16.5^\circ$ ),  $\sim 4$  km high thrust ramps that cut the Miocene-Oligocene strata. The thrust ramp links the main Taiwan décollement to a décollement at 6 km in lower Miocene units and is currently located at the rear of the thrust belt near the boundary between the Central Range and Western Foothills.

The burial and exhumation history recorded by the AFT and AHe cooling ages captures the transition from subduction to arc-continent collision as part of the southward progressing collisional-system. Modern day equivalents of the burial and

exhumation history captured by the AFT and AHe data are seen to the south, and the more evolved equivalents of the events are evident to the north.

## 4.2 Introduction

The Western Foothills fold-and-thrust belt lies at the edge of the Taiwan orogen which forms from the oblique collision of the Luzon arc and the Chinese Continental margin (Figure 4.1). The obliquity of the Luzon arc to the Chinese continental margin results in a southward propagating collision so that the southern section of the thrust belt is its youngest part. The youngest southern part of the thrust belt is currently the most active accommodating upward of 30 mm/yr of plate convergence (Suppe, 1984; Yu et al., 1997; Shyu et al., 2005; Huang et al., 2000; 2006). As collision propagates to the south, subduction is replaced by arc-continent collision. The southern part of the Western Foothills records this first stage of the arc-continent collision providing an excellent location to understand the transition from accretion to collision and investigate the processes that form the more mature Taiwan orogen to the north.

The Taiwan Western Foothills contain a series of NE-SW striking, west-verging thrusts and fault-related folds which form a series of ridges and valleys creating classic fold-and-thrust belt topography. The structures in southern Taiwan can be traced from the developed fold-and-thrust belt southward into the depositional basins and thrust structures in the submarine Kaoping slope and Manila trench accretionary prism (Figure 4.1 and 4.2, Liu et al., 1997; 2004 Shyu et al., 2005). To the east, the southern fold-and-thrust belt is bounded by the Tulungwun or Laonung fault at the edge of the Central Range, and to the west the thrust belt is bounded by the undeformed coastal plain (Figure 4.2).

Geologic cross-sections through the thrust belt show a series of foreland propagating thrust-ramps that either sole into décollements in the Pliocene, Miocene, and perhaps Oligocene passive-margin strata (Suppe, 1980; 1983, Hung & Wiltschko, 1993; Hung et al., 1999; Hickman et al., 2002; Huang et al., 2004) or continue as steeply dipping faults into the Pre-Miocene basement (Mouthereau et al., 2001).

Rapid uplift and shortening is occurring along a shallowly dipping blind thrust-fault beneath the Chiayi Hills at the western edge of the thrust belt that appears to accommodate almost all of the convergence in the southern Taiwan thrust belt (Hung et al., 1999; Huang et al., 2004; Shyu et al., 2005). The series of prominent NW-SE striking west-verging thrust-faults that outcrop across the Western Foothills are not active on geomorphic or geodetic time scales (Shyu et al., 2005).

Geologic cross-sections provide a 'static picture of thrust fault evolution in the thrust belt. Balanced cross-sections of thrust belts typically assume faults have propagated sequentially into the foreland but there is evidence for 'out-of-sequence' faulting (Mouthereau et al., 2001). Low-temperature radiometric dating techniques such as apatite fission track (AFT) and apatite (U-Th)/He (AHe) can provide a chronology of erosion, and, by inference, the deformation history. A dense suite of apatite fission track thermochronometric ages in southern Taiwan (Chapter 3) presents an excellent opportunity to investigate the burial, exhumation and kinematics of the developing southern Taiwan thrust-belt.

The AFT data in western Taiwan document a general southward and westward propagating collision (Chapter 3). The AFT and AHe ages record spatially varying amounts of burial and complex kinematics associated with thrust faulting and fault-bend folding (Chapter 3). To interpret the complexities in the AFT and AHe ages, we use a 2d thermal-kinematic-thermochronometric numerical model of thrust faulting and fault-bend-folding. The density of AFT data allows for detailed thermal-kinematic modeling of the burial and exhumation recorded by a thermochronometric age to place good constraints on the timing, rate of exhumation, and nature and geometry of thrust faults, and date the onset of arc-continent collision.

### **4.3 Tectonic Setting of Taiwan**

The Taiwan orogen forms from the collision of the Luzon island arc, on the Philippine Sea plate and the Asian continental margin on the Eurasian plate. Collision is occurring at ~80-90 mm/yr (Yu et al, 1997; Sella et al., 2002). Convergence is

partitioned between two major zones of shortening, one at the Longitudinal Valley fault in eastern Taiwan and the other at the frontal thrust of the Western Foothills fold-and-thrust belt (Yu et al, 1997, Hsu et al., 2003). The Luzon arc is oblique to the Chinese continental shelf causing collision to propagate southward with time at a rate of around 60–90 km/my (Suppe, 1981; Byrne & Liu, 2002, Liu et al, 2001). Collision began first in the north and is only just beginning in the south around the latitude of this study.

#### **4.4 Geology of the Western Foothills fold-and-thrust belt**

Like all convergent orogens, the Taiwan orogen is flanked by a fold-and-thrust belt its edge. The Western Foothills are a classic example of a fold-and-thrust belt. A sequence of NE-striking parallel thrust faults deform passive margin and synorogenic sediments creating a series of repeating Miocene and Pliocene stratigraphic sections. The fold-and-thrust belt is one of 6 geological regions. The others are, from west to east, the Hsüehshan Range, the Central Range, the Longitudinal Valley, and the Coastal Range (Figure 4.1).

##### *4.4.1 Stratigraphy of the southern Western Foothills.*

The southern Western Foothills contains late Oligocene to Neogene shallow marine to shelf sedimentary rocks and synorogenic upper Pliocene and Pleistocene rocks. The older late-Oligocene, Miocene and early-Pliocene sediments are intercalated marine silts muds, and interspersed sands, deposited on the shelf and slope of the Eurasian continental passive margin (Ho, 1988). The Miocene depositional basin progressively deepens to the south recorded by the progressive fining and thickening of the Miocene stratigraphic units, and the lack of carbonaceous material that exists in northern Taiwan (Chang and Chi, 1983; Covey, 1984; Ho, 1988). The changing depth of the Miocene basin from east to west and north to south, superimposed by eustatic sea level fluctuations, causes spatially rapid lithostraphic variations, and unit boundaries that are gradational or interfingering. The complex stratigraphy has resulted in local

formation names and unit correlations based mainly on fossils rather than lithology (Chang and Chi, 1983, Ho, 1988).

From around the middle Pliocene the sediment source to the depositional basin changed from being fed from Eurasia, to being fed from the east by the newly emerging Taiwan orogen. At the latitude of our study, sedimentation in the basin ceased in the early Pleistocene after deposition of shallow marine and terrestrial conglomerates that mark the emergence of this part of the Western Foothills with the onset of collision (Ho, 1988, Chang and Chi, 1983, Chen et al., 2001).

#### *4.4.2 Structure of the southWestern Foothills fold-and-thrust belt.*

The Western foothills contains a sequence of north-northeast striking thrust faults that deform the Neogene stratigraphy (Figure 4.2). The thrust faults have a ramp and flat geometry. Fault ramps sole into common décollement layers and beds deform above changes in the fault dip creating fault-bend-folds (Suppe, 1980). There are 5 major faults in our study region, the Lunhou, Chutouchi, Pingshi, Chishan and Tulungwun faults. These faults are intersected by many smaller fault splays (figure 4.2). The southern foothills is bounded to the east by the Tulungwun fault, a steep thrust-fault that divides the Western Foothills fold-and-thrust belt from rocks of the Central Range. In our study area, the Tulungwun fault separates the upper Miocene Changshikeng formation from the lower Miocene Changshan formation. Just to the south, the Tulungwun fault is a sharp topographic boundary dividing Miocene stratigraphy in the hangingwall from thick Quaternary deposits of the Pingtung plain in the footwall (Figure 4.2). Despite this sharp topographic boundary and large stratigraphic separation across the fault, there is no evidence for recent thrust activity, although the Tulungwun fault may have been reactivated as a strike-slip fault (Hickman et al., 2002; Lacombe et al., 2003). The depositional Pingtung plain pinches out northward and ends just south of our study area (Figure 4.2).

To the west of the Tulungwun fault, Miocene, Pliocene, and in the Lunhou thrust sheet Pleistocene stratigraphic units outcrop in the thrust sheets. As is typical in

fold-and-thrust belts, the vertical stratigraphic separation across the thrust faults is relatively minor.

Presently, deformation is accommodated by a blind fault or faults in the footwall of the Chukou thrust that form the Niushan anticline and the Chiayi hills (Suppe, 1980; Shyu et al., 2005; Huang et al., 2004; Shyu et al., 2005)). Geodetically measured shortening rates across this structure are around 30 mm/yr (Yu et al., 1997, Hsu et al., 2003.) The western most fault, the Chukou fault which is also called the Lunhou fault, may have been active as recently as 38 ka but there is no geomorphic or geodectic evidence for recent activity on this or any of the other mapped faults that outcrop in the region (Shyu et al., 2005).

#### **4.5 Thermochronometry in SW Taiwan**

Apatite fission track is a radiometric dating technique that uses the damage tracks in the apatite crystal lattice left by the spontaneous fission of Uranium. An apatite fission track (AFT) age records the time since material cooled through a closure temperature zone above which all tracks anneal and below which all tracks are retained. The primary mechanism of cooling and exhumation in the Western Foothills fold-and-thrust belt is erosion related to brittle deformation along thrust fault structures. These ages record cooling in response to motion along thrust faults and constrain the timing of the thrust structures in the southern Western Foothills.

Depending on the amount of exhumation, AFT ages are ‘reset’, ‘partially-reset’, or ‘unreset’. ‘Unreset’ material is exhumed from above the closure temperature and retains a pre-collisional age. These ages do not document cooling, but they do place an upper limit on the total amount of exhumation. ‘Partially-reset’ AFT samples record that material has not been buried to temperatures sufficient for all fission tracks to fully anneal, but age population analysis can provide a young age that records the most recent cooling (Brandon et al. 1992; Brandon, 2002). ‘Reset’ AFT samples have been buried to temperatures sufficient for fission tracks in apatite to fully anneal before being exhumed.

In the southern thrust-belt, AFT ages exist in Lunhou, Chutouchi, Pingshi, Chishan, and Tulungwun thrust sheets (Chapter 3, Figure 4.2). West of the Pinghi thrust, all samples are unreset indicating exhumation from above the AFT closure temperature. Samples in the Pingshi thrust are unreset and partially-reset, and samples in the Tulungwun and Chishan thrust sheets are partially- or fully-reset. The unreset ages west of the Pingshi thrust do not record the time these thrust faults were active but do record that this material has been exhumed from above the AFT closure temperature. The cooling ages in the partially- and fully-reset samples in the Pingshi, Chishan and Tulungwun faults record erosion associated with motion along these thrusts and can potentially be used to date these structures.

In the southern foothills, cooling ages range from 4.1 Ma to 0.5 Ma (Figure 4.2). The very youngest ages in the hinterland of the thrust belt are good evidence of rapid, recent exhumation despite the lack of geodetic or geomorphic indicators of convergence. The youngest cooling ages along the southern transect are located in the hanging wall of the Pingshi and Chishan thrusts, they are: 0.55 Ma, sample 35\_04; 0.54 Ma, sample 33\_01; 1.0 Ma, sample 34\_04, 1.2 Ma, sample 33\_04; and 1.3 Ma sample 21\_01. Samples 33\_04 and 21\_01 are partially-reset, and 33\_01, 34\_04 and 35\_04 are fully reset. These youngest cooling ages record the most recent exhumation span a very narrow, approximately 5 km wide.

The youngest cooling ages do not appear to record exhumation along the west-verging thrust fault exposed at the surface. The thermochronometric age pattern generated by a west verging surface breaking fault would result in a sharp break in age across a fault, and the youngest ages and the most deeply exhumed material would be in the hangingwall immediately next to the fault ( Chapter 2). This is not what is observed. The fully reset material with the youngest cooling ages is located in the middle of the Chishan thrust sheet, while samples closer to the Pingshi, Chutouchi and more frontal thrusts are partially-reset with older cooling ages. There is no sharp change in AFT age across the Chishan thrust.

Instead of a surface breaking-thrust, the older ages toward the foreland, and the distribution of reset and partially-reset material, indicate exhumation over a buried thrust ramp (Bollinger et al., 2004; 2006; Huerta & Rodgers 2006; Chapters 2 & 3, Figure 4.3). The youngest ages (samples 33\_01 and 35\_04) are interpreted to record the ‘ramp-reset zone’ across a blind thrust (Figure 4.3).

Located only 5 km to the east of the youngest sample (35\_04), AFT cooling ages of 3 Ma exist in the footwall and hangingwall of the Tulungwun fault (Figure 4.2). The 3 Ma ages cross the Tulungwun fault consequently do not record cooling from motion along this fault.

The 3 Ma ages from around the Tulungwun fault significantly pre-date exhumation at ~ 1-0.5 Ma recorded by the youngest AFT ages in the center of the Chishan thrust sheet. Thus the zone of youngest cooling ages recording motion above the buried thrust fault span < 10 km. The limited spatial extent of the young ages places tight constraints on the kinematics of thrust exhumation and geometry of the thrust fault (hatched region, Figure 4.2). To investigate these complex thermochronometric age patterns and constrain the geometry of the buried ramp, we use the thermal-kinematic thrust fault model described in Chapter 2.

#### **4.6 Thrust fault model**

Thrust fault related exhumation is a 2 (or 3)-dimensional process that is not captured in a 1-dimensional approach to interpreting AFT ages. Complex thrust kinematics are evident in the rapid variations in cooling rate and burial depth recording by AFT ages in the Western Foothills (Figure 4.2). To appropriately interpret the thermochronometric ages we use a 2-dimensional thermal-kinematic model of thrust faulting and folding that is constrained by the stratigraphy and structure of the southern section of the western-foothills fold-and-thrust belt.

Our approach uses the present day stratigraphy, structure, and the time and amount of exhumation recorded by the AFT ages, to construct a sequence of cross-sections at different stages in deformation along a transect crossing the study area. The



cross sections show the timing, significance and geometry of the thrust structures that have built the southern fold-and-thrust belt (Figure 4.2). The cross sections are constrained by previously published geologic cross sections, geologic maps, and the patterns of thermochronometric age in the thrust belt. Below, we describe our numerical model, and the geological and thermochronological constraints that we used to build our preferred model of deformation. The preferred model describes the exhumation and kinematics of deformation in the thrust belt over the last 1 Ma.

#### *4.6.1 Numerical Model*

The numerical model couples a 2-dimensional kinematic-structural and 2-dimensional advection-diffusion thermal model to produce temperature-time histories. The temperature-time histories are used to calculate fission track annealing and He retention to predict low-T thermochronometric ages that results from thrust exhumation. This model is described in detail in Chapter 2. The kinematic model is *2DMove* (*Midland Valley*) which allows representation of diverse styles of deformation in a fold-and-thrust belt. We use the fault-parallel flow deformation in the kinematic modeling software *2DMove* to generate of fault-bend-folds (Suppe, 1980). The velocity field from the kinematic model field is fed into a finite-element, advection-diffusion thermal model tracking the thermal response to the faulting and fault-related folding. The approach generates material cooling histories that we use to calculate thermochronometric age.

The assumptions of this approach are 1) exhumation in the Western Foothills occurs by erosion related to thrust faulting and fault-bend-folding, and 2) erosion is totally efficient, permitting no topography. These assumptions apply in the Western Foothills because there is very little topography in the study area, all samples are collected within 300 m elevation, and uplift and erosion rates are very rapid and related to active structures (Dadson et al., 2003).

#### 4.6.2 Building the thermal-kinematic model

##### *Constraints on Ramp Dip*

Above a thrust ramp, the group of youngest AFT and AHe cooling ages is created by material exhumed constantly from the closure temperature to the surface and thus constrains vertical exhumation rate (point P, Figure 4.3, Chapter 2). The vertical exhumation rate is controlled by the rate of fault slip and the thrust-ramp dip. In the southern Western Foothills, the rate of fault slip can be constrained by the geodetically measured shortening rate to be  $\sim 30$  mm/yr (Yu et al., 1997). Using the measured shortening, the dip of the ramp and resulting vertical exhumation rate along the cross-section was derived by running a series of models with varying the thrust-ramp dips to isolate the best fit model. For 30 mm/yr of horizontal shortening, the youngest thermochronometric cooling ages along the cross section are fit best by a  $\sim 16.5^\circ$  dipping thrust ramp producing  $\sim 8.5$  mm/yr of vertical exhumation. Our thermo-kinematic modeling shows that, with 30 mm/yr of shortening, a shallower ramp dip lowers the exhumation rate producing AFT ages older than observed, and a steeper dip results in ages younger than observed. Our finding of a  $16.5^\circ$  dipping ramp is similar to the  $18^\circ$  dip suggested for the ramps at the front of the thrust (Suppe, 1980).

##### *Depth of the Décollements.*

The shallowly dipping blind ramp identified by the young AFT ages, must step between two décollements. There is structural and stratigraphic evidence for a décollement at the base of the middle-upper Miocene Changshikeng formation (Nanchuang formation, Figure 4.2). The Changshikeng formation is exposed in the hangingwall of the Lunhou, Chutouchi and Pingshi thrust sheets and runs parallel to the faults. The Changshikeng formation also outcrops in the Chishan thrust sheet, but is deformed into many small scale folds and rather than paralleling a thrust hanging-wall flat. This relationship shows the thrust steps down the stratigraphic section to expose deeper units. Further evidence of a lower décollement is the existence of lower Miocene Mushan formation in imbricate thrust sheets beneath the Chiayi hills (Suppe, 1980, 1983, figure 4.2).

There is no obvious décollement in the Chishan or Tulungwun thrust sheets but two possible décollement horizons have been identified. Suppe (1980; 1983) places a décollement in the lower Miocene Mushan formation at ~6-8 km to explain the structures beneath the Chukou fault. Hung & Wiltschko (1993) Hung et al. (1999) and Hickman et al. (2002), place a deeper décollement at 9-13 km in the lower Miocene or upper Oligocene strata. This deeper décollement is around the level of the main Taiwan décollement that is seismically imaged to the north (Carena et al., 2002) and the depth of the main décollement constrained by GPS dislocation modeling (Hsu et al., 2003).

Here, our preferred model includes three décollements. An upper décollement in the Changshikeng formation that is well constrained by surface structure and stratigraphy, a décollement in the lower Miocene following the interpretation of Suppe, 1980, and a décollement at 10 km, the approximate depth of the main Taiwan décollement. These three décollements are linked by two ramps. One thrust ramp beneath the Chishan thrust sheet linking the main Taiwan décollement to the décollement in the lower Miocene stratigraphy, and a second thrust ramp at the front of the thrust belt that links the upper and lower Miocene décollements. Motion above the ramp that links the upper two décollement layers forms the growing structure beneath the Chiayi hills (Suppe, 1980; Shyu et al., 2006).

The depth of the upper-Miocene Changshikeng formation, which contains one décollement, is ~5 km (Suppe, 1980; Mouthereau et al., 2001; Hickman et al., 2002). A depth of around 5 km is consistent with the partially and fully-reset AFT samples in Changshikeng formation, the partially reset samples indicating exhumation from depths around the fission track partial annealing zone, and 5 km is about the depth to the AFT partial annealing zone for typical crustal geothermal gradients (Figure 4.2).

The deeper décollement in our model is at the approximate depth of the main Taiwan décollement which is seismically imaged to the north (Carena et al., 2002). A décollement at approximately this depth has been suggested by Hung & Wiltschko, (1993), Hung et al. (2000), and Hickman et al. (2002). We interpret this as vertical exhumation above the ramp linking the main Taiwan décollement and the décollement

in the lower-Miocene units that exhumes material through the AFT closure temperature producing the young cooling ages observed at the eastern edge of our transect. Without the existence of this deeper décollement, exhuming material from beneath the AFT closure temperature would require multiple imbricate thrust ramps. The active ramp in such an imbricate thrust system would be active as an ‘out-of-sequence’ thrust coincident with and in the same décollement levels as the thrust-ramp beneath the Chiayi hills.

The middle décollement in our model is in the lower Miocene strata at around 6 km. The middle décollement is required because a ramp between the depth of the Changshikeng formation at 5 km, and the depth of the main Taiwan décollement at 10 km, generates a zone of AFT reset ages that are wider than observed. A shorter thrust ramp generates a narrower zone of reset ages (Chapter 2).

#### *4.6.4 Evidence for a migrating thrust ramp*

The AFT cooling ages record a thrust ramp beneath the hinterland of the thrust belt that is not fixed but migrates with time. These youngest cooling ages become older toward the foreland at a rate of 0.5 Ma over 5 km (Figure 4.2). For a non-migrating ramp, this gradient would be produced by 10 km/Myr of horizontal slip (Bollinger et al., 2004; 2006; Huerta and Rogers, 2006) which is a third of the geodetically measured rate of shortening (Yu et al., 1997). The pattern of AFT ages generated by a non-migrating thrust ramp with a horizontal slip rate at the geodetically measured 30 mm/yr would span a zone much wider than the 5-10 km observed. Also, an individual non-migrating thrust ramp with the geometry described, exhumes material from insufficient depths to expose reset AFT ages. A longer thrust ramp would exhume material from greater depths, but a longer ramp widens the zone of reset ages beyond what is observed.

These AFT ages can be used to determine the rate of ramp migration. Using the approach outlined in Chapter 2, the rate of ramp migration is calculated using the oldest cooling age (1.0 Ma, sample 34\_04, figure 4.2) which records the onset of thrust

exhumation, and the youngest cooling age (0.5-0.6 Ma, samples 35\_04, 33\_01, figure 4.2):

$$\text{Foreland age gradient} = \frac{\text{Distance between oldest cooling age \& youngest cooling age}}{(\text{oldest cooling age} - \text{youngest cooling age})}$$

$$\text{Foreland age gradient} = \frac{5 \text{ km}}{(1.0 \text{ Ma} - 0.5 \text{ Ma})} = 10 \text{ km/Myr}$$

$$\begin{aligned} \text{Rate of ramp migration} &= \text{Horizontal velocity} - \text{Foreland age gradient} \\ &= 30 \text{ mm/yr} - 10 \text{ mm/yr} = \mathbf{20 \text{ mm/yr for 1 Ma}} \end{aligned}$$

#### 4.6.5 Ramp spacing and amount of slip on the ramp

We choose a ramp spacing of 10 km which is the approximate distance separating surface faults and fits the width and distribution of the young AFT data. The narrowest width of reset ages is achieved when the slip along each fault approximately equals the fault spacing. If slip is less than this, the zone of young ages widens toward the hinterland. If slip is much greater than the fault spacing, the zone of young, reset ages widens toward the foreland. Assuming a fault spacing of 10 km, the thermochronometric age distribution constrains the amount of slip along each fault to be ~ 10 km.

#### 4.6.6 Onset of thrust exhumation

The data is best fit when thrust faulting begins at 1 Ma, which is marked by the oldest reset cooling age in the fold-thrust belt (sample 34\_04) that typically indicates thrust initiation (Chapter 2). The YPA observed in samples 33\_04, 1.2 Ma and 33\_01, 1.3 Ma could potentially record thrust initiation but a slightly earlier onset of thrust motion at ~1.2 Ma widens the zone of reset and partially reset AFT ages generating a poorer fit between the model and data. We interpret that the youngest age populations in samples 33\_04 and 33\_01 are partially-reset and do not date thrust motion.

## 4.7 Discussion

### 4.7.1 Modeled collision-related exhumation

The fault geometry and kinematics described by the modeled deformation sequence is a migrating thrust ramp that links the main Taiwan décollement at 10 km to a décollement at 6 km in the lower Miocene section (Figure 4.4 & 4.5). Three fault ramps are activated sequentially. Once one fault becomes active, the other fault is deactivated (Figure 4.5). The total model run time is 1 Ma. Faults 1 and 2 slip for 11 km and fault 3 slips for 8 km. All faults dip at 16.5° and slip at 30 mm/yr. The model generates a thermochronometric age pattern that closely matches the pattern observed (Figure 4.4A).

Although not shown, increasing or decreasing the amount of slip along any of the faults widens the zone of young AFT ages that record thrust exhumation beyond what is observed. Increasing the length of the ramp widens the zone of reset AFT ages, and decreasing and increasing the fault dip causes a mismatch between the modeled and observed youngest AFT age (0.5 Ma).

Samples 35\_04 and 33\_01 in the center of the Chishan thrust sheet are modeled as having experienced the greatest amount of exhumation since 1 Ma (Figure 4.6B). Moving away from this point, material is exhumed from progressively shallower depths. Samples around the Tulungwun fault are modeled as being exhumed from the AFT partial annealing zone and are partially-reset (Figures 4.6C & D). Sample 34\_04 is modeled as being exhumed through the AFT closure temperature at 1 Ma with the first fault motion (Figure 4.6A). To the west of sample 34\_04, material is modeled as being exhumed from the partial annealing zone consistent with the partially-reset AFT ages recorded by samples 21\_01 and 33\_04. The onset of thrusting at 1 Ma is consistent with the increase in the rate of sedimentation into the southern part of the foreland basin at around this time (Chang and Chi, 1983; Chen et al., 2001; Monthereau, 2001).

The model predicts material around the Tulungwun fault to be partially or unreset, but reset ages are observed (Figure 4.2). However, the reset ages in the hangingwall of the Tulungwun fault and at the rear of the Chishan thrust sheet are at

least 1.5 Ma older than the cooling event we model and, although these ages indicate cooling, it is probably not related to arc-continent collision. Because the Tulungwun fault 'reset' ages record an earlier cooling event, the model prediction of unreset and partially reset ages around the Tulungwun fault is consistent with those observed. The significance of these older cooling ages are discussed in more detail below.

The kinematic model of collision related thrust faulting describes uplift above three shallowly dipping thrust fault ramps creating a large anticline structure beneath the Chishan thrust sheet (Figure 4.5). The detailed structure in the Chishan thrust sheet is complex, but an anticline structure like the one generated in the model exists in the balanced cross-sections of Hickman et al. (2002) and is interpreted in the cross sections from the 1:50000, Central Geologic Survey geologic map, Chishan sheet (MOEA, 1999).

#### *4.7.2 Apatite (U-Th)/He ages*

In the majority of samples, AHe repeat grain ages show considerable scatter (Figure 4.2, Chapter 3). We interpret the data scatter to result from partial-resetting of the (U-Th)/He system and radiation damage that alters the AHe closure temperature of each grain (Farley, 2000; Green et al., 2006; Schuster et al., 2006; and Flowers et al., 2007). Consistent grain ages record deeper exhumation from beneath the AHe and radiation damage closure temperatures. AHe ages from samples 33\_04, and 34\_04, yield consistent AHe ages of ~0.4 Ma which are interpreted to result from deeper exhumation. The remaining samples AHe grain ages are not consistent recording shallower amounts of exhumation. Our model fits the amounts of burial recorded by the observed AHe ages, predicting deeper exhumation in the center of the Chishan thrust sheet and shallower exhumation east and west (Figures 4.4, 4.5). The zone of reset AHe ages generated in our model is slightly wider than observed, but this may reflect different amounts of radiation damage in the measured ages which is not considered in our thermochronometric model.

#### 4.7.3 *Pre-collision Burial*

Partially-reset and unreset samples, and the cooling ages recorded by reset and partially-reset samples, document sample location and depth of exhumation prior to the modeled deformation sequence. At 1 Ma, samples that have a cooling age  $< 1$  Ma were below the AFT closure temperature zone, and material that is partially-reset, unreset, or has a cooling age  $> 1$  Ma was above the closure temperature zone. The reset and unreset samples show that the stratigraphy was not flat-laying at 1 Ma because the AFT closure temperature zone did not parallel the stratigraphic layers (Figure 4.5D & 4.7).

The pre-1 Ma sample location and the structure of the stratigraphic layers could result from either thrust faulting that differentially uplift samples, or from sediment burial. The structure of the Chishan thrust sheet argues against differential uplift from thrust motion prior to 1 Ma. There is no fault separating the 3 Ma aged samples at the rear of the Chishan thrust from  $< 1$  Ma aged samples in the center and front of thrust sheet (Figure 4.7 Ma). Also, there is no evidence for a buried fault and thrust-anticline centered around the Tulungwun fault. Instead, the Changshikeng formation is the only stratigraphic unit outcropping in the Chishan thrust sheet and the formation displays many small scale folds overprinting a broad anticline centered at the front the of the Chishan thrust sheet. It is more likely the pre-exhumation age distribution record a purely depositional feature.

The geometry of this depositional feature is similar to the geometry of the present-day basin depositional basin which extends from the Pintung plain southward to depositional basins offshore (Chiang et al., 2003, Figure 4.2 & 4.6). Given the space-time equivalence in the southward propagating collisional system, the existence of the Pingtung and offshore basins provides support for the existence of an equivalent feature at the latitude of our transect at 1 Ma.

The Chishan fault and probably the Pingshi fault pre-date the thrust exhumation that began at 1 Ma and must have been active prior to burial. Therefore, these faults are likely accretionary prism faults formed by the subduction of the Eurasian plate beneath the Phillipine sea plate and pre-date the onset of arc-continent collision. Modern



versions of these subduction related thrust faults exist today in the Manila trench accretionary prism to the south of Taiwan.

Burial equivalent to that recorded by the AFT data prior to 1 Ma is currently occurring on the Kaoping slope offshore southern Taiwan. Large quantities of sediment shed from the growing Taiwan orogen are carried by longitudinal rivers such as the Laonung River and deposited over inactive faults in the accretionary prism and inactive faults buried beneath the Pingtung plain (Figure 4.2, Liu et al., 1997; 2004; Huang et al., 2004; Chiang et al., 2005; Shyu et al., 2005; Chiang & Yu, 2006). The Pingtung plain is rapidly loaded with sediment and is subsiding by as much as 13 mm/yr (Shyu et al., 2005; Ching et al., 2007).

Local burial in a paleo-Pingtung plain and Kaoping slope basin explains the differential burial recorded by samples collected from the same stratigraphic depth. For example, sample 34\_04 is fully reset, and sample 33\_04 is partially-reset even though they are both stratigraphically above material that is unreset (Figure 4.2). Samples 34\_04 and 33\_04 were beneath the depositional basin, but samples from equivalent stratigraphic units to the west were not buried and remain unreset.

Post exhumation burial of the Chishan thrust sheet also reconciles seemingly inconsistent amounts of exhumation recorded by the two different thermochronometers AFT and AHe. Sample 28\_04 has a fully reset apatite fission track ages of 3.2 Ma indicating cooling through the AFT partial annealing zone at this time. Seemingly at odds with this, (U-Th)/He ages from the same sample are scattered, recording partial resetting of this lower closure temperature thermochronometer (Figure 4.3). Post-exhumational burial in a deposition basin explains this confusing result if sample 28\_04 at first cools through the AFT closure temperature at 3.2 Ma. Post-cooling, burial in the depositional basin partially resets the lower closure temperature AHe system, but is insufficient to reset the AFT system. The AFT and AHe ages from sample 23\_04 also record this signal of post-cooling burial.

#### 4.7.4 Pre-Collision exhumation

At the rear of the Chishan thrust sheet and in the hanging wall of the Tulungwun fault, there are a group of reset AFT ages recording exhumation around 3.5 Ma pre-dating the modeled onset of thrusting at 1 Ma (Figure 4.2). The ages pre-date the generally accepted timing for the onset of collision in southern Taiwan and this older cooling event is perplexing. 3.5 Ma ages are approximately coincident with the cessation of island arc-volcanism at this latitude recorded by the build up of limestone reefs on volcanic islands at 3.1-2.9 Ma. These reefs were then accreted to the east coast of Taiwan at around 1 Ma (Huang et al., 1995). There is an 3.7-3.5 Ma unconformity at the base of the Pliocene stratigraphy at the southern tip of the Hengchung Peninsula that records the sub-aerial emergence of the old forearc ridge (Huang et al., 2006). Our AFT ages provide support the sub-aerial exposure of the Hengchung Peninsula and the hinterland portion of the thrust belt at ~ 3-4 Ma.

Exhumation at 3.5 Ma is not related to slip along the thrust faults in the Western Foothills. The Pingshi thrust could not have exhumed material in the Chishan and Tulungwun thrust sheets at 3 Ma because the deepest exhumed material in a thrust sheet is located the hanging wall immediately next to the fault and sample 36\_04 in the immediately next to the Pingshi fault is unreset. 3.5 Ma could record motion along the Chishan thrust, but only if the Chishan thrust had a geometry different to that interpreted here and has a much greater stratigraphic offset than appears (Figure 4.5 D). It is more likely that the 3.5 Ma ages record exposure and erosion of the accretionary prism that is unrelated to thrusting (Lee et al., 2006).

Prior to burial in the accretionary slope depositional basin as described above, samples with the youngest ages (1.2-0.5 Ma, samples 21\_01, 33\_01, 34\_04, & 35\_04) may have recorded the same ~3.5 Ma ages but this signal was erased by burial. Marine sediments preserved in the Chutouchi and Lunhou thrust sheets shows at least the western portion of the thrust belt was submerged at 3.5 Ma and remained submerged until ~ 1 Ma. The marine Maopu shale deposited around 3.5 Ma contains turbidites that

may record sub-aerial exposure of the Hengchun Peninsula and perhaps very eastern part of the foothills (Mouthereau et al., 2001).

The 3-4 Ma ages that exist either side of the Tulungwun fault indicate there has been no significant thrust motion along the fault since at least 3 Ma (Figure 4.2). The 4 Ma aged sample in the footwall of the Tulungwun fault makes it unlikely that this fault is responsible for the uplift of the Hengchung Peninsula but we can not rule this out. The sample in the footwall of the Tulungwun fault is slightly (0.5 Ma) older than material in the hangingwall recording possible motion at ~2.5-3.5 Ma, the age of samples in the hangingwall. There is no evidence for motion along Tulungwun fault more recently than 2 Ma thus the sharp topographic boundary between the Pingtung plain and the Hengchung Peninsula to the south is purely depositional.

Subaerial exposure of the Hengchun Peninsula has been interpreted as a stage of ‘initial arc continent collision’ (Huang et al., 2000; 2006), but uplift and exhumation may be a purely an accretionary prism process and occur during subduction of oceanic crust beneath the Luzon arc, rather than thrust-faulting that accommodates the collision of the Luzon arc with the Chinese continental margin (McIntosh et al., 2005).

#### **4.8 Alternative interpretation: Backthrust**

Mouthereau et al., (2001) interpret an eastward-verging backthrust between the westward-verging Chishan fault and the Tulungwun fault that would separate the 3.5 Ma from the <1 Ma AFT ages. The sharp break in AFT cooling ages appear initially to support this interpretation. Thermal-kinematic modeling shows a backthrust does generate AFT ages that match those observed (Figure 4.8). However, the east-verging back-thrust that needs to extend from the surface to a depth of at least 7 km in order to exhume material with reset AFT ages and to 10 km to match the observed age distribution. There is no geomorphological or geological evidence for such a significant feature in the Chishan thrust sheet. Instead, the Miocene Changshikeng formation is gently folded to almost flat and is the only formation outcropping in the Chishan thrust sheet making a back-thrust an unlikely scenario.

#### **4.9 Summary of exhumation and thrust faulting in the southern western-foothills fold-thrust belt.**

The prominent surface breaking west-verging thrust faults, the Pingshi and Chutouchi, and perhaps the Chishan fault are accretionary prism faults that pre-date arc-continent collision. These accretionary prism faults are west-verging thrust faults that sole into a décollement in the Miocene Changshikeng formation. These accretionary prism faults form the classic ridge and valley topography of the southwestern thrust belt and the hangingwall fault-related fold structures.

At around 3.5 Ma, the eastern part of the subduction accretionary prism became sub-aerially exposed. Sub aerial exposure of the of the eastern portion of the accretionary prism, the Hengcheng Peninsula, and perhaps the hinterland portion of the Western Foothills, is not attributed to motion and uplift along the thrust faults exposed in the southern Western Foothills.

After 3.5 Ma, sediment rapidly accumulated in a 'wedge top depozone' on the eastern part of the accretionary prism (Chiang et al., 2004, DeCelles & Giles, 1996), burying the inactive accretionary prism fault, the Chishan fault. This depositional process is occurring to the south today.

The onset of arc-continent collision is marked by motion above a shallowly dipping thrust ramp beneath the Chishan thrust sheet at 1 Ma that rapidly exhumes material at the rear of the thrust belt. The thrust ramp links two décollement layers, one décollement in the lower Miocene, and the main Taiwan décollement in a deeper stratigraphic layer. Over time, the ramp migrates toward the foreland accreting lower Miocene and perhaps upper Oligocene stratigraphy. Motion along the thrust ramp creates an anticline that exposes older stratigraphy at the rear of the thrust belt.

Using current kinematic models, slip is passed out into the coastal plain along the top décollement. This scenario is consistent with the geomorphology, and GPS measurements show that the bulk of shortening appears to occur beneath the Chukou fault and in the Chiayi Hills (Figure 4.2). Compared to the shortening accommodated by the 'triangle zone' features at the front of the thrust belt (Suppe, 1980; 1983; Huang et

al., 2004), the fault-bend-fold formed above the deeper thrust ramp accommodates small amounts of shortening, but generates rapid exhumation.

As collision continues, the ramp at the rear of the thrust belt will expose older stratigraphy and the overlying accretionary prism faults will be removed by erosion above the active thrust ramp at the rear of the thrust belt. Thus although Oligocene rocks of the Hsüeshan Range are not exposed at the latitude of our study, an implication of this deformation model is that the Hsüeshan Range will grow southward as deeper units are exposed above the active ramp.

#### **4.10 Conclusions**

The thrust faults modeled in this study have a relatively simple geometry. However, even simple thrust faults with multiple thrust ramps can generate complex exhumation patterns that can not be established using an approach that does not consider the 2-dimensional kinematics that characterize thrust exhumation. This study shows that it is possible to use 2-dimensional kinematic-thermal models like the one used here to understand the detailed cooling histories recorded by thermochronometric data and constrain the timing and geometry of burial and thrust fault deformation which can not be captured with one-dimensional approach.

The thermal kinematic modeling in this study helps understand the history of burial and exhumation in southern Taiwan recorded by the thermochronometric data. The history of burial and exhumation captured by the thermochronometric data describes the burial and thrust faulting that mark the transition from subduction to collision. The cooling histories that capture the onset of collision in southern Taiwan are consistent with a relatively constant southward and westward progressing exhumation.

**Table 4.1** Thermal Model Parameters.  
Parameters used in thermal and thermochronometric model.

<b>Model Parameter</b>	<b>Value</b>
Specific heat	1000 J kg <sup>-1</sup> K <sup>-1</sup>
Thermal conductivity	2.5 Wm <sup>-1</sup> K <sup>-1</sup>
Radiogenic Heat Production	1 μW/m <sup>3</sup>
length scale of heat production	10 km (exponential decay)
Upper Boundary Condition	20 °C
Rock density	2500 (kg/m <sup>3</sup> )
Lower Boundary Condition	0.03 W/m <sup>2</sup>
Model Depth	30 km
Model Width	130 km
Time step	0.03 Ma
Dpar	1.87
Padding used in thermochronometric model	2 Ma

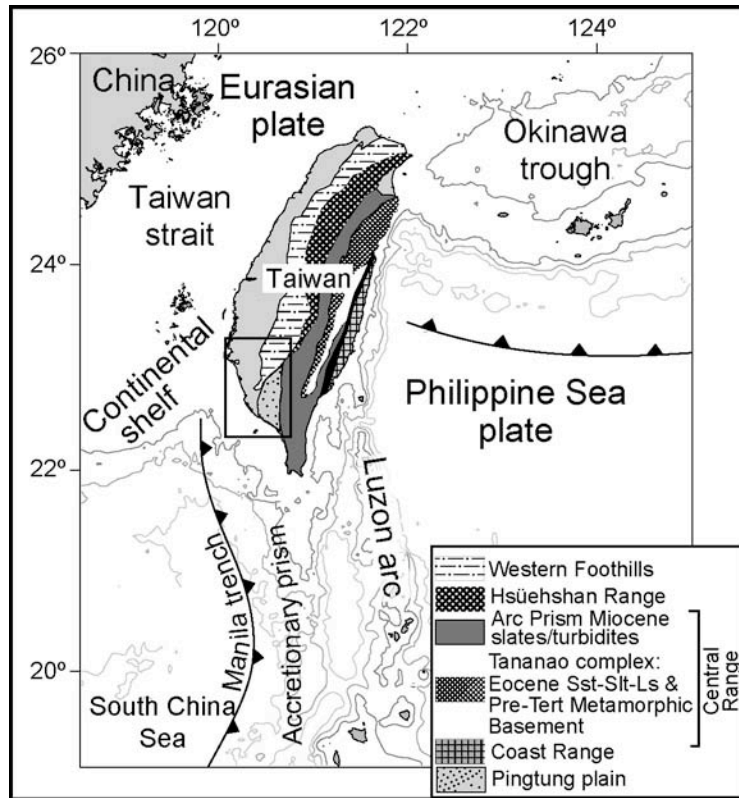


**Figure 4.1** Tectonic Setting and Geologic units of Taiwan.

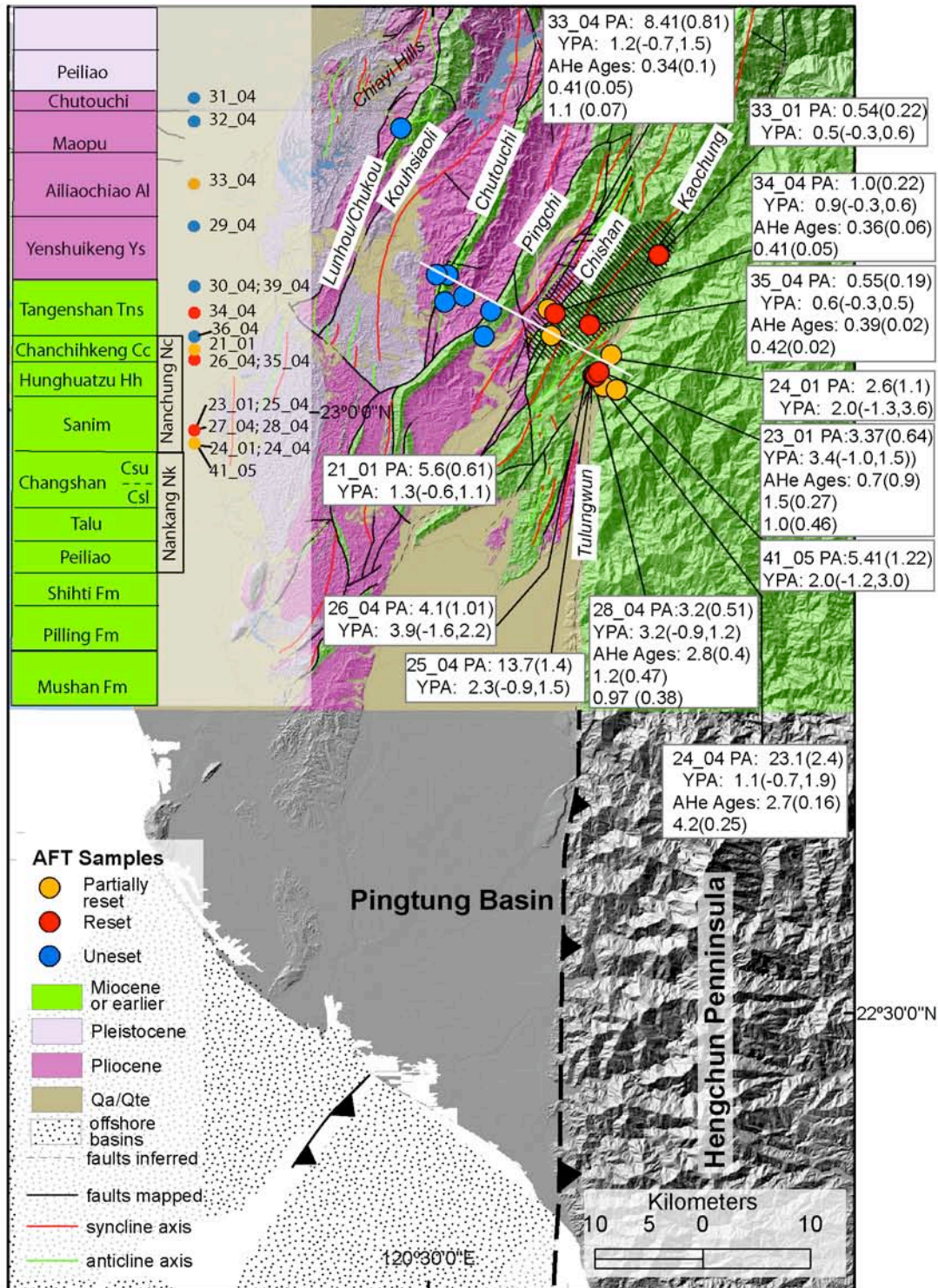
After Ho, 1988; Lundberg et al., 1997; Subuet and Hsu, 1997; Fisher et al., 2002; Lamcombe et al., 2003. Base map from Stolar et al., 2007 showing 1, 2, & 3 km bathymetry. Black box shows location of figure 4.2.

**Figure 4.2** Geologic map, stratigraphy and thermochronometric sample location.

Location of map shown on figure 4.1. Structure and stratigraphy from Chinese Petroleum corporation 1:100000 Chai-i sheet, 1986. Sample locations and thermochronometric age of reset and partially reset samples. Fission track ages: given as Pooled ages (PA)  $\pm 2$  s and young peak age (YPA) with asymmetric 95% confidence intervals. He ages: (U-Th)/He in apatite grain ages  $\pm 95\%$  confidence intervals. White line shows the location of the model cross section shown in figure 4.4. Age classification as reset, unreset and partially reset from Chapter 3. Cross-hatched region shows zone of young cooling ages that are interpreted to record exhumation above a thrust ramp. Inset shows generalized stratigraphy compiled from Tensi et al., 2006, Ho, 1988, and MOEA 1:50000 Central Geologic Survey Maps, 1999, Chasien Sheet; Lee et al., 2002; Huang et al., 2004) with samples stratigraphic units. Offshore piggy-back basins from Chiang et al., 2005.



120°30'0"E



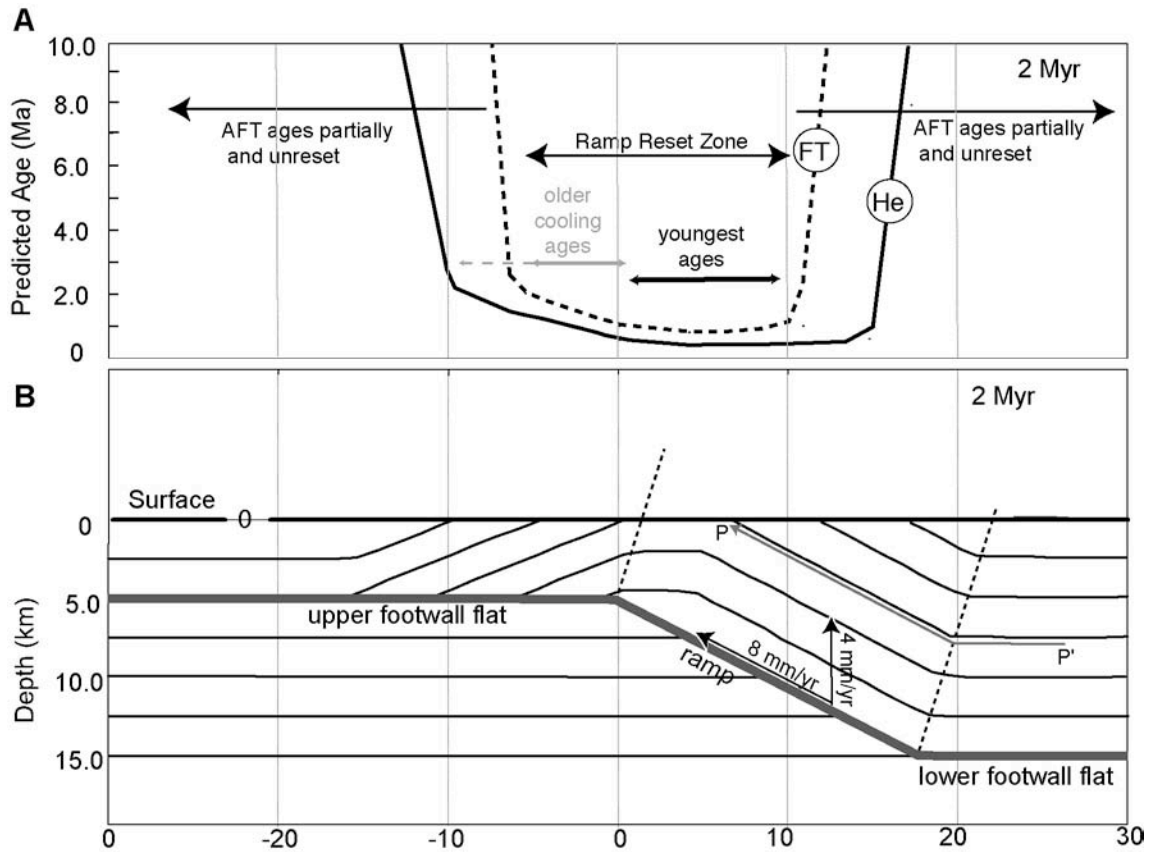
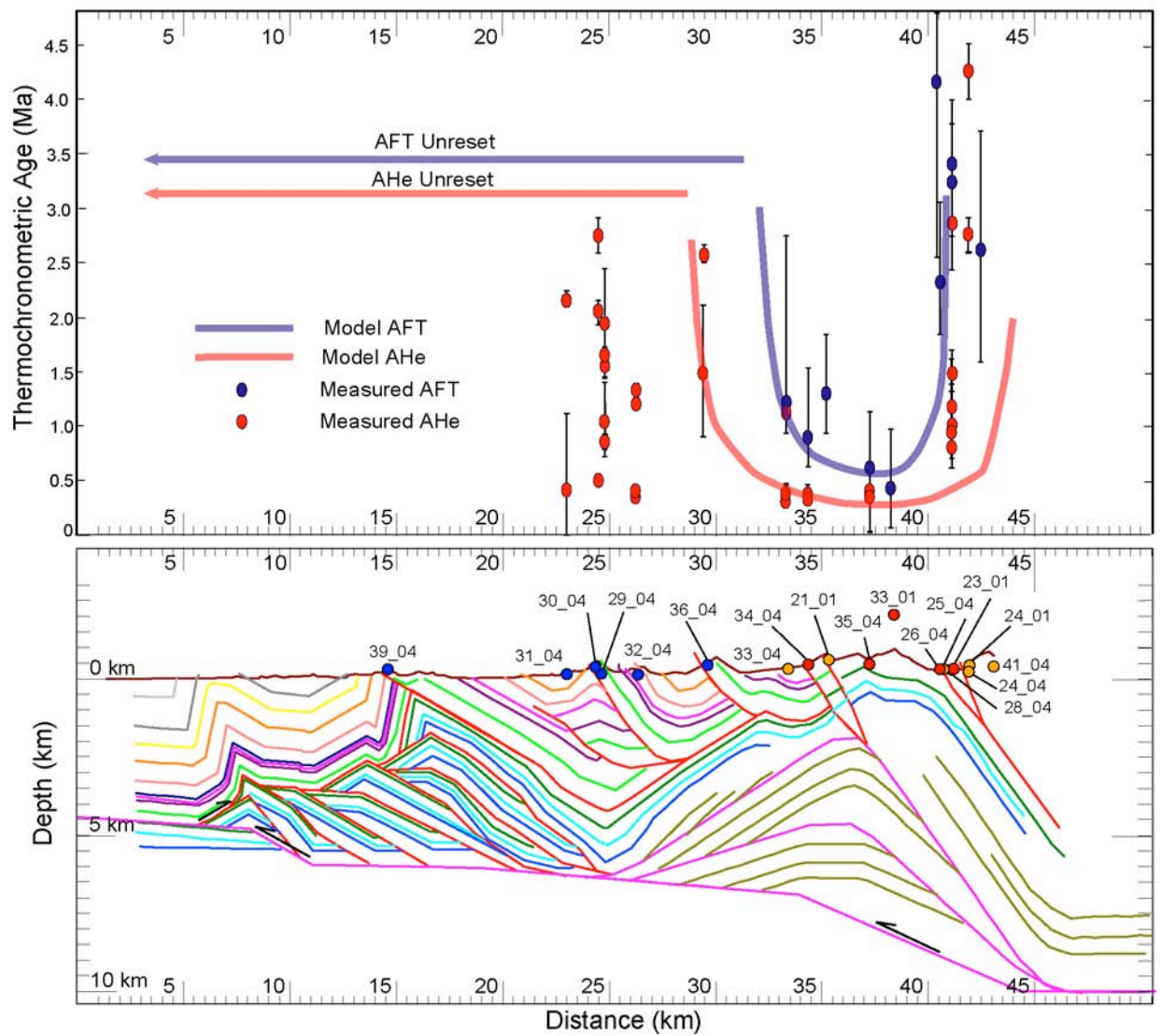


**Figure 4.3** Example of thermo-kinematic-thermochronometric model.

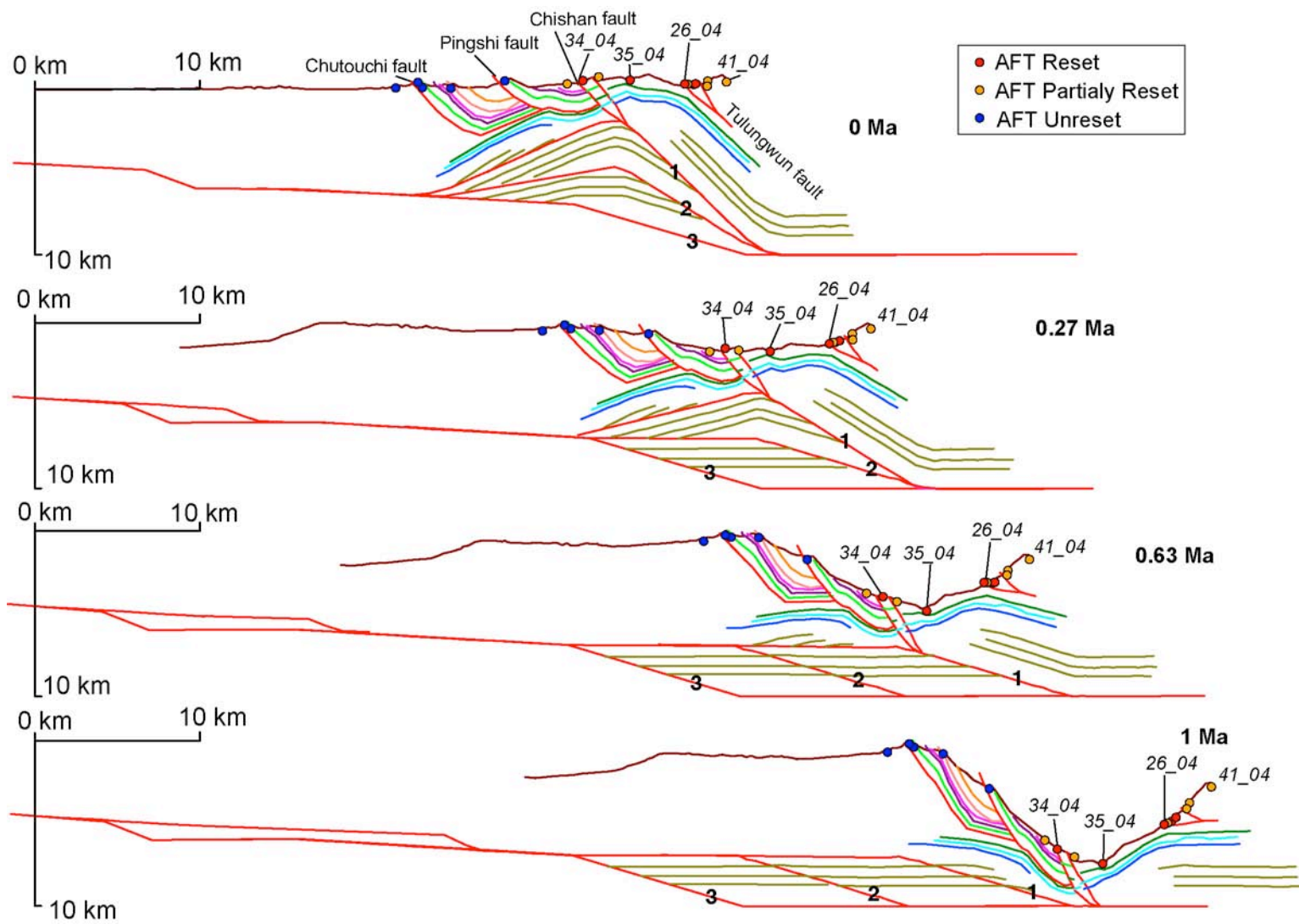
Example of thermo-kinematic model for a single fault with a flat-ramp-flat geometry and resulting AFT and AHe ages. Fault slips at 8 mm/yr for 2 Ma. A) Apatite fission track and (U-Th)/He ages generated by kinematics shown in B. Ages form a 'u-shaped' pattern formed by reset, partially reset, and unreset thermochronometric ages. B) Fault-bend-fold generated using the fault-parallel flow algorithm of 2DMove. Point P shows example of cooling history of material with the youngest AFT and AHe ages.

**Figure 4.4** Results of preferred thermal-kinematic-thermochronometric model of thrust deformation over the last 1 Ma.

A) Predicted and observed AFT and AHe age formed by thrust sequence shown in figure 4.5 and described in text. Thermal and thermochronometric model parameters shown in table 4.1. Solid blue line is model generates AFT ages, solid red line is modeled AHe age. Blue and red circles are observed AFT and AHe ages. AFT is pooled age for reset samples  $\pm 2\sigma$  and young peak age for partially reset samples with asymmetric 95% confidence intervals, AHe ages  $\pm 95\%$  confidence intervals (Figure 4.2). B) Final deformed geologic section. Frontal structures beneath the Lunhou fault are not modeled. The structures shown are modified from Suppe, 1980; 1983. The deformation modeled is three thrust structures beneath the Chishan thrust sheet with the geometry described in the text. Arrow show direction of relative fault motion. There is good agreement between modeled and observed AFT and AHe data. Scattered observed AHe ages from the same sample are interpreted as partially reset.



**Figure 4.5** Kinematic Model of thrusting in southern Taiwan over the last 1 Ma. Red (AFT reset), blue (AFT unreset) and orange (AFT partially reset) dots are sample locations. Faults (red lines) are activated sequentially, fault 1 to 3 (numbers shown on faults). Kinematic model shown at 1 Ma and the end of each faults activity, at 1 Ma, 0.63 Ma, 0.27 Ma and present. Faults 1 & 2 slip for 11 km, fault 3 slips for 8 km. All faults dip at 16.5° and slip at 30 mm/yr. Thermochronometric age generated by this deformation sequence shown in figure 4.4. Depth and temperature history for samples labeled shown in figure 4.5. The Chihsan, Pinghsi and Chutouchi faults (labeled) have not been active for the last 1 Ma.



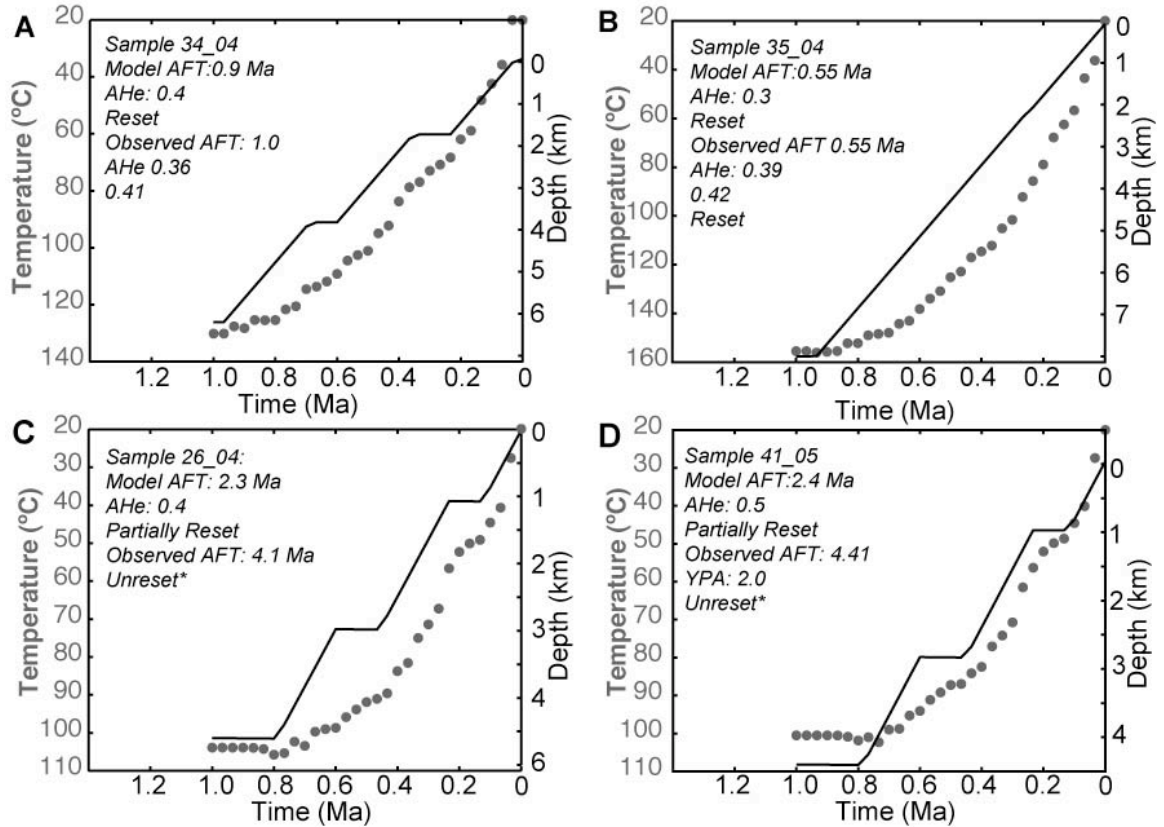


**Figure 4.6** Model generated temperature-depth histories of samples 34\_04, 35\_04, 26\_04 & 41\_01. A - D show temperature and depth histories generated by the kinematic model shown in Figure 4.4 & 4.5. Grey circles show temperature, solid black line is depth. Model predicted and observed AFT and AHe ages for each sample. AFT is pooled age and YPA is AFT young peak age. A) Sample 35\_04 AFT age records initial thrust motion. It is exhumed above the ramp of each fault and transported laterally by faults 1 and 2. B) Sample 34\_04 AFT age is exhumed at a constant rate above the ramp of all three faults. This sample is exhumed from the greatest depths and records the youngest cooling ages. C & D) Sample 26\_04 and 41\_05 are exhumed from above the AFT closure temperature and does not record the modeled thrust exhumation. \* 26\_04 is reset and 41\_05 is partially-reset, but are defined as unreset here because we interpret it is not reset by the burial and exhumation in the last 3 Ma.

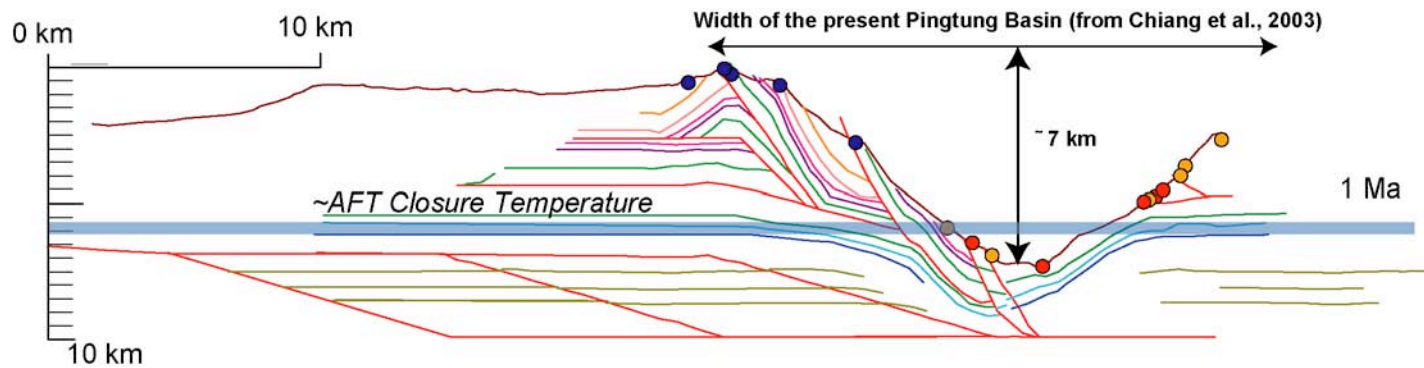


**Figure 4.7** Samples and 'undeformed' structure prior to thrust deformation at 1 Ma.

The amount of burial is recorded by the distribution of reset and unreset AFT ages AFT cooling ages. Thick blue line shows schematic AFT closure temperature. At 1 Ma, samples with AFT cooling age < 1 Ma were below the closure temperature, samples with AFT age > 1 Ma were above the closure temperature, partially-reset and unreset samples were at or above the AFT closure temperature. The pattern of burial recorded by the AFT ages is a basin whose geometry is similar to the present day Pingtung basin to the south. Surface-breaking faults are accretionary prism faults that pre-date thrusting related to arc-continent collision.



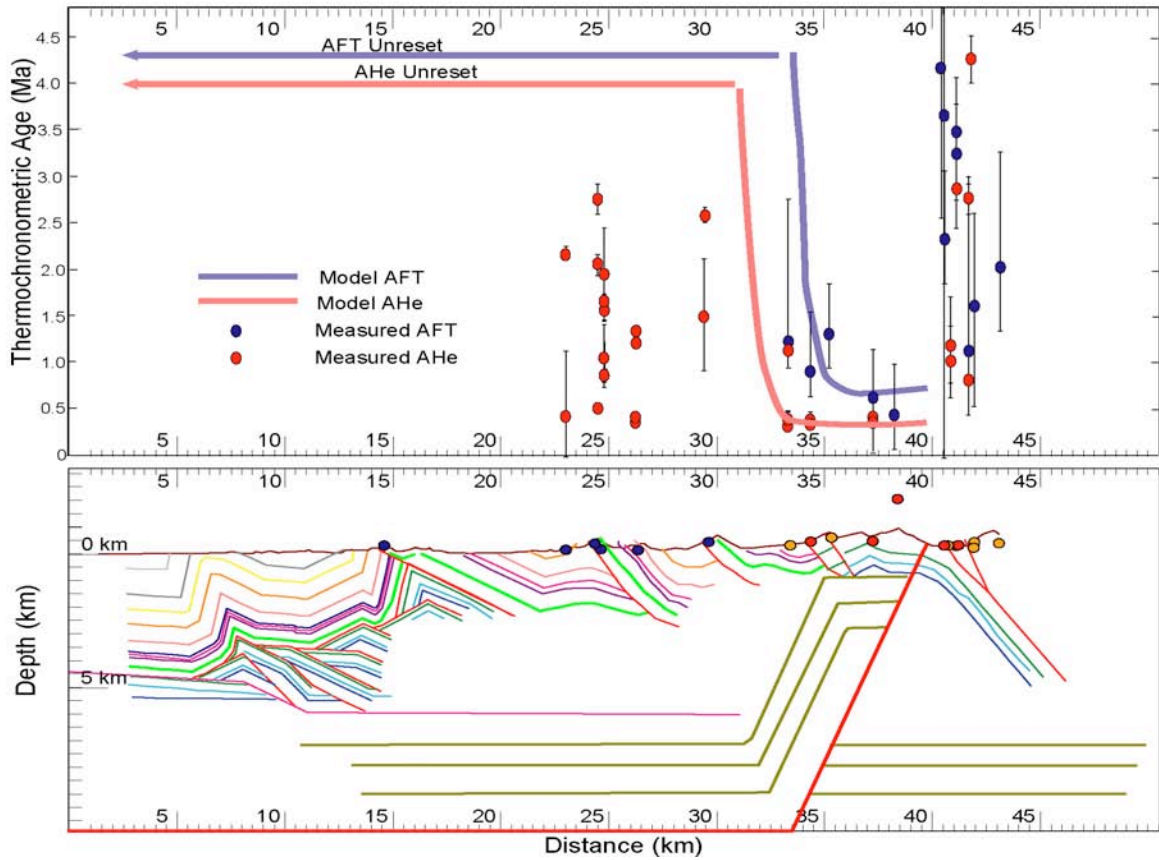


**Figure 4.8** Backthrust thermo-kinematic-thermochronologic model.

Interpretation of backthrust between the 3 Ma and 0.5 Ma AFT cooling ages. The backthrust ramp (red line) dips at  $60^\circ$ , slips at 15 mm/yr and extends from 10 km to the surface. The model produces a fairly good fit to the data but there is not geologic or geomorphic evidence for such a significant feature. In the backthrust model, the older AFT ages to the east of the youngest ages is partially annealed rather than recording earlier thrusting as it is in our preferred model. Stratigraphy at the surface stratigraphy from our preferred model, frontal structures from Suppe, 1980, 1983. Dark green lines show structure formed by backthrust.

#### Notes to Chapter 4

- Bollinger, L., Avouac, J. P., Beyssac, O., Catlos, E. J., Harrison, T. M., Grove, M., et al. (2004). Thermal structure and exhumation history of the Lesser Himalaya in central Nepal. *Tectonics*, 23, TC5015.
- Bollinger, L., Henry, P., & Avouac, J. P. (2006). Mountain building in the Nepal Himalaya: Thermal and kinematic model. *Earth and Planetary Science Letters*, 244, 58-71.
- Brandon, M.T., 2002, Decomposition of mixed grain-age distributions using BINOMFIT. On Track, v. 24, p. 13-18 (informal report in newsletter)
- Brandon, M. T., & Vance, J. A. (1992). Tectonic evolution of the Cenozoic Olympic subduction complex, Washington State, as deduced from fission track ages for detrital zircons. *American Journal of Science*, 292(8), 565-636.
- Byrne, T. B., & Liu, C. (2002). Introduction to the geology and geophysics of Taiwan. *Special Paper - Geological Society of America*, 358, v-viii.
- Carena, S., Suppe, J., & Kao, H. (2002). Active detachment of Taiwan illuminated by small earthquakes and its control of first-order topography. *Geology*, 30(10), 935-938 .
- Chang, S.S.L.&Chi, W.-R. (1983) Neogene nanoplankton biostratigraphy in Taiwan and the tectonic implications. *Pet. Geol. Taiwan*, 19, 93-147.
- Chen, W., Ridgway, K. D., Horng, C., Chen, Y., Shea, K., & Yeh, M. (2001). Stratigraphic architecture, magnetostratigraphy, and incised-valley systems of the Pliocene-Pleistocene collisional marine foreland basin of Taiwan. *Geological Society of America Bulletin*, 113(10), 1249-1271.
- Chiang, C., & Yu, H. (2006). Morphotectonics and incision of the Kaoping submarine canyon, SW Taiwan orogenic wedge. *Geomorphology*, 80(3-4), 199-213.
- Chiang, C., Yu, H., & Chou, Y. (2004). Characteristics of the wedge-top depozone of the southern Taiwan foreland basin system. *Basin Research*, 16(1), 65-78.
- Ching, K., Rau, R., Lee, J., & Hu, J. (2007). Contemporary deformation of tectonic escape in SW Taiwan from GPS observations, 1995-2005. *Earth and Planetary Science Letters*, 262(3-4), 601-619.
- Covey, M. (1984). Lithofacies analysis and basin reconstruction, Plio-Pleistocene western Taiwan foredeep. *Petroleum Geology of Taiwan*, 20, 53-83.

- Dadson, S. J., Hovius, N., Chen, H., Dade, W. B., Hsieh, M., Willett, S. D., Hu, J., Horng, M., Chen, M., Stark, C., Lague, D., Lin, J., (2003). Links between erosion, runoff variability and seismicity in the Taiwan orogen. *Nature*, 426(6967), 648-651.
- DeCelles, P. G., & Giles, K. A. (1996). Foreland basin systems. *Basin Research*, 8(2), 105-123.
- Farley, K. A. (2002). (U-Th)/He dating; techniques, calibrations, and applications. *Reviews in Mineralogy and Geochemistry*, 47, 819-843.
- Flowers, R. M., Shuster, D. L., Wernicke, B. P., & Farley, K. A. (2007). Radiation damage control on apatite (U-Th)/He dates from the Grand Canyon region, Colorado Plateau. *Geology (Boulder)*, 35(5), 447-450.
- Fruneau, B., Pathier, E., Raymond, D., Deffontaines, B., Lee, C. T., Wang, H. T., Angelier, J., Rudant, J., Chang, C. (2001). Uplift of Tainan Tableland (SW Taiwan) revealed by SAR interferometry. *Geophysical Research Letters*, 28, 3071-3074.
- Green, P. F., Crowhurst, P. V., Duddy, I. R., Japsen, P., & Holford, S. P. (2006). Conflicting (U Th)/He and fission track ages in apatite: Enhanced He retention, not anomalous annealing behaviour. *Earth and Planetary Science Letters*, 250, 407-427.
- Hickman, J. B., Wiltschko, D. V., Hung, J., Fang, P., & Bock, Y. (2002). Structure and evolution of the active fold-and-thrust belt of southwestern Taiwan from Global Positioning System analysis. *Special Paper - Geological Society of America*, 358, 75-92.
- Ho, C. S. (1988). *An Introduction to the Geology of Taiwan:- Explanatory Text of the Geologic Map of Taiwan, 2nd ed..* Taipei, Taiwan: Central Geological Survey.
- Hsu, Y., Simons, M., Yu, S., Kuo, L., & Chen, H. (2003). A two-dimensional dislocation model for interseismic deformation of the Taiwan mountain belt. *Earth and Planetary Science Letters*, 211(3-4), 287-294.
- Huang, C., Yuan, P. B., & Tsao, S. (2006). Temporal and spatial records of active arc-continent collision in Taiwan; a synthesis. *Geological Society of America Bulletin*, 118(3-4), 274-288.

- Huang, C., Yuan, P. B., Lin, C., Wang, T. K., & Chang, C. (2000). Geodynamic processes of Taiwan arc-continent collision and comparison with analogs in Timor, Papua New Guinea, Urals and Corsica. *Tectonophysics*, 325(1-2), 1-21.
- Huang, C., Yuan, P. B., Song, S., Lin, C., Wang, C., Chen, M., Shyu, C., Karp, B. Tectonics of short-lived intra-arc basins in the arc-continent collision terrane of the Coastal Range, eastern Taiwan. *Tectonics*, 14(1), PAGES 19–38.
- Huang, M., Hu, J., Hsieh, C., Ching, K., Rau, R., Pathier, E., Fruneau, B., Deffontaines, B. (2006). A growing structure near the deformation front in SW Taiwan as deduced from SAR interferometry and geodetic observation. *Geophysical Research Letters*, 33, L12305.
- Huang, S., Yang, K., Hung, J., Wu, J., Ting, H., Mei, W., Hsu, S., Lee, M. (2004). Deformation Front Development at the Northeast Margin of the Tainan Basin, Tainan–Kaohsiung Area, Taiwan. *Marine Geophysical Researches*, 25(1), 139-156.
- Huerta, A. D., & Rodgers, D. W. (2006). Constraining rates of thrusting and erosion; insights from kinematic thermal modeling. *Geology (Boulder)*, 34(7), 541-544.
- Hung, J., & Wiltschko, D. V. (1993). Structure and kinematics of arcuate thrust faults in the Miaoli-Cholan area of western Taiwan. *Petroleum Geology of Taiwan*, 28, 59-96.
- Hung, J., Wiltschko, D. V., Lin, H., Hickman, J. B., Fang, P., & Bock, Y. (1999). Structure and motion of the southwestern Taiwan fold and thrust belt. *Diqiu Kexue Jikan = TAO*, 10(3), 543-568.
- Lacombe, O., Mouthereau, F., Angelier, J., Chu, H., & Lee, J. (2003). Frontal belt curvature and oblique ramp development at an obliquely collided irregular margin; geometry and kinematics of the NW Taiwan fold-thrust belt. *Tectonics*, 22(3).
- Lee, Y., Chen, C., Liu, T., Ho, H., Lu, H., & Lo, W. (2006). Mountain building mechanisms in the Southern Central Range of the Taiwan Orogenic Belt -- From accretionary wedge deformation to arc-continental collision. *Earth and Planetary Science Letters*, 252(3-4), 413-422.
- Liu, Deffontaines, Lu, & Lallemand. (2004). Deformation Patterns of an Accretionary Wedge in the Transition Zone from Subduction to Collision Offshore Southwestern Taiwan. *Marine Geophysical Researches*, 25(1), 123-137.

- Liu, C., Huang, I. L., & Teng, L. S. (1997). Structural features off southwestern Taiwan. *Marine Geology*, 137(3-4), 305-319.
- Liu, T., Hsieh, S., Chen, Y., & Chen, W. (2001). Thermo-kinematic evolution of the Taiwan oblique-collision mountain belt as revealed by zircon fission track dating. *Earth and Planetary Science Letters*, 186(1), 45-56.
- Mouthereau, F., Lacombe, O., Deffontaines, B., Angelier, J., & Brusset, S. (2001). Deformation history of the southwestern Taiwan foreland thrust belt; insights from tectono-sedimentary analyses and balanced cross-sections. *Tectonophysics*, 333(1-2), 293-322.
- Sella, G. F., Dixon, T. H., & Mao, A. (2002). REVEL: A model for Recent plate velocities from space geodesy. *Journal of Geophysical Research*, 107(B4), 2081.
- Shuster, D. L., Flowers, R. M., & Farley, K. A. (2006). The influence of natural radiation damage on helium diffusion kinetics in apatite. *Earth and Planetary Science Letters*, 249(3-4), 148-161.
- Shyu, J. B. H., Sieh, K., Chen, Y., & Liu, C. (2005). Neotectonic architecture of Taiwan and its implications for future large earthquakes. *Journal of Geophysical Research*, 110, B08402.
- Suppe, J., & Anonymous. (1981). Mechanics of mountain-building and metamorphism in Taiwan. *Chung Kuo Ti Ch'ih Hsueh Hui Chuan Kan = Memoir of the Geological Society of China*, 4, 67-89.
- Suppe, J. (1980). Imbricated structure of Western Foothills Belt, southcentral Taiwan. *Petroleum Geology of Taiwan*, (17), 1-16.
- Suppe, J. (1983). Geometry and kinematics of fault-bend folding. *American Journal of Science*, 283(7), 684-721.
- Suppe, J., Chen, C., Chen, J., Lee, C., & Pan, K. (1984). Kinematics of arc-continent collision, flipping of subduction, and back-arc spreading near Taiwan. *Chung Kuo Ti Ch'ih Hsueh Hui Chuan Kan = Memoir of the Geological Society of China*, 6, 21-33.
- Yu, S., Chen, H., & Kuo, L. (1997). Velocity field of GPS stations in the Taiwan area. *Bulletin of the Institute of Earth Sciences*, 17, 43-44.

## **Chapter 5**

### **Summary and Global Applications**

This dissertation is focused on the classic Taiwan Western Foothills fold-and-thrust belt, but the results are globally applicable. Foreland verging thrust structures and fault related folds lie at the edge of all convergent margins with the same ramp and flat thrust structures, fault-bend folds, and transient kinematic patterns observed in Taiwan. The modeling techniques used to investigate the temporal evolution of fault structures in western Taiwan and the thermochronometric patterns predicted by the numerical model apply to fold-and-thrust belts world-wide.

The distribution of thermochronometric ages generated by thrust exhumation defines a 'U-shaped' pattern. The U-shaped pattern exists in material exhumed by motion along single and multiple thrust faults. The base of the 'U-shape' is formed by young thermochronometric cooling ages above the thrust ramp. These youngest cooling ages are surrounded by older cooling thermochronometric ages, and partially-reset and unreset thermochronometric ages. The details of the shape depend on the thrust geometry, the total slip along the fault, and the thermochronometric system used.

Material with the youngest reset cooling ages at the base of the U-shape is cooled at a near-constant rate after passing through the closure temperature. Identifying the youngest ages comprising the flat 'base' of the cooling age pattern thus permits direct comparison between thermochronometric ages and modern geomorphic and geodetic estimates of deformation and exhumation.

In multiple thrust fault settings, variable cooling produces older cooling ages recorded either side of the youngest cooling ages. In these settings, faults are typically spaced closely enough that material in the hangingwall of a fault in the hinterland is also exhumed by younger forelandward faults. As material is exhumed by multiple faults, material in the hangingwall of one fault may record slip along a younger fault. The time that each fault is active is preserved, including initial faulting, but exhumation caused by slip along each thrust is not only recorded in the hangingwall of that same

fault. As a result, in a foreland propagating thrust sequence the model predicted cooling ages show no step change across each fault unless there is out-of-sequence faulting.

This U-shaped thermochronometric age pattern predicted by the numerical modeling is evident in the new apatite fission track and (U-Th)/He data collected from western Taiwan. The thermochronometric age patterns in western Taiwan are consistent with a migrating buried thrust fault ramp that is located today beneath the hinterland of the Western Foothills or the eastern part of the Hsüehshan Range.

The ramp forms with the onset of arc-continent collision. The thermochronometric cooling ages in western Taiwan record vertical exhumation through the apatite fission track and apatite (U-Th)/He closure temperatures above this thrust ramp, followed by horizontal transport above an upper décollement. Older cooling ages observed in the west of the thrust belt do not record a slower exhumation rate which would be the interpretation using a 1d model. Instead the older ages in the west of the thrust-belt record earlier cooling above the thrust ramp, but at the same rapid rate recorded by the youngest sample ages from central Taiwan.

In Taiwan, there is evidence that the thrust ramp migrates with time. In the model, a migrating thrust ramp exhumes material from the greatest depth and generates a large anticline structure centered above the active thrust ramp. The anticline contains multiple faults which are old thrust ramps exhumed by younger thrust ramps. Such a large anticline structure exists in the center of the Hsüehshan Range in northern and central Taiwan, and at the rear of the Western Foothills in southern Taiwan. Rocks in the core of the anticline are the most deeply exhumed rocks in western Taiwan and coincide with the youngest cooling ages. Thus, I interpret that the thrust structures that crop out along each of our transects are exhumed through the closure temperature to the surface by the motion along the main Taiwan décollement.

There is abundant geodetic and geomorphic evidence for rapid uplift, erosion, and shortening focused at the deformation front. The deformation front lies ~20-30 km west of the young thermochronometric cooling ages. Although the geodetic records of short-term shortening and the thermochronometric record of long-term exhumation are

spatially separated, they are entirely consistent with one another. These records, which average over different time scales, according to my model reflect different parts of the same single fault system with two different thrust ramps. The thermochronometric ages record exhumation over a lower thrust ramp that soles to a depth beneath the depths to the apatite fission track and (U-Th)/He closure temperatures, and subsequent horizontal advection. The short-term geomorphic and geodetic measure of vertical exhumation and erosion record an upper thrust ramp that soles into a décollement which above the depths to the apatite fission track and apatite (U-Th)/He closure temperatures. The frontal thrust ramp is best described as a triangle zone, where rocks in the fault hangingwall are wedged into the footwall generating the rapid shortening recorded in geodetically and geomorphically across the frontal structures. These two ramps, the upper and the lower, are linked by a décollement that is at or above the apatite fission track and apatite (U-Th)/He closure temperatures.

This pattern of exhumation is consistent with the thermochronology. In addition, the pattern of deformation I describe explains the stratigraphy, structure, and the patterns of geodetically measured shortening across western Taiwan. There is no evidence for out-of-sequence thrusting in the thrust belt and the deformation is consistent with a steady, self-similar westward and southward propagating thrust system with a geometry similar to today. The migrating single thrust system with two thrust ramps explains the uplift and exhumation across Taiwan without needing any additional mechanisms or drivers of uplift, erosion, and exhumation. The fault system and distribution of deformation seen today have existed through time and the thrust structures in the foothills and throughout western Taiwan play an integral part in arc-continent collision and mountain building.

The southward propagation to collision is reflected in the distribution of oldest and youngest thrust cooling ages. The oldest thermochronometric record of thrust faulting is 3.5 Ma along the northern and central transects, and 1 Ma in the south showing the progressively younger onset of collision in the south. The youngest cooling age is 0.5 Ma in central and southern Taiwan and 1.2 Ma in northern Taiwan recording



that thrust faults in northern Taiwan are no longer accommodating collision. Thus the overall deformation history documented by thermochronometric ages in western Taiwan is a steady southward progressing collision that is accommodated by westward propagating thrust faults and fault-related folding of sediments of the Asian passive margin.

### *Global Applications*

The results presented here are applicable to convergent orogens and thrust systems world wide. The ‘U-shaped’ distribution of low-T thermochronometric ages is evident in the Himalaya (Arne et al., 1997; Bollinger et al., 2004; 2006; Theide et al., 2006) the Bolivian Andes (Barnes et al., 2006), the European Alps (Malusa et al., 2005), the Brooks Range of Alaska (Blythe et al., 1996), and the Sevier thrust belt (Huerta and Rodgers, 2006).

In the Himalaya, a U-shaped thermochronometric age patterns with the youngest thermochronometric ages at the rear of the mountain belt significantly behind the deformation front, geodetic shortening focused at the deformation front, and rapid transitions from reset to unreset material over short distances unrelated to mapped thrust structures, have been used to argue for out-of-sequence faulting, climate-driven erosion, or changes in the tectonic setting (Wobus et al., 2003; Theide et al., 2004; Huntington et al., 2006; 2007). However, the structural, stratigraphic, geodetic and thermochronometric patterns are consistent with a steady, self-similar development of a single, linked thrust system like the fault system I describe in Taiwan and this pattern of deformation is consistent with the conventional view of forward propagating thrust faulting with no out-of-sequence faulting. Thus although the distribution of geodetic shortening, long-term exhumation and the relation to mapped structures appear at first incongruous, exactly these patterns are to be expected based on my kinematic-thermal-thermochronologic model and are those observed in Taiwan.

The modeled migrating buried thrust ramp generates an anticline or duplex structure in the center of the thrust belt, and shallower foreland verging thrust structures

at the deformation front. This structural pattern is seen in convergent orogenic belts world wide including the Andes (Barnes et al., 2006), the Himalaya (Bollinger et al., 2004; 2006), the European Alps (Escher et al., 1988), and the Sevier (DeCelles & Coogan, 2007). Thus, this thrust fault geometry and resulting pattern of uplift and exhumation are very likely applicable in all convergent orogenic belts. Hence, thermochronometric ages should be interpreted in light of the results of this study.

This study also raise questions about the widely applied age-elevation relationship. Age-elevation relationships are commonly used to interpret exhumation rates by assuming that material at high elevations passed through the closure isotherms before material at low elevations, and that all material passes vertically through the closure temperature at the same rate. Although theoretically, samples for age-elevation transects are thought of as being collected along a vertical transect this is impossible and in reality these transects are horizontally distributed. In a fold-and-thrust belt, the vertical and lateral kinematics of thrust faulting and the development of the thrust belt mean an age elevation transect spanning from the foreland to the hinterland records the sequential activation of thrusts in addition to any change in elevation. This greatly complicates an age-elevation interpretation and the technique should be used with extreme caution in thrust fault settings.

The studies in this dissertation highlight the necessity and power of using thermo-kinematic-thermochronologic modeling to understand cooling histories recorded by thermochronometric data in thrust and fold settings like western Taiwan.

### Notes to Chapter 5

- Arne, D., Worley, B., Wilson, C., Chen, S., Foster, D., Luo, Z., Liu, S., Dirks, P. (1997). Differential exhumation in response to episodic thrusting along the eastern margin of the Tibetan Plateau, *Tectonophysics*, 280, 239–256.
- Barnes, J. B., Ehlers, T. A., McQuarrie, N., O'Sullivan, P. B., & Pelletier, J. D. (2006). Eocene to recent variations in erosion across the central Andean fold-thrust belt, northern Bolivia: Implications for plateau evolution. *Earth and Planetary Science Letters*, 248, 118-133.
- Blythe, A., Bird, J., Omar, G. (1996) Deformation history of the central Brooks range, Alaska; results from fission-track and  $^{40}\text{Ar}/^{39}\text{Ar}$  analyses. *Tectonics* 15(2), 440-455.
- Bollinger, L., Avouac, J. P., Beyssac, O., Catlos, E. J., Harrison, T. M., Grove, M., et al. (2004). Thermal structure and exhumation history of the Lesser Himalaya in central Nepal. *Tectonics*, 23, TC5015.
- Bollinger, L., Henry, P., & Avouac, J. P. (2006). Mountain building in the Nepal Himalaya: Thermal and kinematic model. *Earth and Planetary Science Letters*, 244, 58-71.
- DeCelles, P., Coogan, J., (2007). Regional structure and kinematic history of the Sevier fold-and-thrust belt, central Utah. *Geological Society of America Bulletin*, 119 (3-4). 508-512
- Escher, A., Masson, H. and Steck, A. (1988). Coupes géologiques des Alpes occidentales suisses. *Mémoires de Géologie*, 2, p. 11.
- Huerta, A.D., Rodgers, D.W. (2006). Constraining rates of thrusting and erosion: Insights from kinematic thermal modeling *Geology*, 34(7), 541–544.
- Huntington, K. W., Blythe, A. E., & Hodges, K. V. (2006). Climate change and late Pliocene acceleration of erosion in the Himalaya. *Earth and Planetary Science Letters*, 252(1-2), 107-118.
- Huntington, K. W., Ehlers, T. A., Hodges, K. V., & Whipp, D. M. W. (2007). Topography, exhumation pathway, age uncertainties, and the interpretation of thermochronometer data. *Tectonics*, 26, TC4012.

- Malusa, M. G., Polino, R., Zattin, M., Bigazzi, G., Martin, S., Piana, F., 2005, Miocene to Present differential exhumation in the Western Alps: Insights from fission track thermochronology. *Tectonics* 24, TC3004, doi:10.1029/2004TC001782.
- Thiede, R.C., Arrowsmith, J.R., Bookhagen, B., McWilliams, M.O., Sobel, E.R., Strecker, M.R. (2005). From tectonically to erosionally controlled development of the Himalayan orogen, *Geology* 33(8), 689–692.
- Wobus, C. W., Hodges, K. V., & Whipple, K. X. (2003). Has focused denudation sustained active thrusting at the Himalayan topographic front? *Geology*, 31(10), 861-864.

## REFERENCES

- Arne, D., Worley, B., Wilson, C., Chen, S., Foster, D., Luo, Z., Liu, S., Dirks, P. (1997). Differential exhumation in response to episodic thrusting along the eastern margin of the Tibetan Plateau, *Tectonophysics*, 280, 239–256.
- Banerjee, P., Bürgmann, R. (2002). Convergence across the northwest Himalaya from GPS measurements, *Geophysical Research Letters*, 29(13),30
- Barnes, J. B., Ehlers, T. A., McQuarrie, N., O'Sullivan, P. B., & Pelletier, J. D. (2006). Eocene to recent variations in erosion across the central Andean fold-thrust belt, northern Bolivia: Implications for plateau evolution. *Earth and Planetary Science Letters*, 248, 118-133.
- Benedetti, L., Tapponnier, P., King, G.C.P., Meyer, B. & Manighetti, I. (2000). Growth folding and active thrusting in the Montello region, Veneto, northern Italy. *Journal of Geophysical Research*, 105, 739– 766.
- Blythe, A. E., Murphy, J., & OSullivan, P. B. (1997). Tertiary cooling and deformation in the south-central Brooks Range: Evidence from zircon and apatite fission-track analyses. *Journal of Geology*, 105(5), 583-599.
- Blythe, A.E., Bird, J.M., and Omar, G.I. (1998). Constraints on the cooling history of the central Brooks Range, Alaska, from fission-track and  $^{40}\text{Ar}/^{39}\text{Ar}$  analyses, in Oldow, J.S., and Av Lallemand, H. G., eds., *Architecture of the Central Brooks Range Fold and Thrust Belt, Arctic Alaska: Boulder, Colorado, Geological Society of America Special Paper 324*, 163-177.
- Bollinger, L., Avouac, J. P., Beyssac, O., Catlos, E. J., Harrison, T. M., Grove, M., et al. (2004). Thermal structure and exhumation history of the Lesser Himalaya in central Nepal. *Tectonics*, 23, TC5015.
- Bollinger, L., Henry, P., & Avouac, J. P. (2006). Mountain building in the Nepal Himalaya: Thermal and kinematic model. *Earth and Planetary Science Letters*, 244, 58-71.
- Brandon, M. T., & Vance, J. A. (1992). Tectonic evolution of the Cenozoic Olympic subduction complex, Washington State, as deduced from fission track ages for detrital zircons. *American Journal of Science*, 292(8), 565-636.
- Brandon, M. T. (1992). Decomposition of fission-track grain-age distributions. *American Journal of Science*, 292(8), 535-564.

- Brandon, M.T. (2002). Decomposition of mixed grain-age distributions using BINOMFIT. *On Track*, v. 24, p. 13-18 (informal report in newsletter)
- Brandon, M. T., Roden-Tice, M. K., & Garver, J. I. (1998). Late Cenozoic exhumation of the Cascadia accretionary wedge in the Olympic Mountains, Northwest Washington State. *Geological Society of America Bulletin*, 110(8), 985-1009.
- Braun, J. (2002). Quantifying the effect of recent relief changes on age – elevation relationships, *Earth and Planetary Science Letters*, 200, 331–343.
- Brewer, J. (1981). Thermal effects of thrust faulting. *Earth and Planetary Science Letters*, 56, 233-244.
- Brewer, I. D., & Burbank, D. W. (2006). Thermal and kinematic modeling of bedrock and detrital cooling ages in the central Himalaya. *Journal of Geophysical Research*, 111(B9).
- Brown, R.W. and Summerfield, M.A. (1997). Some Uncertainties in the Derivation of Rates of Denudation from Thermochronologic Data, *Earth Surface Processes and Landforms* 22(3), 239-248.
- Bullen, M.E., Burbank, D.W.; Garver, J.I. (2003). Building the northern Tien Shan; integrated thermal, structural, and topographic constraints. *Journal of Geology* 111(2), 149-165.
- Bullen, M E; Burbank, D W; Abdrakhmatov K. Y., Garver, J. (2001). Late Cenozoic tectonic evolution of the northwestern Tien Shan; new age estimates for the initiation of mountain building. *Geological Society of America Bulletin*, vol.113, 12, 1544-1559.
- Burbank, D.W., Vergés, J., Munoz, J.A., and Betham, P. (1992). Coeval hindward- and forward-imbricating thrusting in the south-central Pyrenees, Spain: Timing and rates of shortening and deposition *Geological Society of America Bulletin*, 3–17.
- Burbank, D.W., Meigs, A., and Brozovic, N. (1996). Interactions of growing folds and coeval depositional systems: *Basin Research*, v. 8, p. 199-223.
- Burbank, D.W., Blythe, A.E., Putkonen, J., Pratt-Sitaula, B., Gabet, E., Oskin, M., Barros, A., and Ojha, T.P. (2003). Decoupling of erosion and precipitation in the Himalayas, *Nature* 426, 652-655.

- Bürgmann, R., Arrowsmith, R., Dumitru, T., and McLaughlin, R., (1994). Rise and fall of the southern Santa Cruz Mountains, California, from fission tracks, geomorphology, and geodesy, *Journal of Geophysical Research*, 99, 20181-20, 202.
- Byrne, T. B., & Liu, C. (2002). Introduction to the geology and geophysics of Taiwan. *Special Paper - Geological Society of America*, 358, v-viii.
- Carena, S., Suppe, J., & Kao, H. (2002). Active detachment of Taiwan illuminated by small earthquakes and its control of first-order topography. *Geology*, 30(10), 935-938 .
- Chapple, W.M., (1978) Mechanics of thin-skin fold-and-thrust belts. *Geological Society of America Bulletin*, 89 (8), 1189-1198
- Coward, M. P., De Donatis, M., Mazzoli, S., Paltrinieri, W., Wezel, F. (1999) Frontal part of the northern 85222 fold and thrust belt in the Romagna-Marche area (Italy): Shallow and deep structural styles. *Tectonics* 18(3), 559–574
- Covey, M. (1984). Lithofacies analysis and basin reconstruction, Plio-Pleistocene western Taiwan foredeep. *Petroleum Geology of Taiwan*, 20, 53-83.
- Dadson, S. J., Hovius, N., Chen, H., Dade, W.B., Lin, J. C., Hsu, M.-L., Lin, C.-W., Horng, M.-J., Chen, T.-C., Milliman, J., Stark, C. P. (2004). Earthquake-triggered increase in sediment delivery from an active mountain belt. *Geology* 32, 733-736.
- Dahlstrom, C. D. A. (1970). Structural geology in the eastern margin of the Canadian Rocky Mountains. *Bulletin of Canadian Petroleum Geology* 18, 332-406
- Dahlstrom, C.D.A. (1969). Balanced cross sections. *Canadian Journal of Earth Sciences*, vol.6, no.4, Part 1, 743-757.
- Davis, D., Suppe, J., Dahlen, F. A. (1983). Mechanics of fold-and-thrust belts and accretionary wedges. *Journal of Geophysical Research* 88, 1153-1172.
- Davy, P., & Gillet, P. (1986). The stacking of thrust slices in collision zones and its thermal consequences. *Tectonics*, 5(6), 913-929.
- DeCelles, P. G., Gray, M. B., Ridway, K. D., Cole, R. B. Srivastava, P., Pequera, N., Pivnik, D. A. (1991). Kinematic history of a foreland uplift from Paleocene synorogenic conglomerate, Beartooth Range, Wyoming and Montana, *Geological Society of America Bulletin* 103(11) 1458–1475.

- DeCelles, P.G., Gautam, M. (1995). History of the Sevier orogenic wedge in terms of critical taper models, Northeast Utah and Southwest Wyoming. *Geological Society of America Bulletin* 107(4), 454-462.
- DeCelles, P., Coogan, J. (2007). Regional structure and kinematic history of the Sevier fold-and-thrust belt, central Utah. *Geological Society of America Bulletin*, 119 (3-4). 508-512
- Donelick, R.A., O'Sullivan, P.B., Ketcham, R.A. (2005). Apatite Fission-Track Analysis. *Reviews in Mineralogy and Geochemistry*. 58(1), 49-94.
- Ducea, M., House, M. A., & Kidder, S. (2003). Late Cenozoic denudation and uplift rates in the Santa Lucia Mountains, California. *Geology (Boulder)*, 31(2), 139-142.
- Ehlers, T.A., Willett, S.D., Armstrong, P.A., Chapman, D.S. (2003). Exhumation of the central Wasatch Mountains, Utah; 2, Thermokinematic model of exhumation, erosion, and thermochronometer interpretation, *Journal of Geophysical Research* 108(B3), 2173.
- Ehlers, T.A., Farley, K.A. (2003). Apatite (U–Th)/He thermochronometry: methods and applications to problems in tectonic and surface processes. *Earth and Planetary Science Letters* 206(1-2), 1-14.
- England, P. C., & Thompson, A. B. (1984). Pressure-temperature-time paths of regional metamorphism; I, Heat transfer during the evolution of regions of thickened continental crust. *Journal of Petrology*, 25(4), 894-928.
- Farley, K.A., Wolf, R.A., Silver, L.T. (1996). The effects of long alpha-stopping distances on (U-Th)/He dates, *Geochim. et Cosmochim. Acta*, 60, 4223-4229.
- Farley, K.A. (2002). (U-Th)/He dating: Techniques, calibrations, and applications, in: Noble Gases in Geochemistry and Cosmochemistry. *Reviews in Mineralogy and Geochemistry*, 47, 819-844.
- Fisher, D. M., Lu, C., & Chu, H. (2002). Taiwan slate belt; insights into the ductile interior of an arc-continent collision. *Special Paper - Geological Society of America*, 358, 93-106.
- Ford, M., Williams, E.A., Artoni, A., Verges, J., Hardy, S. (1997). Progressive evolution of a fault-related fold pair from growth strata geometries, Sant Llorenc de Morunys. SE Pyrenees. *Journal of Structural Geology*, 19, 413-441.



- Fruneau, B., Pathier, E., Raymond, D., Deffontaines, B., Lee, C. T., Wang, H. T. (2001). Uplift of Tainan Tableland (SW Taiwan) revealed by SAR interferometry. *Geophysical Research Letters*, 28, 3071-3074.
- Fuller, C., Willett, S., Fisher, D., & Lu, C. (2006). A thermomechanical wedge model of Taiwan constrained by fission-track thermochronometry. *Tectonophysics*, 425(1-4), 1-24.
- Hardy, S., Poblet, J., McClay, K., and Waltman, D. (1996). Mathematical modelling of growth strata associated with fault-related fold structures, in Buchanan, P.G., and Nieuwland, D.A., Editors, Modern developments in structural interpretation, validation and modelling: Geological Society [London] Special Publication 99, 265–282.
- Hickman, J. B., Wiltschko, D. V., Hung, J.-H., Fang, P., Bock, Y. (2002). Structure and evolution of the active fold-and-thrust belt of Southwestern Taiwan from Global Positioning System analysis. Geological Society of America Special Paper 358, 75-92.
- Hickman, J. B., Wiltschko, D. V., Hung, J., Fang, P., & Bock, Y. (2002). Structure and evolution of the active fold-and-thrust belt of southwestern Taiwan from Global Positioning System analysis. *Special Paper - Geological Society of America*, 358, 75-92.
- Ho, C. S. (1988). *An Introduction to the Geology of Taiwan:- Explanatory Text of the Geologic Map of Taiwan, 2nd ed.* Taipei, Taiwan: Central Geological Survey.
- House, M. A., Gurnis, M., Kamp, P. J. J., & Sutherland, R. (2002). Uplift in the Fiordland region, New Zealand; implications for incipient subduction. *Science*, 297(5589), 2038-2041.
- Hsieh, M., & Knuepfer, P. L. K. (2002). Synchronicity and morphology of Holocene river terraces in the southern Western Foothills, Taiwan; a guide to interpreting and correlating erosional river terraces across growing anticlines. *Special Paper - Geological Society of America*, 358, 55-74.
- Hsieh, M., & Knuepfer, P. L. K. (2001). Middle-late Holocene river terraces in the Erhjen River Basin, southwestern Taiwan--implications of river response to climate change and active tectonic uplift. *Geomorphology*, 38(3-4), 337-372.
- Hsu, Y., Simons, M., Yu, S., Kuo, L., & Chen, H. (2003). A two-dimensional dislocation model for interseismic deformation of the Taiwan mountain belt. *Earth and Planetary Science Letters*, 211(3-4), 287-294.

- Huang, S-T, Yang, K-M., Hung, J-H., Wu, J-C., Ting, H-H., Mei, W-W., Hsu, S-H., Lee, M. (2004). Deformation Front Development at the Northeast Margin of the Tainan Basin, Tainan–Kaohsiung Area, Taiwan. *Marine Geophysical Researches*, 25(1), 139-156.
- Huang, C., Wu, W., Chang, C., Tsao, S., Yuan, P. B., Lin, C., Xia, K., (1997). Tectonic evolution of accretionary prism in the arc-continent collision terrane of Taiwan. *Tectonophysics*, 281(1-2), 31-51.
- Huang, C., Yuan, P. B., & Tsao, S. (2006). Temporal and spatial records of active arc-continent collision in Taiwan; a synthesis. *Geological Society of America Bulletin*, 118(3-4), 274-288.
- Huang, C., Yuan, P. B., Lin, C., Wang, T. K., & Chang, C. (2000). Geodynamic processes of Taiwan arc-continent collision and comparison with analogs in Timor, Papua New Guinea, Urals and Corsica. *Tectonophysics*, 325(1-2), 1-21.
- Huntington, K. W., Blythe, A. E., & Hodges, K. V. (2006). Climate change and late Pliocene acceleration of erosion in the Himalaya. *Earth and Planetary Science Letters*, 252(1-2), 107-118.
- Huntington, K. W., Ehlers, T. A., Hodges, K. V., & Jr, D. M. W. (2007). Topography, exhumation pathway, age uncertainties, and the interpretation of thermochronometer data. *Tectonics*, 26, TC4012.
- Hsieh, M.-L., Knuepfer, P. L. K. (2001). Middle-late Holocene river terraces in the Ehrjen River Basin, southwestern Taiwan - implications of river response to climate change and active tectonic uplift., *Geomorphology* 38, 337-372.
- Hsieh, M.-L., Knuepfer, P. L. K. (2002). Synchronicity and morphology of Holocene river terraces in the southern Western Foothills, Taiwan: a guide to interpreting and correlating erosional river terraces across growing anticlines. In *Geology and geophysics of an arc-continent collision, Taiwan.*, Byrne T. B., Liu, C. S., Editors, 55-74.
- Huerta, A.D., Rodgers, D.W. (2006). Constraining rates of thrusting and erosion: Insights from kinematic thermal modeling *Geology*, 34(7), 541–544.
- Jackson, J., Ritz, J.F., Siame, L., Raisbeck, G., Yiou, F., Norris, R., Youngson, J. & Bennett, E. (2002). Fault growth and landscape development rates in Otago, New Zealand, using in situ cosmogenic  $^{10}\text{Be}$ . *Earth Planet. Sci. Lett.*, 195, 185– 193.

- Karabinos, P. and Ketcham, R. (1988). Thermal structure of active thrust belts. *Journal of Metamorphic Geology*, 6, 559-570.
- Ketcham, R.A., Donelick, R.A. and Carlson, W.D. (1999). Variability of apatite fission-track annealing kinetics: III. Extrapolation to geological timescales. *American Mineralogist*, 84, 1235-1255.
- Kirby, E., Reiners, P.W., Krol, M.A., Whipple, K.X., Hodges, K.V., Farley, K.A., Tang, W. & Chen Z. (2002). Late Cenozoic evolution of eastern margin of the Tibetan Plateau: inferences from  $^{40}\text{Ar}/^{39}\text{Ar}$  and (U/Th)/He thermochronology, *Tectonics*, 21(1), 1001, doi:10.1029/2000TC001246, 2002.
- Lacombe, O., Mouthereau, F., B. Deffontaines, B., and Angelier, J. (1999). Geometry and Quaternary kinematics of fold and-thrust units of southwestern Taiwan., *Tectonics*, 18, 1198-1223.
- Lacombe, O., Mouthereau, F. (2002). Basement-involved shortening and deep detachment tectonics in forelands of orogens: Insights from recent collision belts (Taiwan, western Alps, Pyrenees). *Tectonics*, 21(4).
- Lacombe, O., Mouthereau, F., Angelier, J., Chu, H.-T., Lee, J.-C. (2003). Frontal belt curvature and oblique ramp development at an obliquely collided irregular margin: Geometry and kinematics of the NW Taiwan fold-thrust belt. *Tectonics* 22(3) 1025, doi:10.1029/2002TC001436, 2003.
- Laslett, G.M., Green, P.F., Duddy, I.R., Gleadow, A.J.W. (1987). Thermal annealing of fission tracks in apatite. *Chemical Geology Isotope Geoscience Section* 65(1), 1-13.
- Lee, J., Angelier, J., Chu, H., Hu, J., & Jeng, F. (2001). Continuous monitoring of an active fault in a plate suture zone: a creepmeter study of the Chihshang Fault, eastern Taiwan. *Tectonophysics*, 333(1-2), 219-240.
- Lee, Y., Chen, C., Liu, T., Ho, H., Lu, H., & Lo, W. (2006). Mountain building mechanisms in the Southern Central Range of the Taiwan Orogenic Belt -- From accretionary wedge deformation to arc-continental collision. *Earth and Planetary Science Letters*, 252(3-4), 413-422.
- Liu, T., Hsieh, S., Chen, Y., & Chen, W. (2001). Thermo-kinematic evolution of the Taiwan oblique-collision mountain belt as revealed by zircon fission track dating. *Earth and Planetary Science Letters*, 186(1), 45-56.

- Lundberg, N., Reed, D. L., Liu, C., & Lieske, J. (1997). Forearc-basin closure and arc accretion in the submarine suture zone south of Taiwan. *Tectonophysics*, 274(1-3), 5-23.
- Mailhe, D., Lucazeau, F., and Vasseur, G. (1986) Uplift history of thrust belts; an approach based on fission track data and thermal modelization., *Tectonophysics* 124, 177–191.
- Malusa, M. G., Polino, R., Zattin, M., Bigazzi, G., Martin, S., Piana, F., 2005, Miocene to Present differential exhumation in the Western Alps: Insights from fission track thermochronology. *Tectonics* 24, TC3004, doi:10.1029/2004TC001782
- Mailhe, D., Lucazeau, F., & Vasseur, G. (1986). Uplift history of thrust belts; an approach based on fission track data and thermal modelization. *Tectonophysics*, 124(1-2), 177-191.
- Malusa, M. G., Polino, R., Zattin, M., Bigazzi, G., Martin, S., & Piana, F. (2005). Miocene to present differential exhumation in the Western Alps; insights from fission track thermochronology. *Tectonics*, 24(3).
- Mancktelow, N. S., & Grasemann, B. (1997). Time-dependent effects of heat advection and topography on cooling histories during erosion. *Tectonophysics*, 270(3-4), 167-195.
- McClay, K. R. (1992). Glossary of thrust tectonics terms, in McClay, K. R., ed., *Thrust tectonics*: London, Chapman & Hall, 419-433.
- McQuarrie, N., Horton, B.K., Zandt, G., Beck, S., DeCelles, P.G. (2005). Lithospheric evolution of the Andean fold–thrust belt, Bolivia, and the origin of the central Andean plateau. *Tectonophysics*, 399(1-4), 15-37.
- Medwedeff, D.A. (1989). Growth fault-bend folding at southeast Lost Hills, San Joaquin Valley, California: *American Association of Petroleum Geologists Bulletin*, 73, 54–67.
- Mitra, S. (1986) Duplex structures and imbricate thrust systems: Geometry, structural position and hydrocarbon potential. *Bulletin of the American Association of Petroleum Geologists* 70, 1087-1112. *Memoir*. 171,489-514.
- Molnar, P., & England, P. C. (1990). Temperatures, heat flux, and frictional stress near major thrust faults. *Journal of Geophysical Research*, 95(B4), 4833-4856.

- Moore, M. A., & England, P. C. (2001). On the inference of denudation rates from cooling ages of minerals. *Earth and Planetary Science Letters*, 185(3-4), 265-284.
- Mouthereau, F., Lacombe, O., Deffontaines, B., Angelier, J., & Brusset, S. (2001). Deformation history of the southwestern Taiwan foreland thrust belt; insights from tectono-sedimentary analyses and balanced cross-sections. *Tectonophysics*, 333(1-2), 293-322.
- Naeser, C. W., Faul, H. (1969). Fission track annealing in apatite and sphene., *Journal of Geophysical Research* 74, 705-710.
- Omar, G. I., Lutz, T. M., & Giegengack, R. (1994). Apatite fission-track evidence for Laramide and post-Laramide uplift and anomalous thermal regime at the Beartooth overthrust, Montana-Wyoming. *Geological Society of America Bulletin*, 106(1), 74-85.
- O'Sullivan, P.B., Hanks, C.L., Wallace, W.K., Green, P.F. (1995). Multiple episodes of Cenozoic denudation in the northeastern Brooks Range; fission-track data from the Okpilak Batholith, Alaska. *Canadian Journal of Earth Sciences Journal Canadien des Sciences de la Terre* 32(8), 1106-1118.
- O'Sullivan, P.B., Wallace, W.K. (2002). Out-of-sequence, basement-involved structures in the Sadlerochit. Mountains region of the Arctic National Wildlife Refuge, Alaska: Evidence and implications from fission-track thermochronology. *GSA Bulletin*, 114 (11), 1356–1378.
- Oxburgh, E. R., & Turcotte, D. L. (1974). Thermal gradients and regional metamorphism in overthrust terrains with special reference to the Eastern Alps. *Schweizerische Mineralogische und Petrographische Mitteilungen = Bulletin Suisse de Mineralogie et Petrographie*, 54(2-3), 641-662.
- Parrish, R. R. (1983). 'Cenozoic thermal evolution and tectonics of the coast mountains of British Columbia 1. Fission track dating, apparent uplift rates, and patterns of uplift', *Tectonics*, 2, 601–631.
- Parrish, R. R. (1985). 'Some cautions which should be exercised when interpreting fission track and other data with regard to uplift rate calculations' (abstract), *Nuclear Tracks and Radiation Measurements* 10, 425.
- Ruppel, C.; Hodges, K. V. (1994). Pressure-temperature-time paths from two-dimensional thermal models: Prograde, retrograde, and inverted metamorphism., *Tectonics*, 13(1) 17-44.

- Safran, E.B. (2003). Geomorphic interpretation of low-temperature thermochronologic data: Insights from two-dimensional thermal modeling. *Journal of Geophysical Research*, 108(B4), 2189.
- Shaw, J.H., Suppe, J. (1994). Active faulting and growth folding in the eastern Santa Barbara Channel. *California GSA Bulletin* 106(5) 607-626.
- Shi, Y., & Wang, C. (1987). Two-dimensional modeling of the P-T-t paths of regional metamorphism in simple overthrust terrains. *Geology (Boulder)*, 15(11), 1048-1051.
- Shyu, J. B. H., Sieh, K., Chen, Y., & Chung, L. (2006). Geomorphic analysis of the Central Range Fault, the second major active structure of the Longitudinal Valley suture, eastern Taiwan. *Geological Society of America Bulletin*, 118(11-12), 1447-1462.
- Shyu, J. B. H., Sieh, K., Chen, Y., & Liu, C. (2005). Neotectonic architecture of Taiwan and its implications for future large earthquakes. *Journal of Geophysical Research*, 110, B08402.
- Simoes, M., & Avouac, J. P. (2006). Investigating the kinematics of mountain building in Taiwan from the spatiotemporal evolution of the foreland basin and western foothills. *Journal of Geophysical Research*, 111, B10401.
- Simoes, M., Avouac, J. P., Chen, Y., Singhvi, A. K., Wang, C., Jaiswal, M., Chan, Y., Bernard, S. (2007). Kinematic analysis of the Pakuashan fault tip fold, west central Taiwan: Shortening rate and age of folding inception. *Journal of Geophysical Research*, 112, B03S14.
- Spotila, J.A., Jamie T. Buscher, J.T., Meigs, A.J., Reiners, P.W. (2004). Long-term glacial erosion of active mountain belts., Example of the Chugach–St. Elias Range, Alaska. *Geology*, 32(6), 501–504.
- Stewart, R.J., Brandon, M.T. (2004). Detrital zircon fission-track ages for the "Hoh Formation": Implications for late Cenozoic evolution of the Cascadia subduction wedge., *Geological Society of America Bulletin* 116, 60-75.
- Stolar, D. B., Willett, S. D., & Montgomery, D. R. (2007). Characterization of topographic steady state in Taiwan. *Earth and Planetary Science Letters*, 261(3-4), 421-431.
- Stuwe, K., White, L. and Brown, R. (1994). 'The influence of eroding topography on steady-state isotherms. Application to fission track analysis', *Earth and Planetary Science Letters*, 124, 63–174.

- Sibuet, J., & Hsu, S. (1997). Geodynamics of the Taiwan arc-arc collision. *Tectonophysics*, 274(1-3), 221-251.
- Sibuet, J., Hsu, S., & Debayle, E. (2004). Geodynamic context of the Taiwan Orogen. *Geophysical Monograph*, 149, 127-158.
- Sobel E. R., Oskin, M., Burbank, D., Mikolaichuk A. (2006). Exhumation of basement-cored uplifts: Example of the Kyrgyz Range quantified with apatite fission track thermochronology, *Tectonics* 25, TC2008, doi:10.1029/2005TC001809.
- Spotila, J. A., Buscher, J. T., Meigs, A. J., & Reiners, P. W. (2004). Long-term glacial erosion of active mountain belts; example of the Chugach-St. Elias Range, Alaska. *Geology (Boulder)*, 32(6), 501-504.
- Stuewe, K., White, L., & Brown, R. (1994). The influence of eroding topography on steady-state isotherms; application to fission track analysis. *Earth and Planetary Science Letters*, 124(1-4), 63-74.
- Suppe, J. (1980). Imbricated Structure of Western Foothills Belt, South Central Taiwan., *Petroleum Geology of Taiwan*, 17, 1-16.
- Suppe, J. (1980). A retrodeformable cross section of northern Taiwan., *Geological Society of China Proceedings*, 23, 46-55.
- Suppe, J. (1981). Mechanics of mountain building and metamorphism in Taiwan., *Chung Kuo Ti Ch'ih Hsueh Hui Chuan Kan = Memoir of the Geological Society of China*, 4, 67-89.
- Suppe, J. (1983). Geometry and kinematics of fault-bend folding, *American Journal of Science* 283(7), 684-721.
- Suppe, J. (1984). Kinematics of arc-continent collision, flipping of subduction, and back-arc spreading near Taiwan., *Geological Society of China Memoir* 6, 21-33.
- Suppe, J., Namson, J. (1979). Fault-bend origin of frontal folds of the western Taiwan fold-and-thrust belt., *Petroleum Geology of Taiwan*, 16, 1-18.
- Suppe, J., Chen, C., Chen, J., Lee, C., & Pan, K. (1984). Kinematics of arc-continent collision, flipping of subduction, and back-arc spreading near Taiwan. *Chung Kuo Ti Ch'ih Hsueh Hui Chuan Kan - Memoir of the Geological Society of China*, 6, 21-33.

- Suppe, J., Medwedeff, D.A. (1990). Geometry and kinematics of fault-propagation folding, *Eclogae Geologicae Helvetiae*, 83(3), 409-454.
- Suppe, J., Chou, G.T., and Hook, S.C. (1992). Rates of folding and faulting determined from growth strata, in McClay, K.R., ed., *Thrust tectonics*: London, Chapman & Hall, 105-121.
- Tagami, T., & O'Sullivan, P. B. (2005). Fundamentals of fission-track thermochronology. *Reviews in Mineralogy and Geochemistry*, 58(1), 19-47.
- Teng, L. S. 1990. Geotectonic evolution of late Cenozoic arc-continent collision in Taiwan. *Tectonophysics*, 183(1-4), 57-76.
- Teng, L. S. (1992) Geotectonic evolution of Tertiary continental margin basins of Taiwan. *Petroleum Geology of Taiwan*, 27, 1–19.
- Teng, L. S. (1996). Extensional collapse of the northern Taiwan mountain belt. *Geology (Boulder)*, 24(10), 949-952.
- Tensi, J., Mouthereau, F., & Lacombe, O. (2006). Lithospheric bulge in the West Taiwan Basin. *Basin Research* 18 (3), 277–299. doi:10.1111/j.1365-2117.2006.00296.x
- Tillman, K. S., Byrne, T. B., Teng, L. S., & Huang, C. (1996). Out-of-sequence thrusting in the Taiwan slate belt. *Journal of the Geological Society of China*, 39(2), 189-208.
- Thompson, S.C., Weldon, R.J., Rubin, C.M., Abdrakhmatov, K., Molnar, R. & Berger, G.W. (2002). Late Quaternary slip rates across the central Tien Shan, Kyrgyzstan, central Asia. *J. Geophys. Res.*, 107(B9), 2203.
- Thiede, R.C., Arrowsmith, J.R., Bookhagen, B., McWilliams, M.O., Sobel, E.R., Strecker, M.R. (2005). From tectonically to erosionally controlled development of the Himalayan orogen, *Geology* 33(8), 689–692.
- Twiss, R. J., & Moores, E. M. (1992). *Structural geology*. New York: W.H. Freeman and Company.
- ter Voorde, M., de Bruijne, C.H., Cloetingh, S.A.P.L., Andriessen, P.A.M. (2004). Thermal consequences of thrust faulting: simultaneous versus successive fault activation and exhumation. *Earth and Planetary Science Letters* 223, 395– 413.



- Wesnousky, S.G., Kumar, S., Mohindra, R., Thakur, V.C. (1999). Uplift and convergence along the Himalayan Frontal Thrust of India. *Tectonics* 18, 967–976.
- Whipp, D. M., Ehlers, T. A., Blythe, A. E., Huntington, K. W., Hodges, K. V., & Burbank, D. W. (2007). Plio-Quaternary exhumation history of the central Nepalese Himalaya: 2. Thermokinematic and thermochronometer age prediction model. *Tectonics*, 26, TC3003.
- Willett, S.D., Brandon, M.T. (2002). On steady states in mountain belts, *Geology* 30(2), 175–178.
- Willett, S. D., Fisher, D., Fuller, C., Yeh, E., & Lu, C. (2003). Erosion rates and orogenic-wedge kinematics in Taiwan inferred from fission-track thermochronometry. *Geology (Boulder)*, 31(11), 945-948.
- Willett, S. D., Hovius, N., Brandon, M. T., & Fisher, D. M. (2006). Tectonics, climate, and landscape evolution; introduction. *Special Paper - Geological Society of America*, 398, vii-xi.
- Wobus, C. W., Hodges, K. V., & Whipple, K. X. (2003). Has focused denudation sustained active thrusting at the Himalayan topographic front? *Geology*, 31(10), 861-864.
- Wolf, R.A., Farley, K.A., Silver, L.T. (1996). Helium diffusion and low temperature thermochronometry of apatite. *Geochim. et Cosmochim. Acta*, 60, 4231-4240.
- Wu, F. T., Rau, R., & Salzberg, D. (1997). Taiwan orogeny: thin-skinned or lithospheric collision? *Tectonophysics*, 274(1-3), 191-220.
- Yu, S., Chen, H., & Kuo, L. (1997). Velocity field of GPS stations in the Taiwan area. *Bulletin of the Institute of Earth Sciences*, 17, 43-44.
- Yu, S.-B., Kuo, L.-C., Hsu, Y.-J., Su, H.-H., Liu, C.C., Hou, C.-S., Lee, J.-F., Lai, T.-C., C.C. Liu, Liu, C.-L., Tseng, T.-F., Tsai, C.-S., Shin, T.-C. (2001). Preseismic deformation and coseismic displacements associated with the 1999 Chi-Chi, Taiwan, earthquake., *Bulletin of the Seismological Society of America*., 91 (5), 995-1012.
- Yue, L., Suppe, J., & Hung, J. (2005). Structural geology of a classic thrust belt earthquake: the 1999 Chi-Chi earthquake Taiwan (Mw=7.6). *Journal of Structural Geology*, 27(11), 2058-2083.

Zapata, T., Allmendinger, R.W. (1996). Growth stratal records of instantaneous and progressive limb rotation in the Precordillera thrust belt and Bermejo basin, Argentina, *Tectonics* 15, 1065–1083.

Zeitler, P.K., (1985). Cooling history of the NW Himalaya, Pakistan. *Tectonics*, 4(1), 127-151.

**VITA**

Jane Lock was born in Wellington, New Zealand. She grew up in Manchester, England then moved to New Zealand where received a BSc (honours) degree in geology from Victoria University of Wellington. Jane traveled before moving to the United States where she earned a MSc in geoscience from Pennsylvania State University. She completed a Doctor of Philosophy at the University of Washington from the Department of Earth and Space Science.